AFRL-VA-WP-TR-2003-3088

INVESTIGATION OF THE EFFECT OF CORROSION PITTING ON FATIGUE LIFE OF ALUMINUM STRUCTURE

Eric J. Tuegel

Analytical Structural Mechanics Branch (AFRL/VASM)
Structures Division
Air Vehicles Directorate
Air Force Research Laboratory, Air Force Materiel Command
Wright-Patterson Air Force Base, OH 45433-7542

OCTOBER 2003

Final Report for 01 July 2001 – 31 December 2002

Approved for public release; distribution is unlimited.

STINFO FINAL REPORT

AIR VEHICLES DIRECTORATE
AIR FORCE RESEARCH LABORATORY
AIR FORCE MATERIEL COMMAND
WRIGHT-PATTERSON AIR FORCE BASE, OH 45433-7542

NOTICE

USING GOVERNMENT DRAWINGS, SPECIFICATIONS, OR OTHER DATA INCLUDED IN THIS DOCUMENT FOR ANY PURPOSE OTHER THAN GOVERNMENT PROCUREMENT DOES NOT IN ANY WAY OBLIGATE THE US GOVERNMENT. THE FACT THAT THE GOVERNMENT FORMULATED OR SUPPLIED THE DRAWINGS, SPECIFICATIONS, OR OTHER DATA DOES NOT LICENSE THE HOLDER OR ANY OTHER PERSON OR CORPORATION; OR CONVEY ANY RIGHTS OR PERMISSION TO MANUFACTURE, USE, OR SELL ANY PATENTED INVENTION THAT MAY RELATE TO THEM.

THIS REPORT IS RELEASABLE TO THE NATIONAL TECHNICAL INFORMATION SERVICE (NTIS). AT NTIS, IT WILL BE AVAILABLE TO THE GENERAL PUBLIC, INCLUDING FOREIGN NATIONS.

THIS TECHNICAL REPORT HAS BEEN REVIEWED AND IS APPROVED FOR PUBLICATION.

/s/
Eric J. Tuegel
Engineer
Analytical Structural Mechanics

/s/
James W. Rogers, Major, USAF
Chief
Analytical Structural Mechanics Branch

/s/
David M. Pratt, PhD
Technical Advisor
Structures Division

Do not return copies of this report unless contractual obligations or notice on a specific document require its return.

REPORT DOCUMENTATION PAGE

Form Approved
OMB No. 0704-0188

1. REPORT DATE *(DD-MM-YY)*	2. REPORT TYPE	3. DATES COVERED *(From - To)*
October 2003	Final	07/01/2001 – 12/31/2002

4. TITLE AND SUBTITLE
INVESTIGATION OF THE EFFECT OF CORROSION PITTING ON FATIGUE LIFE OF ALUMINUM STRUCTURE

5a. CONTRACT NUMBER
IN-HOUSE

5b. GRANT NUMBER

5c. PROGRAM ELEMENT NUMBER
62201F

6. AUTHOR(S)
Eric J. Tuegel

5d. PROJECT NUMBER
2401

5e. TASK NUMBER
00

5f. WORK UNIT NUMBER
TN

7. PERFORMING ORGANIZATION NAME(S) AND ADDRESS(ES)
Analytical Structural Mechanics Branch (AFRL/VASM)
Structures Division
Air Vehicles Directorate
Air Force Research Laboratory, Air Force Materiel Command
Wright-Patterson Air Force Base, OH 45433-7542

8. PERFORMING ORGANIZATION REPORT NUMBER
AFRL-VA-WP-TR-2003-3088

9. SPONSORING/MONITORING AGENCY NAME(S) AND ADDRESS(ES)
Air Vehicles Directorate
Air Force Research Laboratory
Air Force Materiel Command
Wright-Patterson Air Force Base, OH 45433-7542

10. SPONSORING/MONITORING AGENCY ACRONYM(S)
AFRL/VASM

11. SPONSORING/MONITORING AGENCY REPORT NUMBER(S)
AFRL-VA-WP-TR-2003-3088

12. DISTRIBUTION/AVAILABILITY STATEMENT
Approved for public release; distribution is unlimited.

13. SUPPLEMENTARY NOTES
This report contains color.

14. ABSTRACT ***(Maximum 200 Words)***

This report presents the results of testing to obtain data on the effect of pitting corrosion on the fatigue life of aluminum specimens. Forty-one coupons of 7075-T6 that had previously been exposed at various USAF bases around the world for up to a year were fatigue tested. The amount of corrosion on each had been previously characterized in terms of mass lost per unit of surface area. Additional characterization of the corrosion with surface roughness traces was done after the fatigue tests.

After a threshold level of corrosion was reached, fatigue life generally decreased with increasing mass loss. Surface roughness generally increased with increasing mass loss as well. However, strong relationships could not be established in either case because of the limited amount of data and the scatter inherent in both fatigue and corrosion.

15. SUBJECT TERMS
fatigue, corrosion, surface roughness, aluminum alloys, 7075-T6

16. SECURITY CLASSIFICATION OF:			17. LIMITATION OF ABSTRACT:	18. NUMBER OF PAGES	19a. NAME OF RESPONSIBLE PERSON (Monitor)
a. REPORT	b. ABSTRACT	c. THIS PAGE			Eric J. Tuegel
Unclassified	Unclassified	Unclassified	SAR	144	19b. TELEPHONE NUMBER *(Include Area Code)* (937) 904-6772

Standard Form 298 (Rev. 8-98)
Prescribed by ANSI Std. Z39-18

Table of Contents

List of Figures

List of Tables

I. Summary

This report presents the results of testing to obtain data on the effect of pitting corrosion on the fatigue life of aluminum specimens. Forty-one coupons of 7075-T6 that had previously been exposed at various USAF bases around the world for up to a year were fatigue tested. The amount of corrosion on each had been previously characterized in terms of mass lost per unit of surface area. Additional characterization of the corrosion with surface roughness traces was done after the fatigue tests.

After a threshold level of corrosion was reached, fatigue life generally decreased with increasing mass loss. Surface roughness generally increased with increasing mass loss as well. However, strong relationships could not be established in either case because of the limited amount of data and the scatter inherent in both fatigue and corrosion.

II. Introduction

This report describes the results of testing to obtain additional data on the effect of pitting corrosion on fatigue life to support the corrosion fatigue life prediction models being developed under the Corrosion Fatigue Structural Demonstration (CFSD) program [1]. Fatigue tests of specimens with laboratory-induced corrosion were performed in CFSD. Samples of 7075-T6 that had been exposed at various U.S. Air Force bases around the world for up to a year were available for fatigue testing. The severity of the corrosion on each sample had been characterized in terms of the mass lost by each sample. The results from these samples were being used to rank the severity (or corrosion potential) of the various bases [2]. A natural extension of this work was to then determine the effect that exposures of differing times at these different bases had on the fatigue life of these samples. Characterization of pit densities, depths, and surface sizes, along with surface roughness might then provide a link between surface condition, which can be inspected in the field, and the reduction in fatigue life.

The number of specimens tested was not sufficient to draw definitive conclusions. However, some trends were identified in the results. All efforts to characterize the pitting damage are documented in this report for future reference.

In addition, Lockheed Martin had some C-130 nose gear wheel well panels that become pitted as a result of stripping the paint during a rework operation. These panels were integrally stiffened and provided an opportunity to see what the effect of widespread pitting would be in a large structure. Unfortunately, a steel-stamped rejection mark was not noticed while preparing the panel for testing. A fatigue crack started from this rejection mark and subsequently grew to failure. This result allows an upper bound to be placed on the stress concentrations at the pits, but does not provide any details on the effect of widespread pitting. Lockheed decided to test specimens cut from the remaining panels so no additional panels were available to try this test again. The test procedure and results are documented in this report for future reference.

III. Approach

Forty-one coupons (41) of 7075-T6 aluminum that had been exposed to natural environment for 3, 6, 9 or 12 months at different USAF bases around the world were obtained from William Abbott of Battelle – Columbus [1]. Another seven (7) as-fabricated coupons were obtained to establish a baseline for the uncorroded condition. The coupons measured 3.0 inch (75 mm) long by 0.5 inch (12.7 mm) wide by 0.031 inch (0.787 mm) thick. The amount of corrosion on each specimen was measured in terms of mass loss per unit of surface area ($\mu g/cm^2$). Only pitting corrosion was observed on the specimens; the polishing marks made as part of preparing the coupons for exposure could still be observed. Determination of what the mass loss means in terms of pit sizes and densities was not undertaken as part of this effort. The location and length of exposure, and the mass loss per unit surface area ($\mu g/cm^2$) as supplied by Mr. Abbott are reported in Table 1.

The coupons were fatigue tested in order to determine the significance of different corrosion levels to fatigue life. After the fatigue tests, surface roughness measurements were made to see if roughness could be correlated with fatigue life or amount of corrosion. Finally, fractography was done on all the failed specimens to identify the fatigue origins.

Specimen No.	Location	Length of Exposure	Mass Loss/Area ($\mu g/cm^2$)
1331	WPAFB	12 Months	142
5607	Kadena	3 Months	163
5608	Kadena	6 Months	128
5615	MacDill	3 Months	250
5616	MacDill	6 Months	464
5618	MacDill	12 Months	467
5635	WPAFB	9 Months	94
5636	Wright-Patterson	3 Months	41
5708	Warner Robbins	3 Months	12
5710A	Eareckson	6 Months	649
5710B	Warner Robins	6 Months	32
5772	Eareckson	3 Months	197
5773	Elmendorf	3 Months	7
5776	Elmendorf	6 Months	65
5829	Diego Garcia	3 Months	68
5830	Diego Garcia	6 Months	103
5832	Diego Garcia	9 Months	216
5854	Warner Robins	12 Months	68
5869	Yeager	12 Months	84
5871	Yeager	3 Months	35
5872	Yeager	9 Months	71
5877	Tyndall	6 Months	316
5878	Tyndall	3 Months	269
5879	Tyndall	12 Months	866
5880	Tyndall	9 Months	507
5893	Portland	3 Months	65
5896	Portland	12 Months	125
5914	Daytona Beach	12 Months	1702
5925	Charleston	3 Months	144
5926	Charleston	9 Months	308
5931	WPAFB	6 Months	69
5932	McChord	3 Months	155
5933	McChord	6 Months	283
5934	McChord	9 Months	345
5944	Travis	9 Months	225
5945	Travis	6 Months	187
5946	Travis	3 Months	105
5967	Charleston	6 Months	191
5969	Charleston	12 Months	380
6002	Daytona Beach	6 Months	804
6008	Daytona	3 Months	1000

Table 1. List of Coupons and Exposures

II.1 Fatigue Test Program

The fatigue tests were performed in Fatigue and Fracture Mechanics Lab of the Air Vehicles Directorate of the Air Force Research Laboratory. These experiments were considered prior-corrosion/fatigue, because the actual fatigue portion was conducted in laboratory air after exposure at the various bases. Prior to testing 0.020 in. (0.51 mm) was milled off of each edge of the gage section to remove any end-grain corrosion damage. This limited the corrosion damage to the top and bottom faces of the specimens. In addition, it was determined that the coupons had been sheared from the large sheet rather than cut. So milling the edges of the gage section away removed some of the plastically deformed region produced by the shear.

The geometry of the fatigue coupons is shown in Figure 1. The fatigue tests were conducted at a constant amplitude, R = 0.1, loading at 15 Hz in lab air. The first several tests were tested at a maximum stress of approximately 23 ksi (158.5 MPa) to obtain fatigue lives greater than 100,000 cycles where it was anticipated that corrosion would have the most effect. However, the large number of tests exceeding 5,000,000 cycles to failure forced the maximum stress to be increased to 32 ksi (220 MPa). This also improved the control of the tests so that all tests had the same maximum stress of 32 ksi (220 MPa).

Optical microscopy and scanning electron microscopy (SEM) examinations were conducted on the fracture surfaces of all coupons tested at a maximum stress of 32 ksi to characterize the critical features that were the origins of the fatigue cracks. Photographs from the optical microscopy are presented in Appendix A. Photographs from the SEM are presented in Appendix B.

II.2 Surface Roughness Measurements

The surface roughness of the specimens was measured with a Precision Devices, Inc., Surfometer. A single 0.25 in. (6.4 mm) trace was made on each specimen as near to the fracture point as possible. The height of the stylus was recorded every 25 μin. (0.64 μm). These traces were made after the fatigue tests so that any scratch by the stylus moving across the surface would not introduce extraneous fatigue origins. Plots of the roughness profiles are in Appendix C.

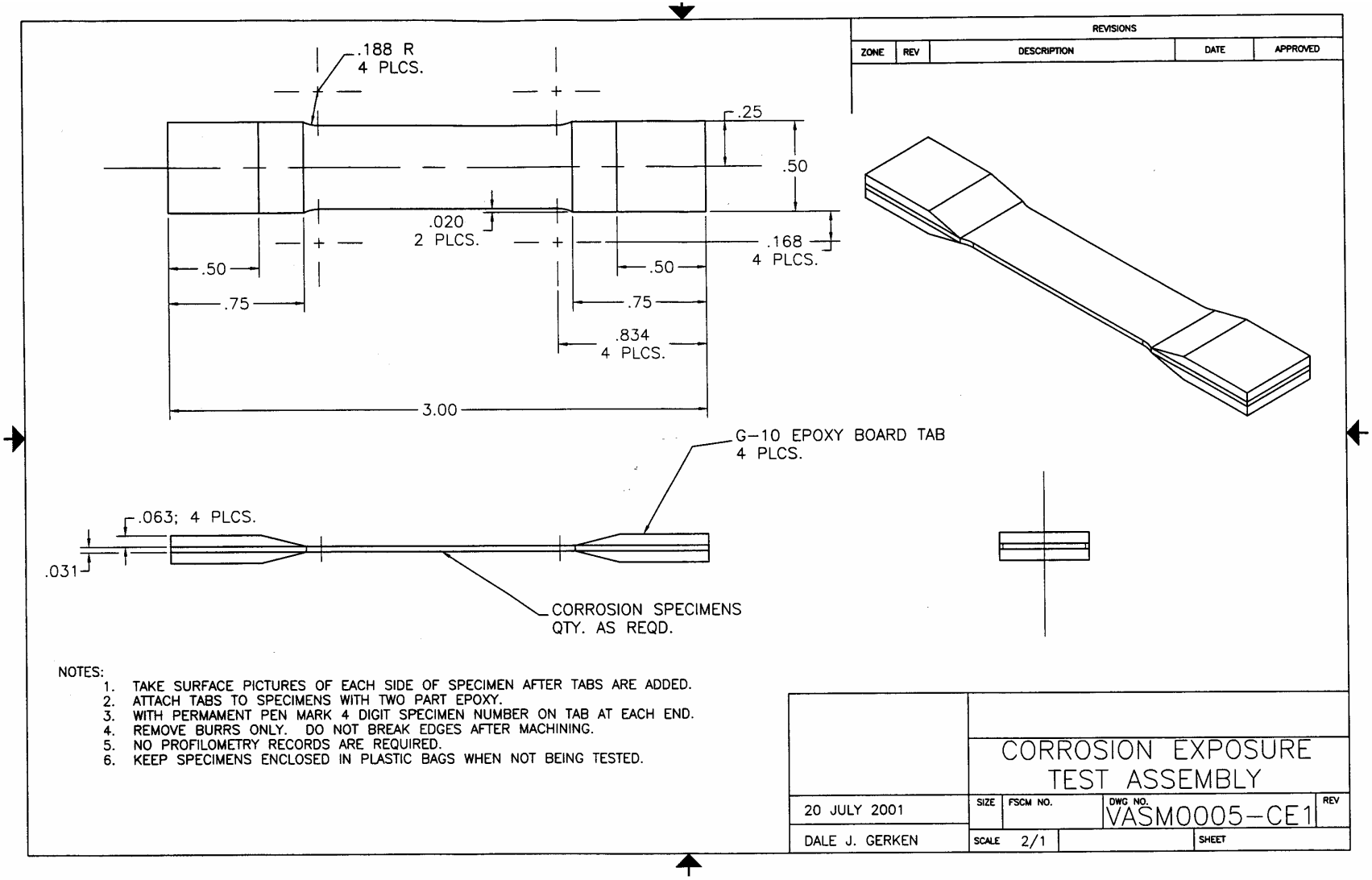

Figure 1. Fatigue test specimen.

IV. Results

III.1 Fatigue Tests

The fatigue lives for the specimens tested at a maximum stress of 23 ksi (158.5 MPa) are reported in Table 2. The fatigue lives for the specimens tested at a maximum stress of 32 ksi (220 MPa) are reported in Table 3.

Specimen ID	Location	Maximum Stress ksi (MPa)	Cycles to Failure
N1	First Baseline	22.4 (154.3)	1,535,787
N2	Second Baseline	22.8 (157.1)	5,000,000[1]
5607	Kadena	22.7 (156.4)	13,591,486[1]
5615	MacDill	23.4 (161.2)	1,038,377
5829	Diego Garcia	22.5 (155)	6,252,110[1]
6008	Daytona	22.8 (157.1)	88,093

[1]Specimen did not fail.

Table 2. Results of Fatigue Tests at a Maximum Stress around 23 ksi (158.5 MPa).

One baseline specimen and two exposed specimens did not fail at the low maximum stress level. These specimens were retested at the higher maximum stress level and had lives comparable to other specimens that had not been previously cycled at the low stress level. It was decided to keep these three data points in the dataset when analysis was performed.

The fracture surfaces of all specimens tested at 32 ksi (220 MPa) maximum stress were examined to determine the failure origin. Not all the fatigue cracks originated at corrosion pits. In one case, the crack originated from a scratch on the surface. The front and back surfaces of the coupons had been roughened prior to exposure at the bases in order to obtain more consistent corrosion results. This particular scratch was a more severe stress concentration than any of the pits.

More frequently, cracks were found starting at a corner of the specimen in the shoulder fillets. The shoulder fillets were sharper than recommended because the coupons were short and we wanted the longest possible gage section to test more of the corroded surface. This type of crack origin may indicate that the stress concentration of the fillet was more severe than any of the pits. The theoretical stress concentration factor for the shoulder fillets is less than 1.08.

The cracks in the baseline specimens began at a corner of the specimens. Some of the longer-lived exposed specimens with low mass losses also had failure origins at a corner. As the mass lost due to corrosion increased, the failure origins moved to the surfaces of the exposed specimens.

The location of the failure origin for each specimen is reported in Table 3. Photographs from the optical examination of the fracture surfaces are presented in Appendix A. The fracture surfaces were next examined in the SEM for detailed examination of the crack origins. Photographs from this examination are presented in Appendix B.

Specimen ID	Location	Cycles to Failure	Failure Origin
N2	Second Baseline	166,130[2]	Edge
N3	Third Baseline	92,036	Edge
N4	Fourth Baseline	86,148	Edge
N5	Fifth Baseline	>3,000,000[1]	
000	New 7075-T6	89,524	Edge
1331	Wright-Patterson	79,807	Surface
5607	Kadena	92,550[2]	Fillet
5608	Kadena	49,517	Fillet
5616	MacDill	79,641	Fillet
5618	MacDill	59,599	Multiple Origins (2 pits, 1 edge)
5635	Wright-Patterson	83,924	Fillet
5636	Wright-Patterson	93,039	Fillet
5708	Warner Robbins	86,844	Fillet
5710A	Eareckson	40,792	Scratch
5710B	Warner Robbins	53,919	Fillet
5772	Eareckson	74,221	Fillet
5773	Elmendorf	54,566	Fillet
5776	Elmendorf	155,745	Corner
5829	Diego Garcia	98,743[2]	Fillet
5830	Diego Garcia	112,107	Fillet
5832	Diego Garcia	58,057	Mult. Pits
5854	Warner Robbins	108,868	Fillet
5869	Yeager	84,467	Fillet
5871	Yeager	118,623	Corner
5872	Yeager	103,001	Fillet
5877	Tyndall	40,789	Surface
5878	Tyndall	52,377	Surface
5879	Tyndall	45,547	Mult. Pits
5880	Tyndall	42,048	Surface
5893	Portland	69,533	Fillet
5896	Portland	79,073	Fillet
5914	Daytona	35,746	Surface
5925	Charleston	47,488	Surface
5926	Charleston	66,887	Surface
5931	Wright-Patterson	150,899	Fillet

[1]Specimen did not fail.
[2]Cycles to failure after previous cycling at lower maximum stress.

Table 3. Results of Fatigue Tests at a Maximum Stress of 32 ksi (220 MPa).

(Continued on next page)

Specimen ID	Location	Cycles to Failure	Failure Origin
5932	McChord	83,908	Fillet
5933	McChord	53,031	Surface
5934	McChord	55,742	Surface
5944	Travis	65,673	Pit
5945	Travis	40,684	Pit
5946	Travis	70,151	Corner
5967	Charleston	54,912	Surface
5969	Charleston	62,898	Surface
6002	Daytona	40,596	Surface

[1]Specimen did not fail.
[2]Cycles to failure after previous cycling at lower maximum stress.

Table 3. Results of Fatigue Tests at a Maximum Stress of 32 ksi (220 MPa).
(Continued from previous page)

III.2 Roughness Measurements

Simple roughness parameters were estimated from the trace for each specimen and are presented in Table 4. The parameters, and the method for calculating them, are as follows:

Average roughness: $R_a = \frac{1}{N}\sum_{n=1}^{N}|r_n|$

RMS roughness: $R_q = \sqrt{\frac{1}{N}\sum_{n=1}^{N}r_n^2}$

Peak: $R_p = |\max(r_n)|$

Valley, $R_v = |\min(r_n)|$

Peak-to-Valley, $R_t = R_p + R_v$

N is the total number of points recorded for each trace and r_n is the nth data point recorded.

Specimen ID	R_a	R_q	R_p	R_v	R_t
N1	17.22	21.41	58.23	82.29	140.52
N2	13.55	17.93	55.94	92.36	148.30
N3	15.69	20.09	52.28	95.03	147.31
0000	9.60	12.50	45.95	56.57	102.52
1331	25.97	36.54	252.85	106.90	359.75
5607	19.28	32.05	79.77	251.85	331.62
5608	21.35	37.96	157.50	235.69	393.19
5615	28.07	49.20	116.73	317.65	434.38
5616	59.59	68.70	153.04	266.15	419.18
5618	18.89	40.39	77.68	405.57	483.25
5635	31.14	40.84	148.23	116.99	265.22
5636	8.33	10.78	27.81	43.85	71.66
5708	6.14	8.11	26.02	39.99	66.01
5710A	14.05	20.52	47.93	109.70	157.63
5710B	9.31	25.27	341.51	37.67	379.18
5772	8.33	10.89	47.36	64.76	112.12
5773	11.45	16.91	36.77	125.96	162.73
5776	10.27	14.37	37.48	118.73	156.21
5829	11.45	16.05	73.79	74.61	148.40
5830	21.72	28.13	128.42	84.91	213.33
5832	32.50	45.28	346.97	96.02	442.99
5854	10.44	14.27	38.26	87.23	125.49
5869	21.03	36.67	139.55	145.13	284.68
5871	14.54	19.31	43.01	112.42	155.43
5872	11.37	14.80	34.64	76.19	110.83
5877	25.69	44.40	103.97	407.22	511.19
5878	28.34	45.84	98.97	295.88	394.85
5879	60.30	82.85	318.43	435.34	753.77
5880	16.85	30.92	58.45	418.16	476.61
5893	8.40	11.02	24.91	82.99	107.89
5896	12.61	16.51	50.27	74.36	124.63
5914	40.26	72.42	170.99	548.64	719.63
5925	12.47	16.02	35.85	69.32	105.17
5926	17.37	23.30	55.98	169.37	225.35
5931	10.58	13.16	34.39	41.12	75.51
5932	16.37	21.12	87.63	86.86	174.49
5933	15.23	24.34	60.58	252.12	312.70

Table 4. Roughness Parameters for Select Specimens.

(continued on next page)

Specimen ID	R_a	R_q	R_p	R_v	R_t
5934	18.85	33.79	79.84	310.61	390.45
5944	12.16	15.45	44.21	57.98	102.19
5945	14.03	18.39	84.35	74.71	159.06
5946	11.84	15.40	39.54	91.34	130.88
5967	11.99	16.28	40.17	88.77	128.94
5969	10.28	14.78	54.72	166.46	221.18
6002	23.72	56.88	73.49	695.80	769.28
6008	43.74	77.37	203.38	478.02	681.40

Table 4. Roughness Parameters for Select Specimens.
(continued from previous page)

V. Discussion

IV.1 Fatigue Tests

The results of the fatigue tests in terms of cycles to failure versus mass loss per unit area are shown in Figure 2 along with an indication of the origin of the crack(s). Lives for pristine baseline specimens are shown along the vertical axis (mass loss of 1 $\mu g/cm^2$ on the log scale) for comparison. Until the mass loss exceeded 140 $\mu g/cm^2$, all the cracks began at a corner usually near the shoulder fillet just like the cracks in the pristine baseline specimens. Between a mass loss of 140 $\mu g/cm^2$ and 200 $\mu g/cm^2$, there is a transition in failure mode. Some of the specimens failed from cracks that originated at a specimen corner while others failed from surface cracks that started at corrosion pits. Above a mass loss of 200 mg/cm2, all the specimens but two failed from surface cracks that started at corrosion pits. The two exceptions to this were both specimens that had been exposed at MacDill with about the same mass loss, 464 and 467 $\mu g/cm^2$. These two specimens had cracks from both corrosion pits and from the specimen corner that linked up. After link-up, the cracks grew on the planes of the corner cracks for both specimens.

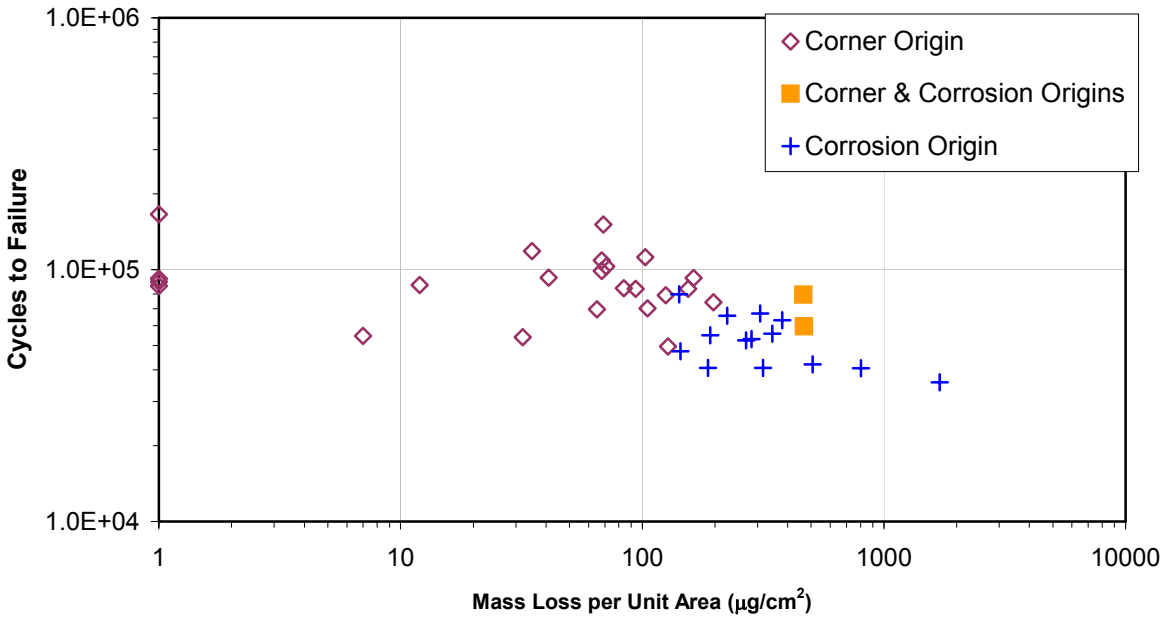

Figure 2. Crack Origin Plotted as a Function of Mass Loss and Cycle to Failure.

The mean fatigue life of the exposed specimens with mass loss of less than 100 µg/cm^2 is about the same as that for the pristine baseline specimens. There does seem to be more scatter in the fatigue lives of the exposed specimens, as well as several lived specimens. When the mass loss becomes greater than 100 µg/cm^2, there is a trend towards decreasing fatigue life with increasing mass loss up to a mass loss of about 1000 µg/cm^2. Around a mass loss of 1000 µg/cm^2, the fatigue lives appear to level off, though there is not enough data with this much mass loss to say conclusively. The minimum fatigue lives obtained for mass losses greater than 100 µg/cm^2 are only slightly shorter than the minimum lives obtained with mass losses less than 100 µg/cm^2, 41,000 cycles versus 54,000 cycles.

These results in relation to the effect of mass loss per unit surface area to fatigue life may be specific to this combination of stress level, material, specimen geometry and coupon fabrication method. However, it is interesting to note the condition of the specimen surfaces in relation to the mass loss as shown in Figure 3. There is little corrosion visible on the exposed surface of specimens with low mass loss per unit area and long fatigue lives (Fig. 3a and 3b). Specimens with greater mass loss per unit area and/or shorter fatigue lives have a great deal more corrosion pitting visible (Fig. 3c and 3d).

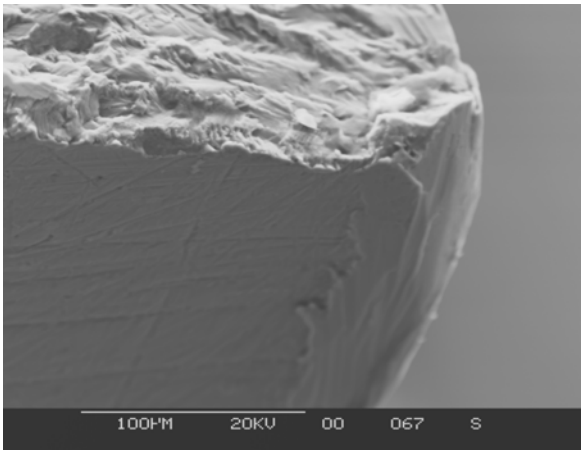

a) 65 µg/cm^2 (155,745 cycles to failure)

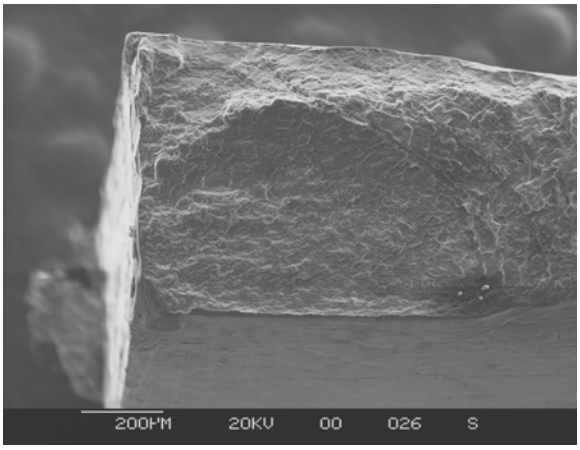

b) 197 µg/cm^2 (74,221 cycles to failure)

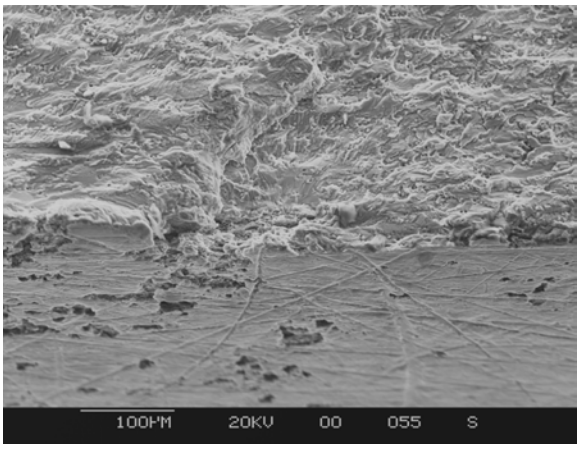

c) 191 µg/cm^2 (54,912 cycles to failure)

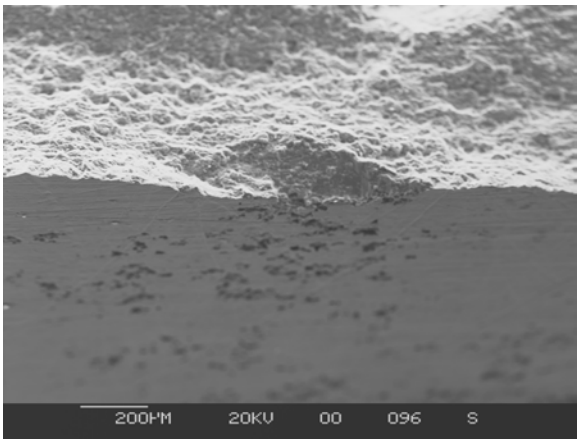

d) 866 µg/cm^2 (45,547 cycles to failure)

Figure 3. Examples of the Amount of Corrosion Pitting Visible on the Exposed Surfaces of Specimens with Different Mass Loss per Unit Surface Area.

The reduction in fatigue life is not necessarily a strong function of the mass loss and length of exposure. This can be seen in Figure 4 where the fatigue lives versus mass loss are plotted for those locations where specimens with different length exposures were tested. Generally, the longer the exposure at a given location, the more mass lost per unit area. Of all the locations with multiple coupons, only Daytona Beach displays a monotonic trend of decreasing fatigue life with increasing mass loss. If there more than two data points for Daytona Beach, it is likely that this consistency would not be maintained. The fatigue lives of specimens exposed at the same location are within the factor of two that is typically quoted for scatter in fatigue tests. If the same scatter factor is still applicable to fatigue tests of corroded specimens, then we would not be able to differentiate between the fatigue lives of a group of specimens exposed at a given location for 3 months from a group exposed at the same location for 12 months. But we might be able to distinguish between specimens exposed at different locations based upon the fatigue lives. Of course, these exposures were limited to one year. It is not known what would happen to the fatigue lives with even longer exposures.

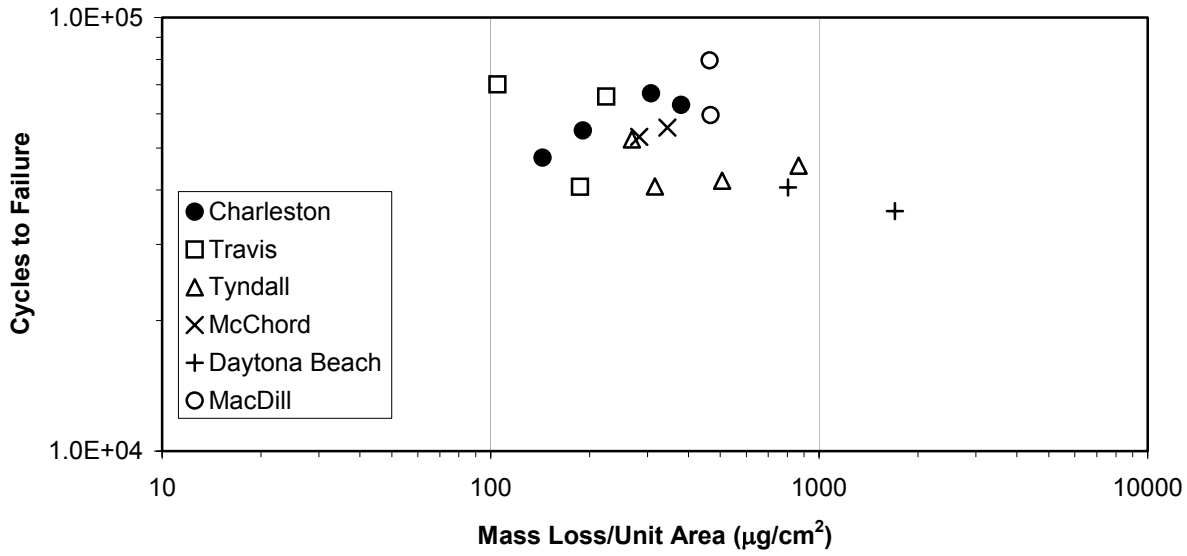

Figure 4: Cycles to Failure vs. Mass Loss per Unit Area Showing Location Where Coupon was Exposed.

IV.2 Surface Roughness

Correlations of the root-mean-square roughness, R_q, and the maximum valley, R_v, with fatigue life are shown in Figures 5 and 6. General trends are observed in both figures but considerably more data is required before we can determine if either of these quantities is a good indicator of the reduction in fatigue life. Since R_a tracks R_q closely and R_q seems to be more sensitive to variations in surface texture, only R_q needs to be looked at. Similarly, R_v represents the deepest hole into the specimen that concentrates stress around it, whereas the maximum peak, R_p, represents a protrusion that is lightly loaded. So we would expect fatigue life to correlate more with R_v than with R_p.

Correlations of Rq and Rv with the mass loss per unit surface area are shown in Figures 7 and 8. Again, general trends are evident but considerably more data is needed before we can determine if either of these quantities is a good indicator of the severity of the corrosion. It is also possible that mass loss per unit surface area is not a measure of corrosion severity. Figures 3b and 3c show the exposed surfaces from two specimens with approximately the same mass loss, but the amount of corrosion visible on the exposed surfaces is very different. There are almost no corrosion pits evident on the surface in Fig. 3b, but the surface in Fig. 3c has numerous corrosion pits.

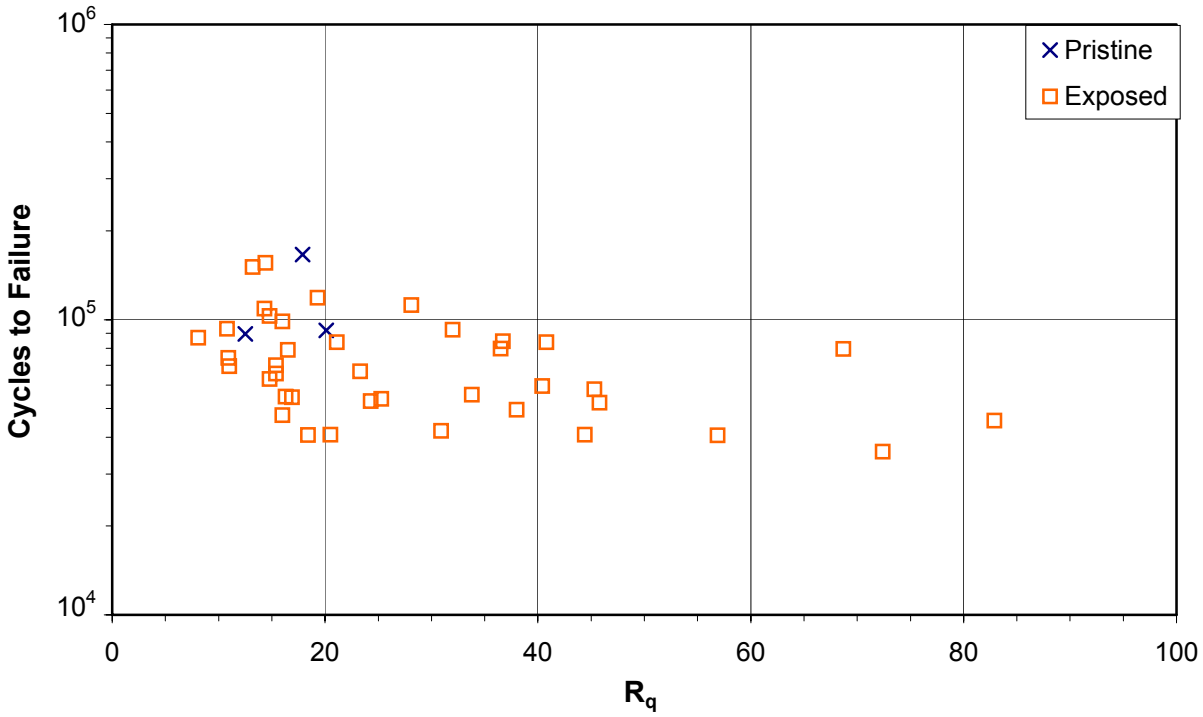

Figure 5. Fatigue Life versus Root Mean Square Roughness, R_q.

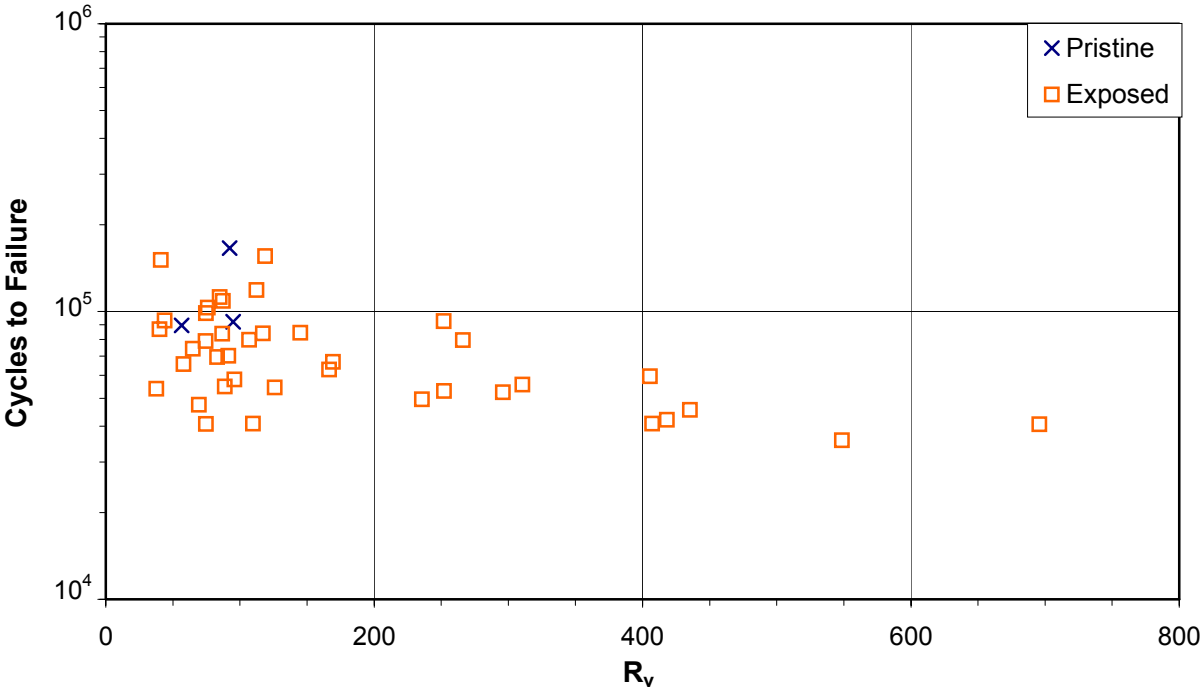

Figure 6. Fatigue Life versus Maximum Valley, R_v.

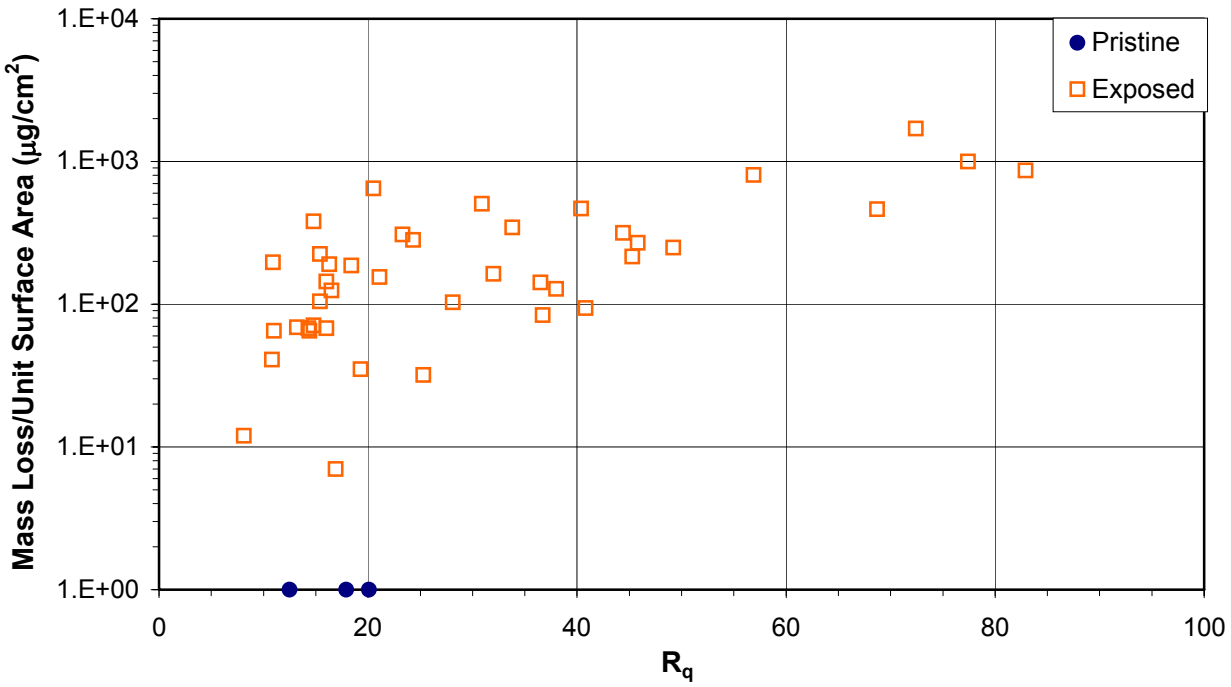

Figure 7. Mass Loss per Unit Surface Area versus Root Mean Square Roughness, R_q.

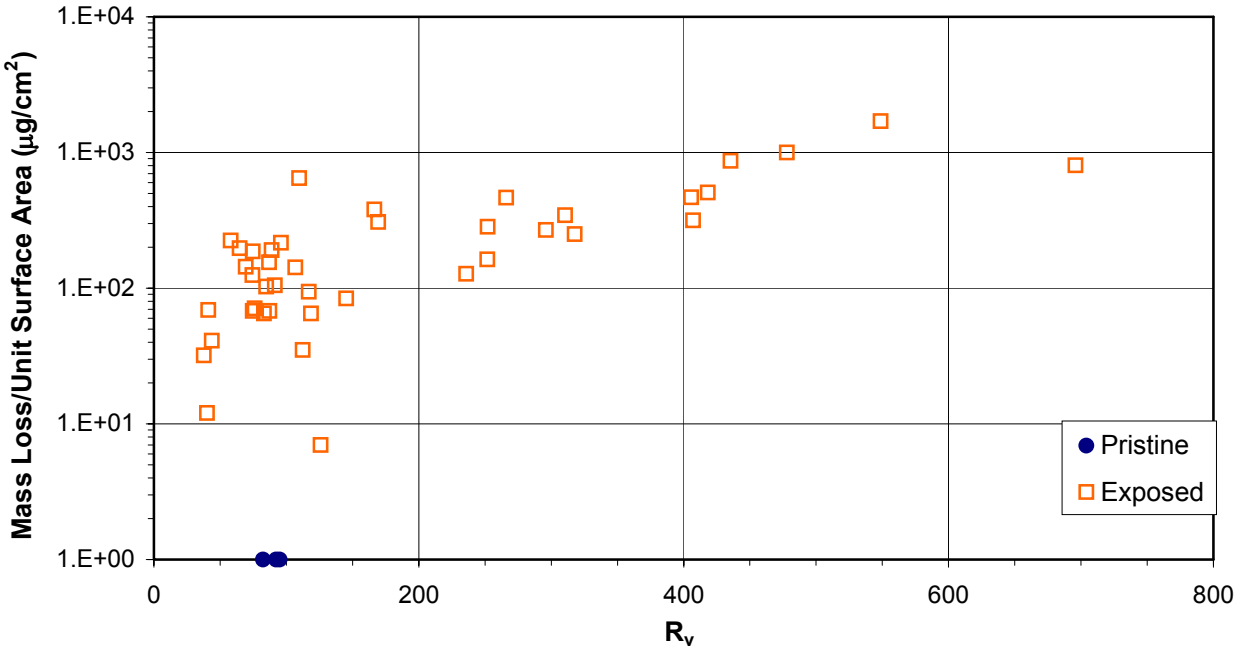

Figure 8. Mass Loss per Unit Surface Area versus Maximum Valley, R_v.

VI. Conclusions

With the limited number of tests performed here, and large amount of scatter associated with corrosion, it is not possible to come to definitive conclusions. Some general observations about the trends seen in the data are:

1. Corrosion does not reduce fatigue life until some threshold level in terms of mass loss is exceeded.

2. Once the threshold level of corrosion is exceeded, fatigue life decreases with increasing mass loss due to corrosion.

3. There is a general trend of decreasing fatigue life as the surface roughness increases as a result of corrosion. There is considerable scatter about the trend curve however.

4. There is a general trend towards increasing surface roughness with increasing mass loss due to corrosion. Again there is considerable scatter in this trend.

VI. References

1. Abbott, W.H., "Final Report of Field Site Reactivity Monitoring," Appendix 4 of **Corrosion Maintenance Improvement (CMI) Final Report**, Contract No. F09650-00-D-0018, S&K Technologies, Feb. 2002.

APPENDIX A: Optical Photomicrographs of Fracture Surfaces

This appendix contains optical photomicrographs of the fracture surfaces of all the specimens tested under the constant amplitude R=0.1 loading with a maximum stress of 32 ksi. After a small amount of flat crack growth on all specimens, slant cracks developed. The angle of the slant faces was very steep; the slant faces being almost parallel to the front and back surfaces of the specimens.

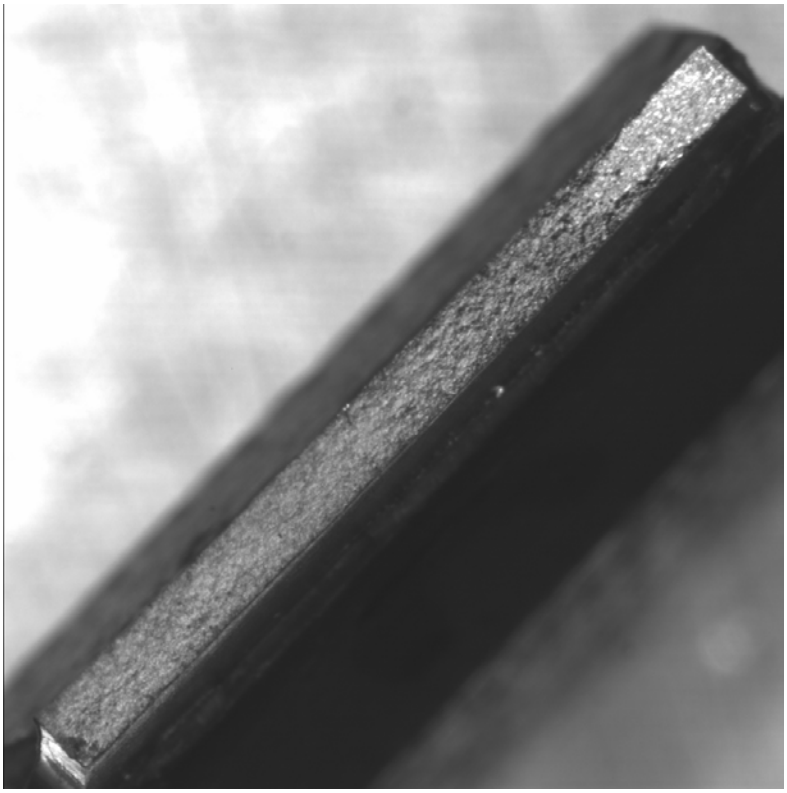

Figure A-1. Fracture Surface of Specimen N2.

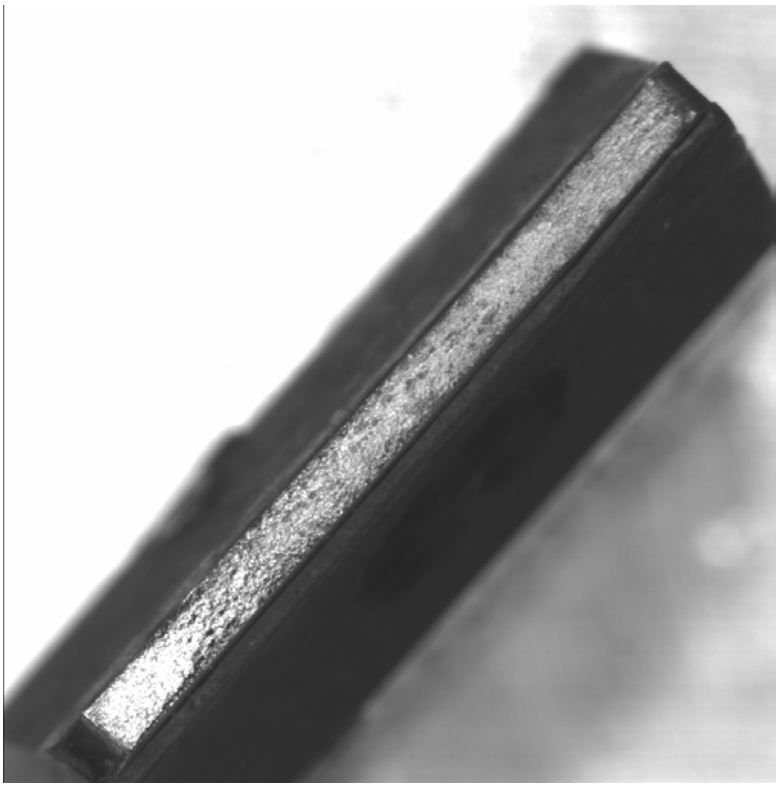

Figure A-2. Fracture Surface of Specimen N4.

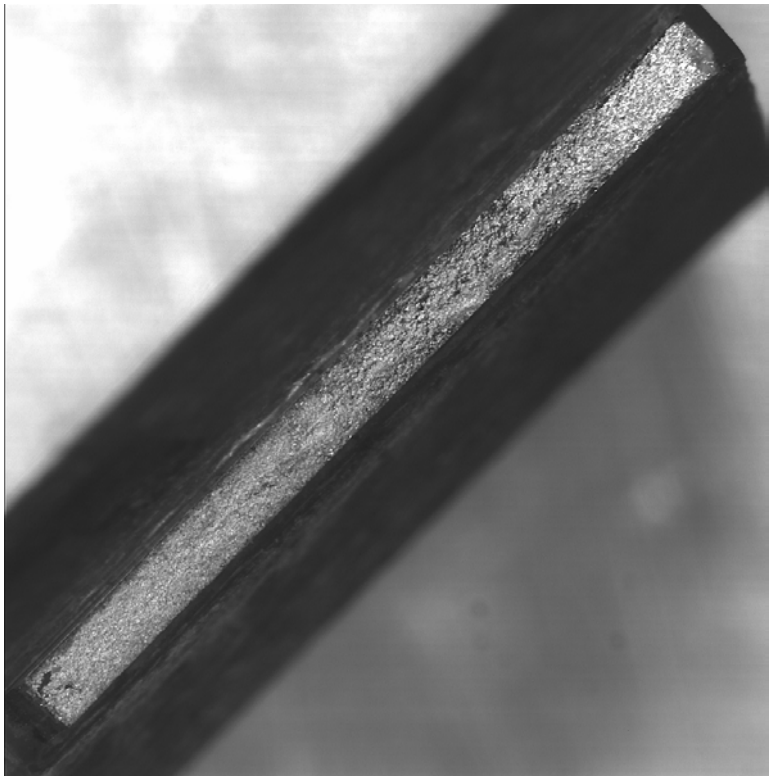

Figure A-3. Fracture Surface of Specimen 0000.

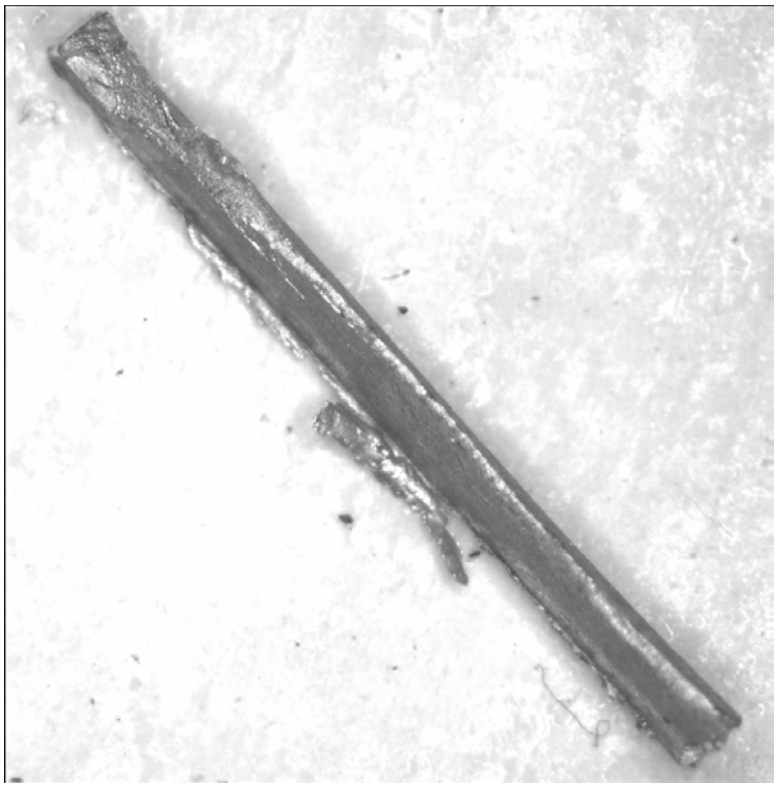

Figure A-4. Fracture Surface of Specimen 1331.

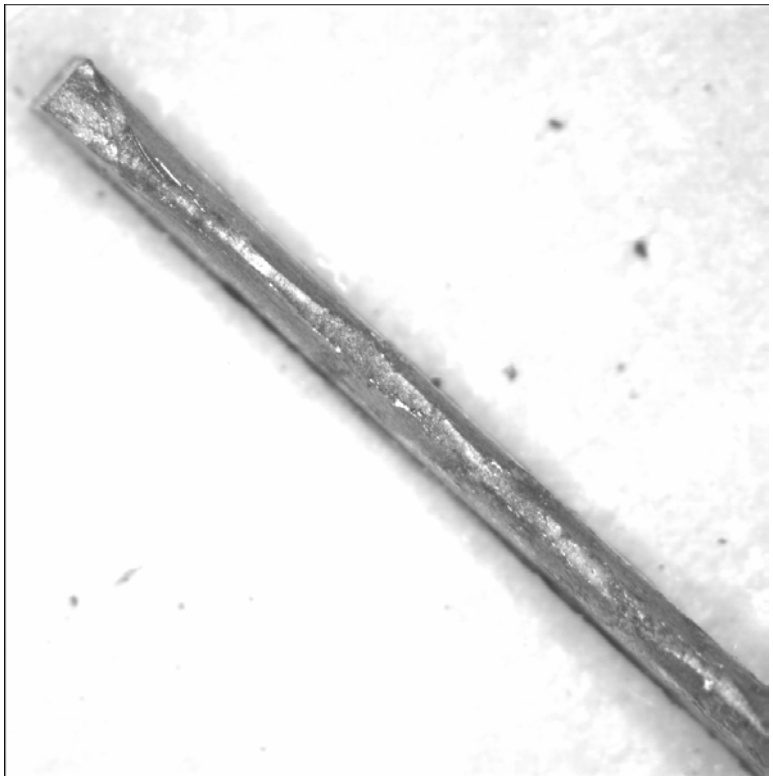

Figure A-5. Fracture Surface from Specimen 5618.

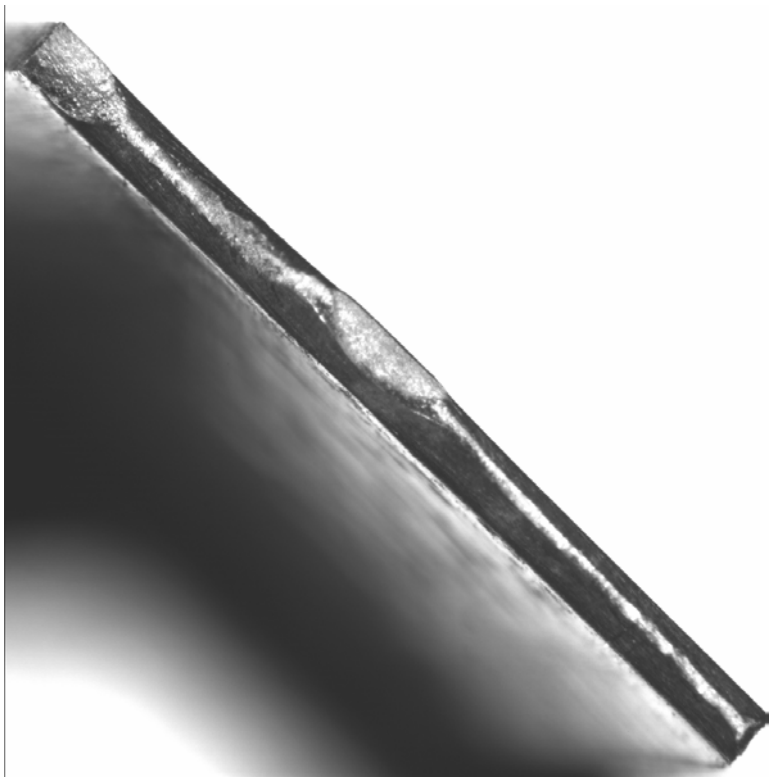

Figure A-6. Fracture Surface of Specimen 5636.

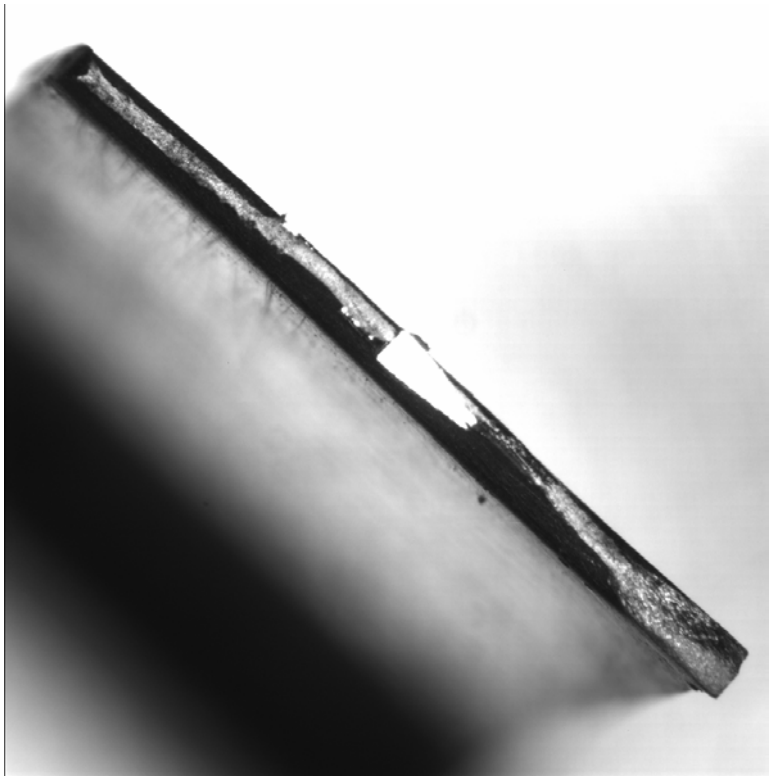

Figure A-7. Fracture Surface of Specimen 5708.

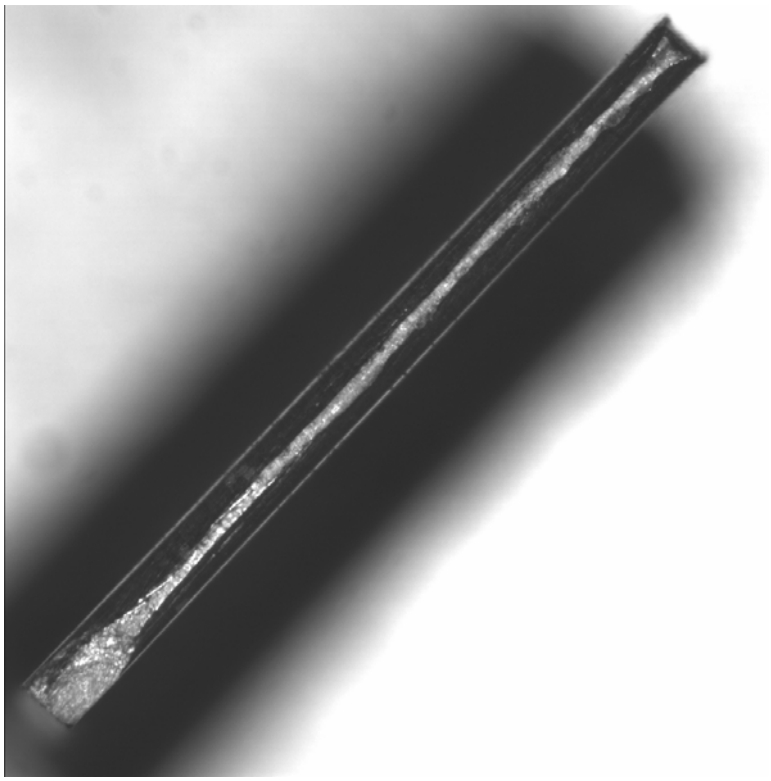

Figure A-8. Fracture Surface of Specimen 5772.

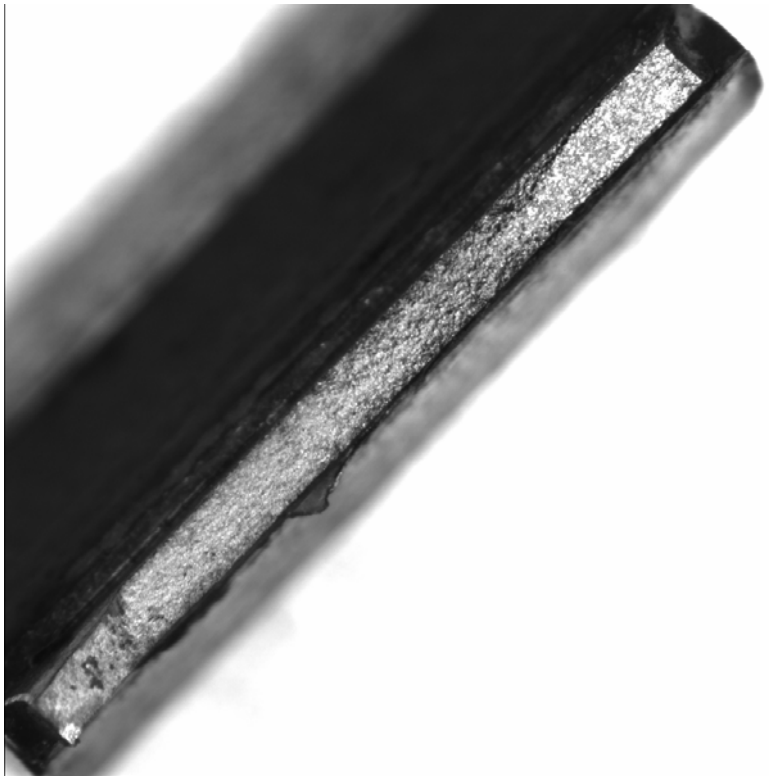

Figure A-9. Fracture Surface of Specimen 5773.

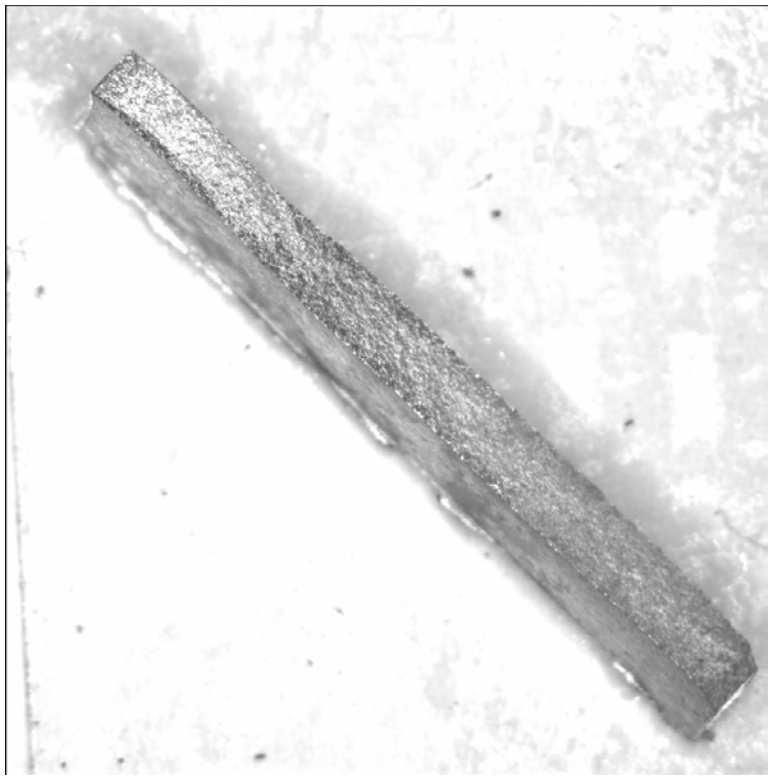

Figure A-10. Fracture Surface of Specimen 5776.

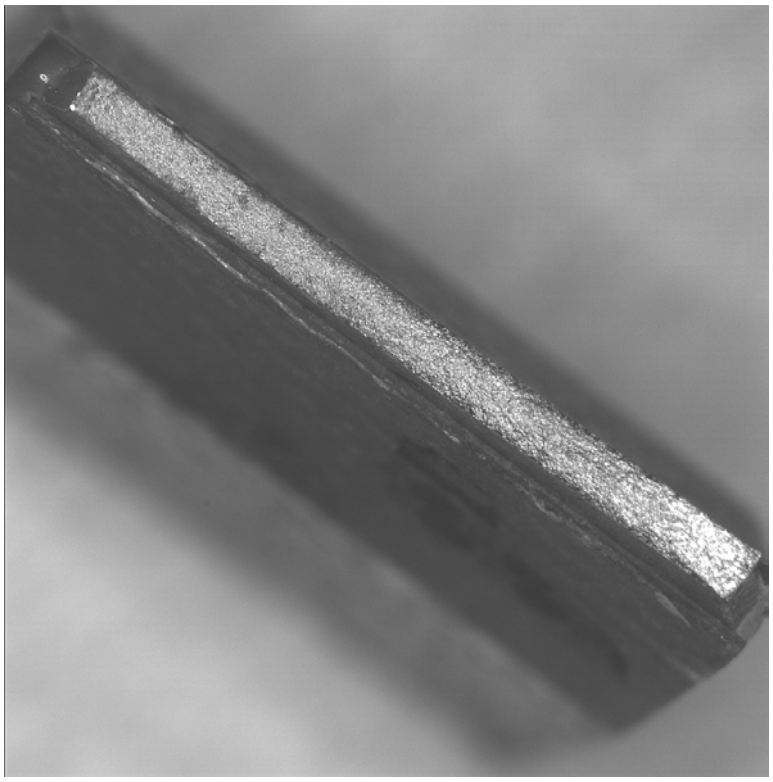

Figure A-11. Fracture Surface of Specimen 5829.

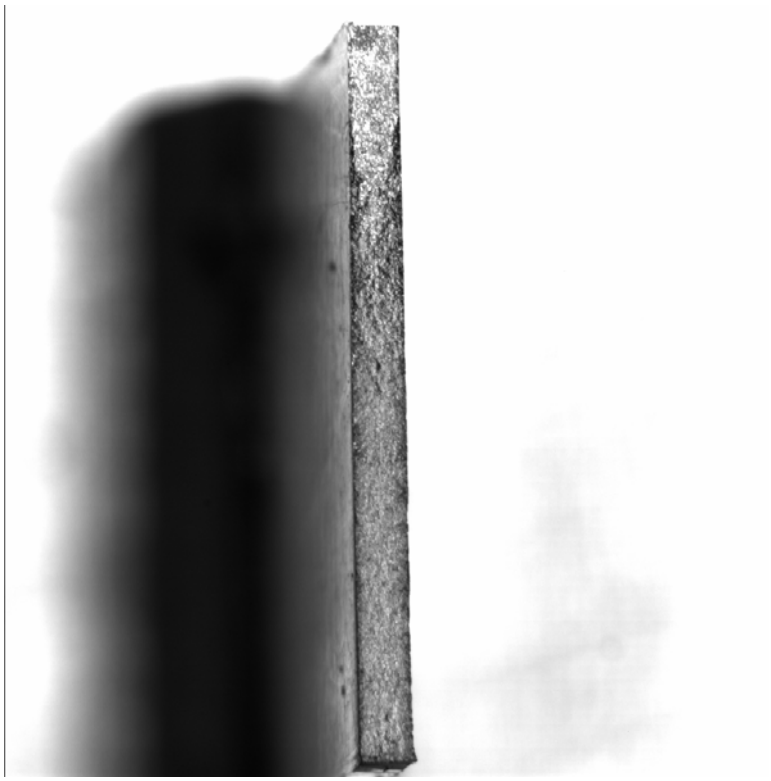

Figure A-12. Fracture Surface of Specimen 5869.

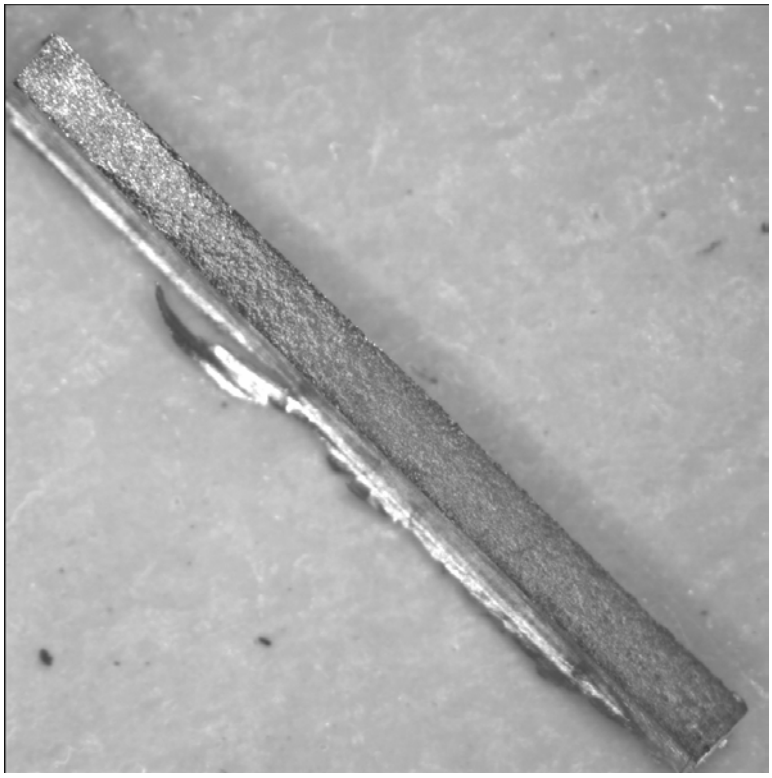

Figure A-13. Fracture Surface from Specimen 5871.

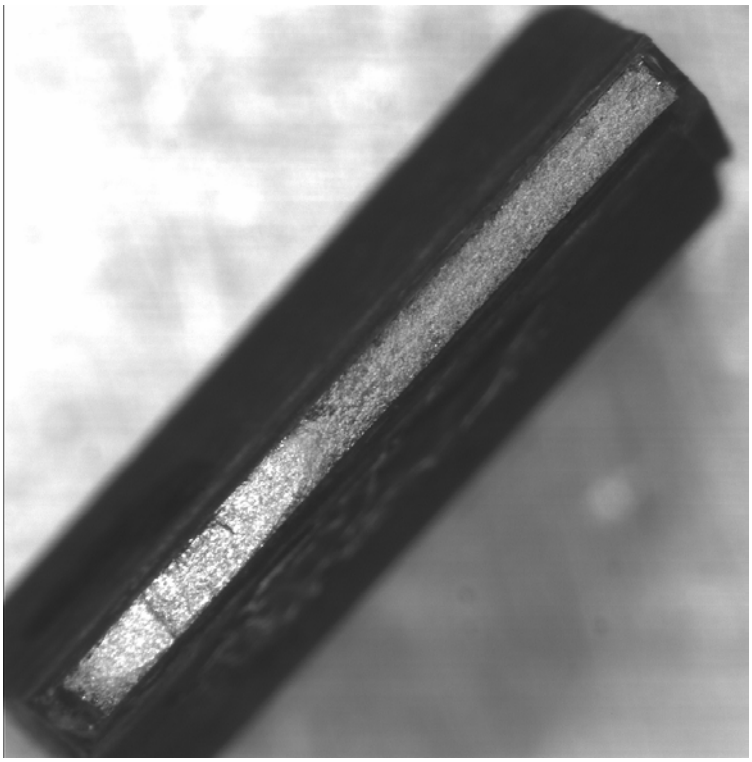

Figure A-14. Fracture Surface of Specimen 5877.

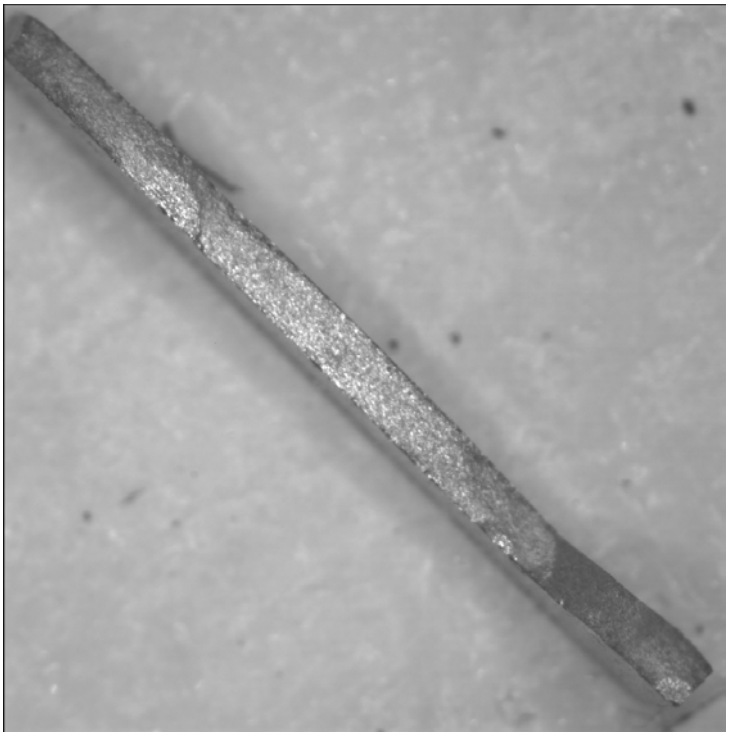

Figure A-15. Fracture Surface of Specimen 5878.

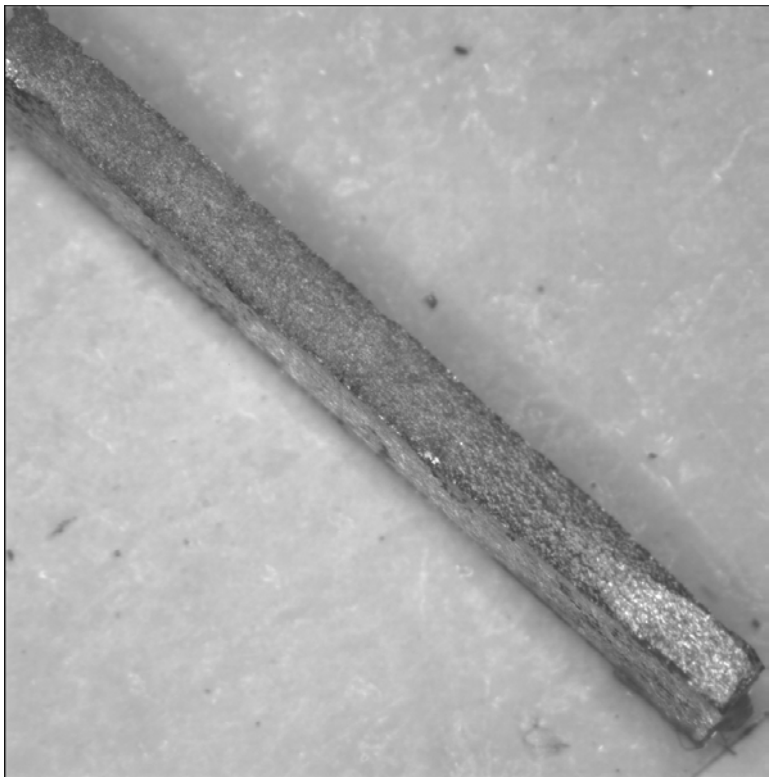

Figure A-16. Fracture Surface of Specimen 5880.

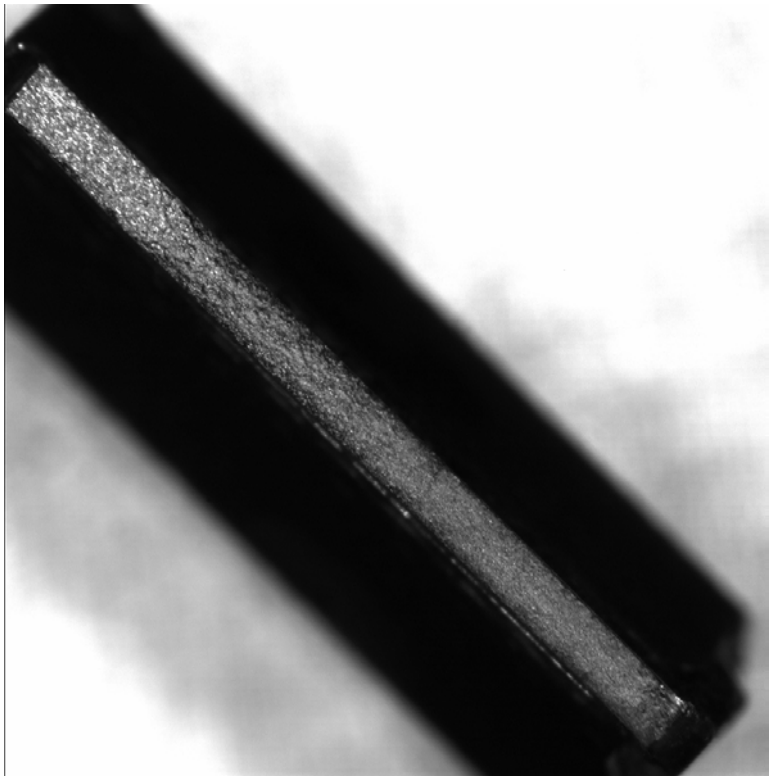

Figure A-17. Fracture Surface of Specimen 5893.

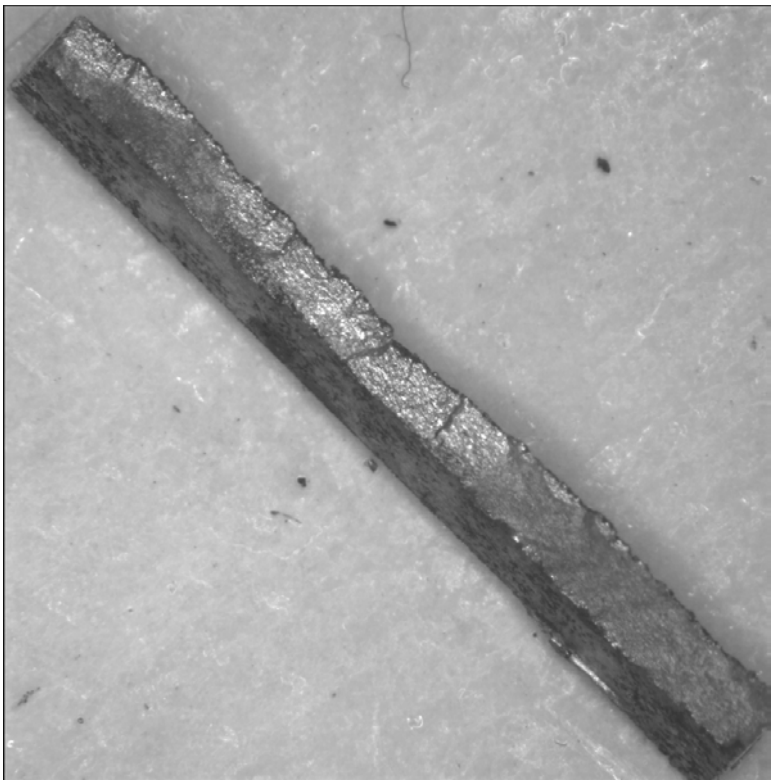

Figure A-18. Fracture Surface of Specimen 5914.

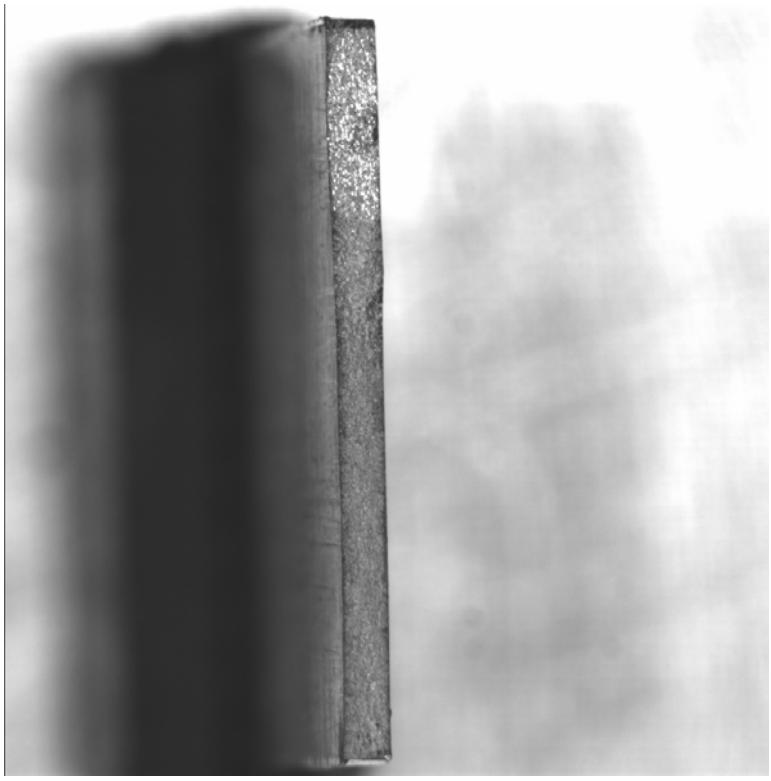

Figure A-19. Fracture Surface of Specimen 5925.

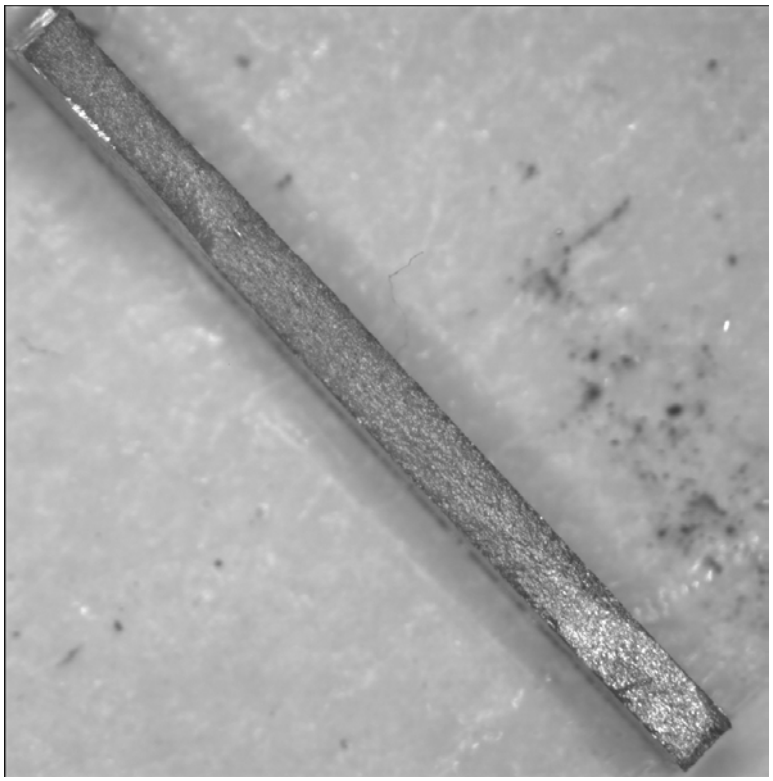

Figure A-20. Fracture Surface of Specimen 5926.

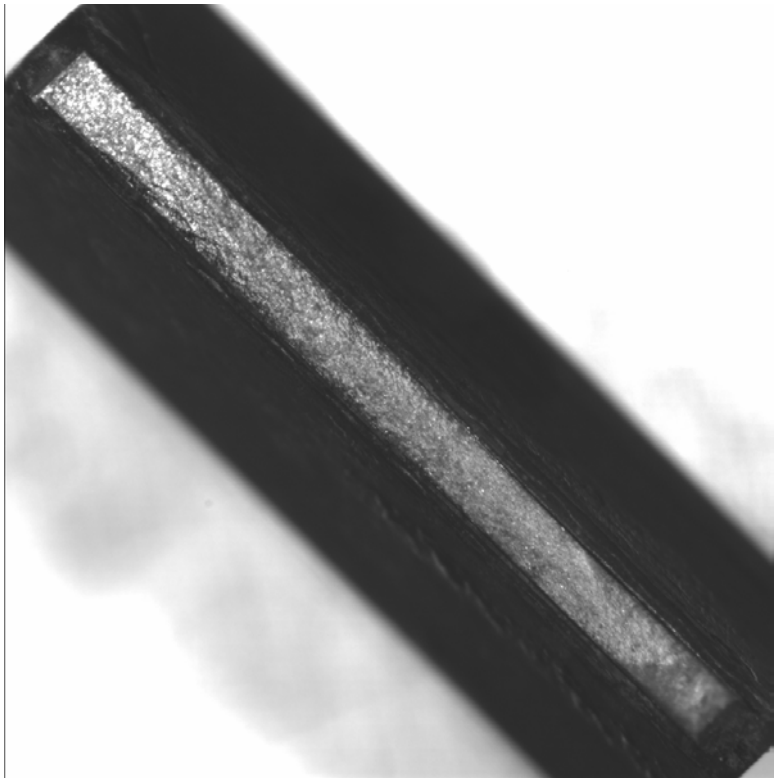

Figure A-21. Fracture Surface of Specimen 5932.

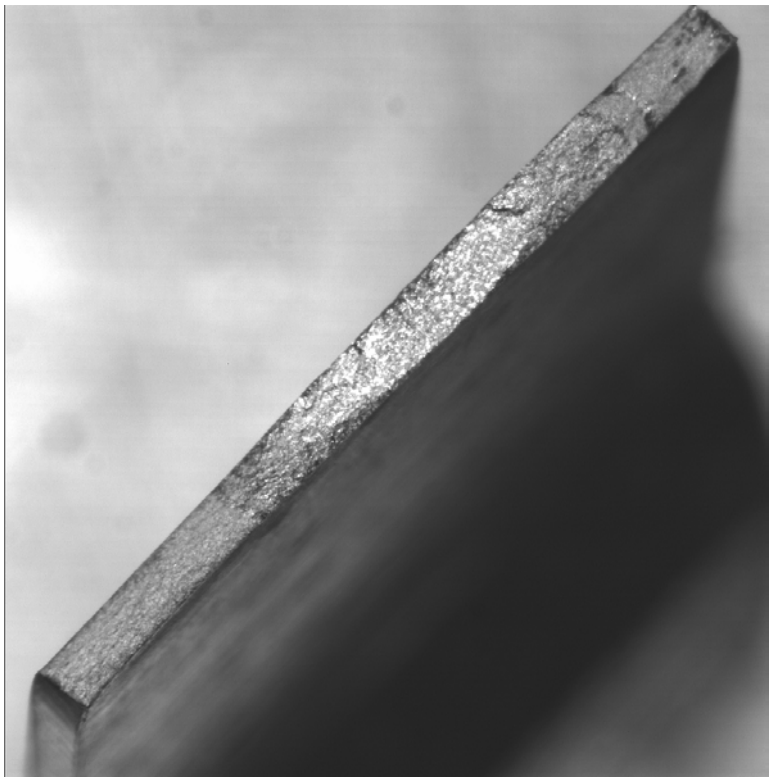

Figure A-22. Fracture Surface of Specimen 5933.

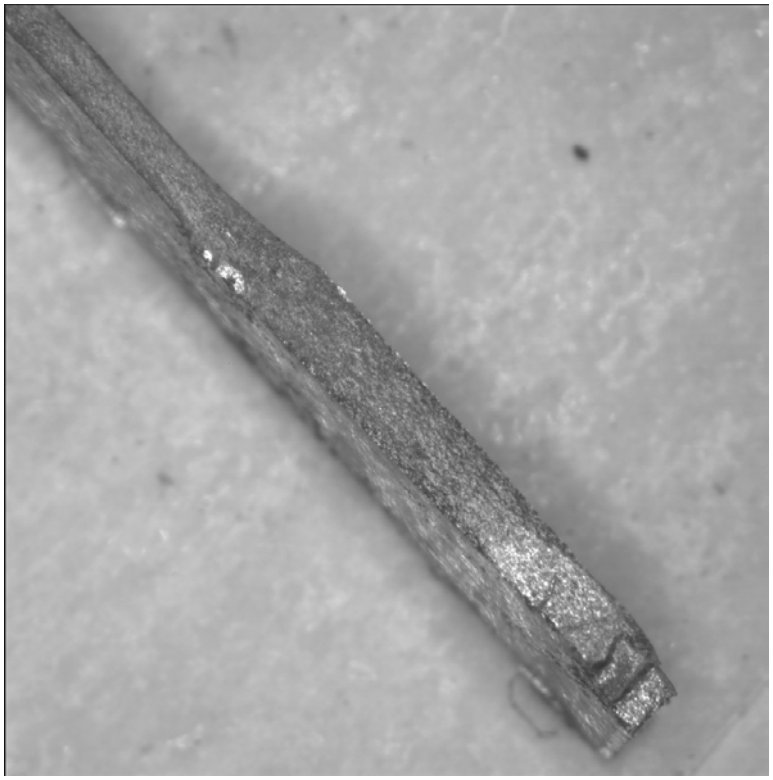

Figure A-23. Fracture Surface of Specimen 5934.

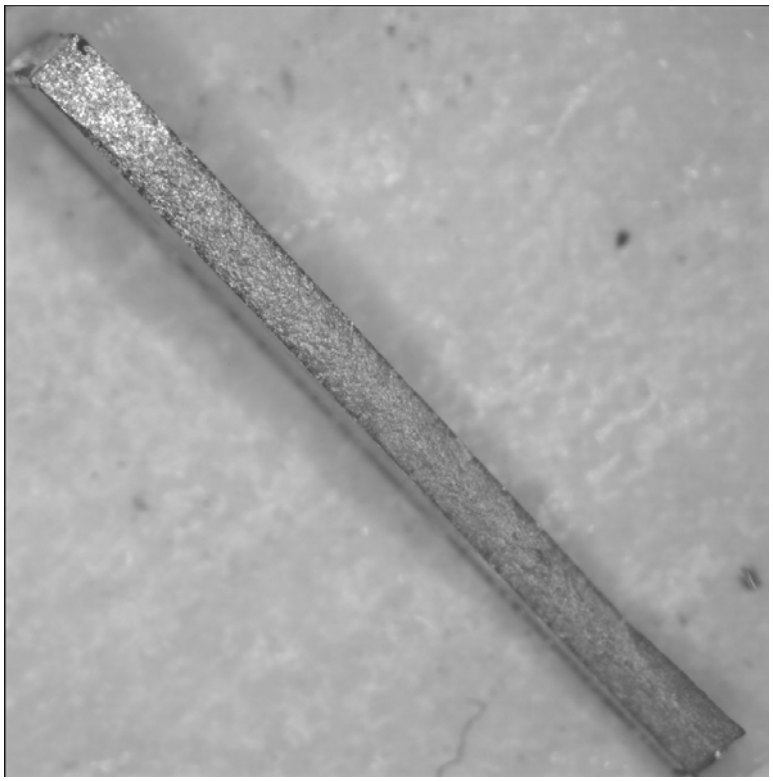

Figure A-24. Fracture Surface of Specimen 5944.

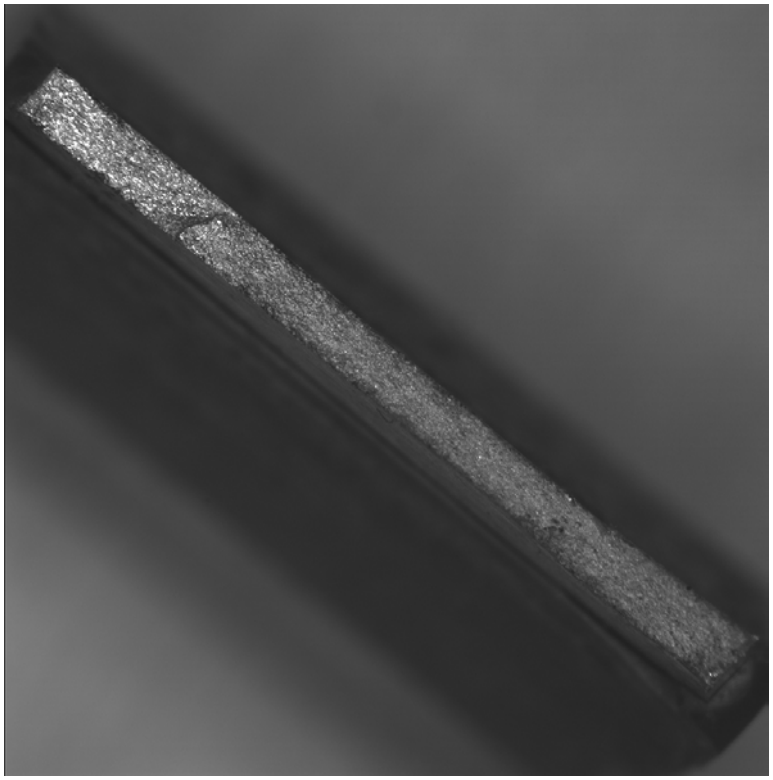

Figure A-25. Fracture Surface of Specimen 5945.

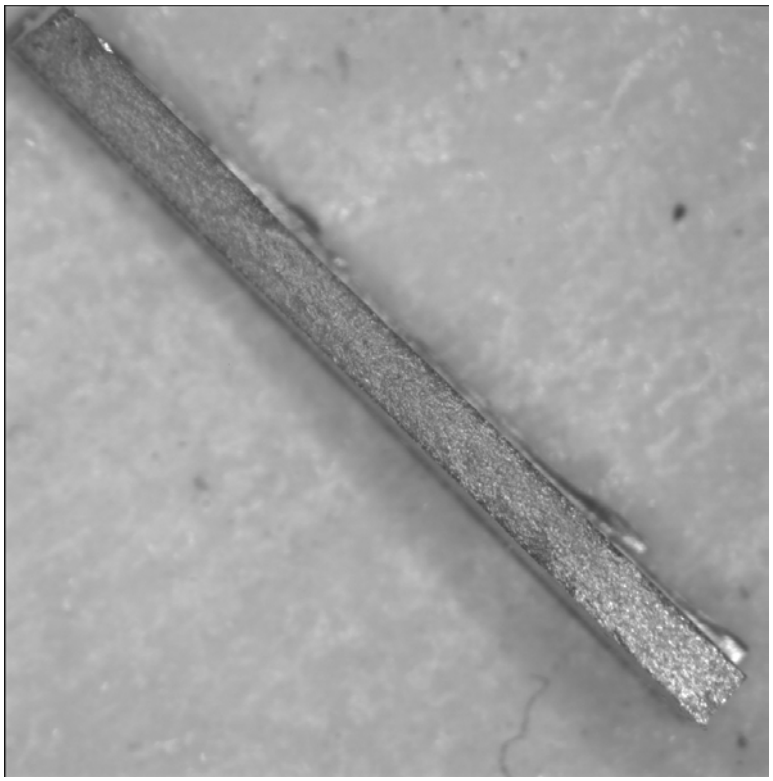

Figure A-26. Fracture Surface of Specimen 5946.

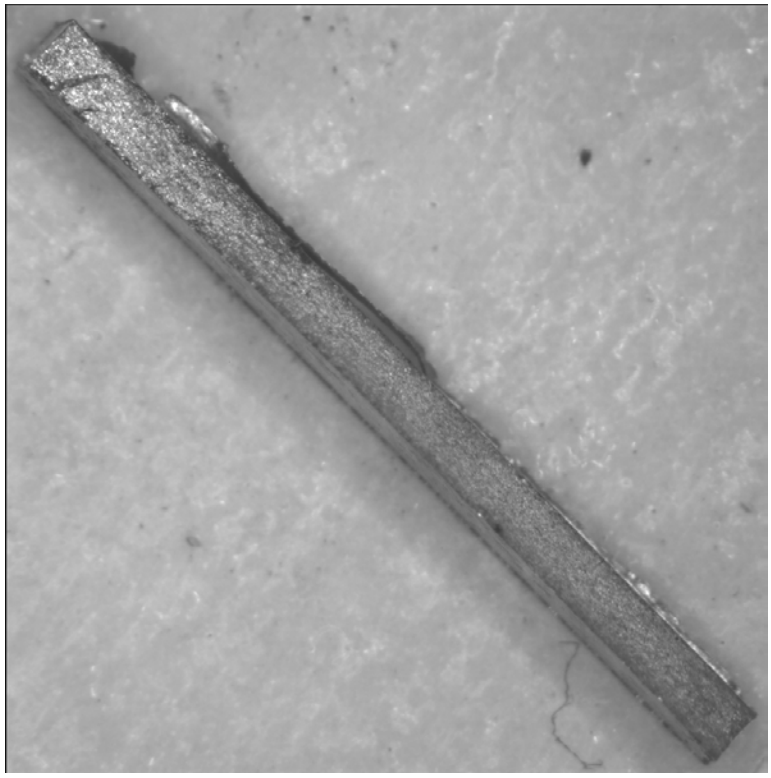

Figure A-27. Fracture Surface of Specimen 5967.

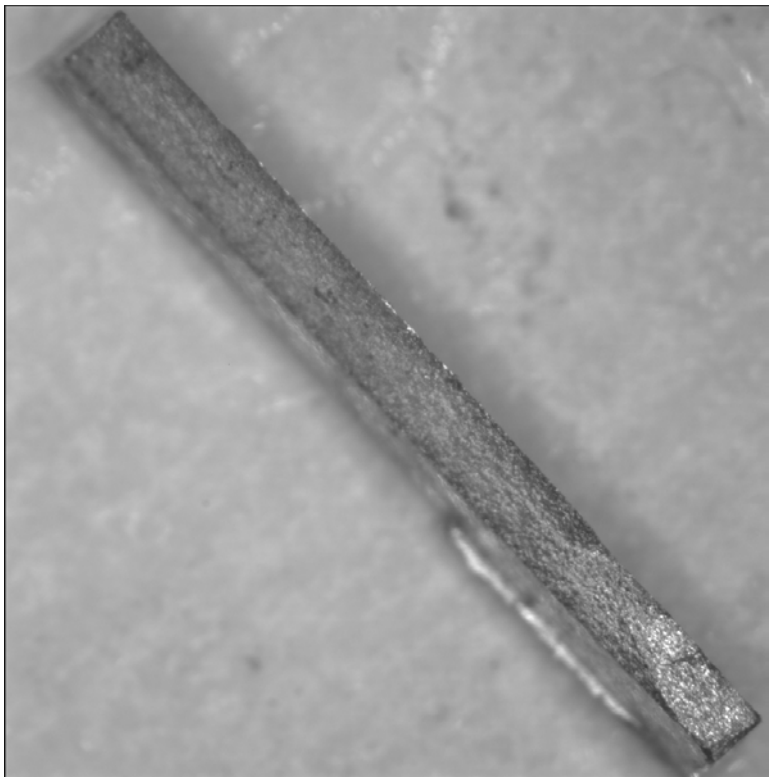

Figure A-28. Fracture Surface of Specimen 5969.

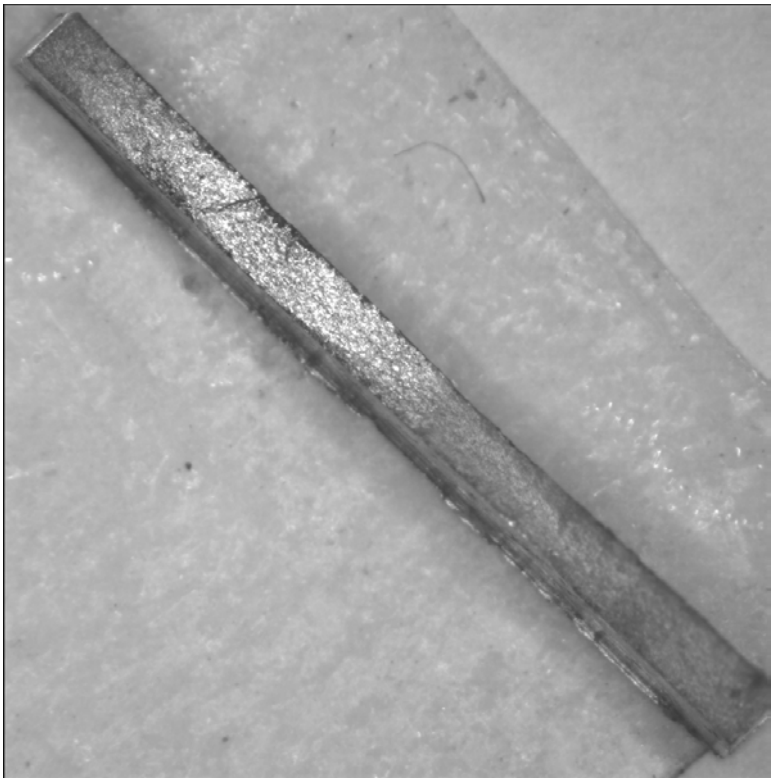

Figure A-29. Fracture Surface of Specimen 6002.

APPENDIX B: Scanning Electron Micrographs of Fracture Surfaces

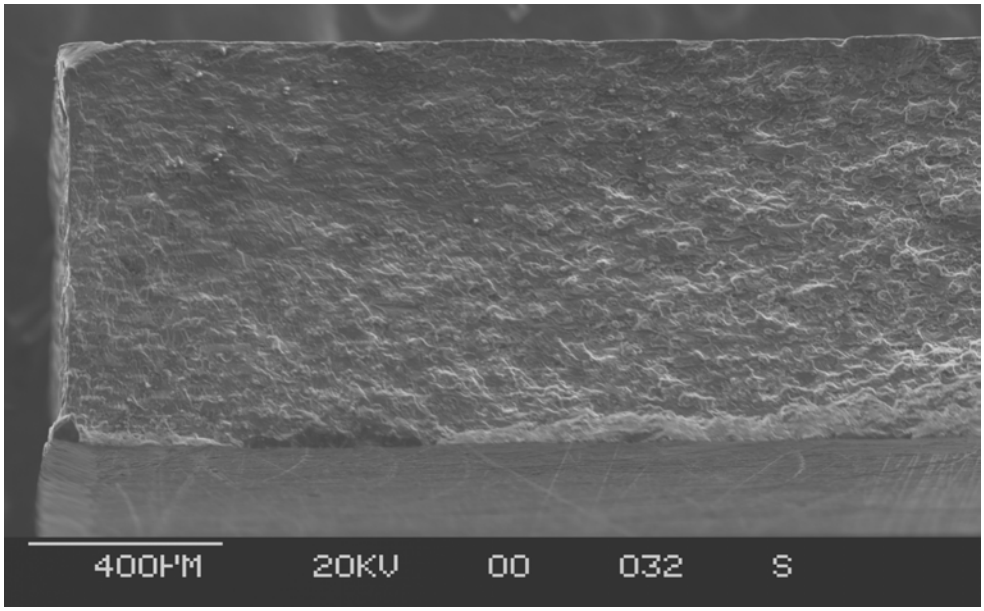

Figure B-1. Fatigue Crack on Fracture Surface of Specimen N3.

Origin is at corner in upper left of photograph.

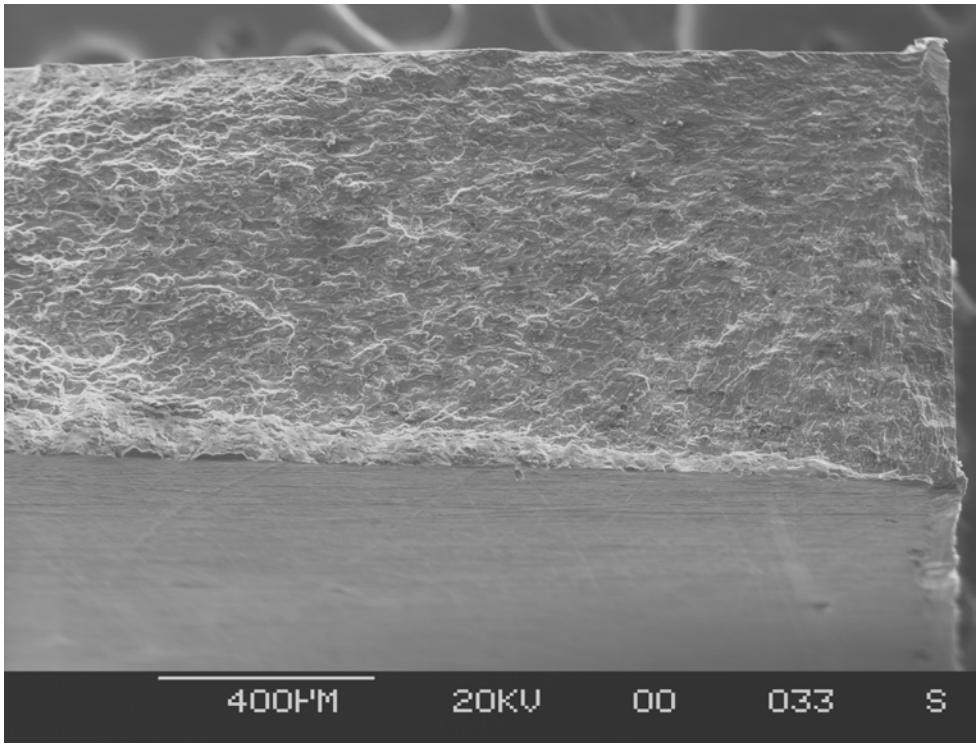

Figure B-2. Fatigue Crack on Fracture Surface of Specimen N4.

Origin is at corner in upper right of photograph.

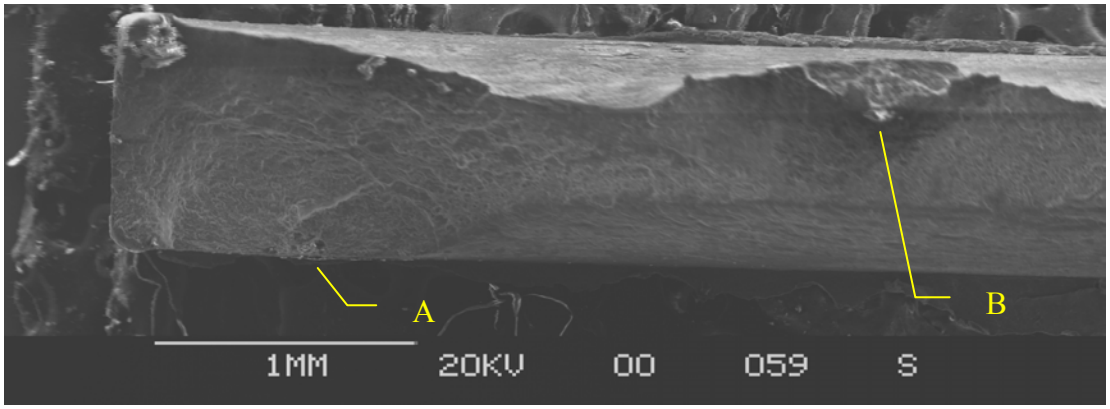

Figure B-3. Fatigue Crack on Fracture Surface of Specimen 1331.

Origins are at A and corner at lower left. Feature B may be origin or just large pit.

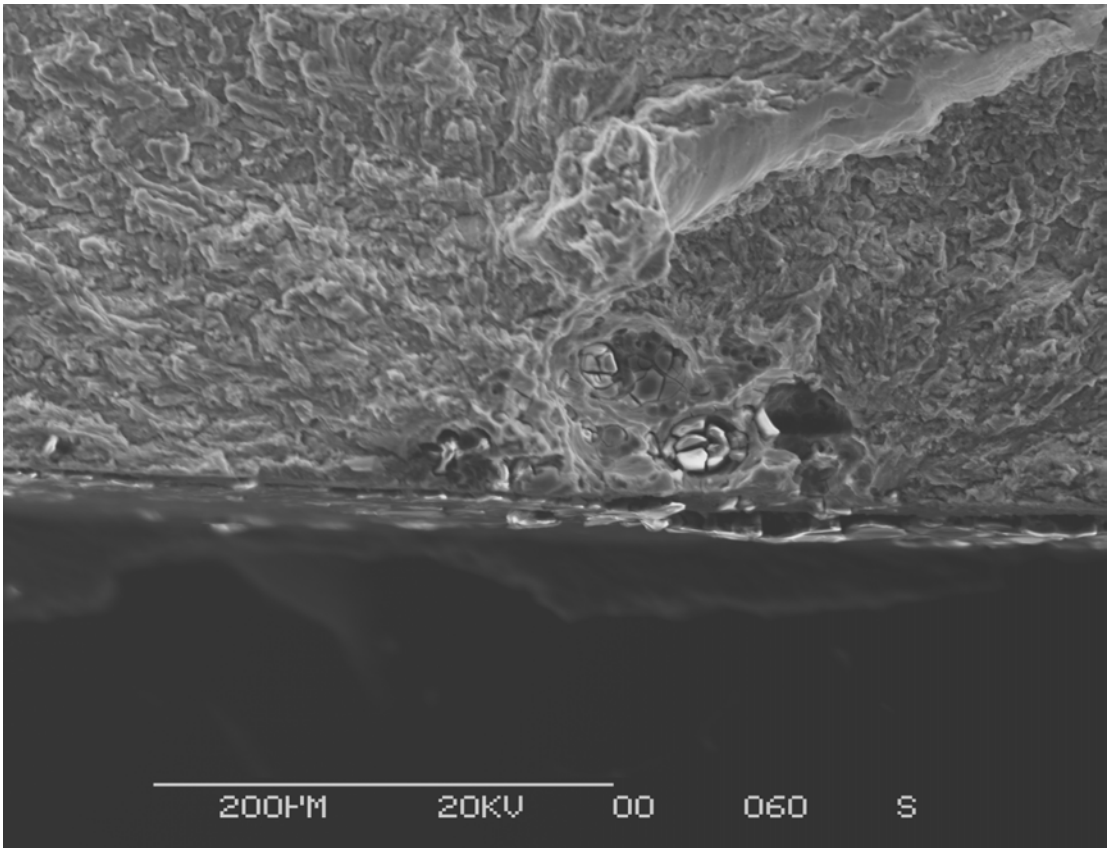

Figure B-4. Crack Origin A (Fig. B-3) on Specimen 1331.

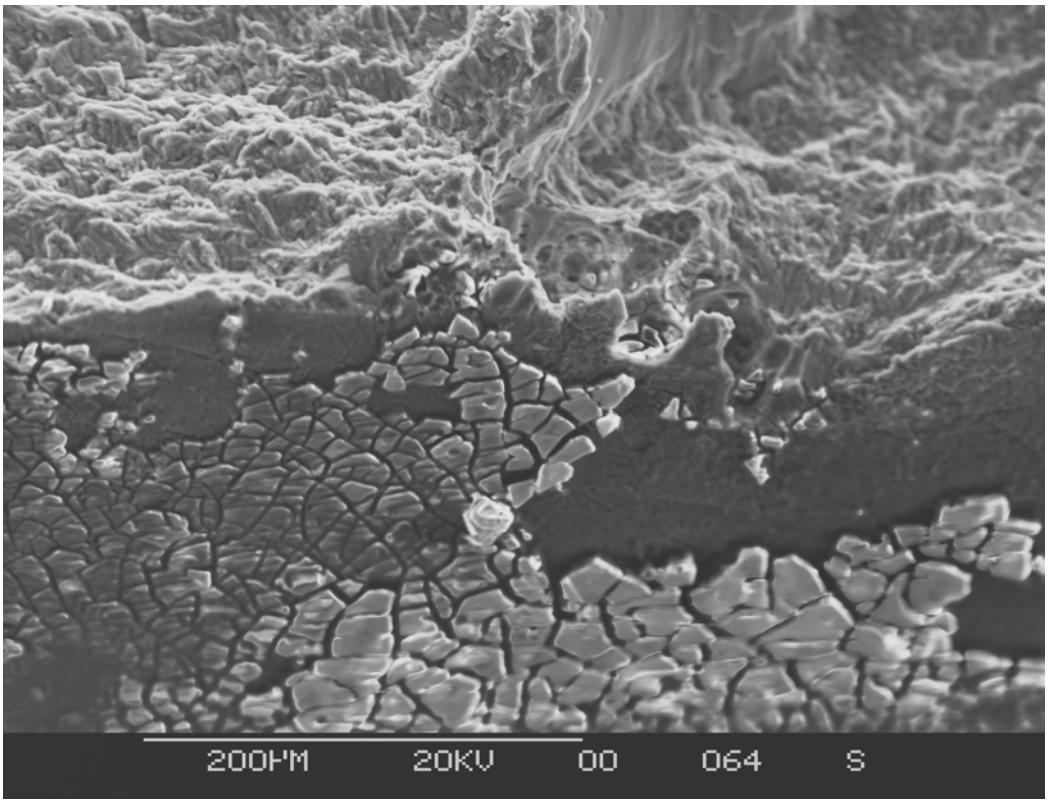

Figure B-5. Surface View of Crack Origin A (Fig. B-3) on Specimen 1331.

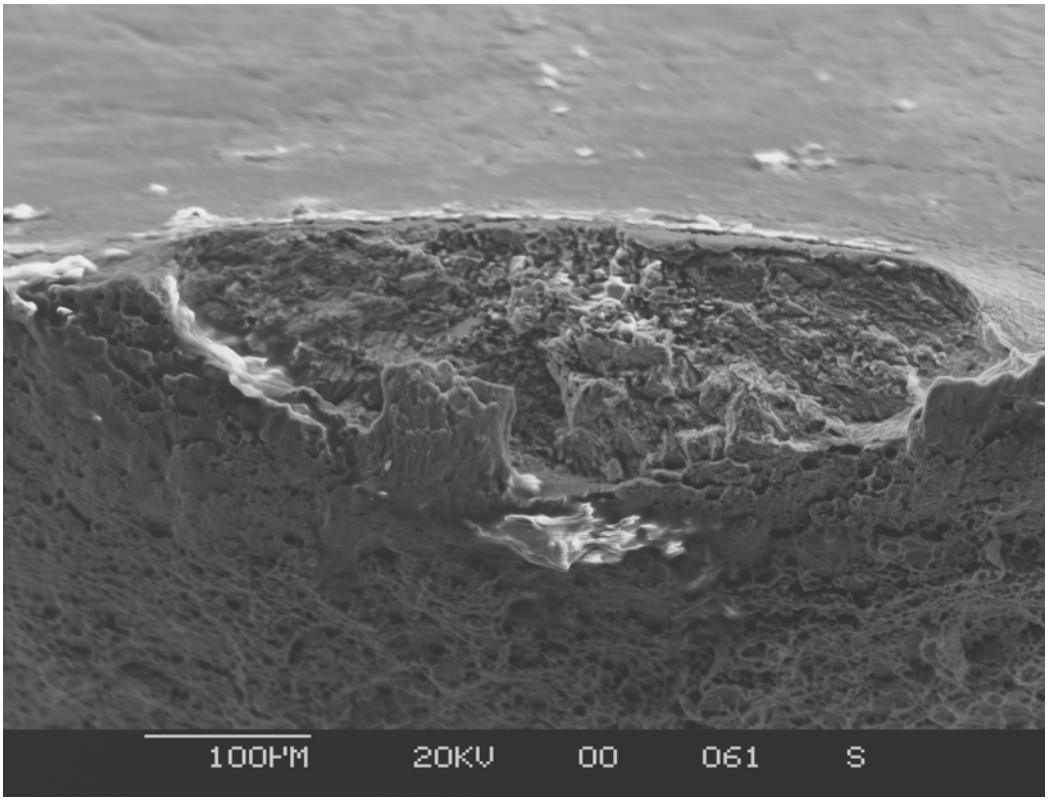

Figure B-6. Feature B (Fig. B-3) on Fracture Surface of Specimen 1331.

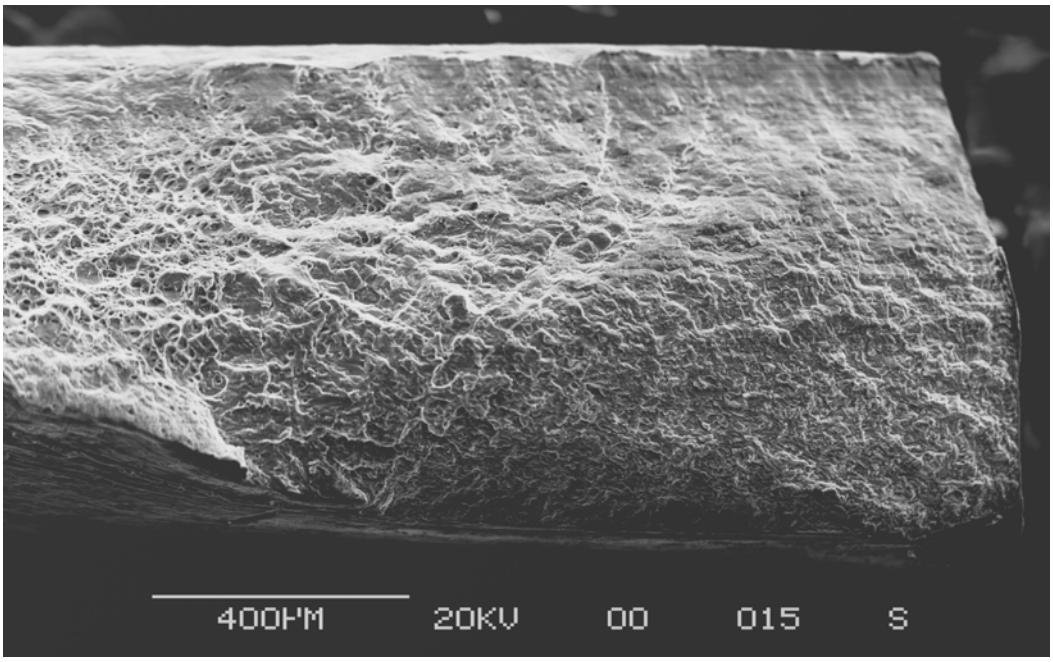

Figure B-7. Fatigue Crack on Fracture Surface of Specimen 5607.

Origin is at corner in lower right of photograph.

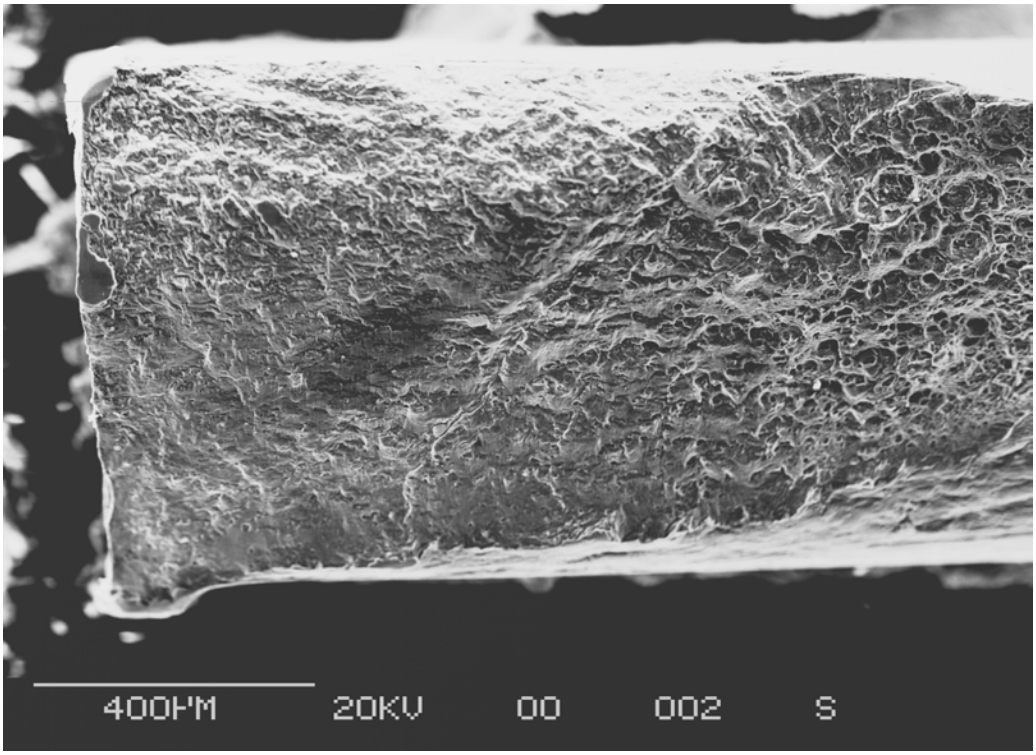

Figure B-8. Fatigue Crack on Fracture Surface of Specimen 5608.

Origin is at corner in upper left of photograph.

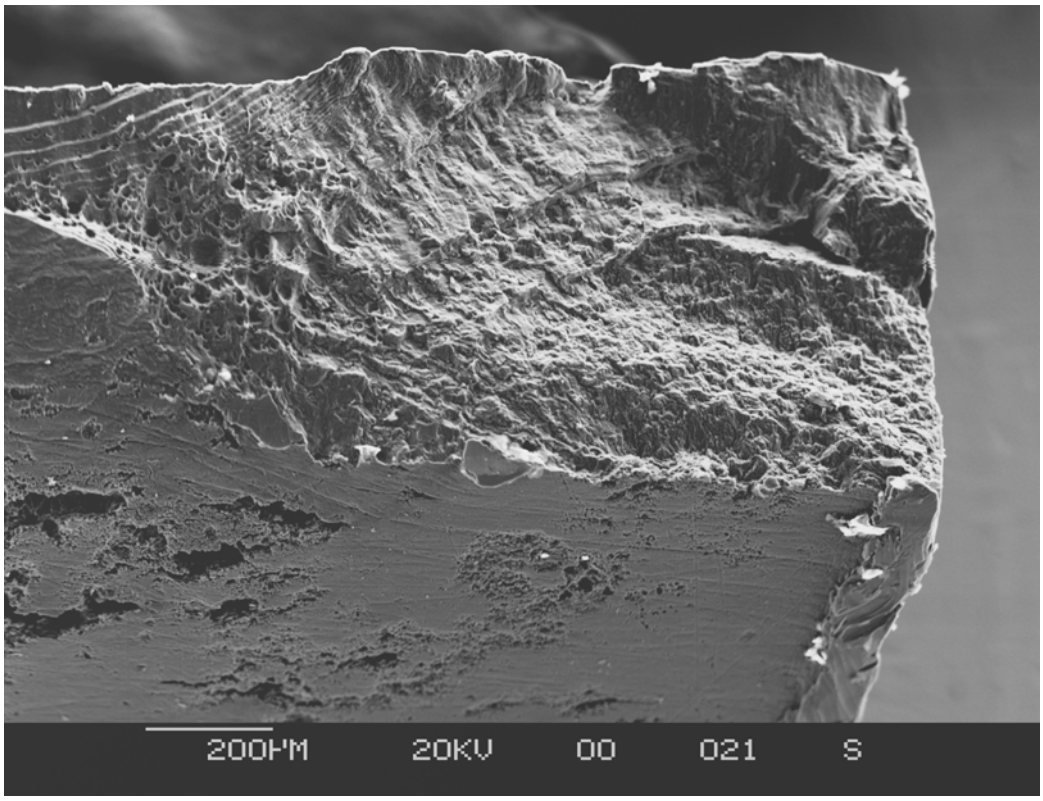

Figure B-9. Fatigue Crack on Fracture Surface of Specimen 5616.

One origin is at a pit, but the dominant crack seems to have come from the corner at lower right.

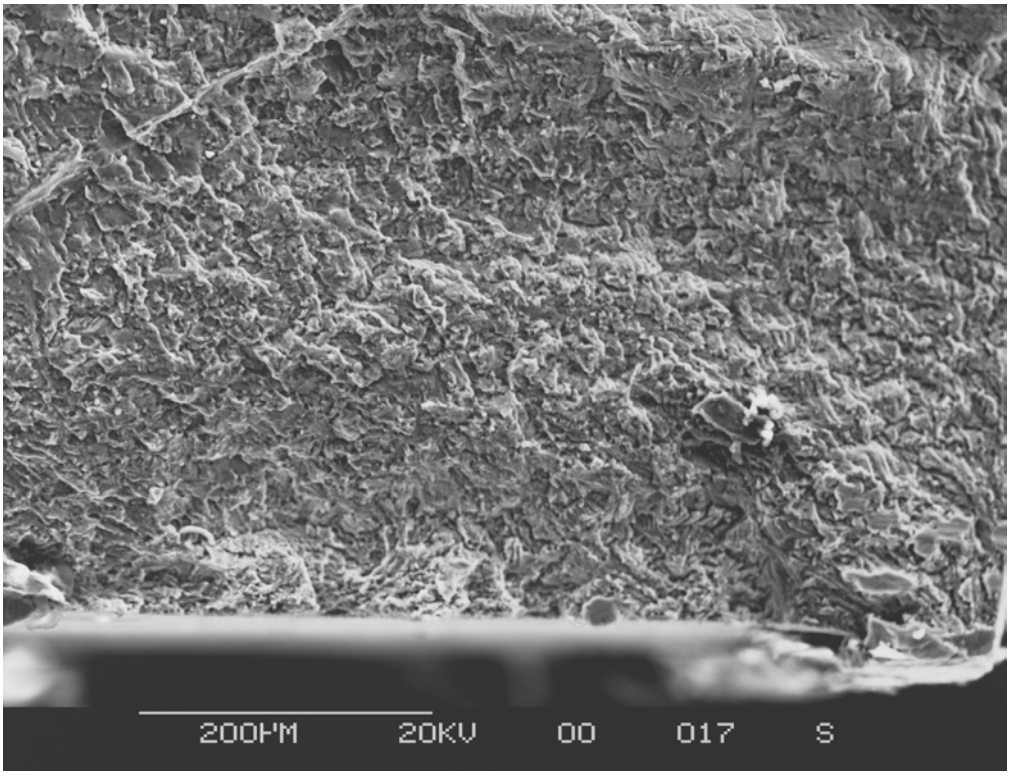

Figure B-10. Origin at Pit (Fig. B-9) on Specimen 5616.

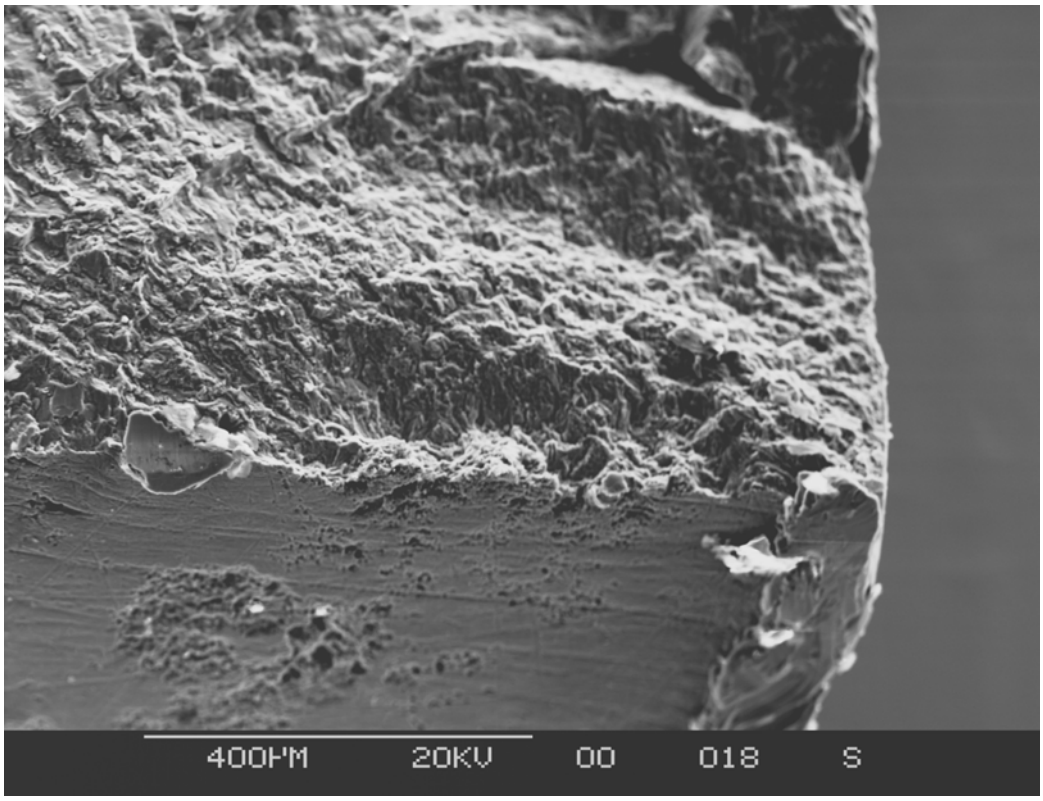

Figure B-11. Close-up Surface View of Origin at Pit on Specimen 5616.

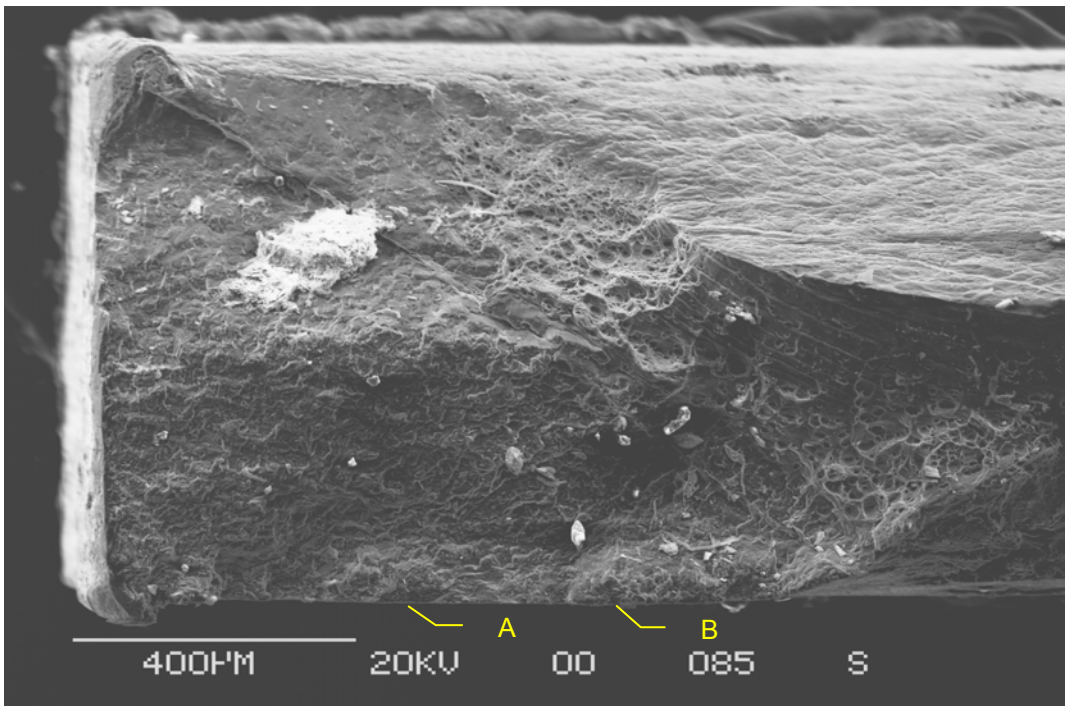

Figure B-12. Fatigue Crack on Fracture Surface of Specimen 5618.

Two origins are along the lower edge of specimen. Dominate crack seems to have come from corner at lower left.

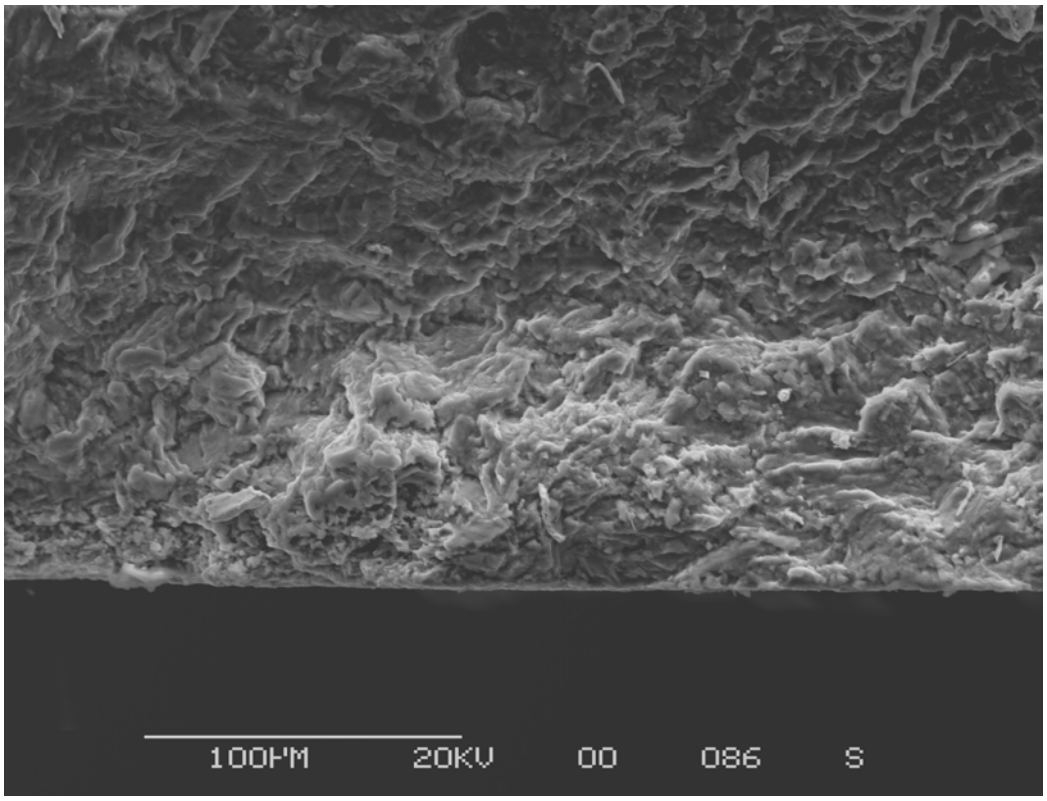

Figure B-13. Origin A (Fig. B-12) on Specimen 5618.

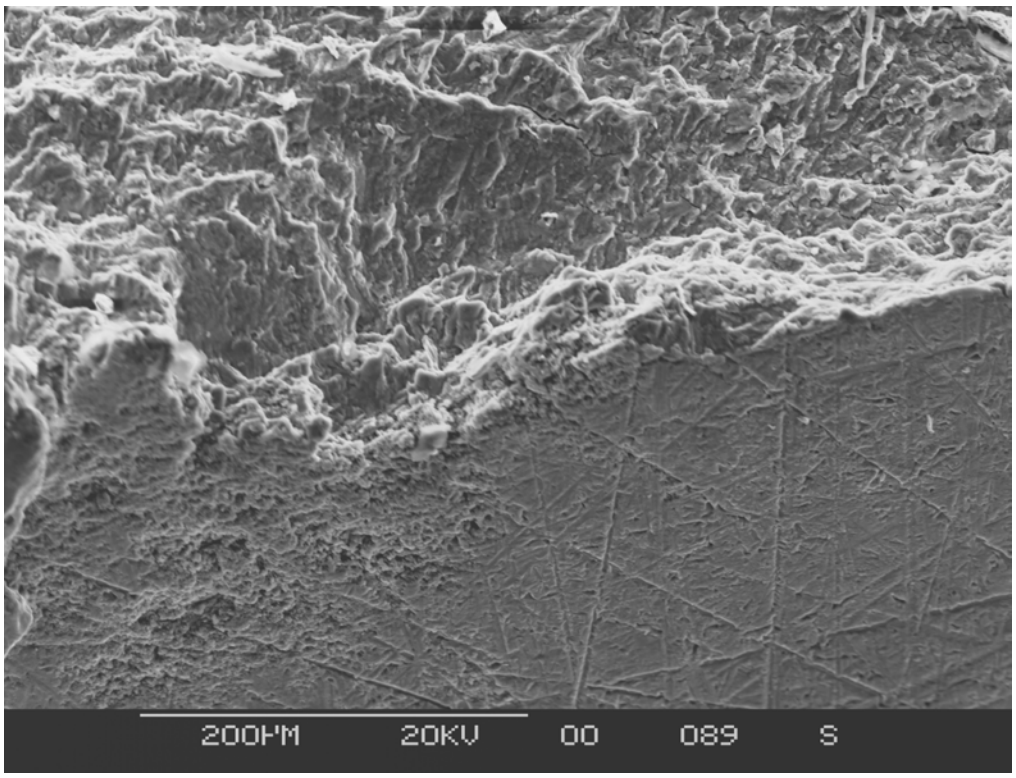

Figure B-14. Surface View of Origin A (Fig. B-12) on Specimen 5618.

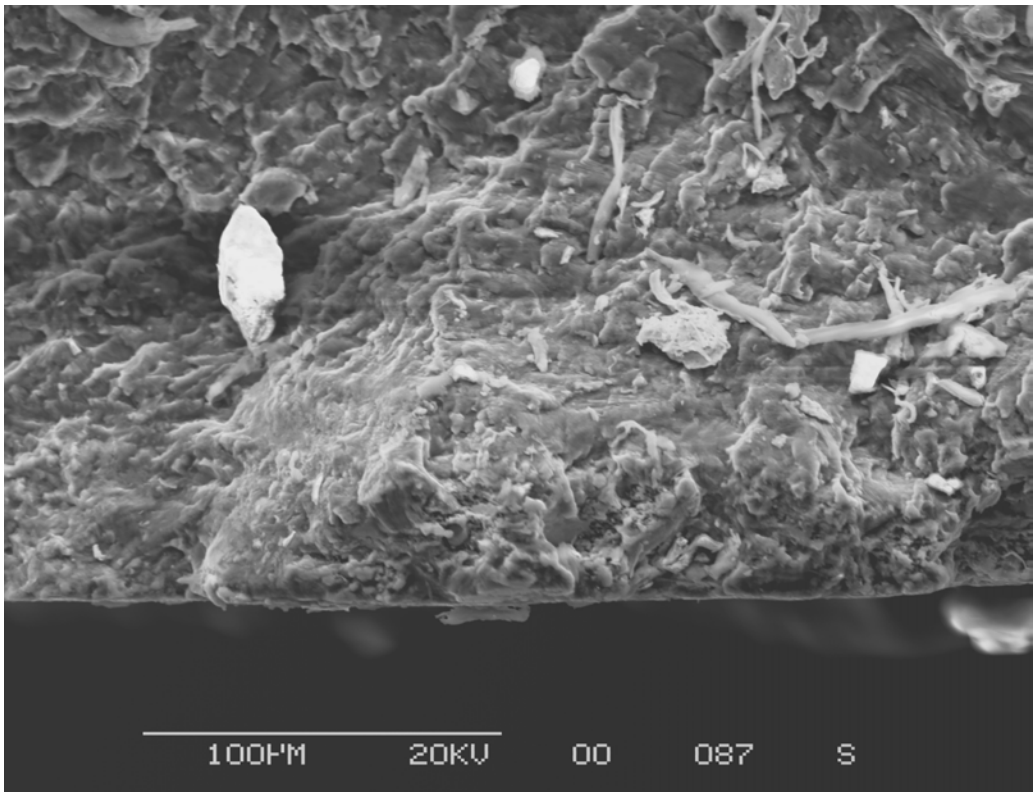

Figure B-15. Origin B (Fig. B-12) on Specimen 5618.

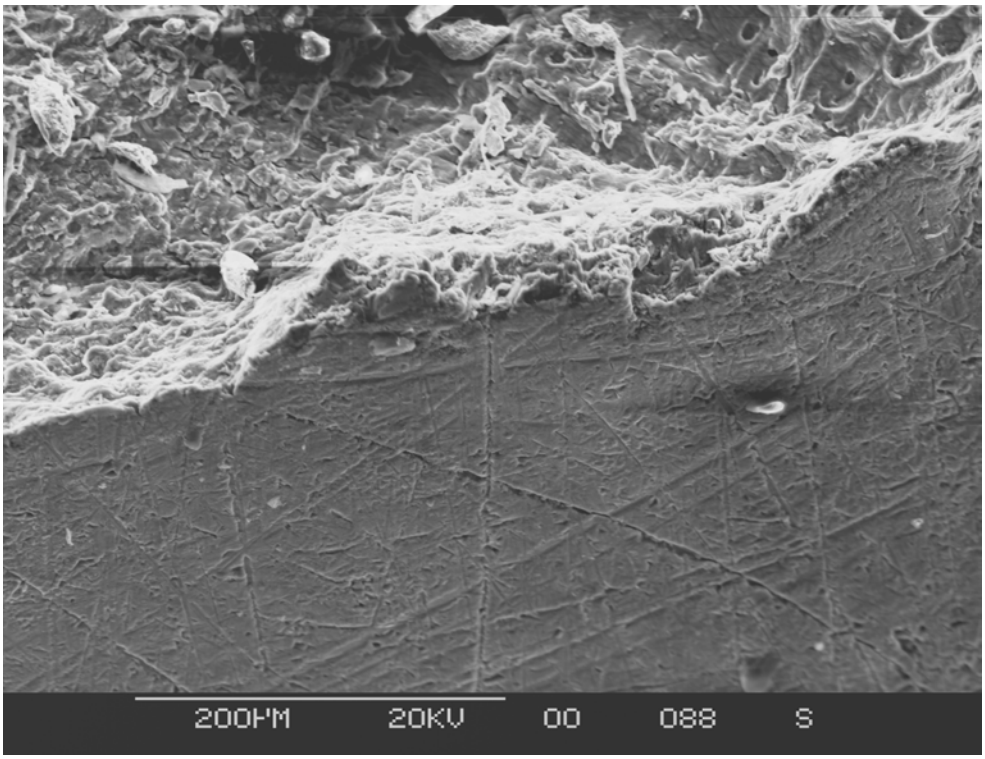

Figure B-16. Surface View of Origin B (Fig. B-12) on Specimen 5618.

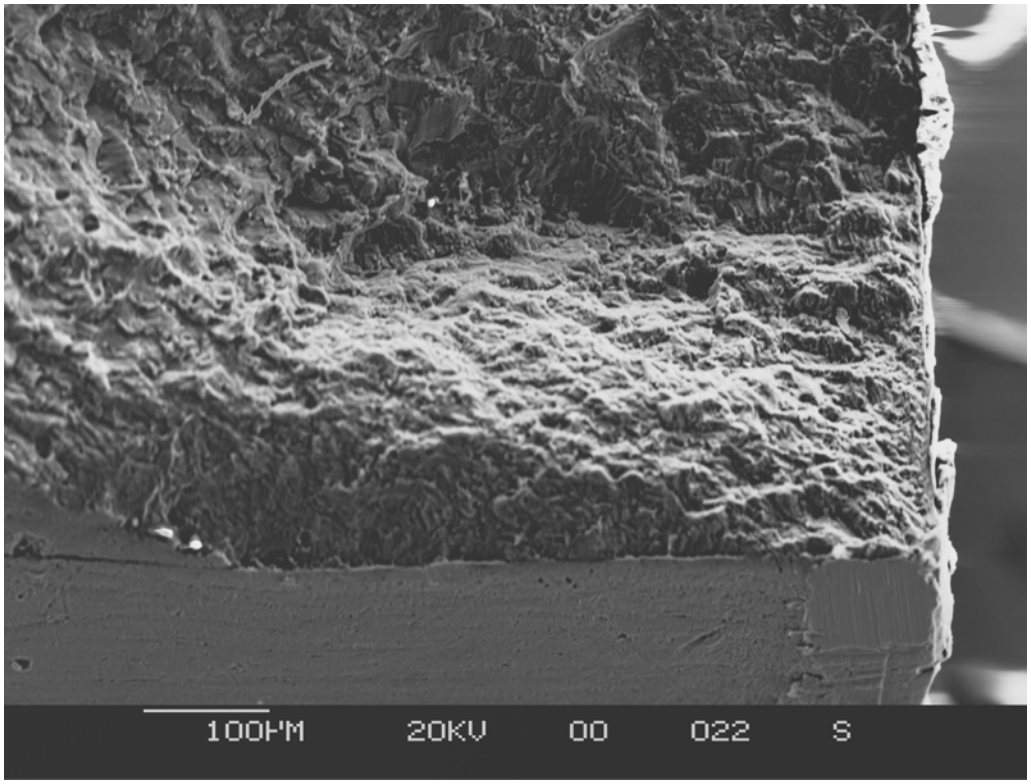

Figure B-17. Fatigue Crack on Fracture Surface of Specimen 5635.

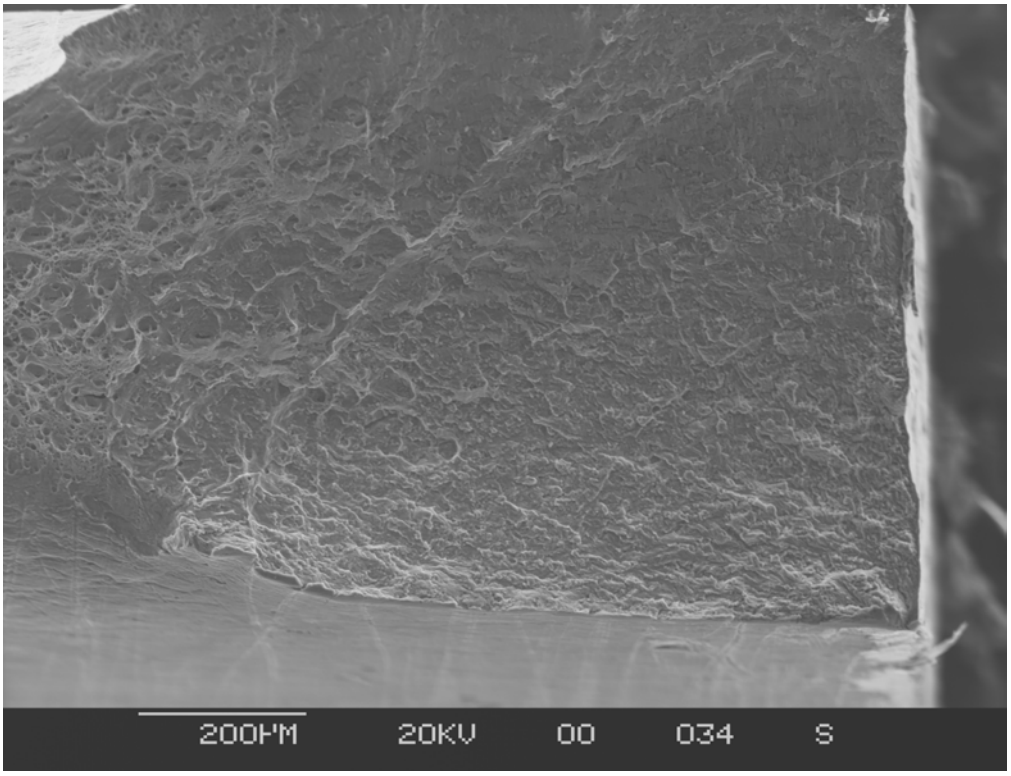

Figure B-18. Corner Fatigue Crack on Fracture Surface of Specimen 5636.

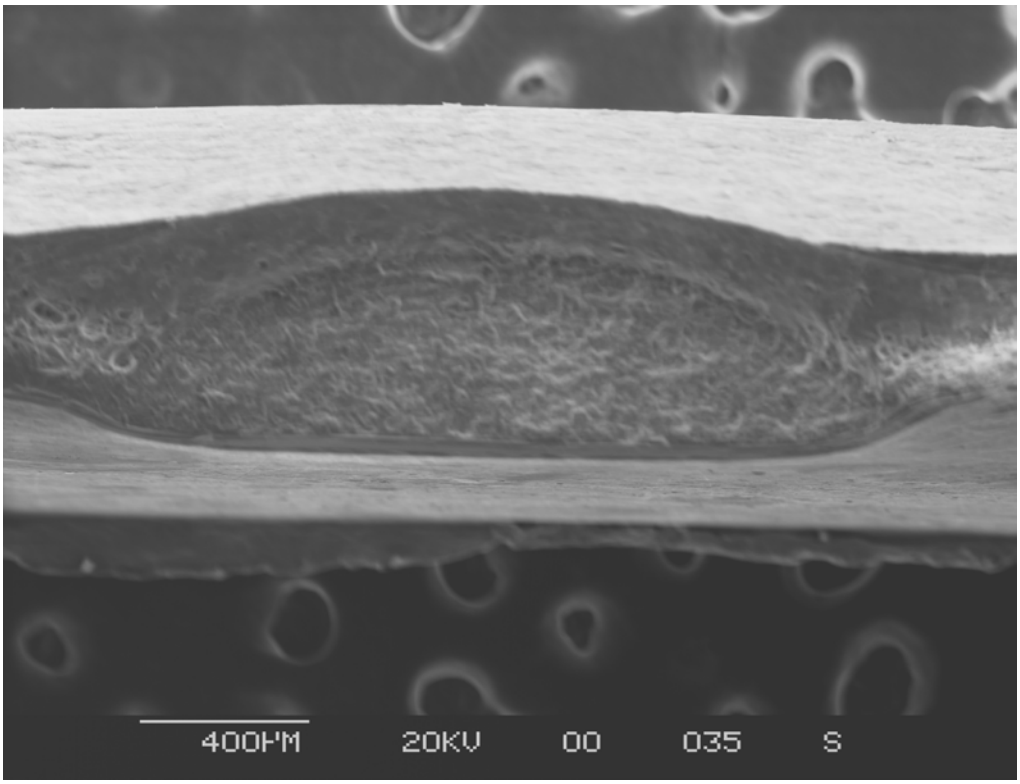

Figure B-19. Edge Crack on Fracture Surface of Specimen 5636.

No corrosion was found at the origin of this crack.

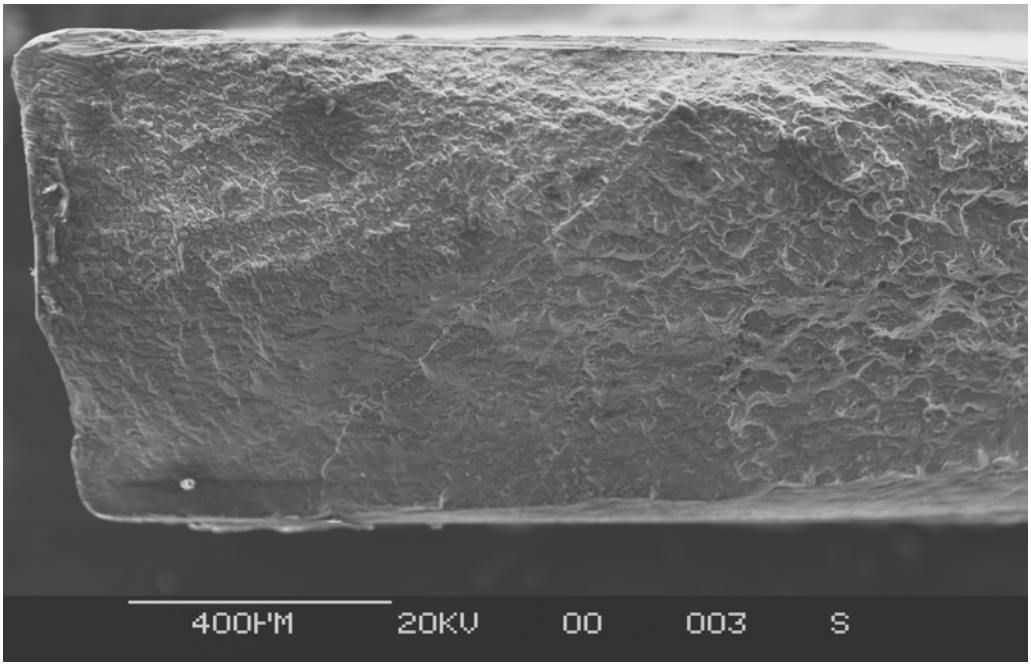

Figure B-20. Fatigue Crack on Fracture Surface of Specimen 5708.

Origin appears to be at corner in upper left of photograph.

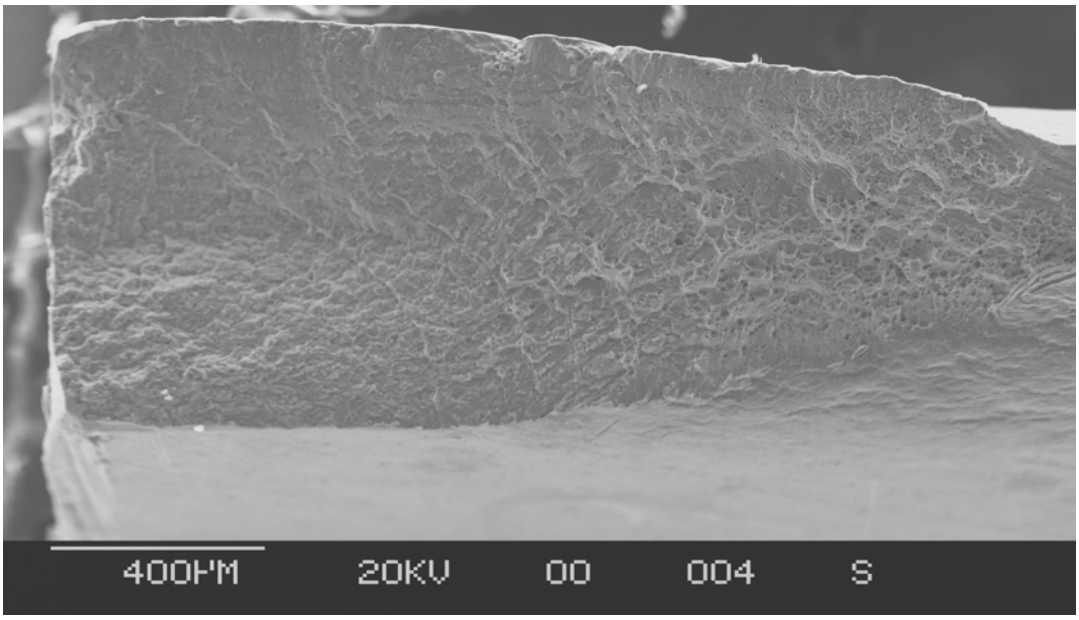

Figure B-21. Fatigue Crack on Fracture Surface of Specimen 5710B.

Origin is at corner in lower left of photograph.

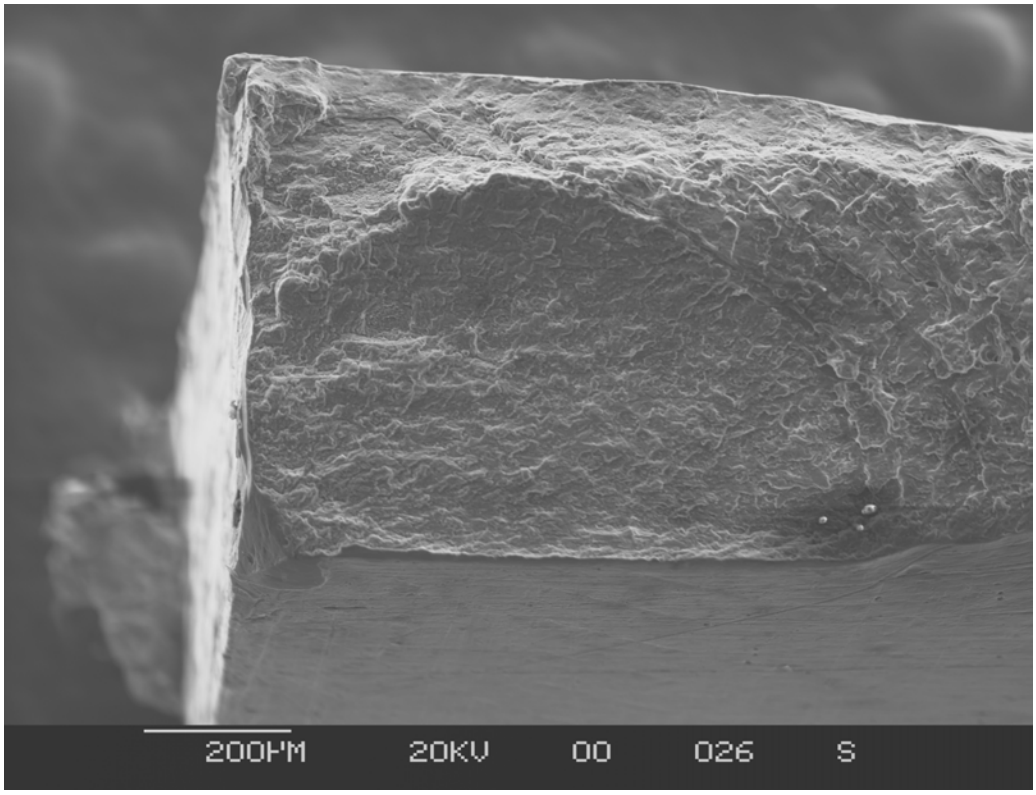

Figure B-22. Fatigue Crack on Fracture Surface of Specimen 5772.

Origin is at corner in lower left of photograph.

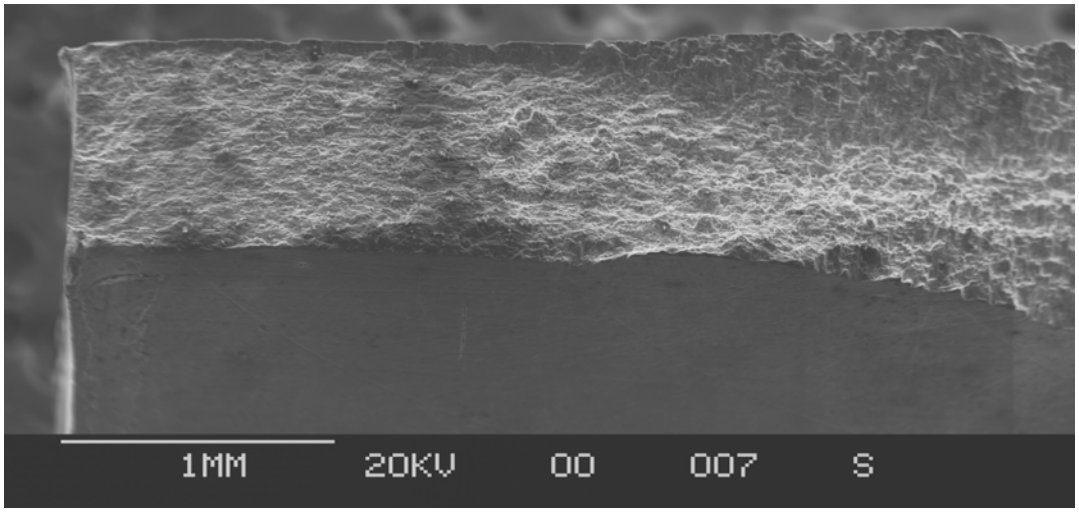

Figure B-23. Fatigue Crack on Fracture Surface of Specimen 5773.

Origin appears to be corner in lower left of photograph.

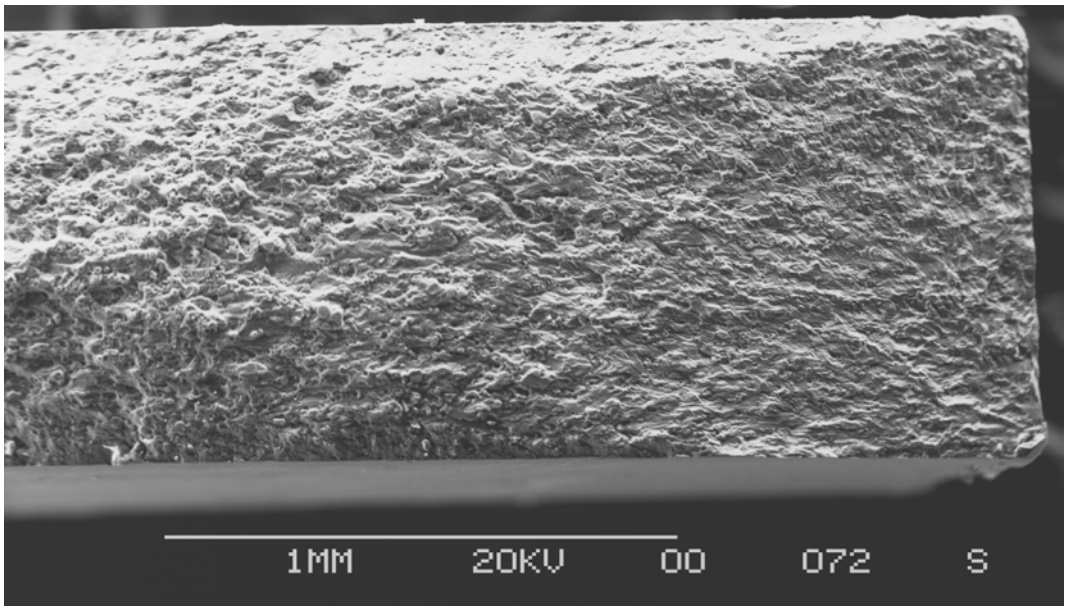

Figure B-24. Fatigue Crack on Fracture Surface of Specimen 5776.

Origin at corner in lower right of photograph.

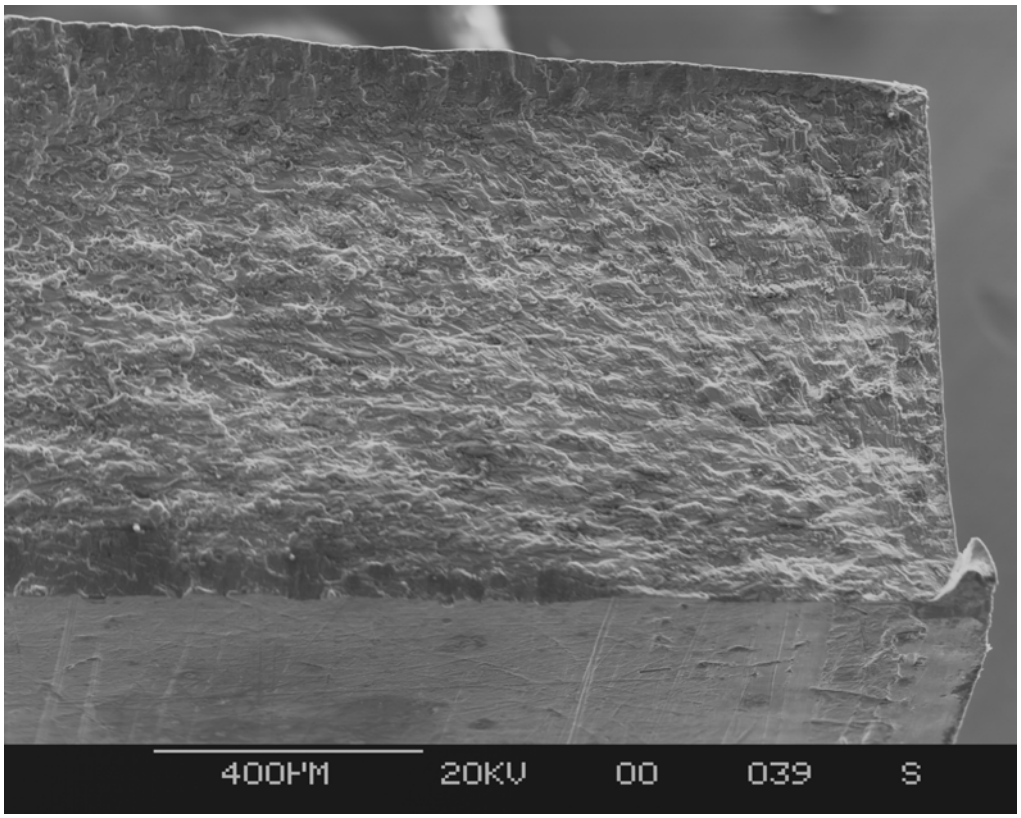

Figure B-25. Fatigue Crack on Fracture Surface of Specimen 5829.

Origin is at corner in lower right of photograph.

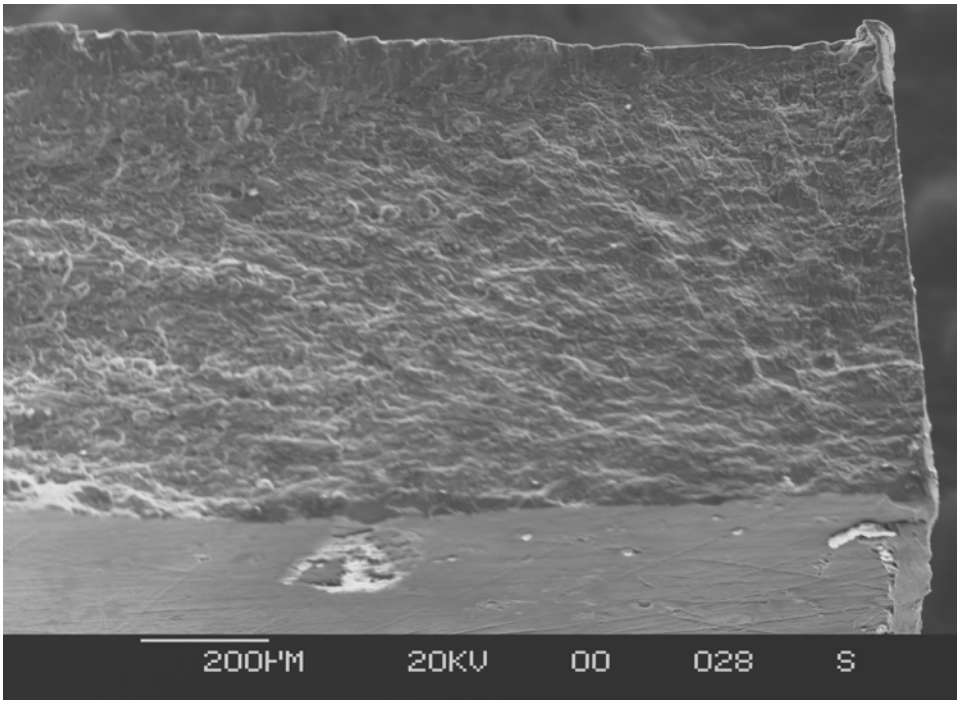

Figure B-26. Fatigue Crack on Fracture Surface of Specimen 5830.

Origin is at corner in lower right of photograph.

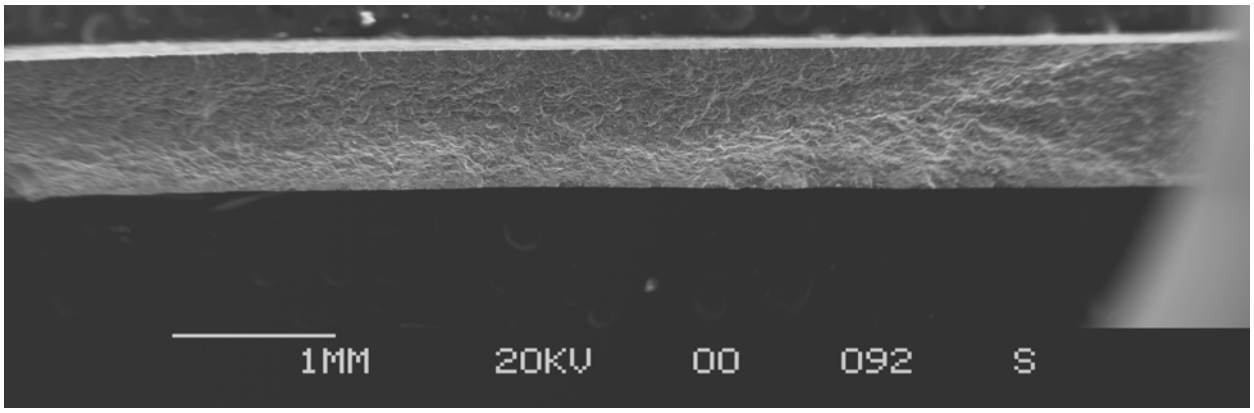

Figure B-27. Fatigue Crack on Fracture Surface of Specimen 5832.

Multiple origins along lower edge of specimen in the photograph.

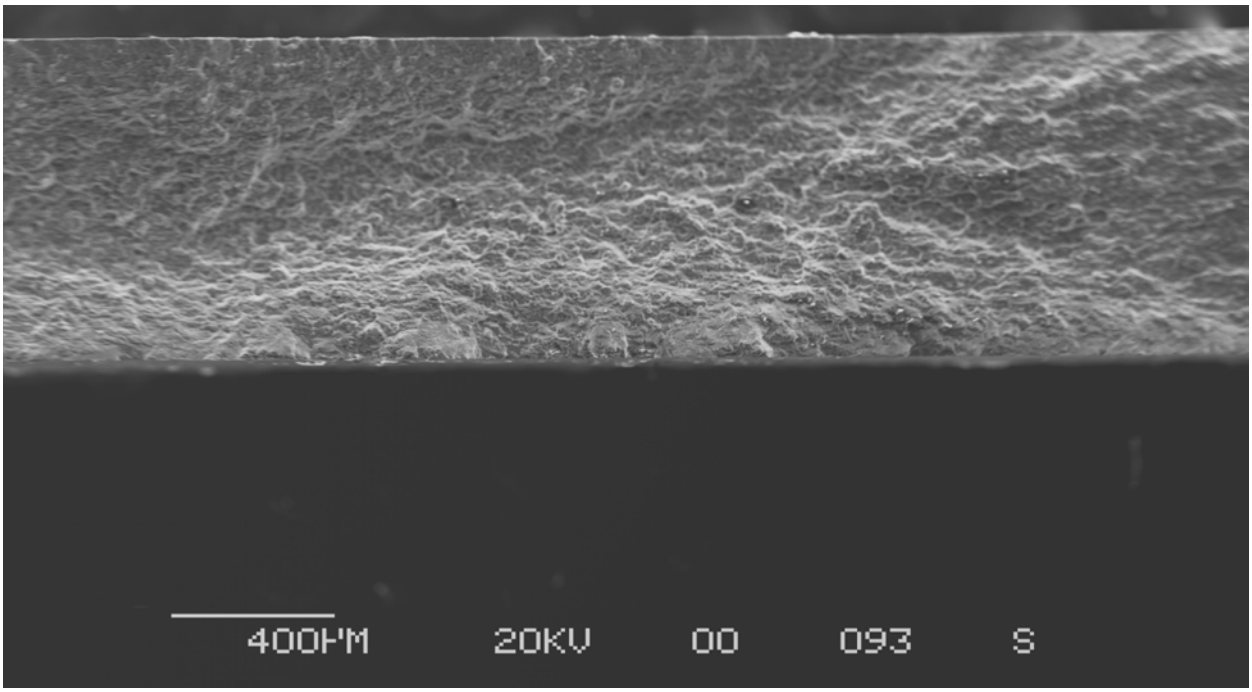

Figure B-28. Multiple Origins for Largest Crack on Specimen 5832.

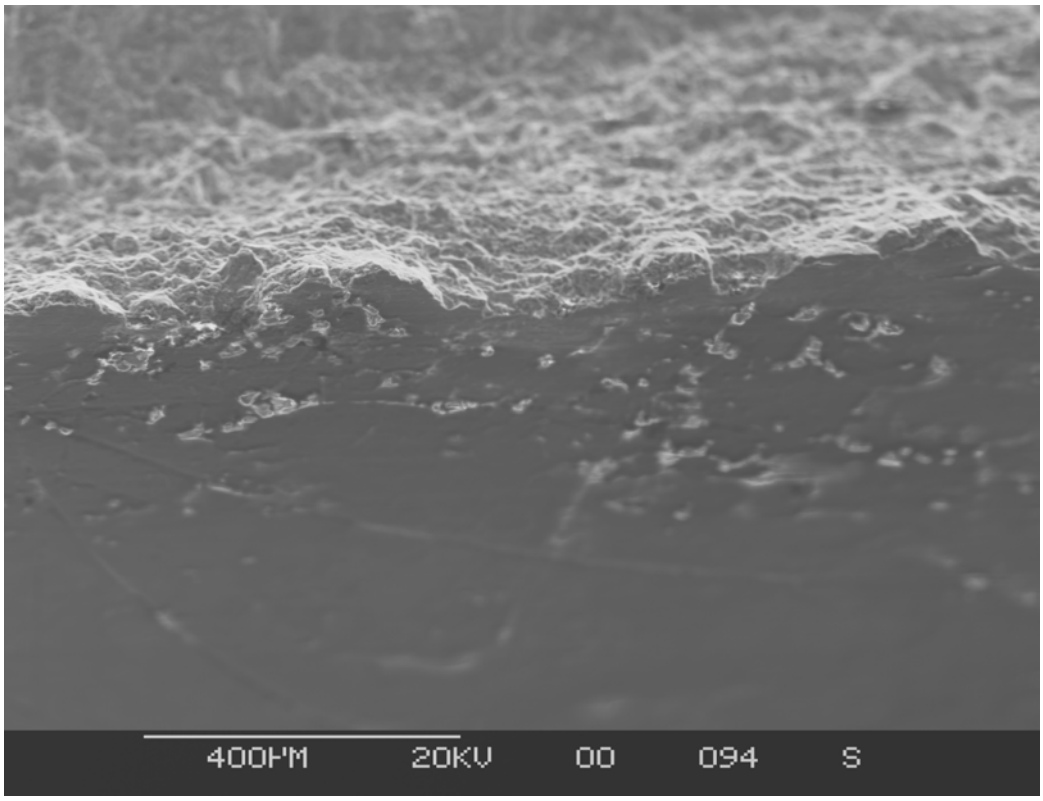

Figure B-29. Surface View of Crack Origins on Specimen 5832.

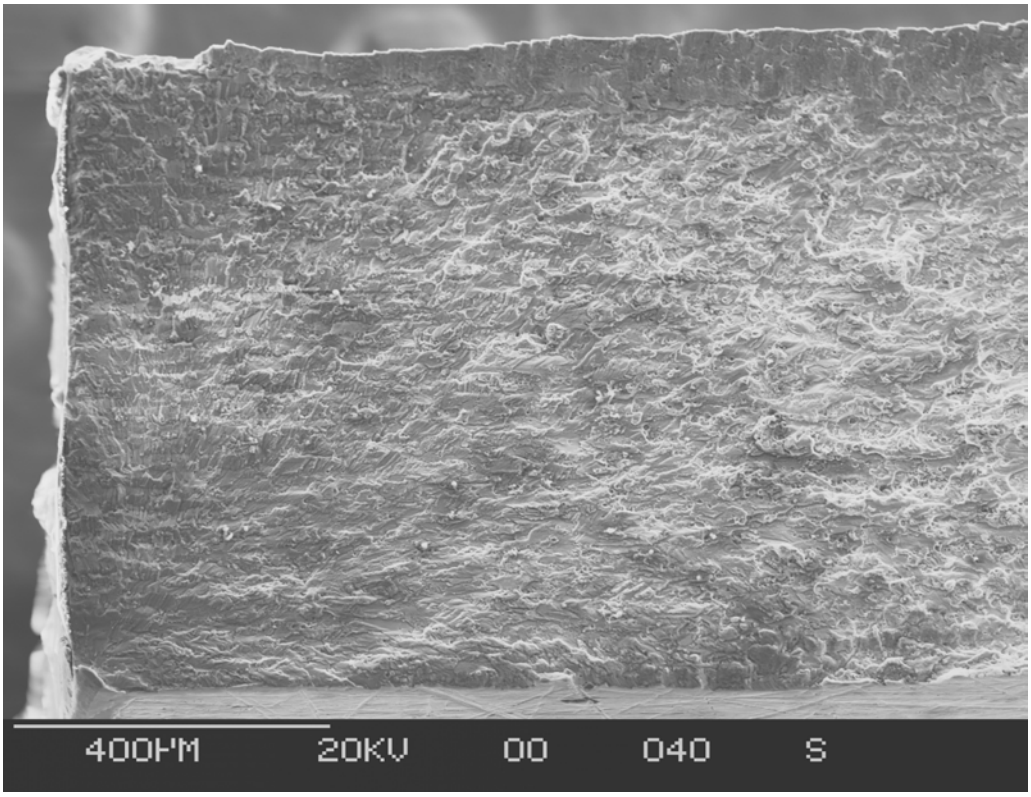

Figure B-30. Fatigue Crack on Fracture Surface of Specimen 5854.

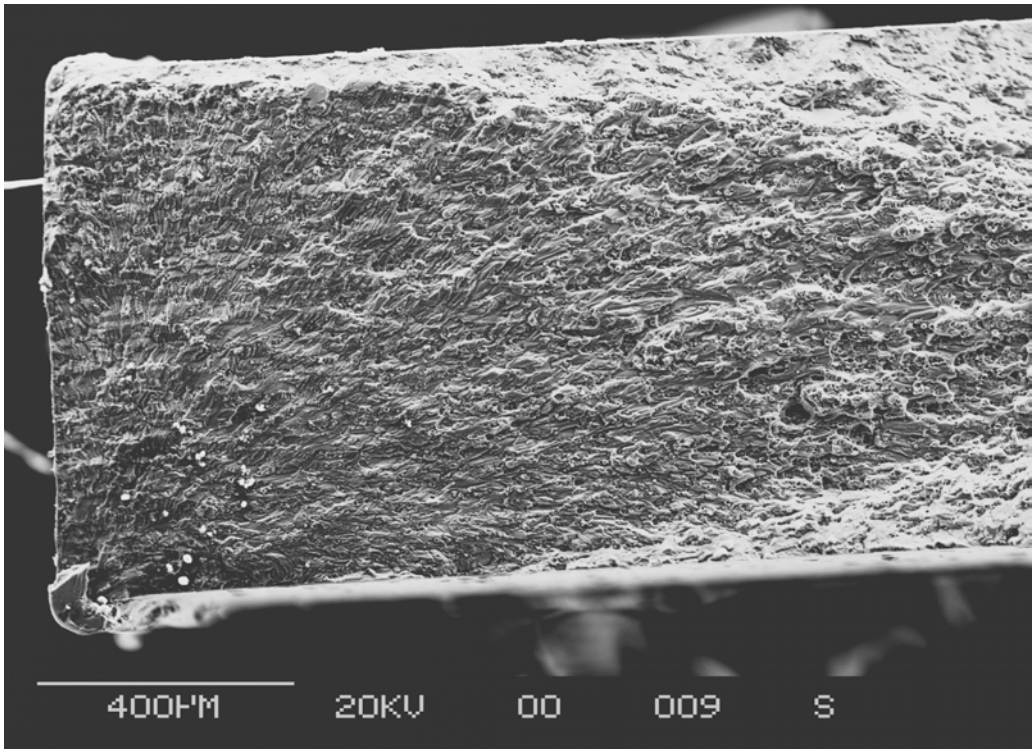

Figure B-31. Fatigue Crack on Fracture Surface of Specimen 5869.

Origin is at corner in lower left of photograph.

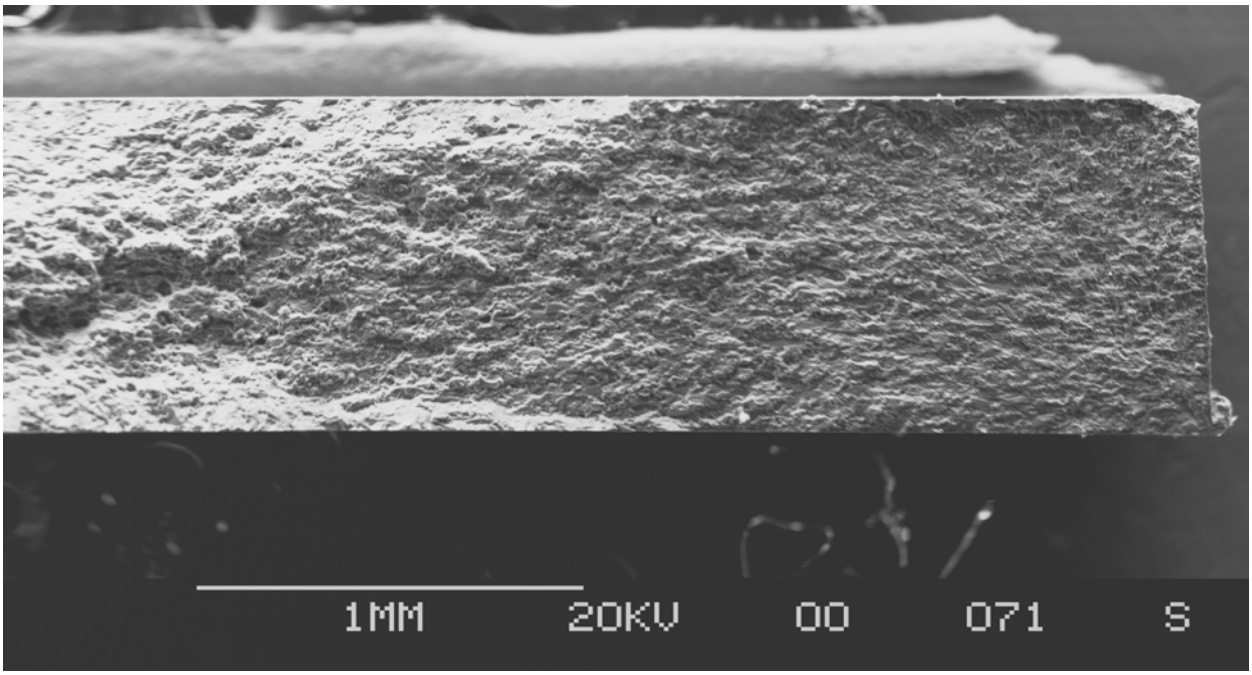

Figure B-32. Fatigue Crack on Fracture Surface of Specimen 5871.

Origin is at corner in lower right of photograph.

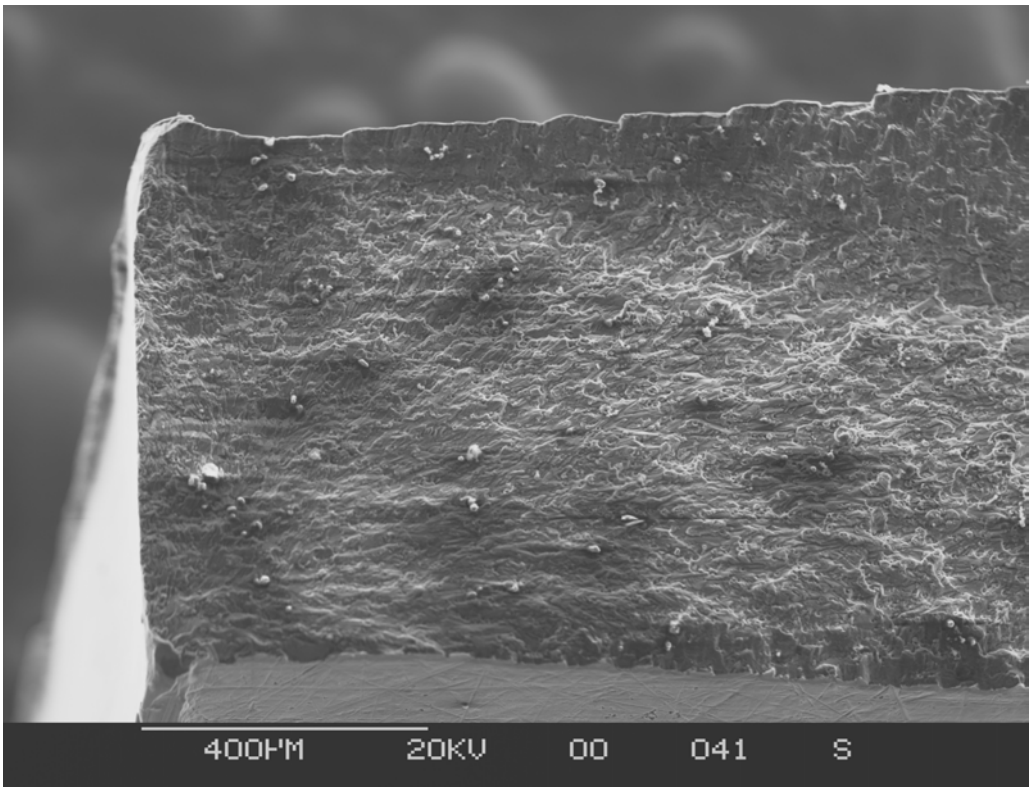

Figure B-33. Fatigue Crack on Fracture Surface of Specimen 5872.

Origin is at corner in lower left of photograph.

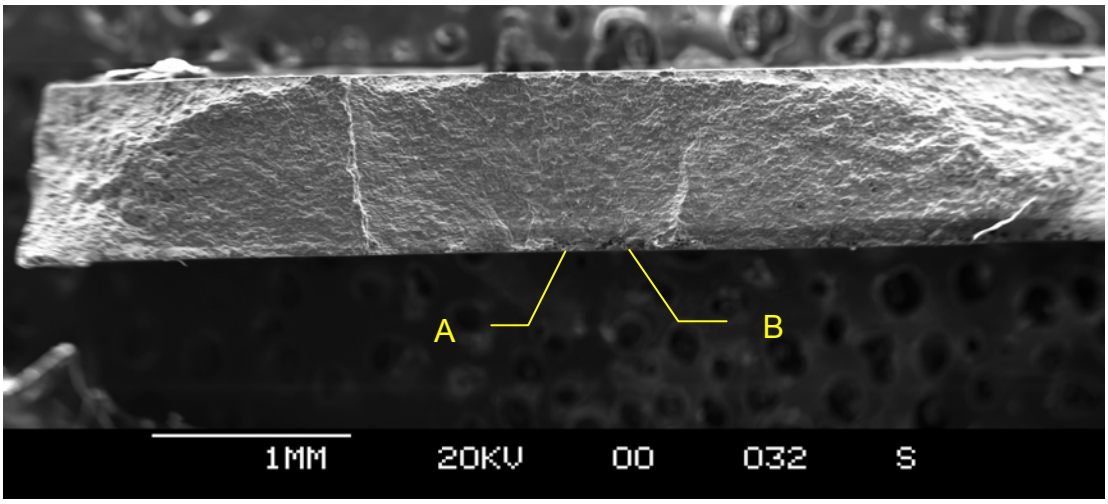

Figure B-34. Fatigue Crack on Fracture Surface of Specimen 5877.

Two identifiable origins are marked. Other origins could not be identified.

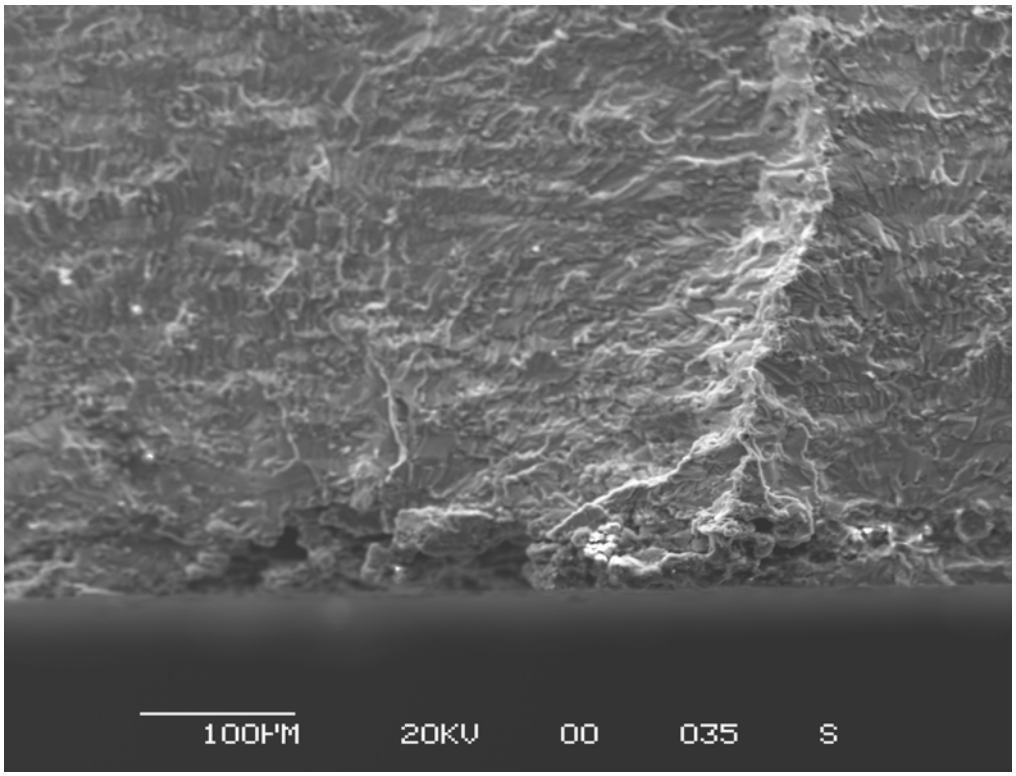

Figure B-35. Crack Origin B (Fig. B-34) on Fracture Surface of Specimen 5877.

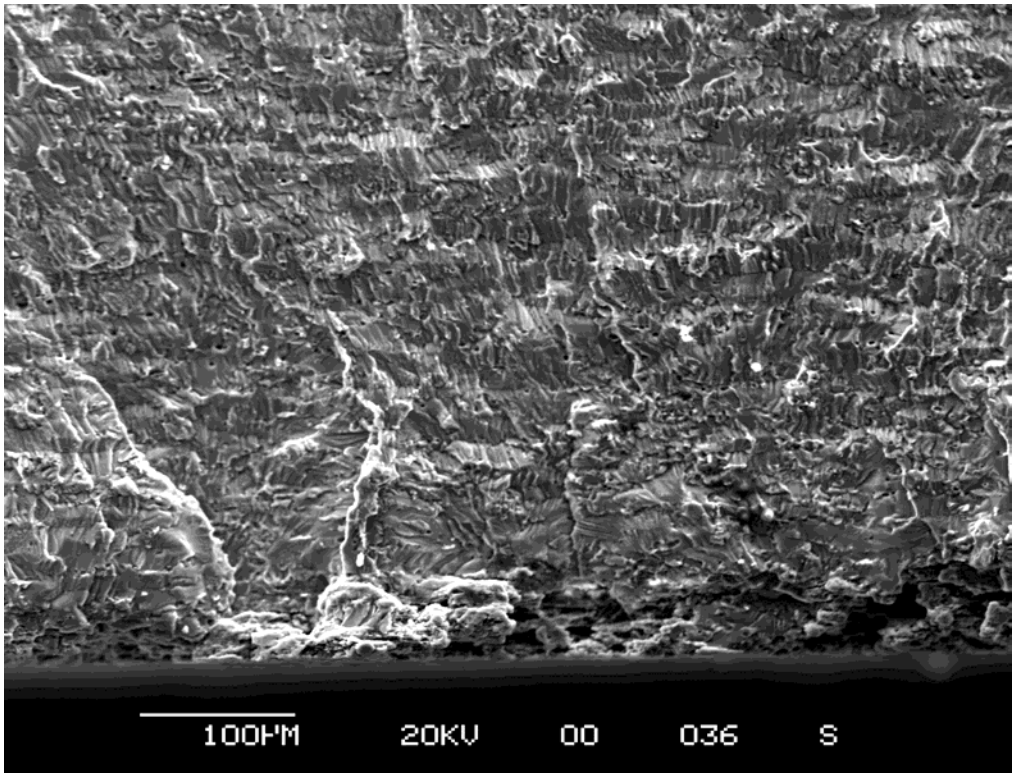

Figure B-36. Crack Origin A (Fig. B-34) on Fracture Surface of Specimen 5877.

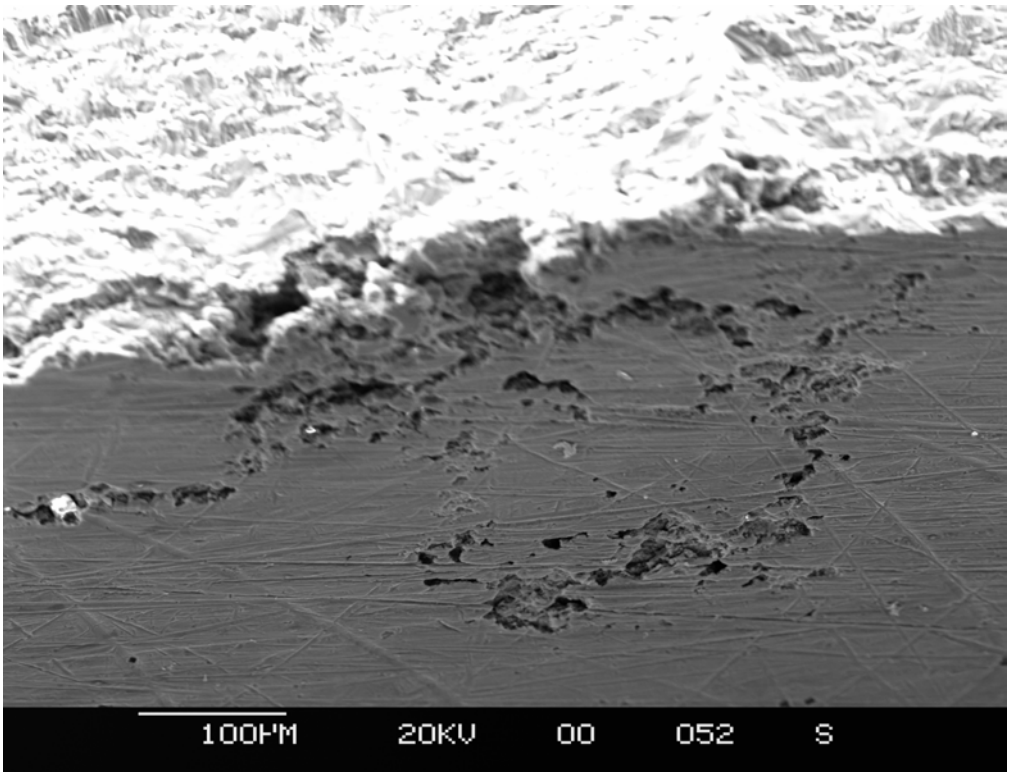

Figure B-37. Surface View of Crack Origin B (Fig. B-34) on Specimen 5877.

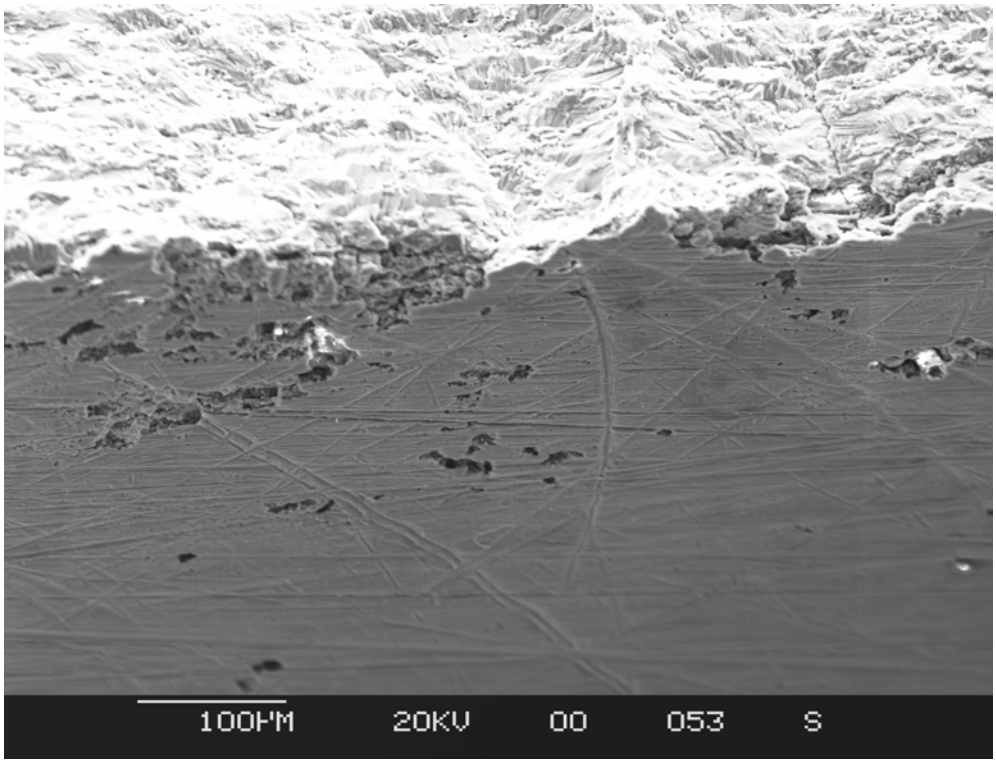

Figure B-38. Surface View of Crack Origin A (Fig. B-34) on Specimen 5877.

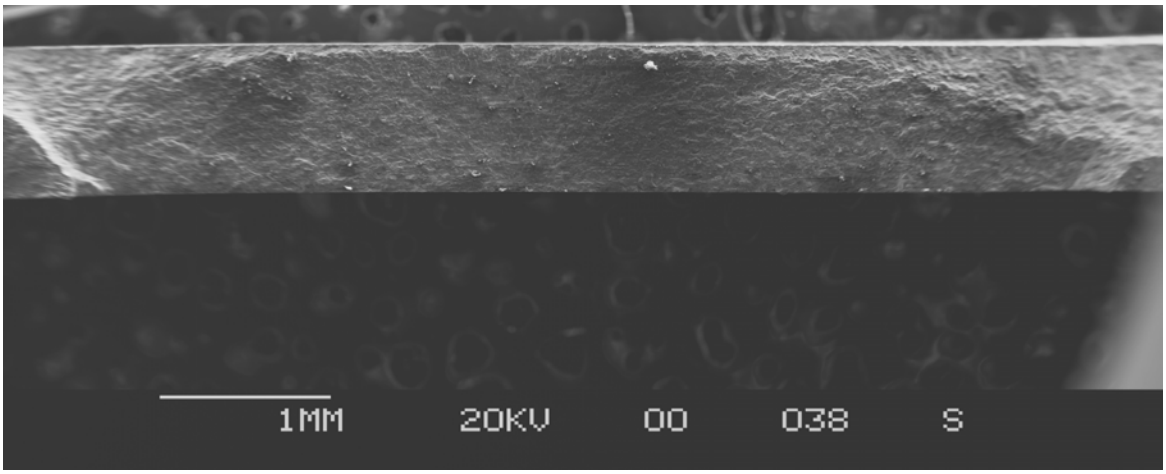

Figure B-39. Primary Fatigue Crack on Fracture Surface of Specimen 5878.

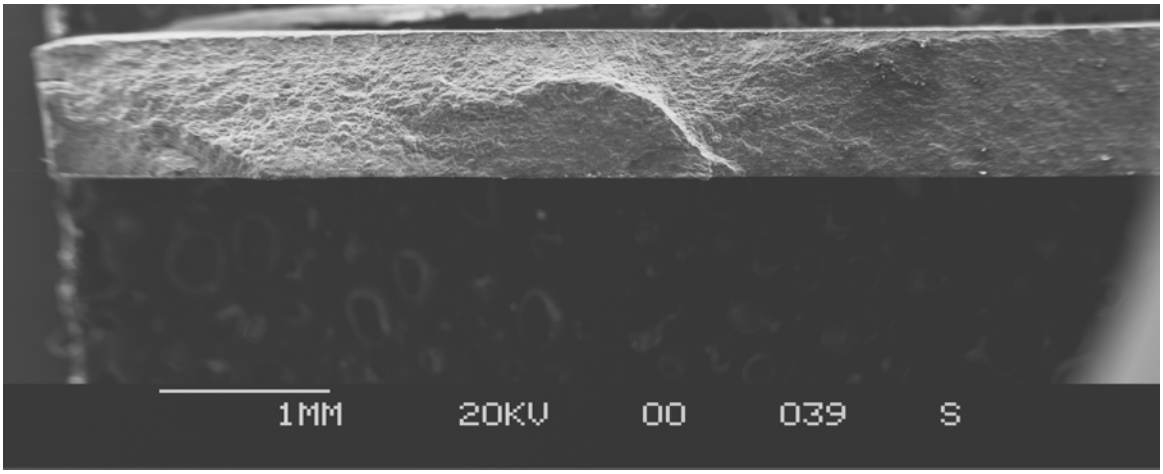

Figure B-40. Second Fatigue Crack on Specimen 5878 to the Left of the Primary Crack in Fig. B-39.

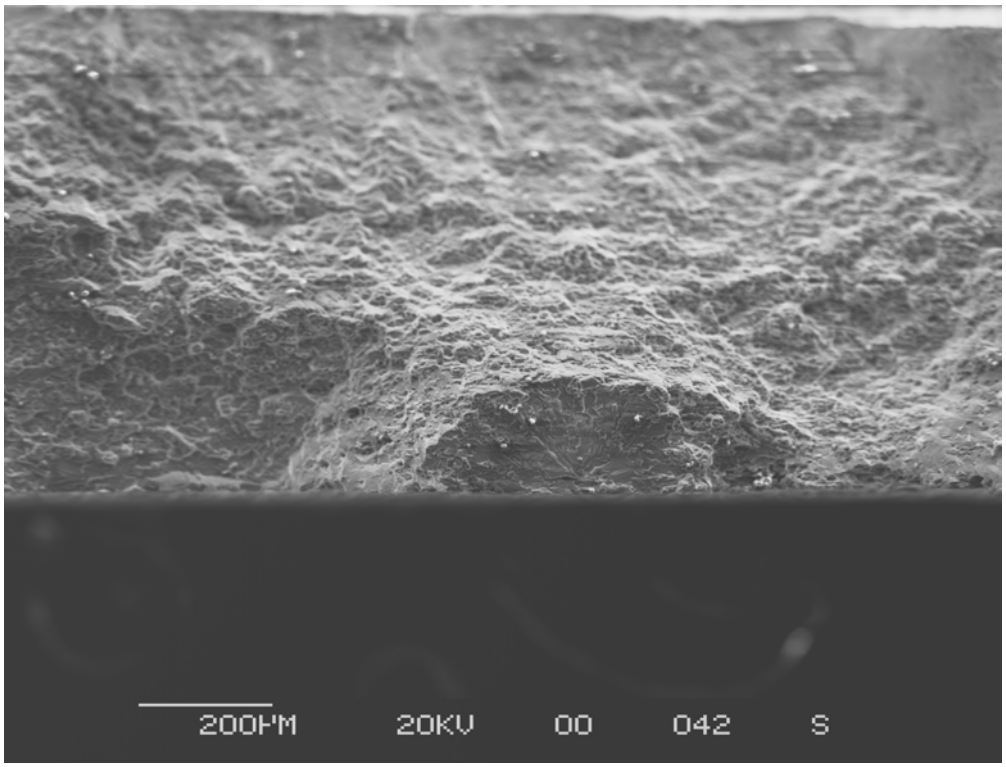

Figure B-41. Third Fatigue Crack on Specimen 5878 to the Right of the Primary Crack in Figure B-39.

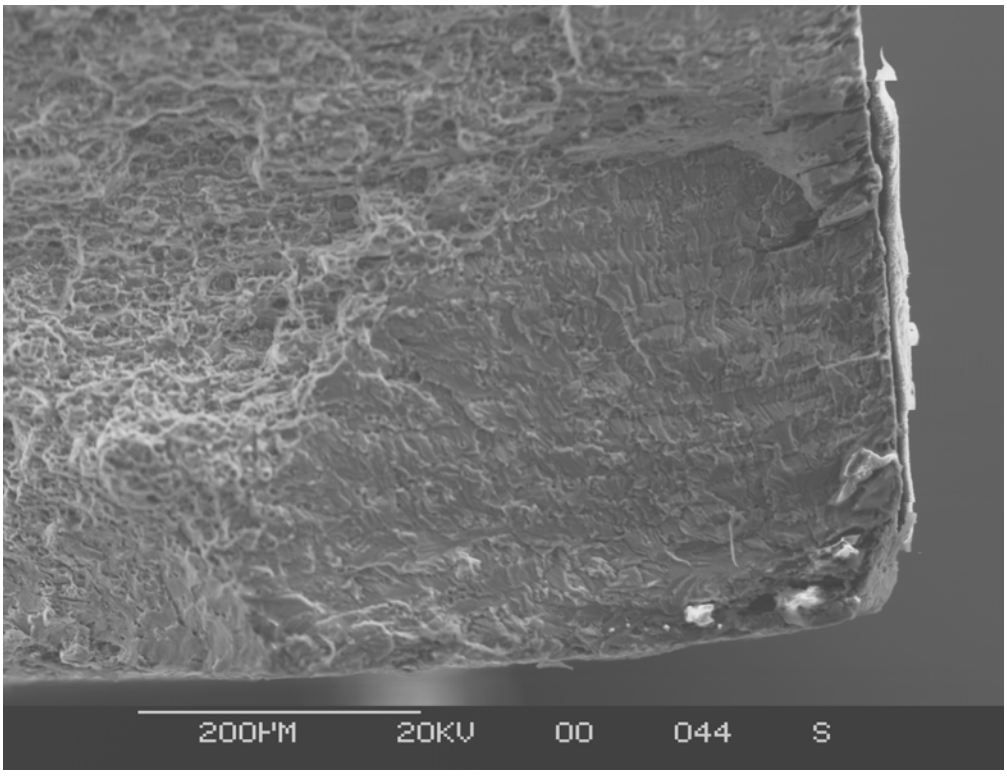

Figure B-42. Fourth Fatigue Crack on Specimen 5878 at the Lower Right Corner of the Specimen Oriented as in Fig. B-39.

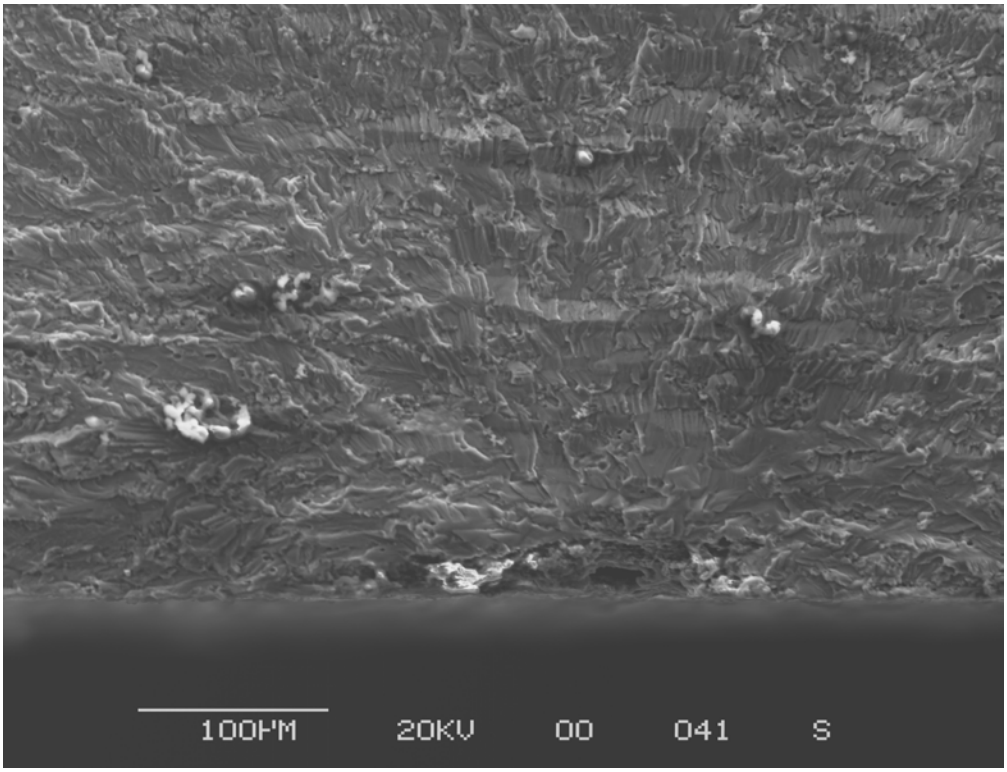

Figure B-43. Origin of Primary Crack in Fig. B-39.

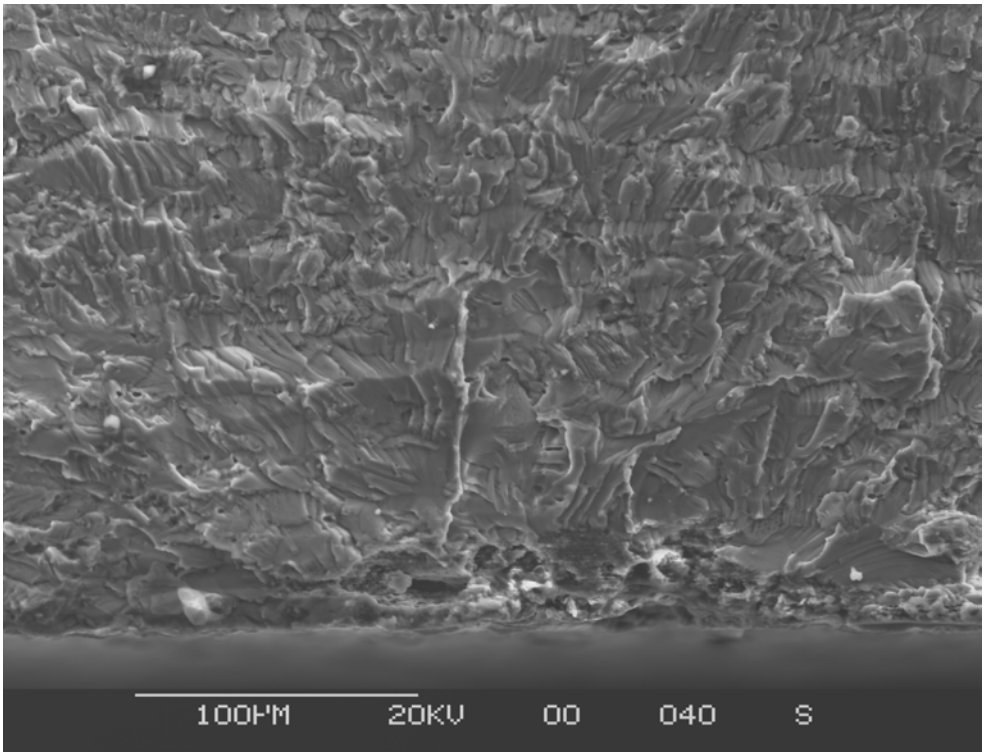

Figure B-44. Origin of Crack in Figure B-40.

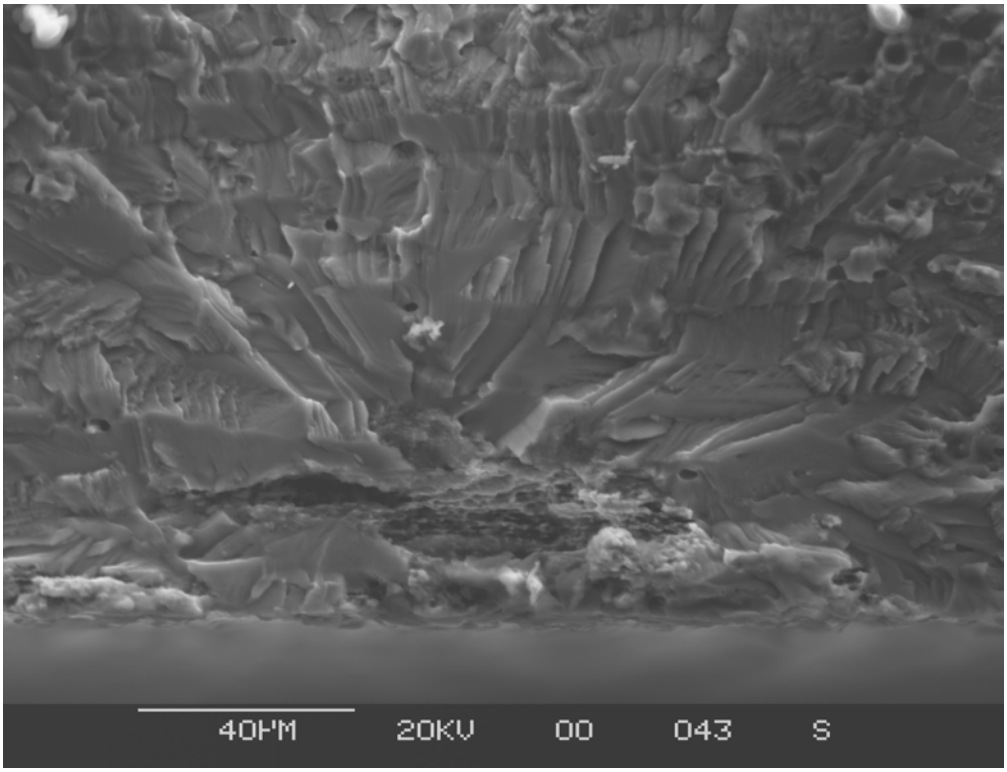

Figure B-45. Origin of Crack in Fig. B-41.

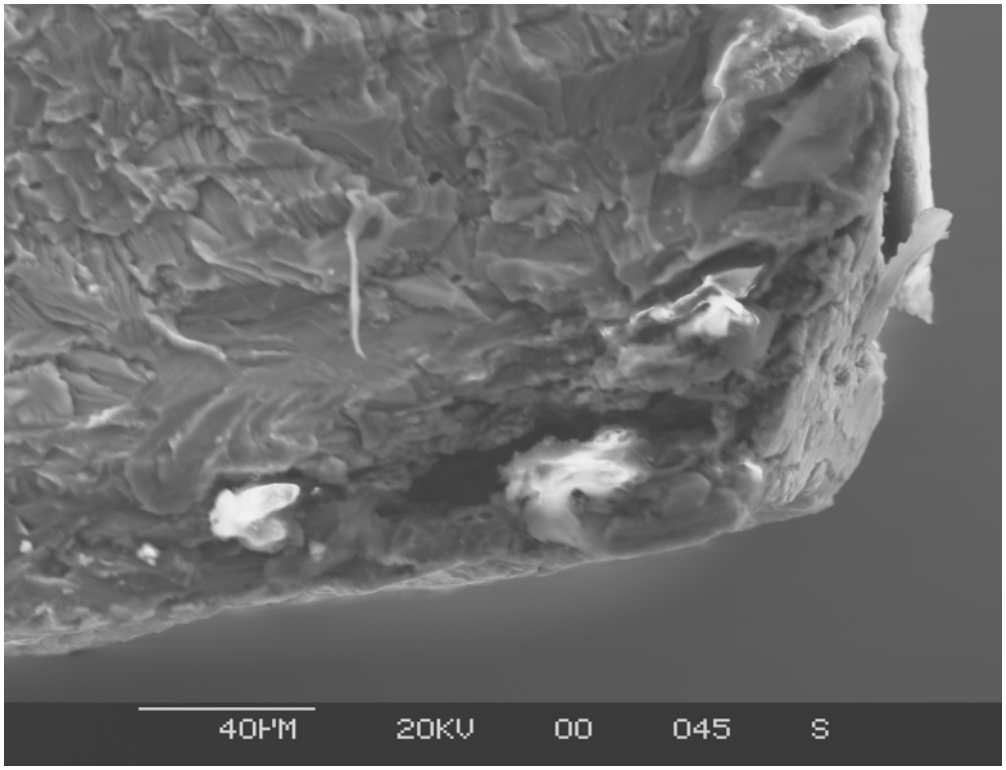

Figure B-46. Origin of Crack in Fig. B-42.

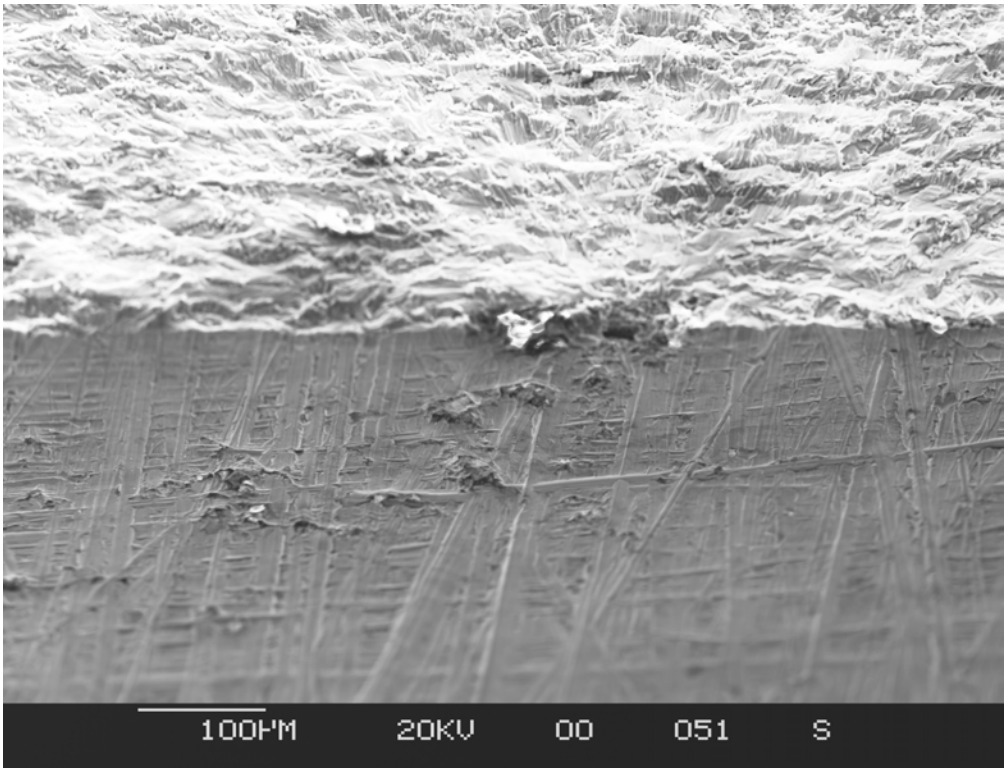

Figure B-47. Front Surface View of Origin of Primary Crack (Fig. B-39).

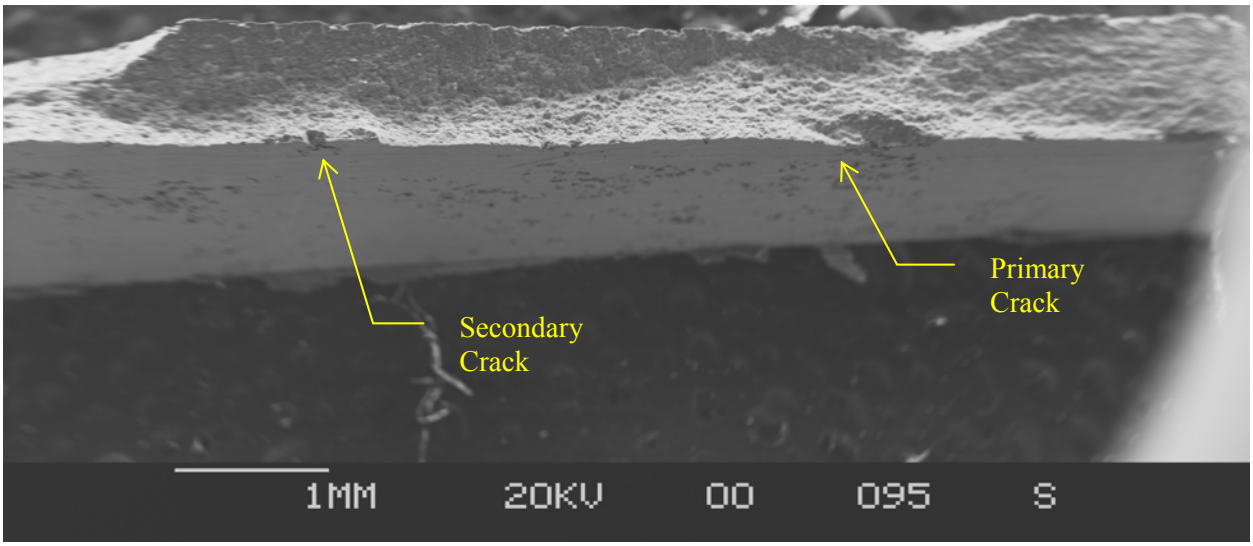

Figure B-48. Fatigue Crack on Fracture Surface of Specimen 5879.

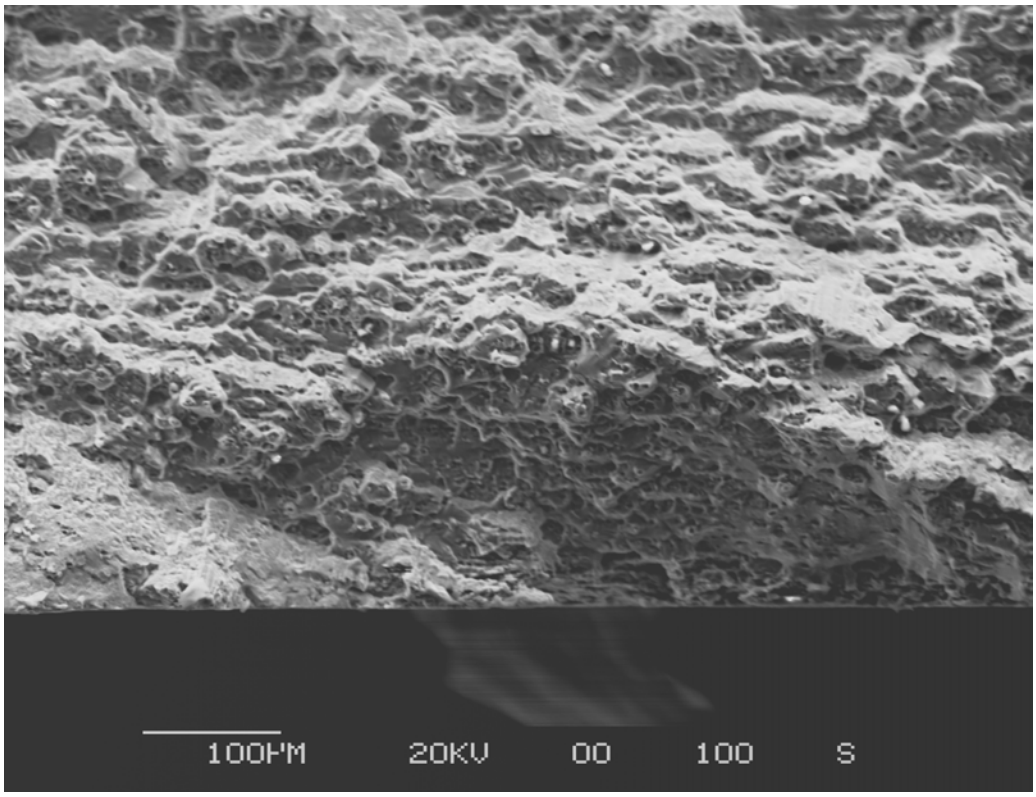

Figure B-49. Origin of Primary Crack on Specimen 5879.

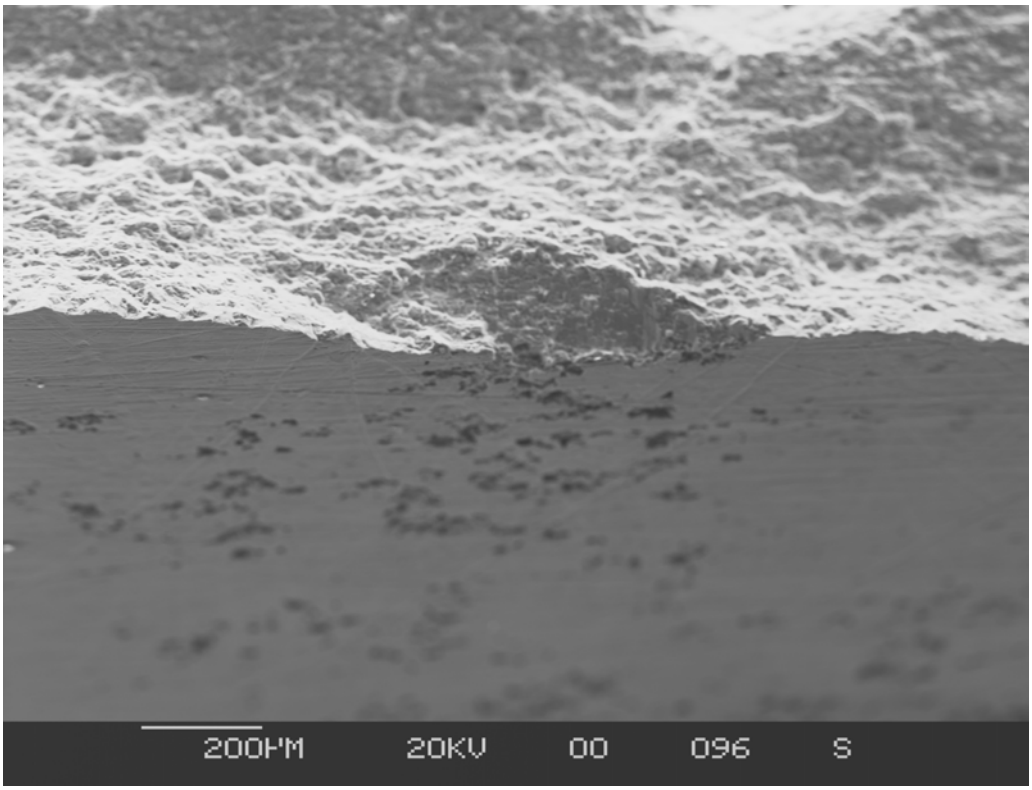

Figure B-50. Surface View of Primary Crack Origin on Specimen 5879.

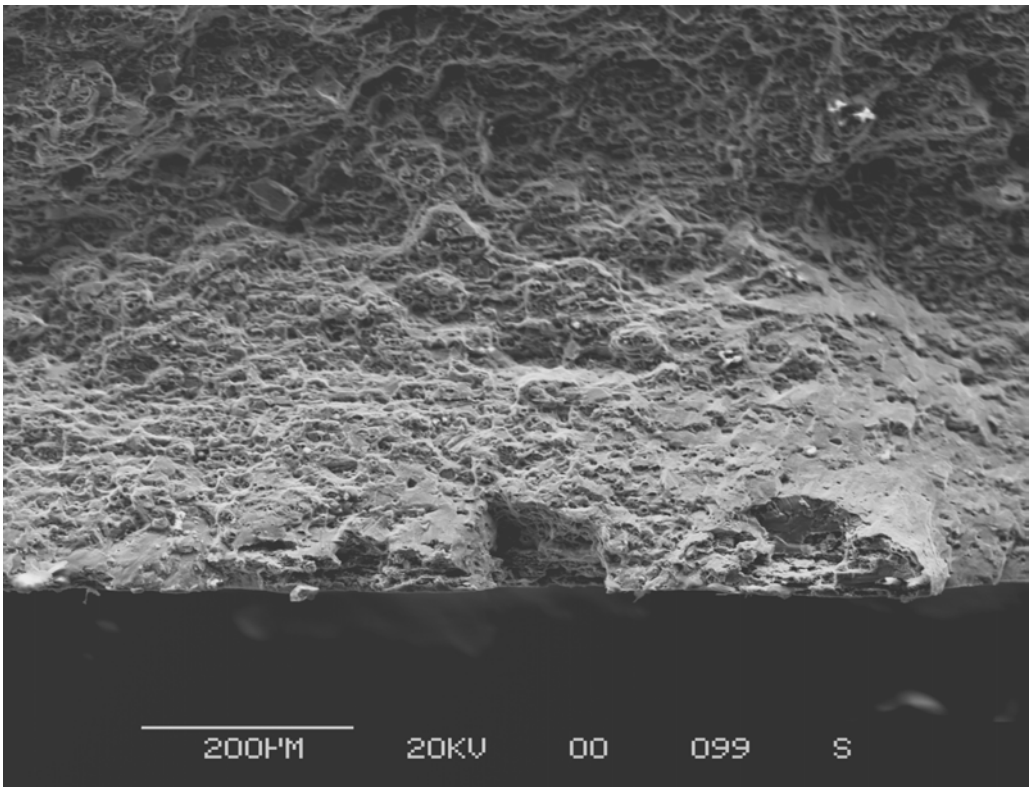

Figure B-51. Secondary Crack Origins on Specimen 5879.

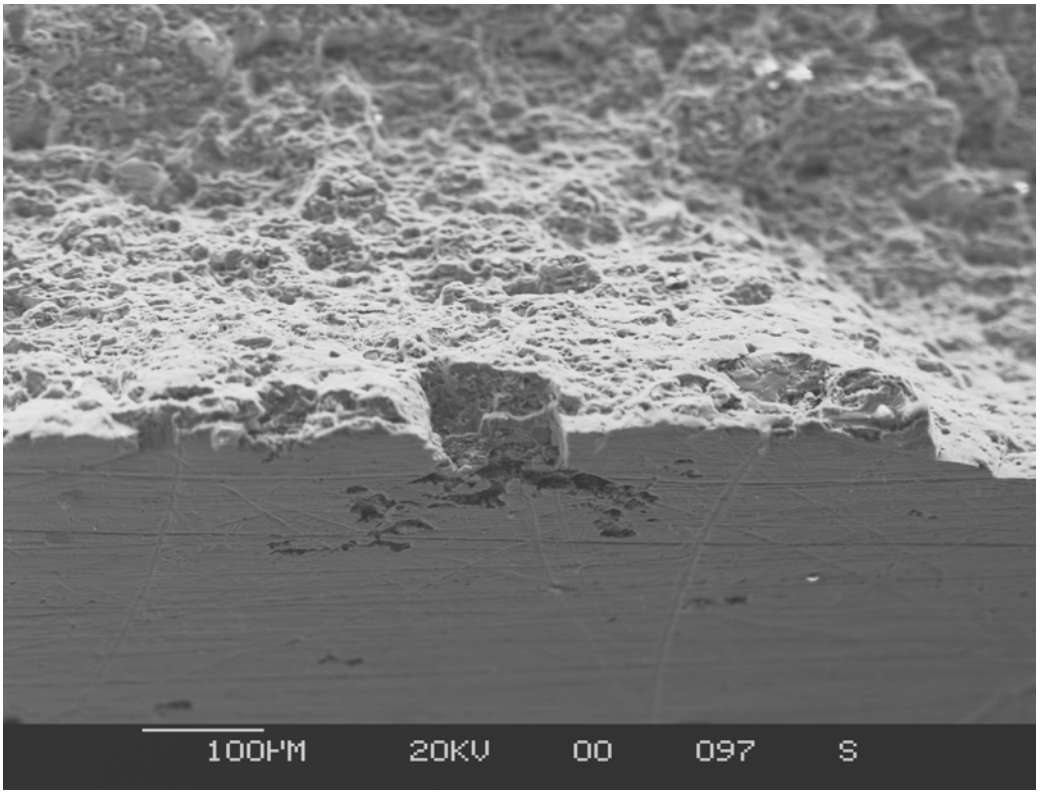

Figure B-52. Surface View of Secondary Crack Origins on Specimen 5879.

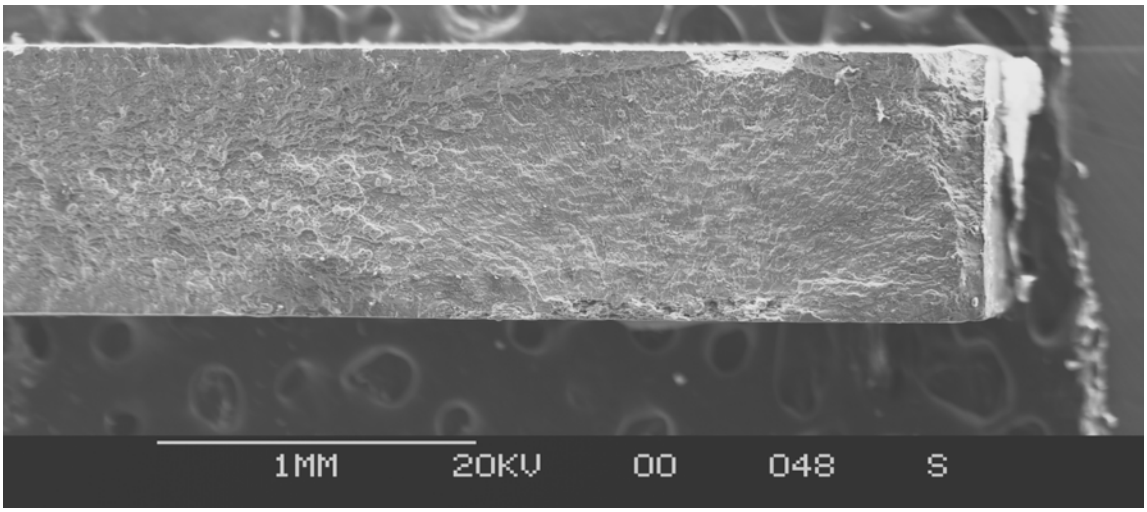

Figure B-53. Crack on Fracture Surface of Specimen 5880.

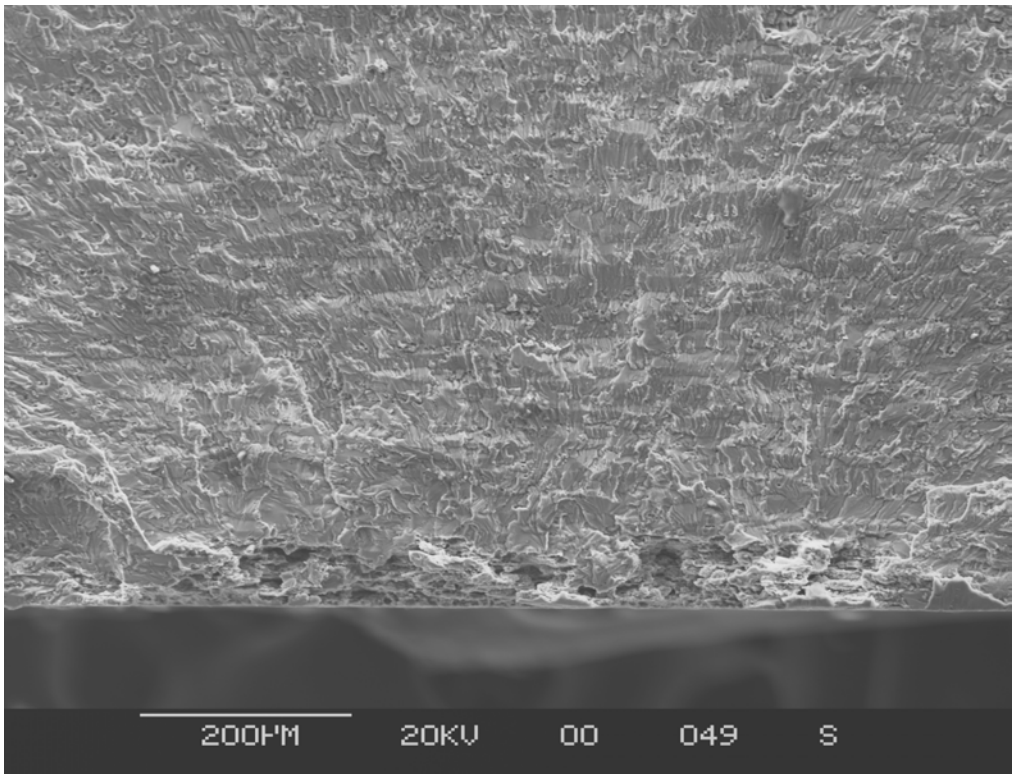

Figure B-54. Origin of Crack on Specimen 5880.

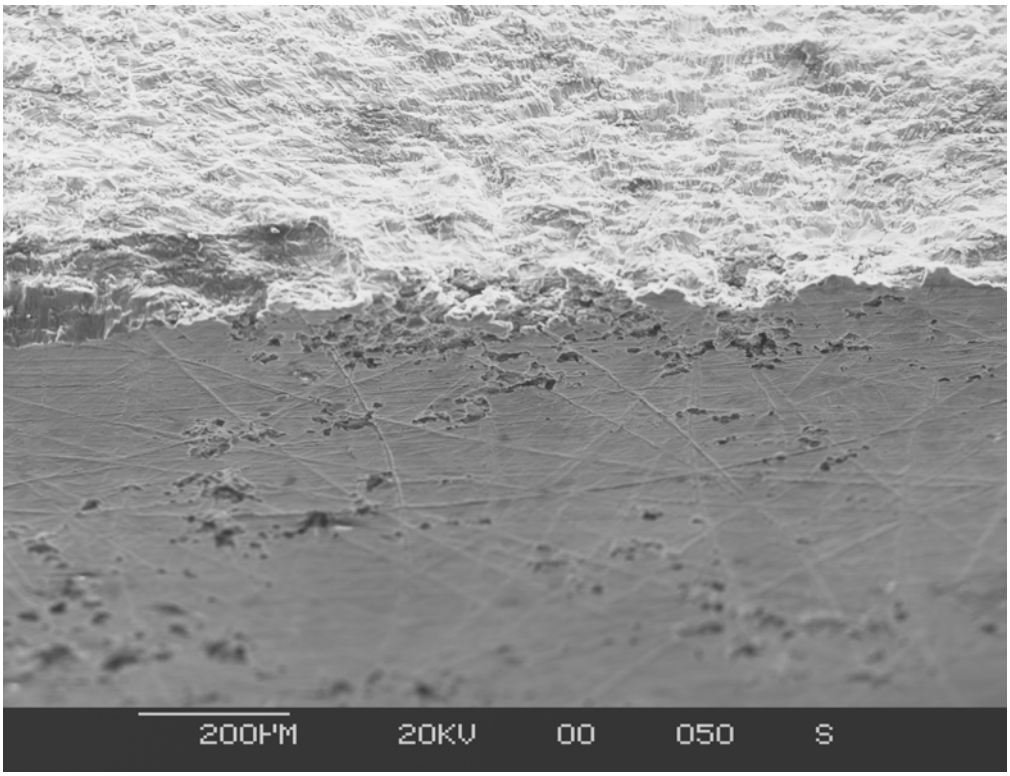

Figure B-55. Front Surface View of Crack Origin on Specimen 5880.

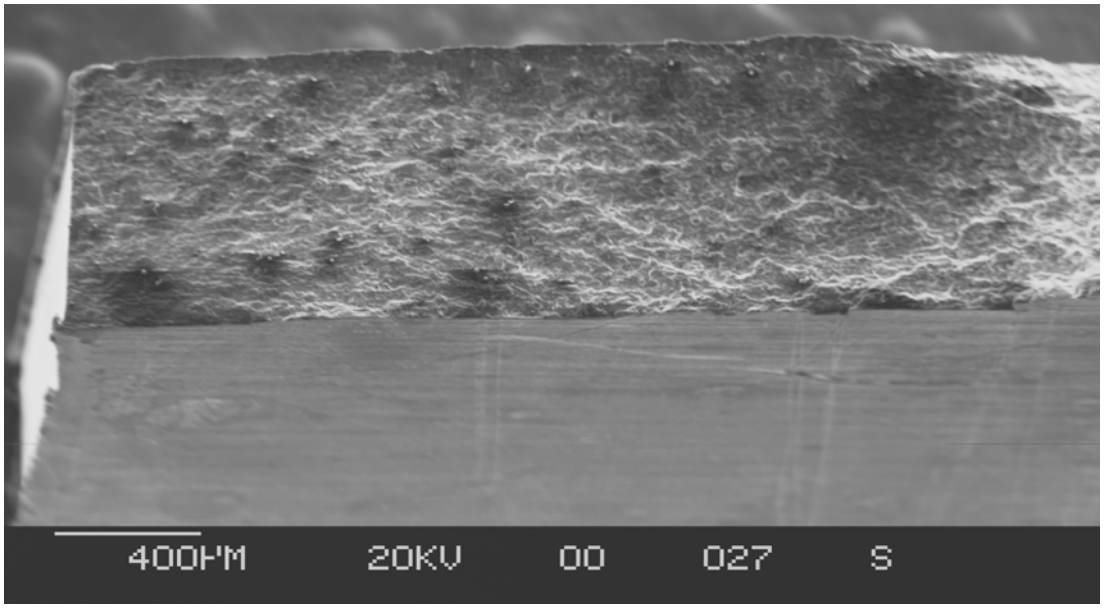

Figure B-56. Fatigue Crack on Fracture Surface of Specimen 5893.

Origin is at lower corner at left in the photograph.

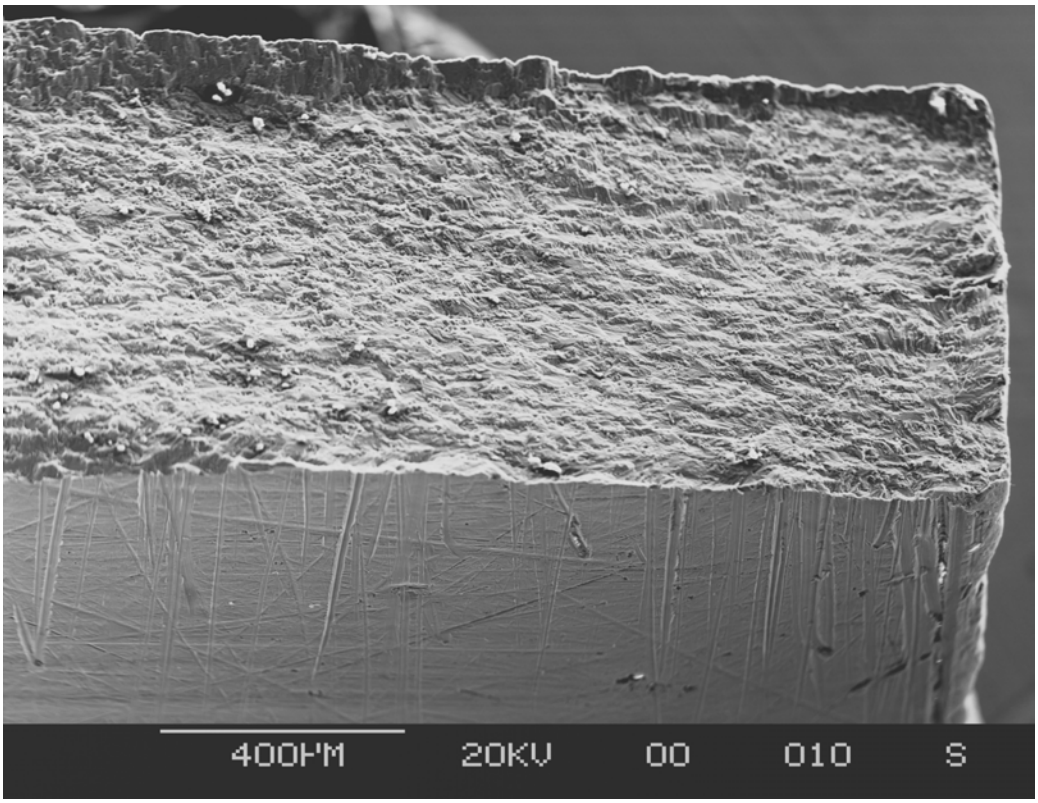

Figure B-57. Fatigue Crack on Fracture Surface of Specimen 5896.

Origin is at lower corner at right in the photograph.

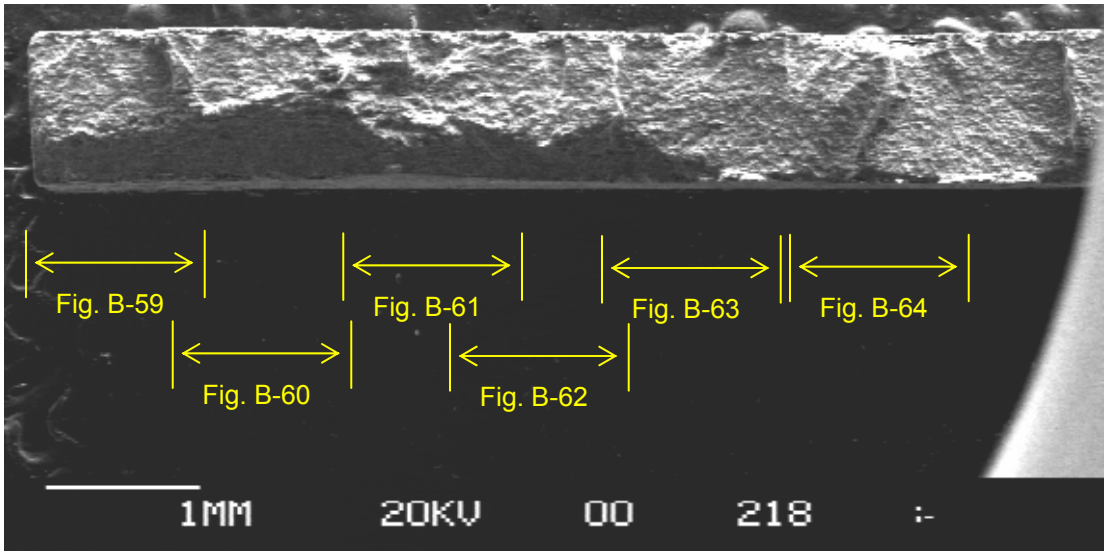

a) Left portion of fracture surface of Specimen 5914

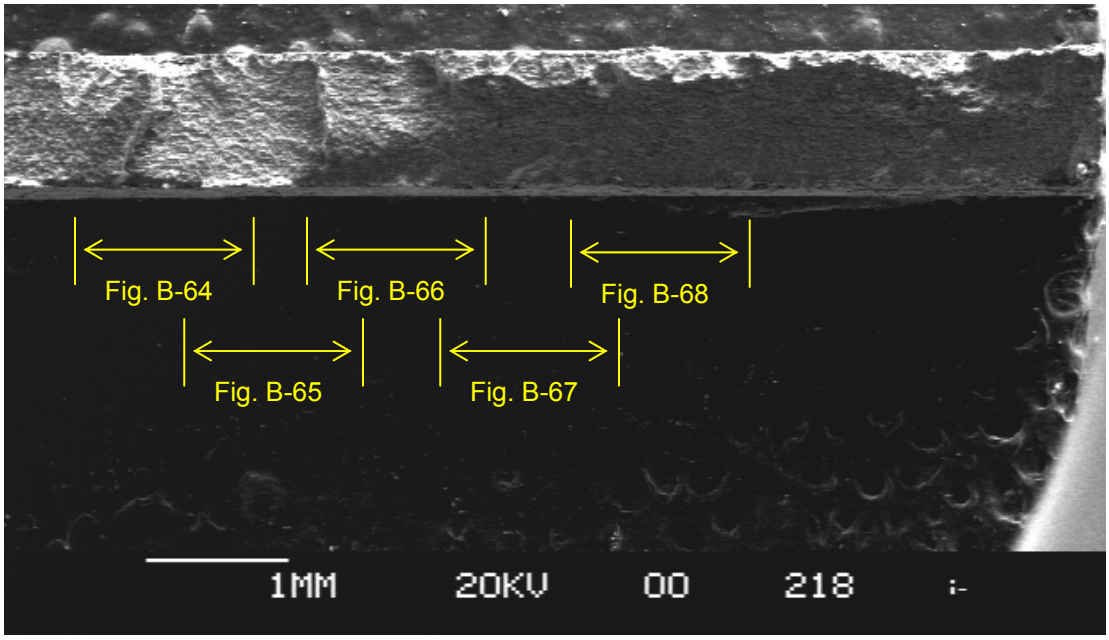

b) Right portion of fracture surface of Specimen 5914

Figure B-58. Multiple Fatigue Cracks on Fracture Surface of Specimen 5914.

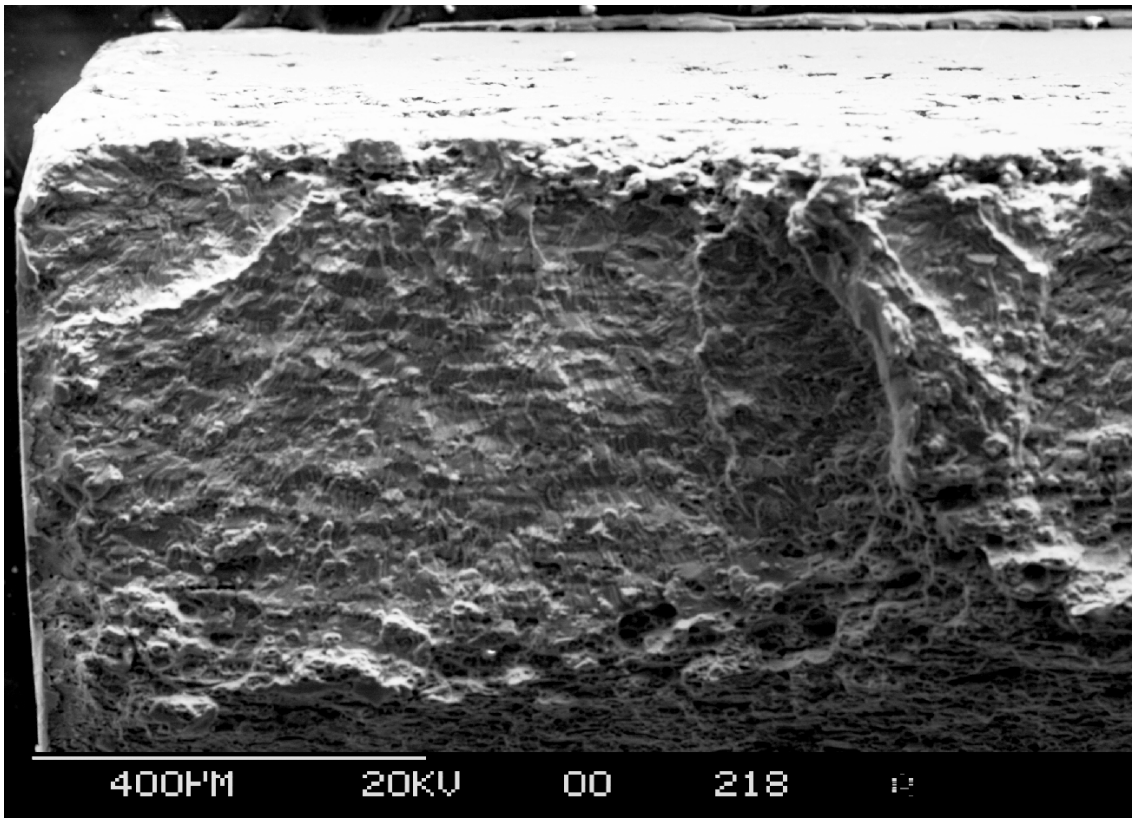

Figure B-59. Crack Origin #1 in Specimen 5914 (seen in Fig. B-58).

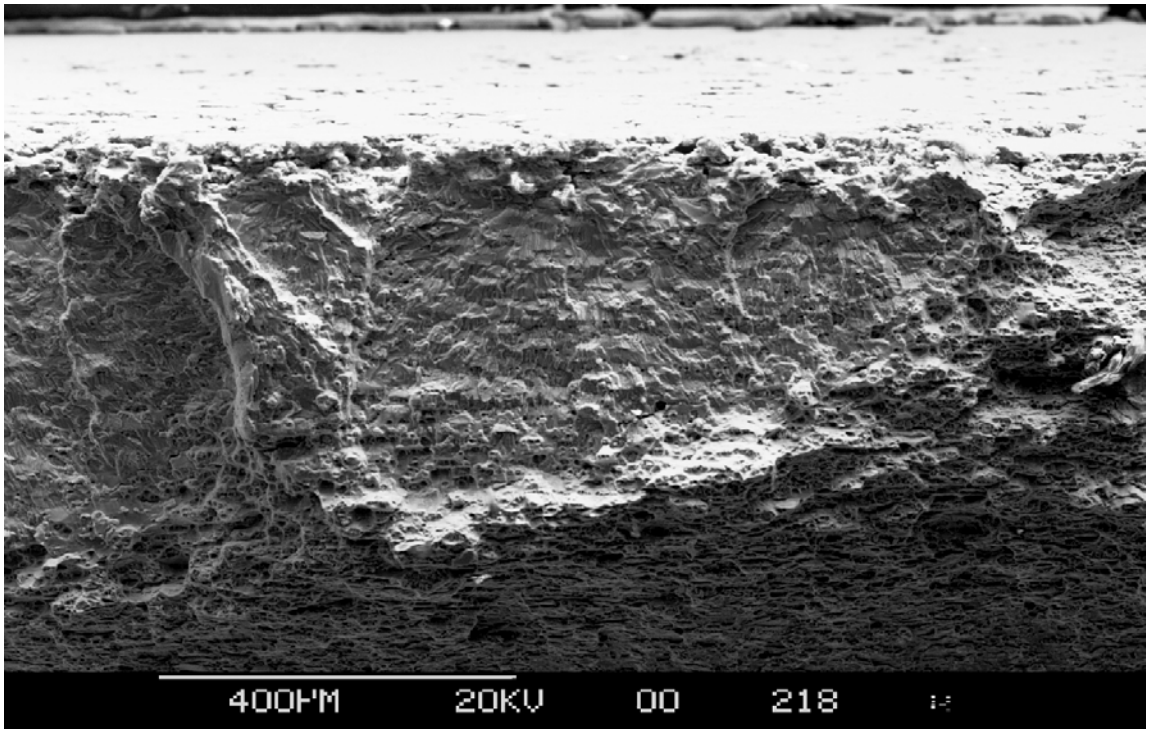

Figure B-60. Crack Origin #2 in Specimen 5914 (seen in Fig. B-58).

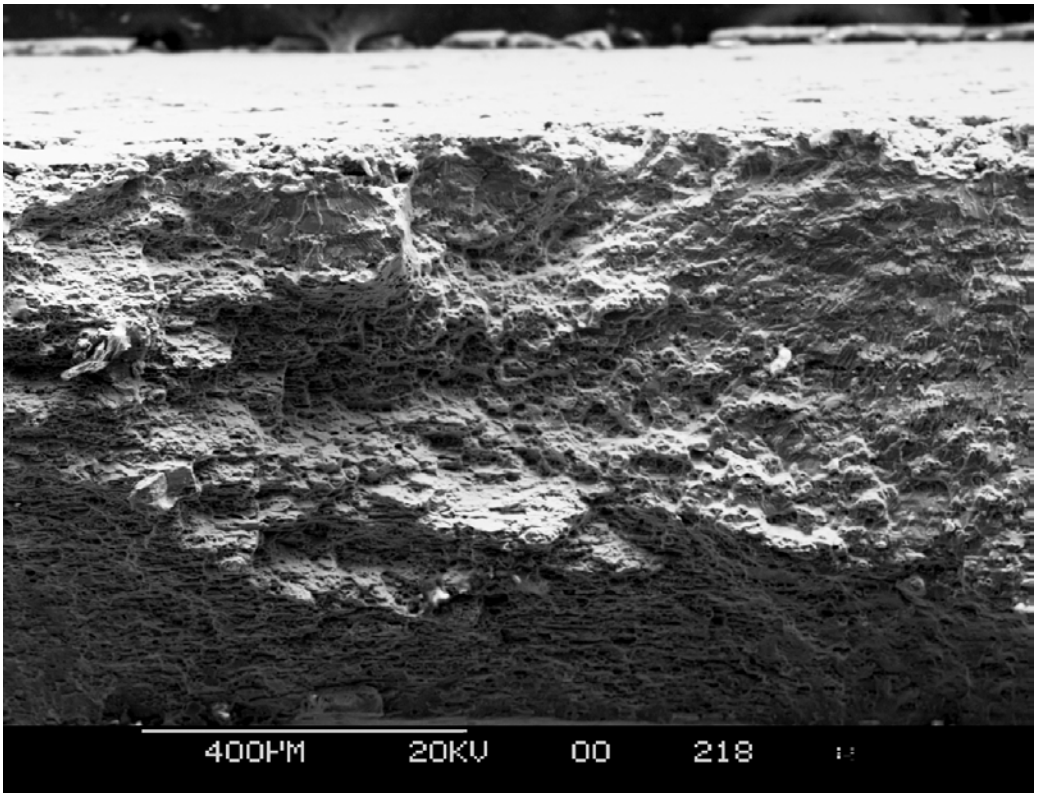

Figure B-61. Crack Origin #3 in Specimen 5914.

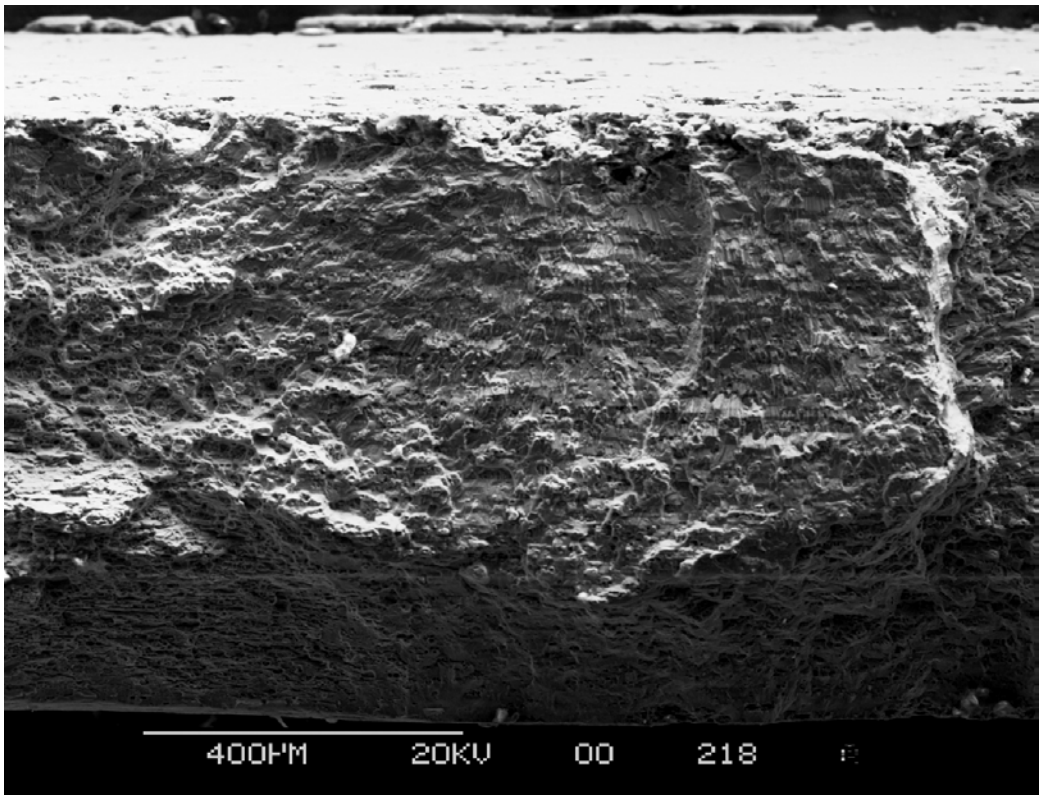

Figure B-62. Crack Origin #4 in Specimen 5914.

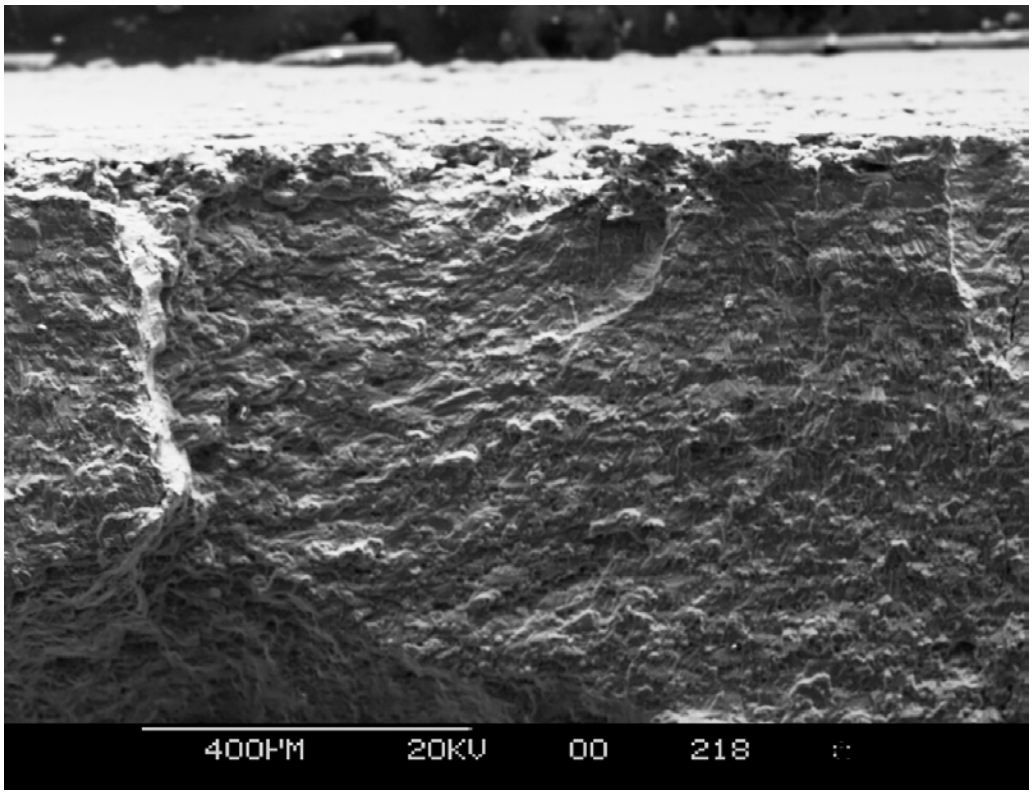

Figure B-63. Crack Origin #5 in Specimen 5914.

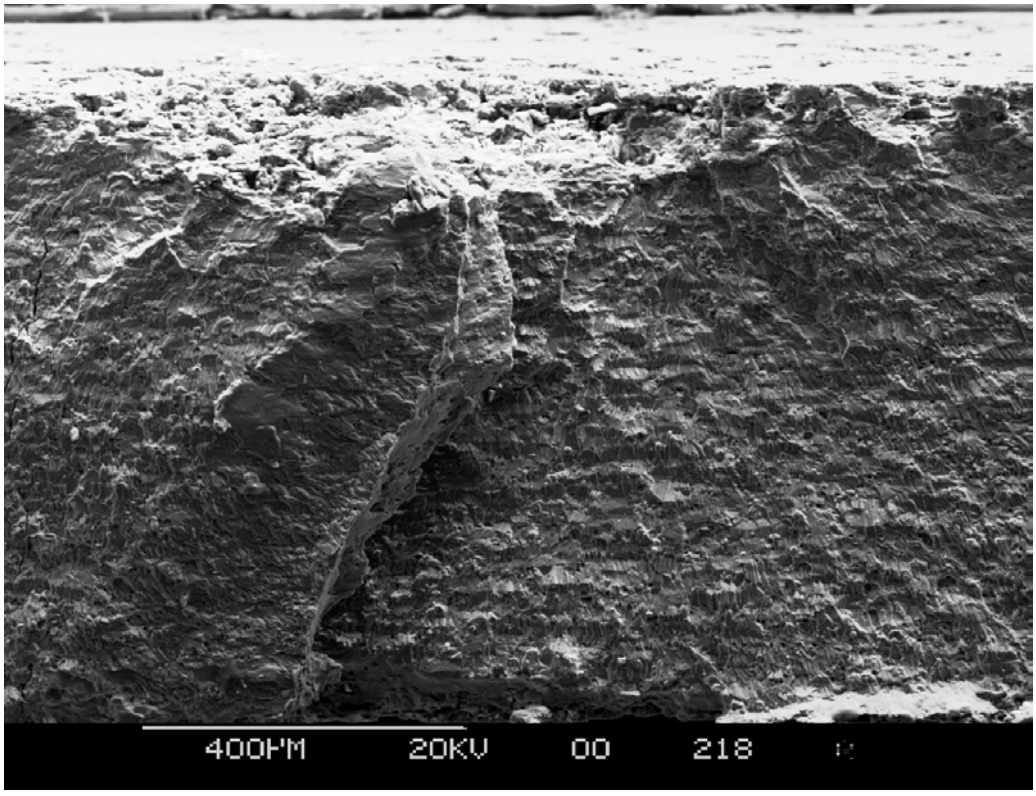

Figure B-64. Crack Origin #6 in Specimen 5914.

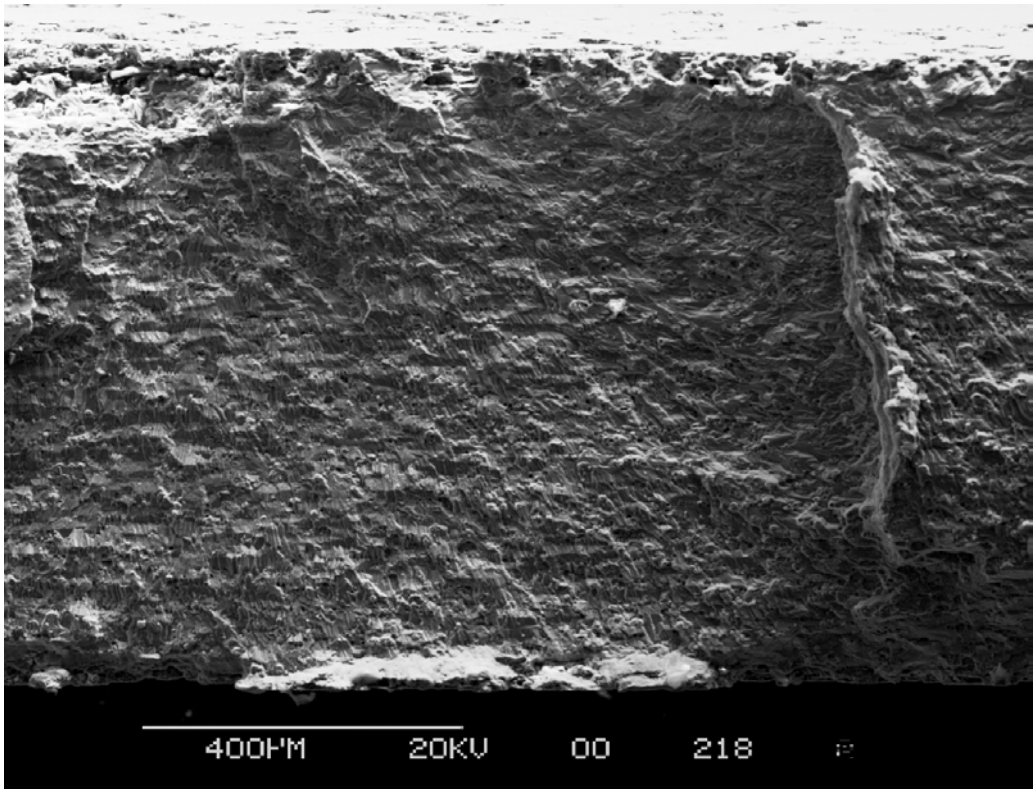

Figure B-65. Crack Origin #7 in Specimen 5914.

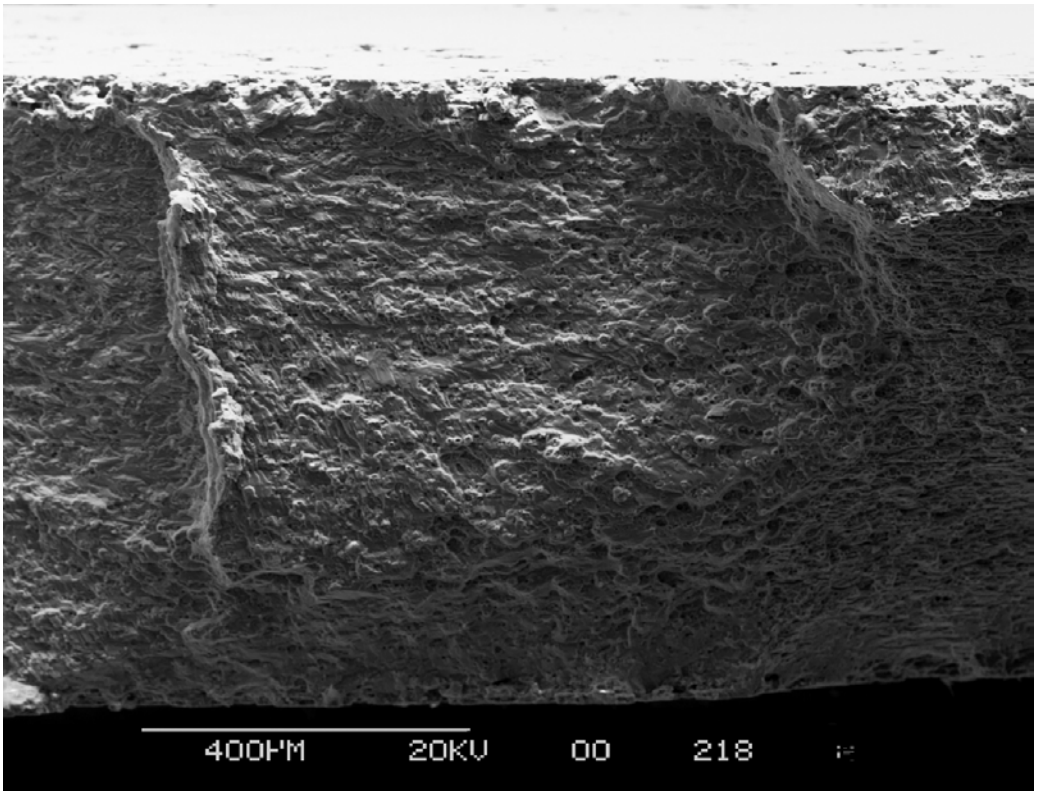

Figure B-66. Crack Origin #8 in Specimen 5914.

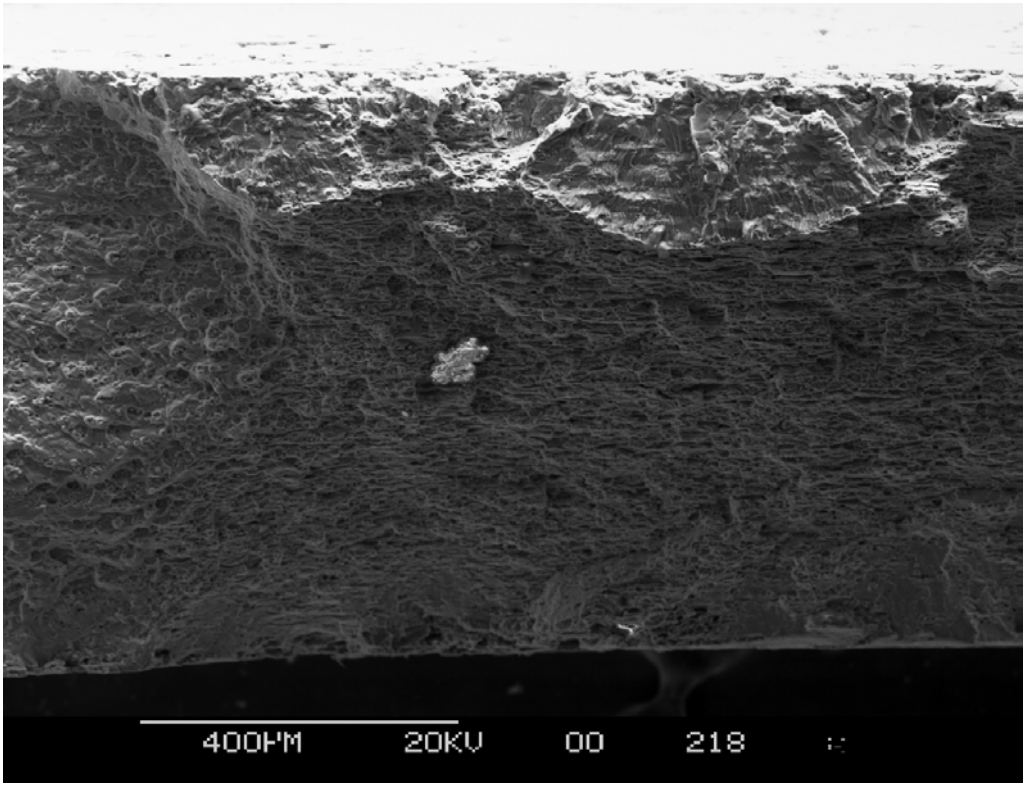

Figure B-67. Crack Origin #9 in Specimen 5914.

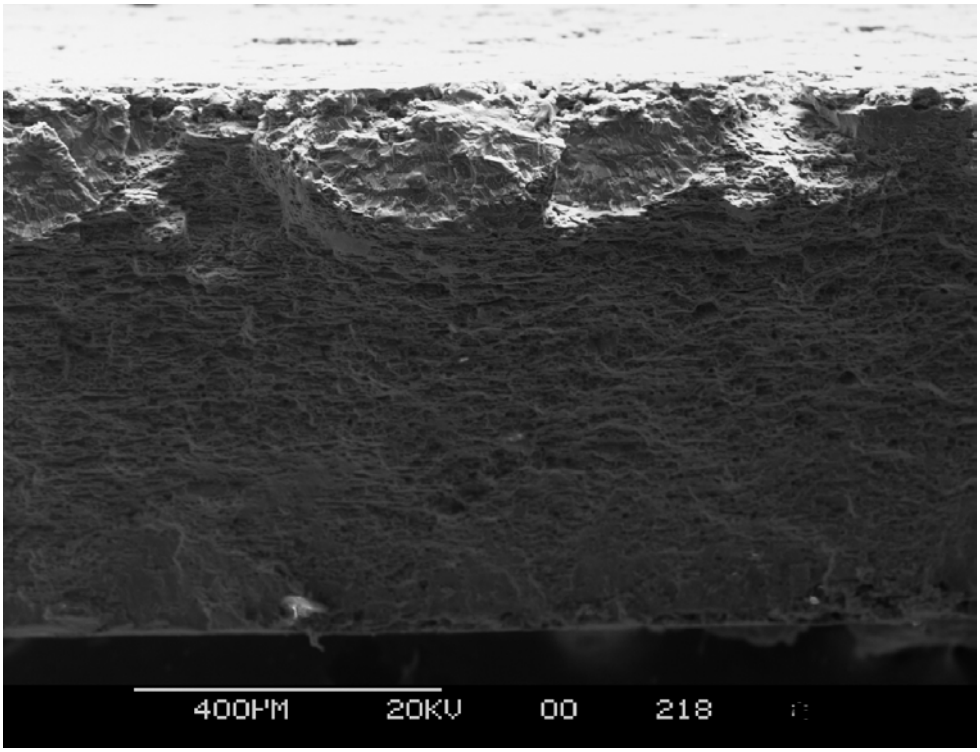

Figure B-68. Crack Origin #10 in Specimen 5914.

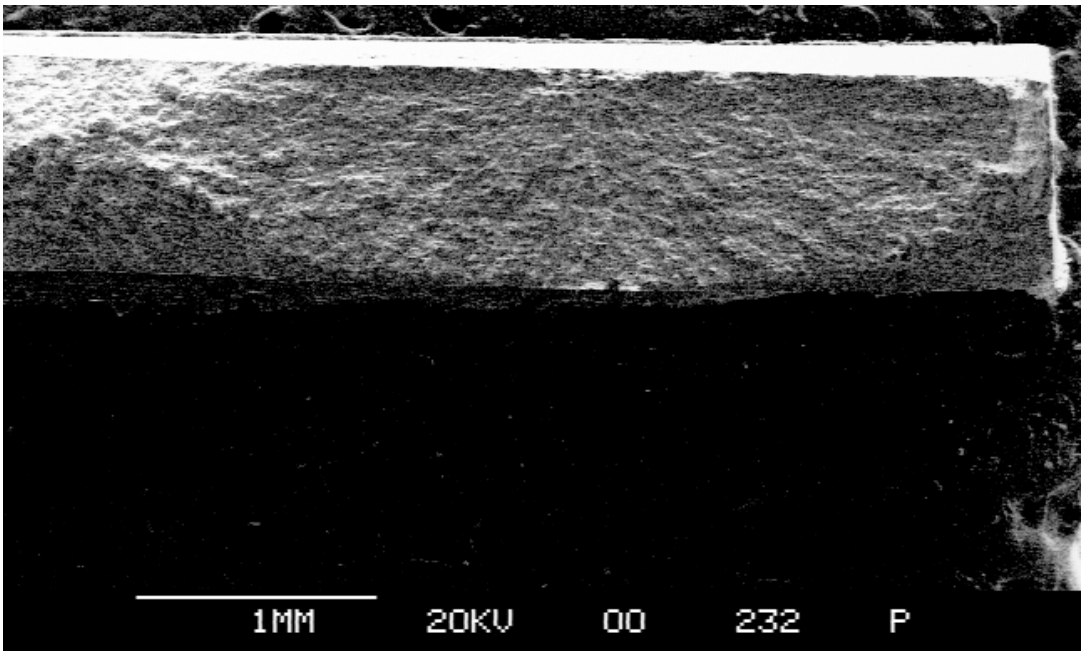

Figure B-69. Fatigue Crack on Fracture Surface of Specimen 5925.

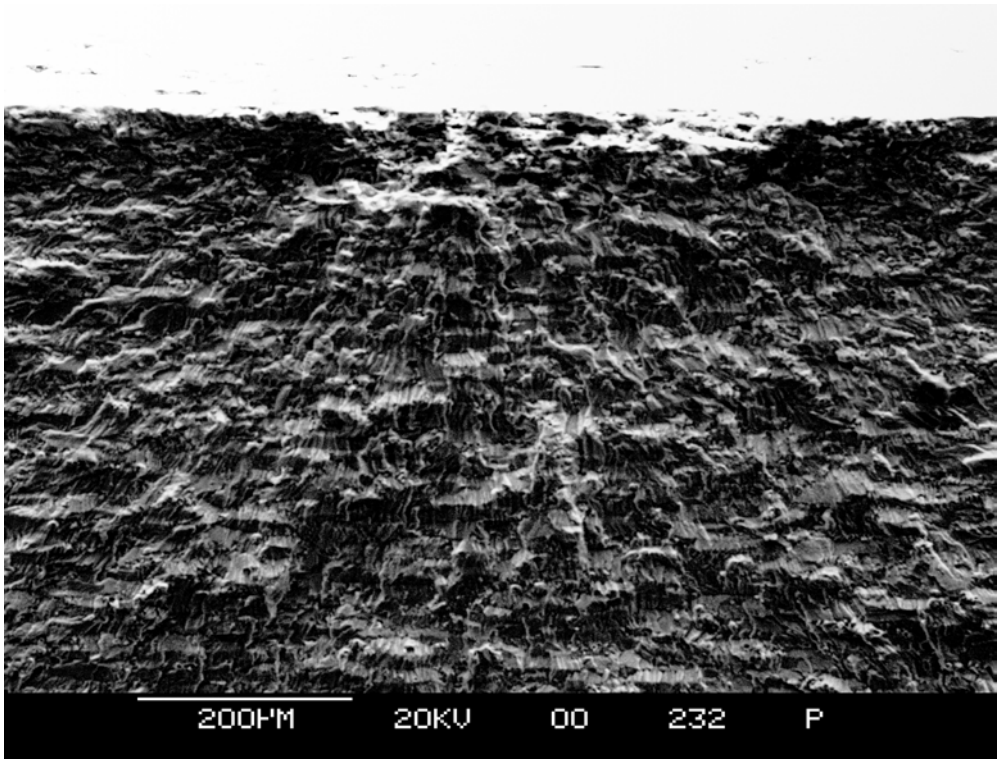

Figure B-70. Pit at origin of crack in Specimen 5925.

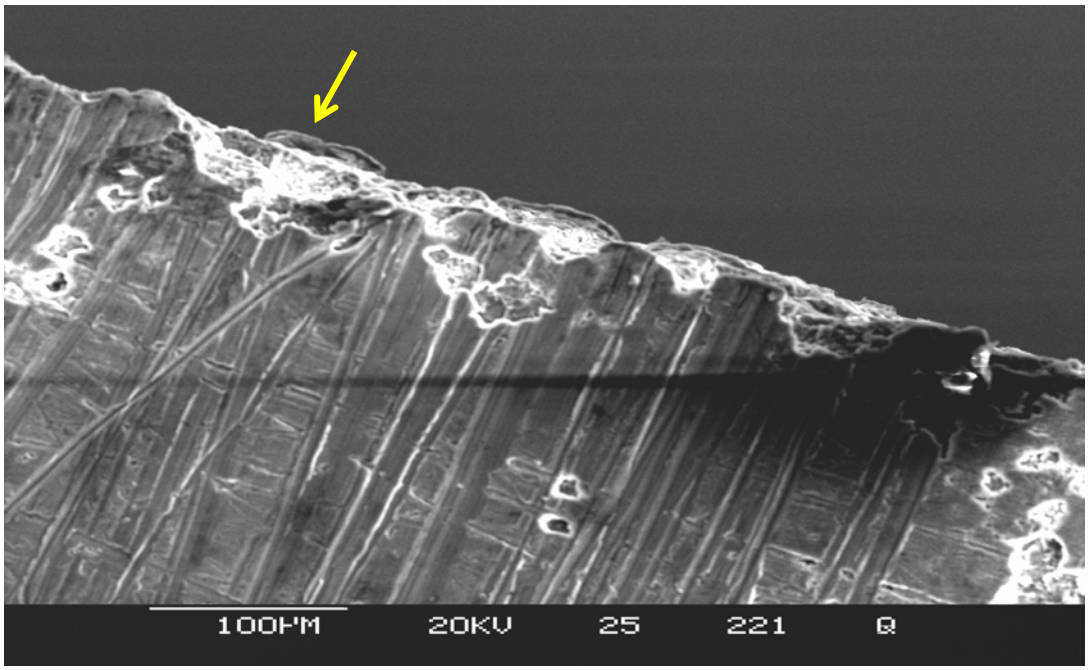

Figure B-71. Pits Along Crack Path in Specimen 5925 Viewed from the Surface of the Specimen.

Crack Nucleating Pit is Indicated by the Arrow.

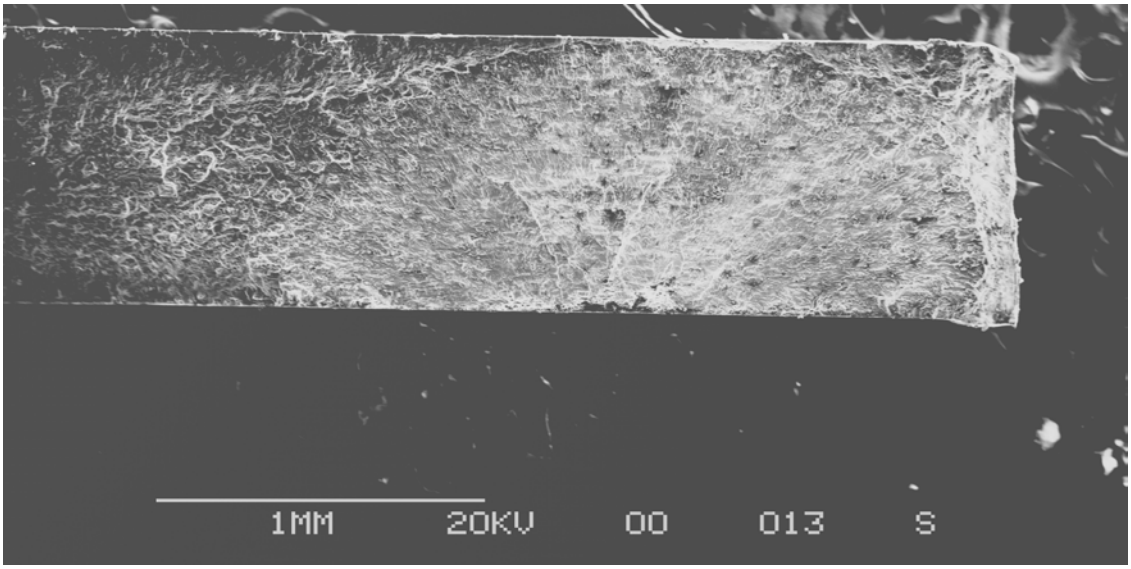

Figure B-72. Fatigue Crack on Fracture Surface of Specimen 5926.

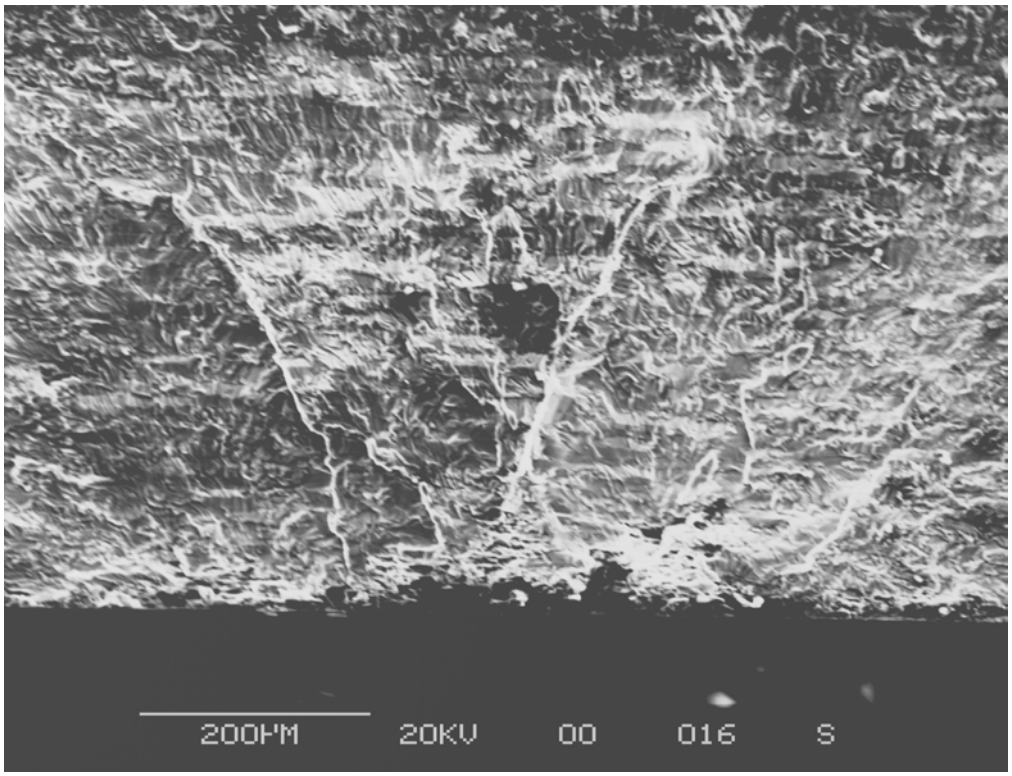

Figure B-73. Origin of Crack on Specimen 5926.

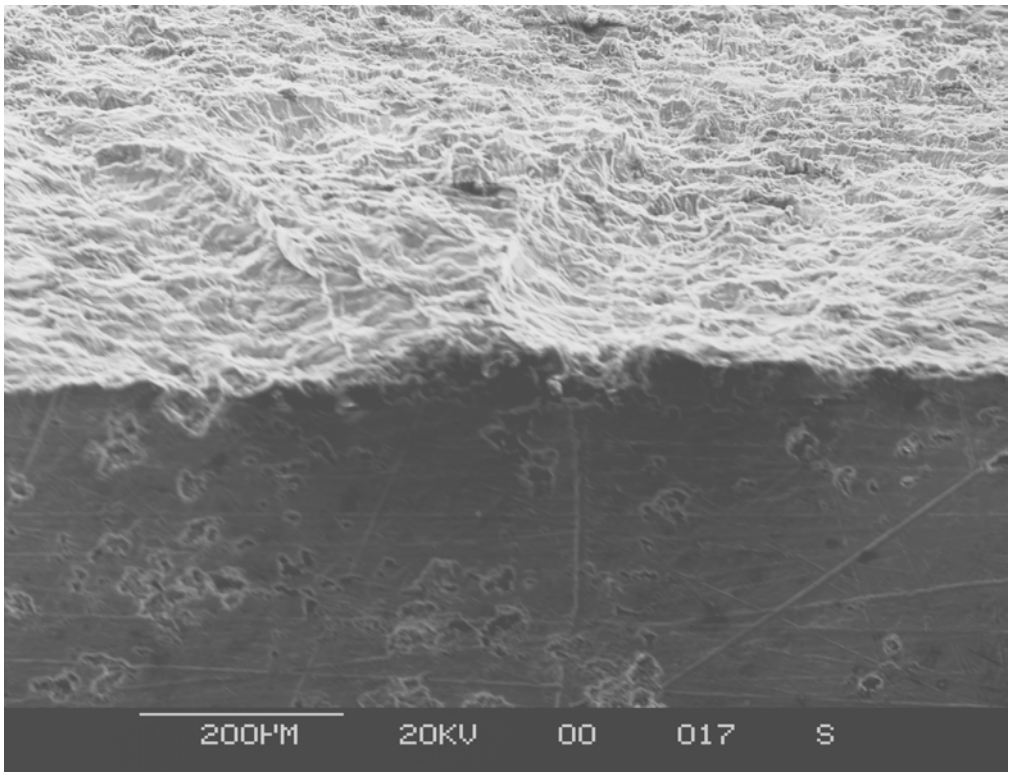

Figure B-74. Surface View of Crack Origin on Specimen 5926.

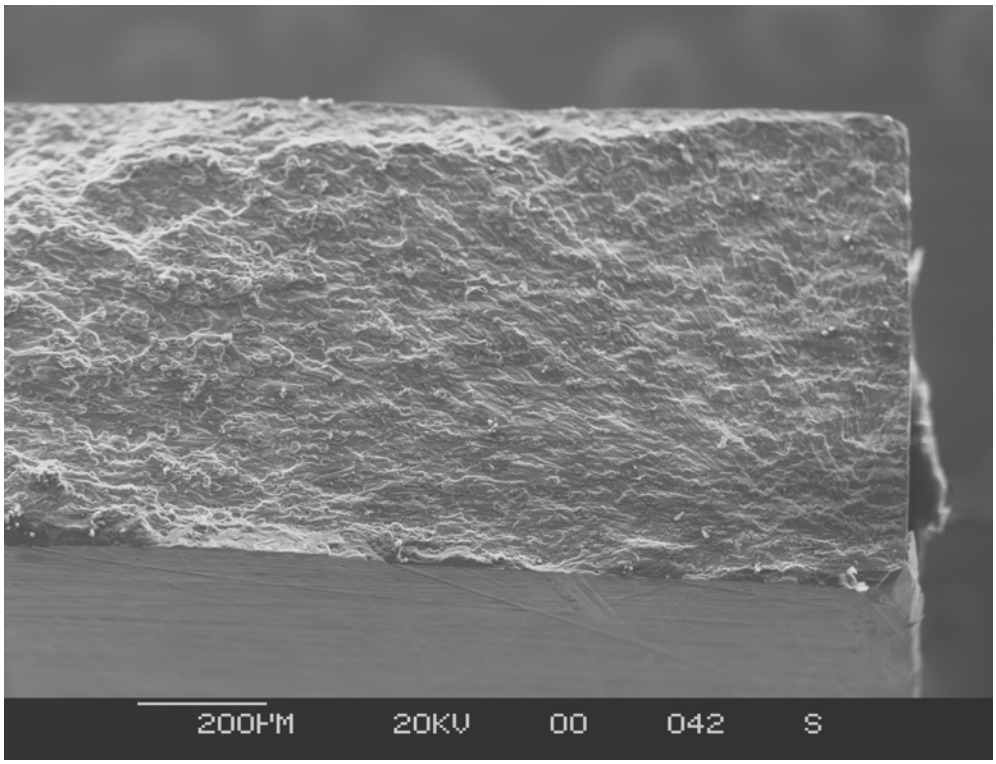

Figure B-75. Fatigue Crack on Fracture Surface of Specimen 5931.

Origin is at corner in lower right of the photograph.

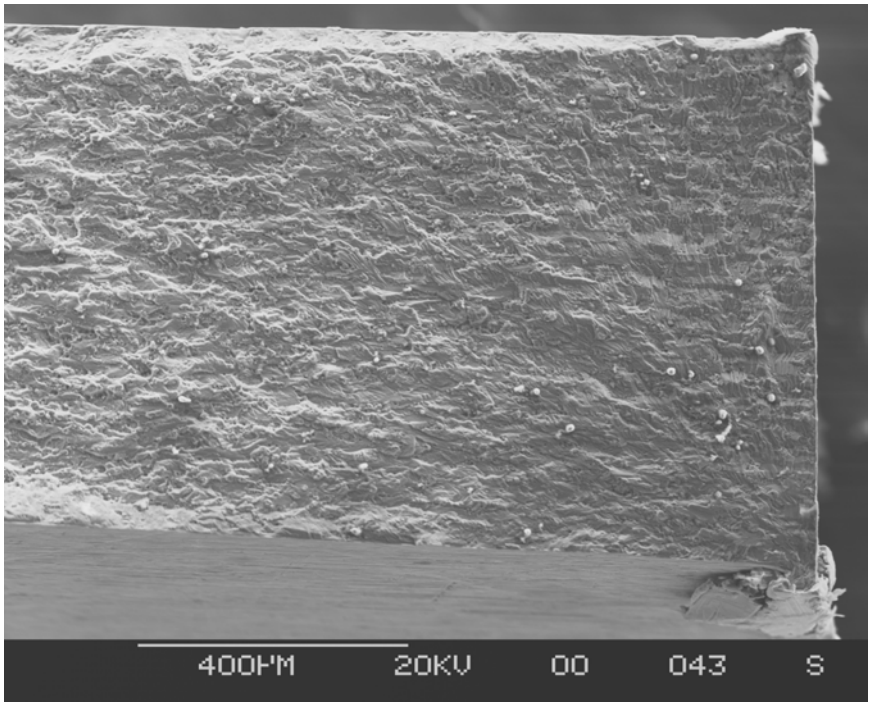

Figure B-76. Fatigue Crack on Fracture Surface of Specimen 5932.

Origin is at corner in lower right of the photograph.

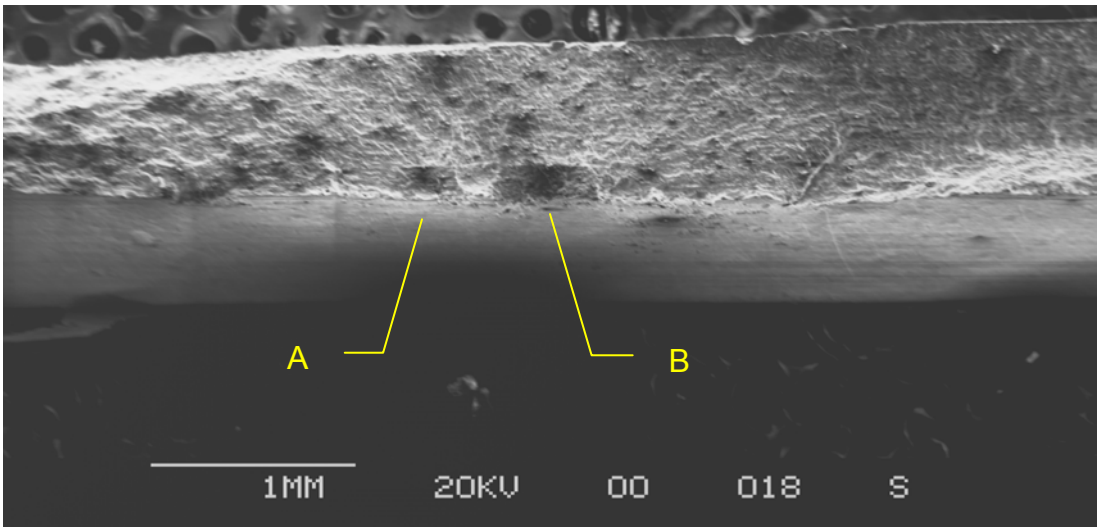

Figure B-77. Fatigue Crack on Fracture Surface of Specimen 5933.

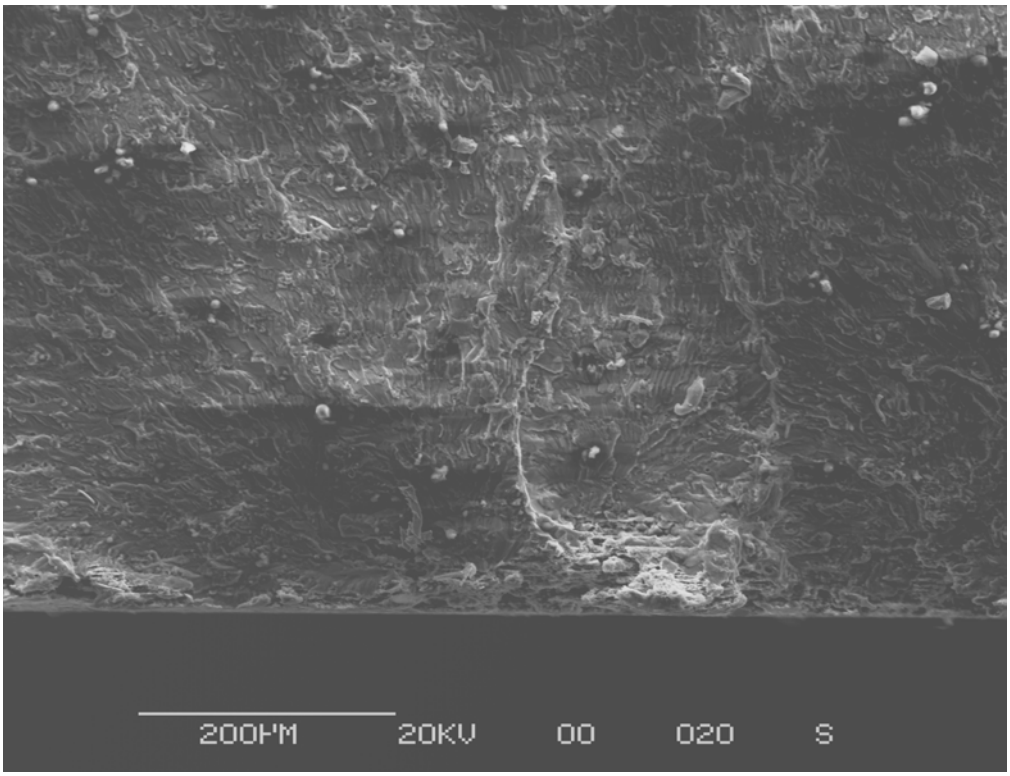

Figure B-78. Origin A (Fig. B-77) on Specimen 5933.

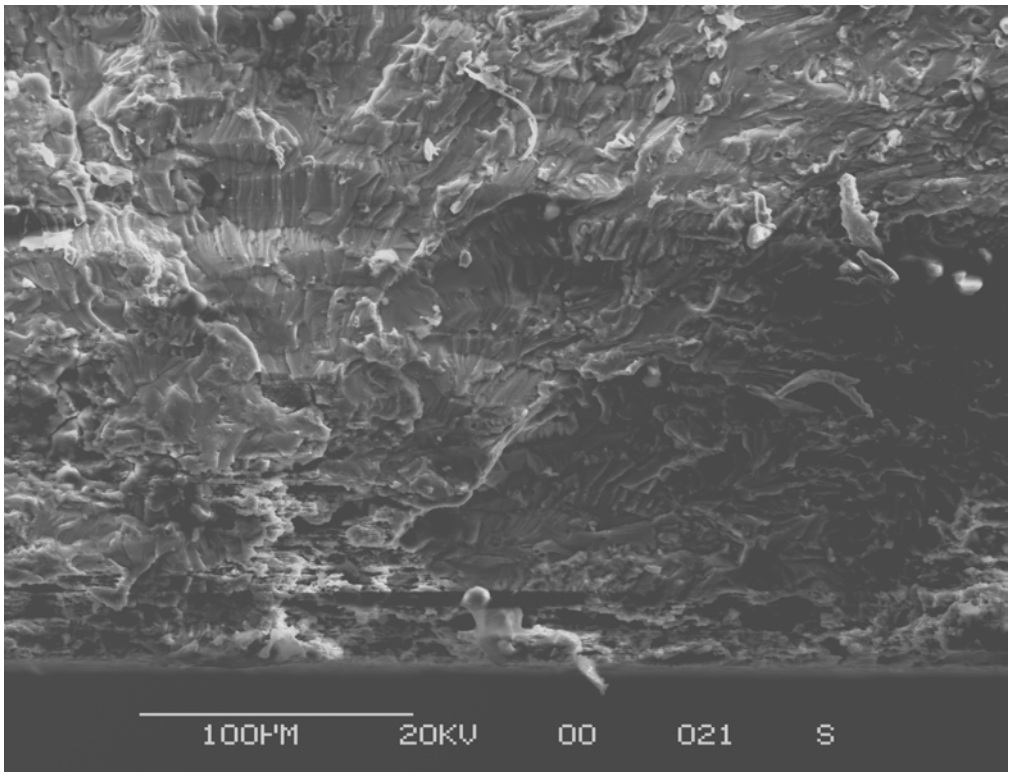

Figure B-79. Origin B (Fig. B-77) on Specimen 5933.

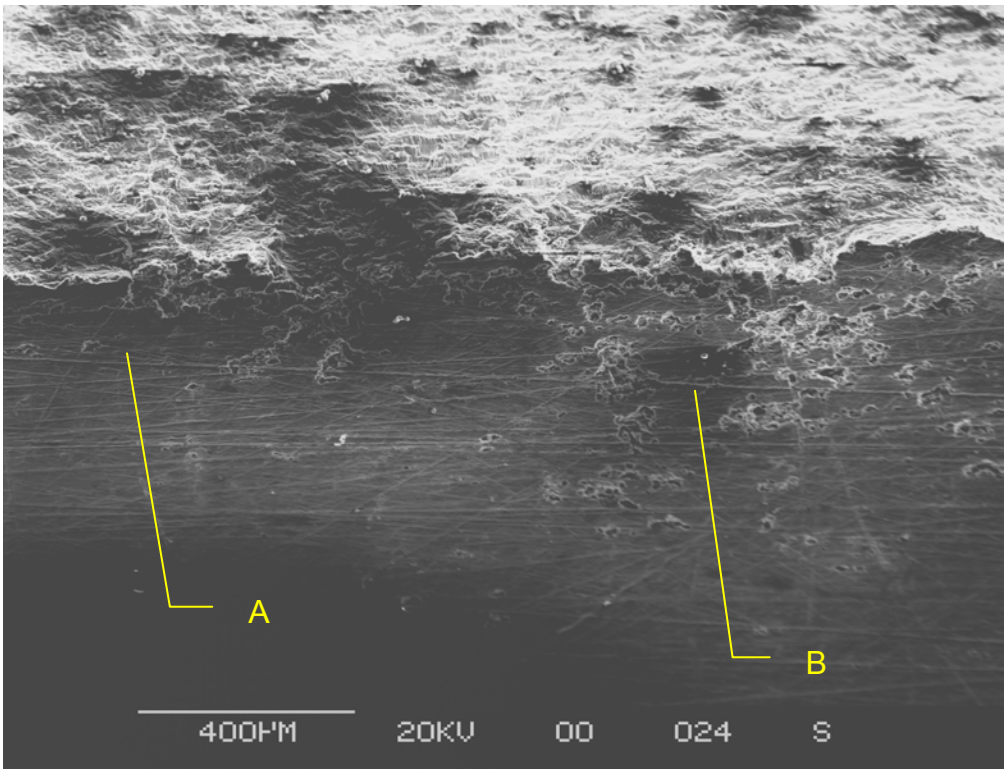

Figure B-80. Surface View of Crack Origins on Specimen 5933.

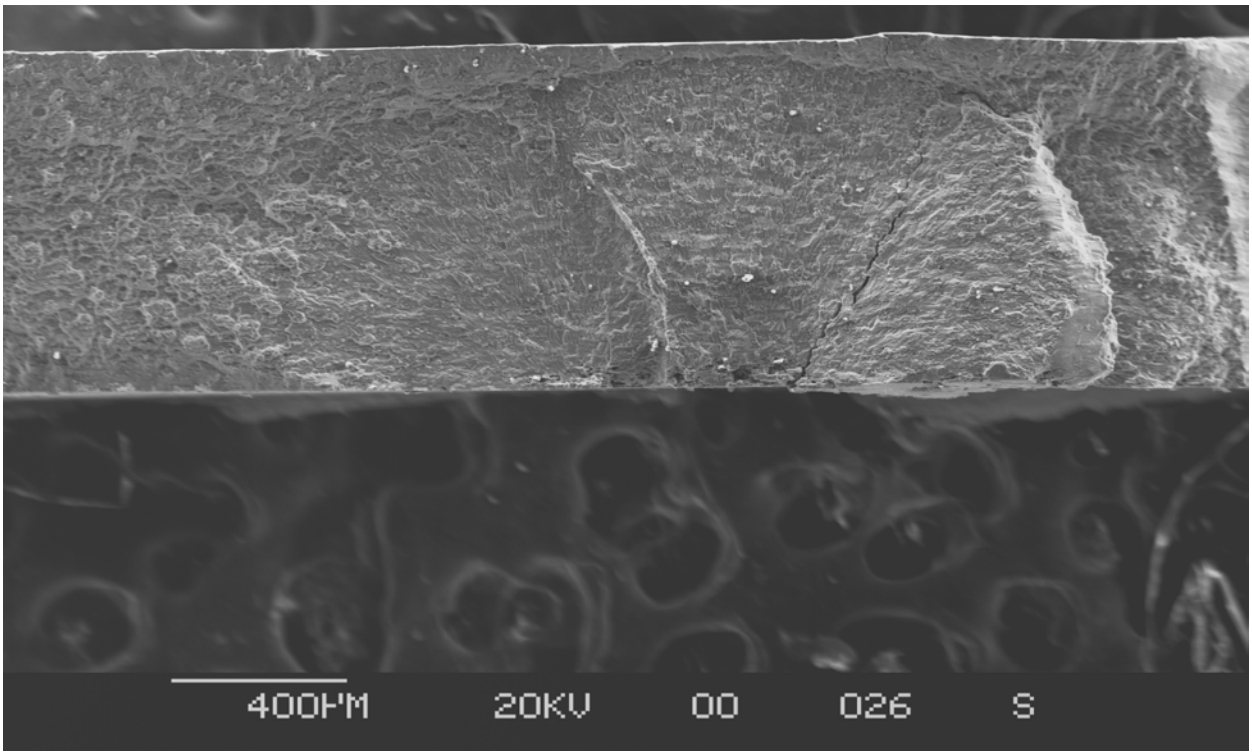

Figure B-81. Fatigue Crack on Fracture Surface of Specimen 5934.

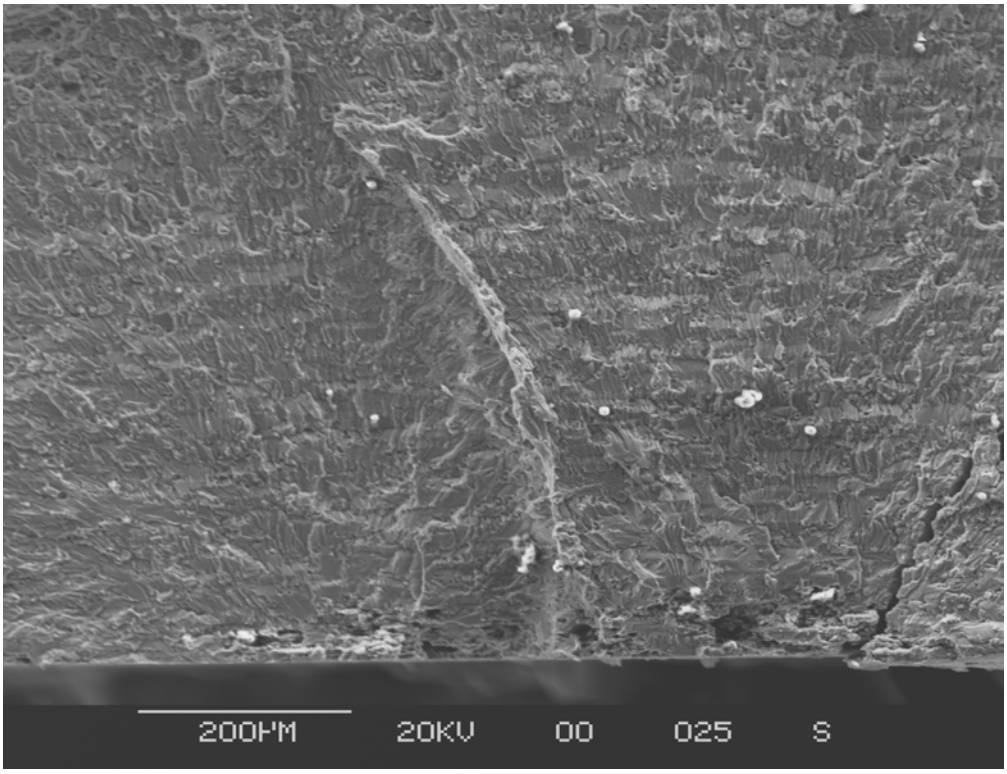

Figure B-82. Origin of Crack on Specimen 5934.

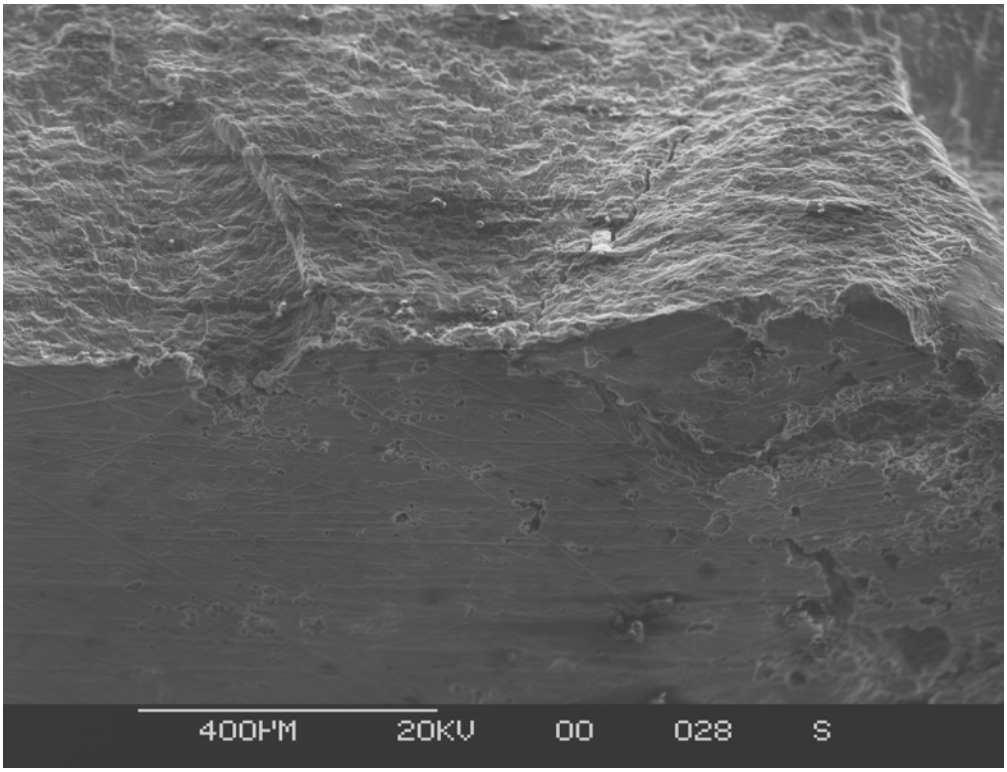

Figure B-83. Surface View of Crack Origins on Specimen 5934.

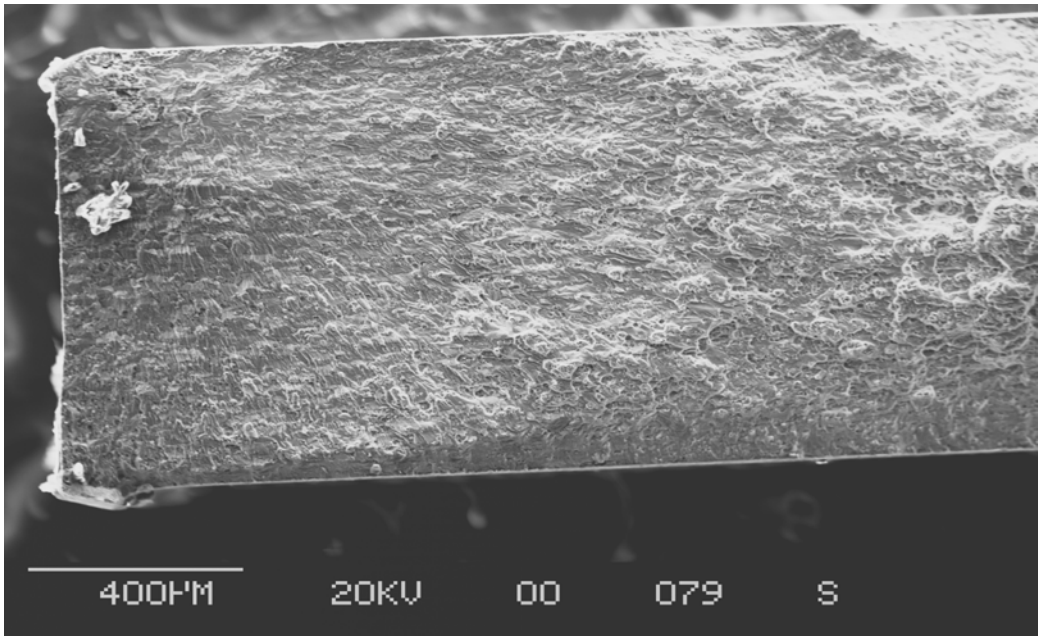

Figure B-84. Fatigue Crack on Fracture Surface of Specimen 5944.

Origin is near corner at upper left in the photograph.

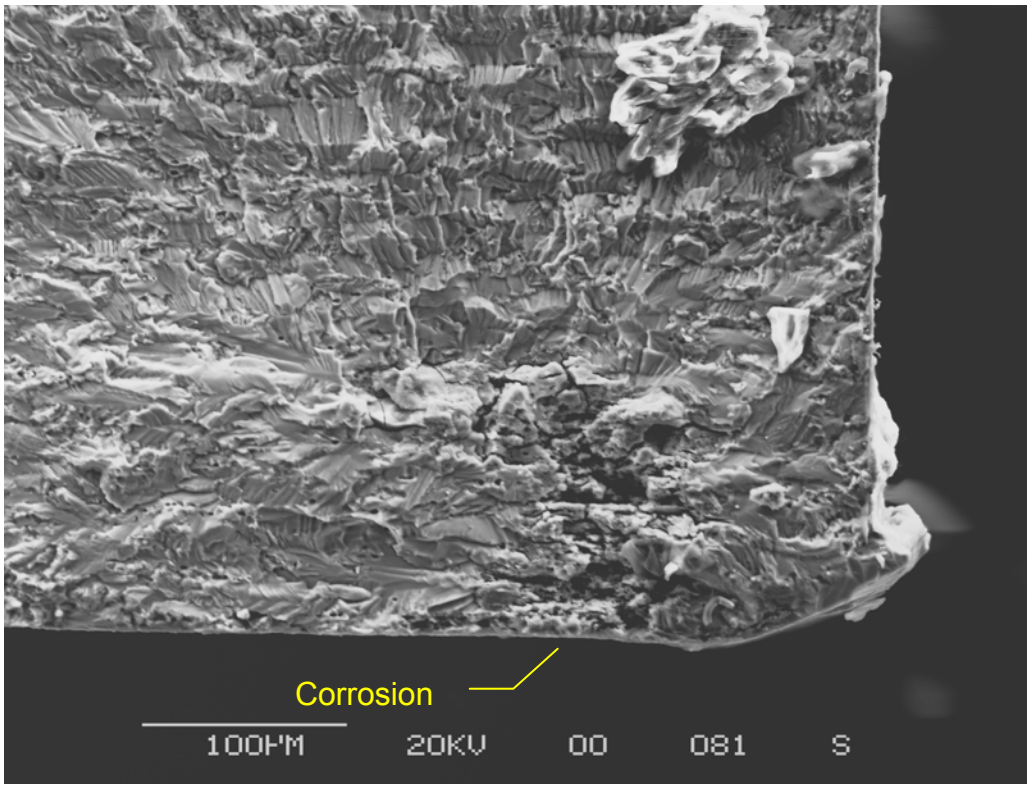

Figure B-85. Crack Origin on Specimen 5944.

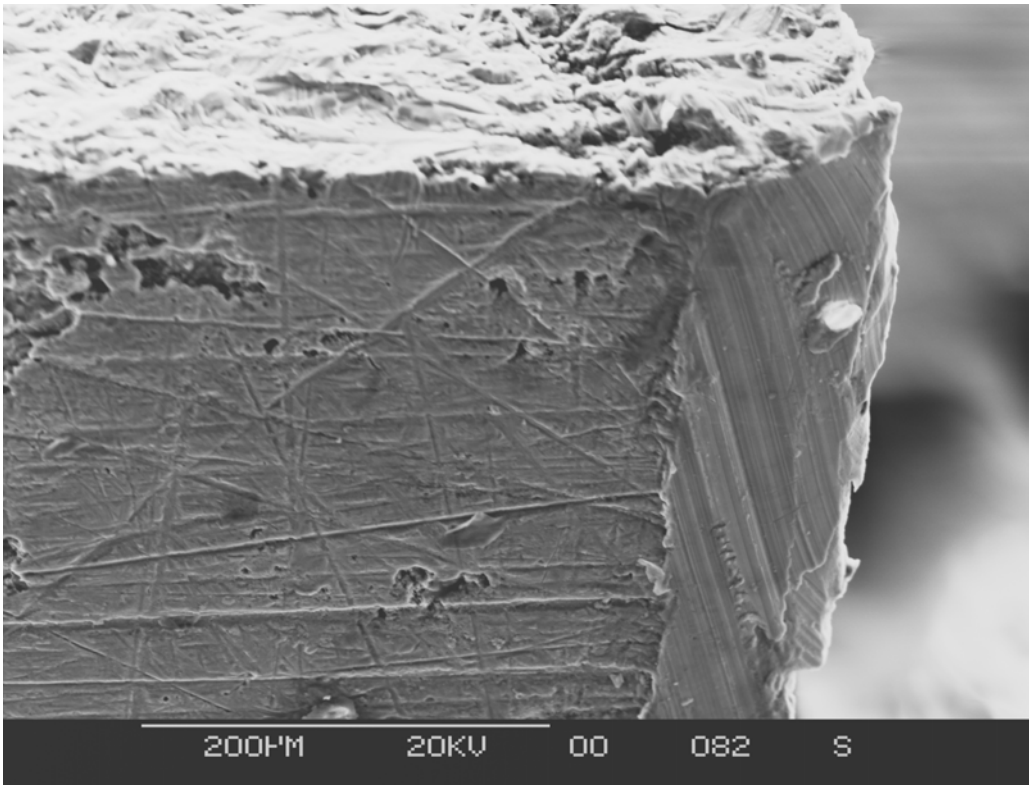

Figure B-86. Surface View of Origin on Specimen 5944.

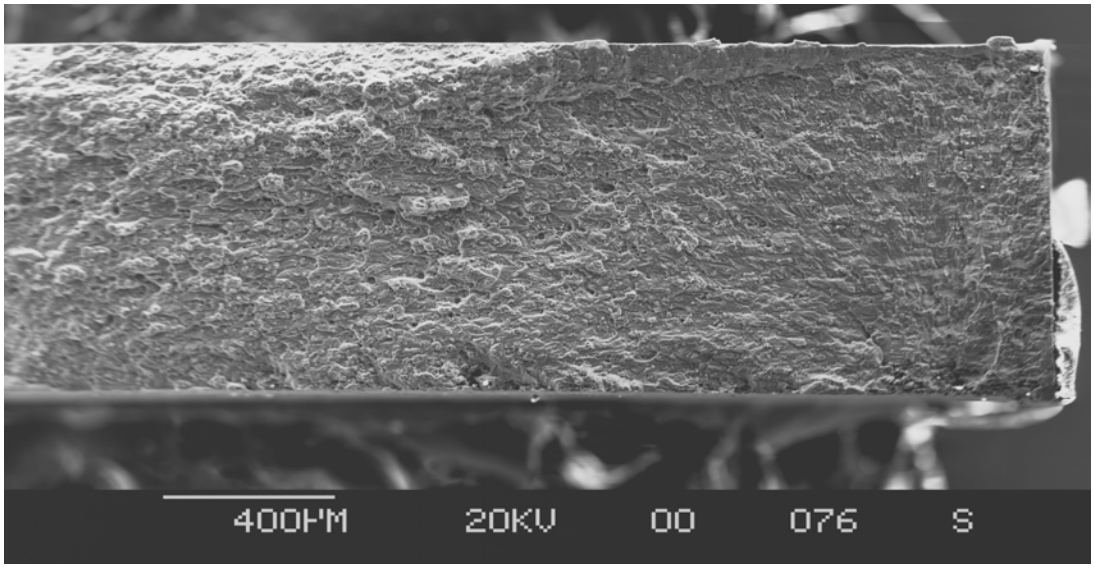

Figure B-87. Fatigue Crack on Fracture Surface of Specimen 5945.

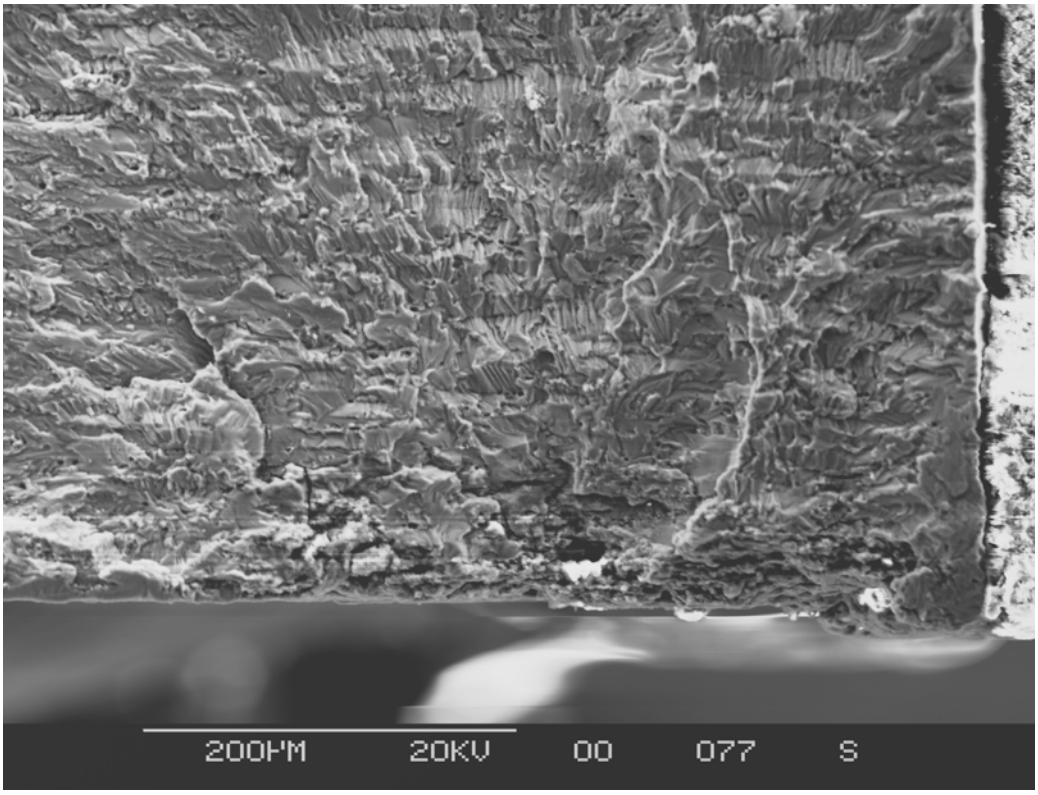

Figure B-88. Crack Origin on Specimen 5945.

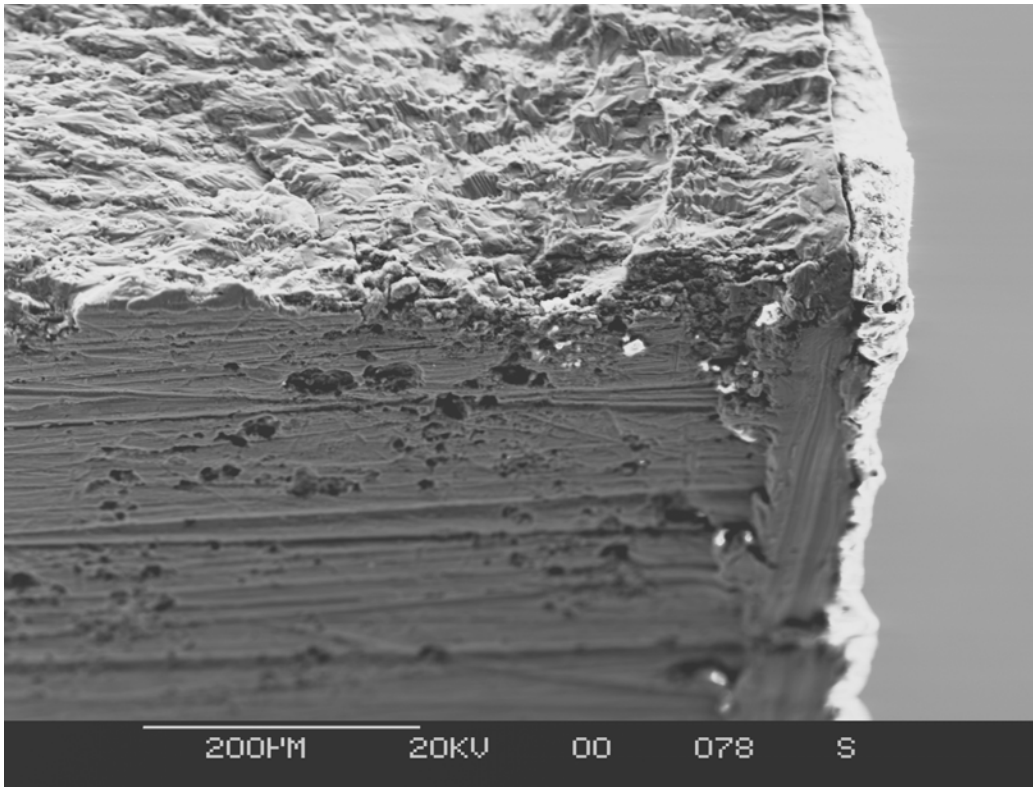

Figure B-89. Surface View of Origin on Specimen 5945.

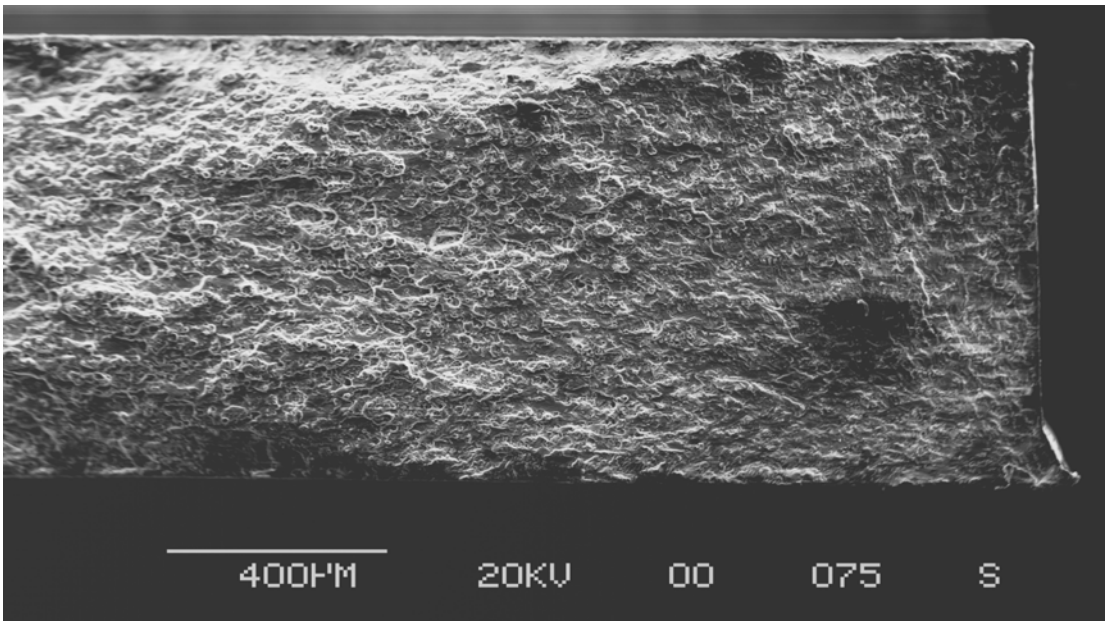

Figure B-90. Fatigue Crack on Fracture Surface of Specimen 5946.

Origin is at corner in lower right of the photograph.

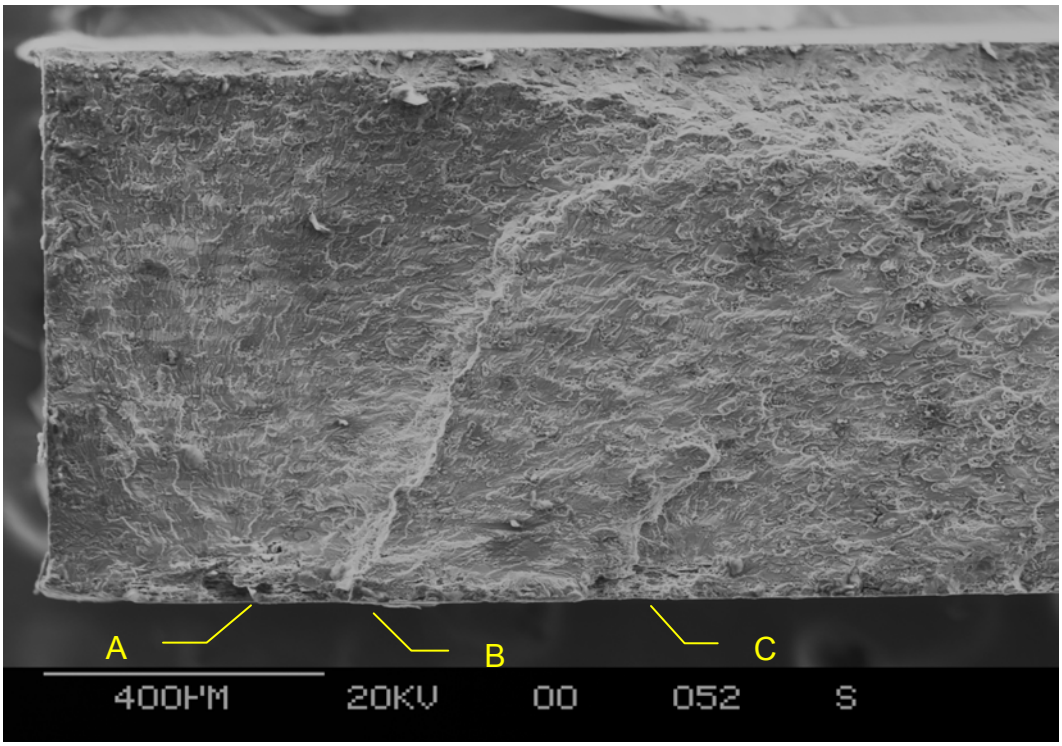

Figure B-91. Fatigue Crack on Fracture Surface of Specimen 5967.

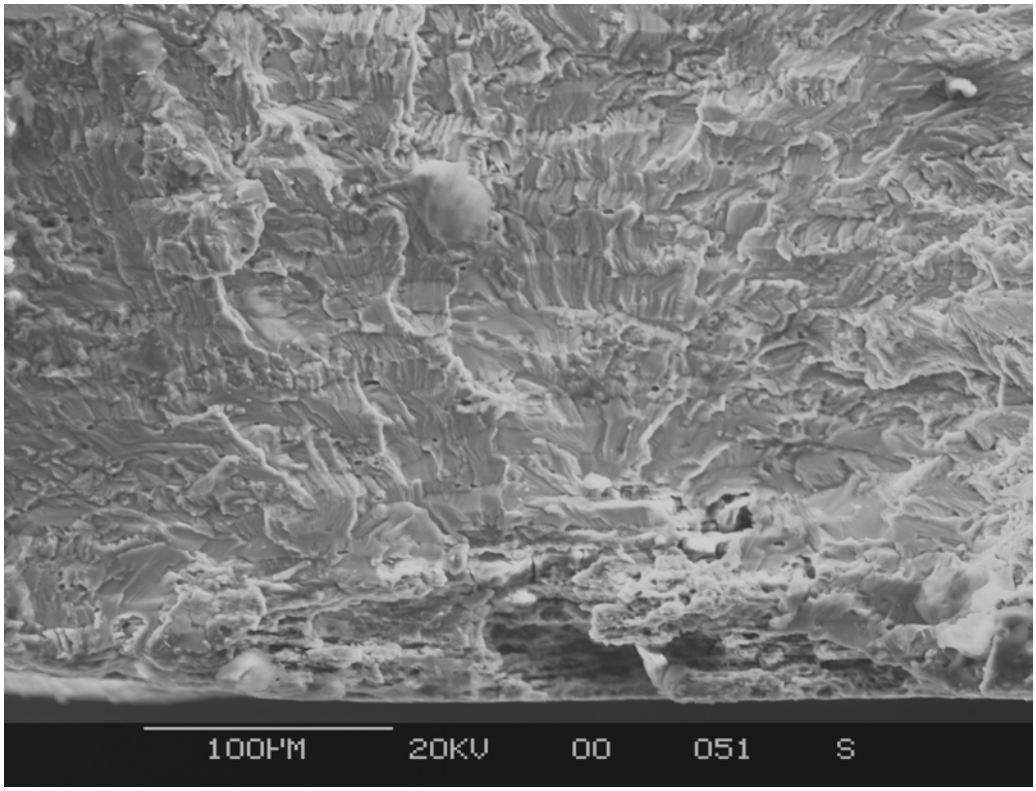

Figure B-92. Crack Origin A (Fig. B-91) on Specimen 5967.

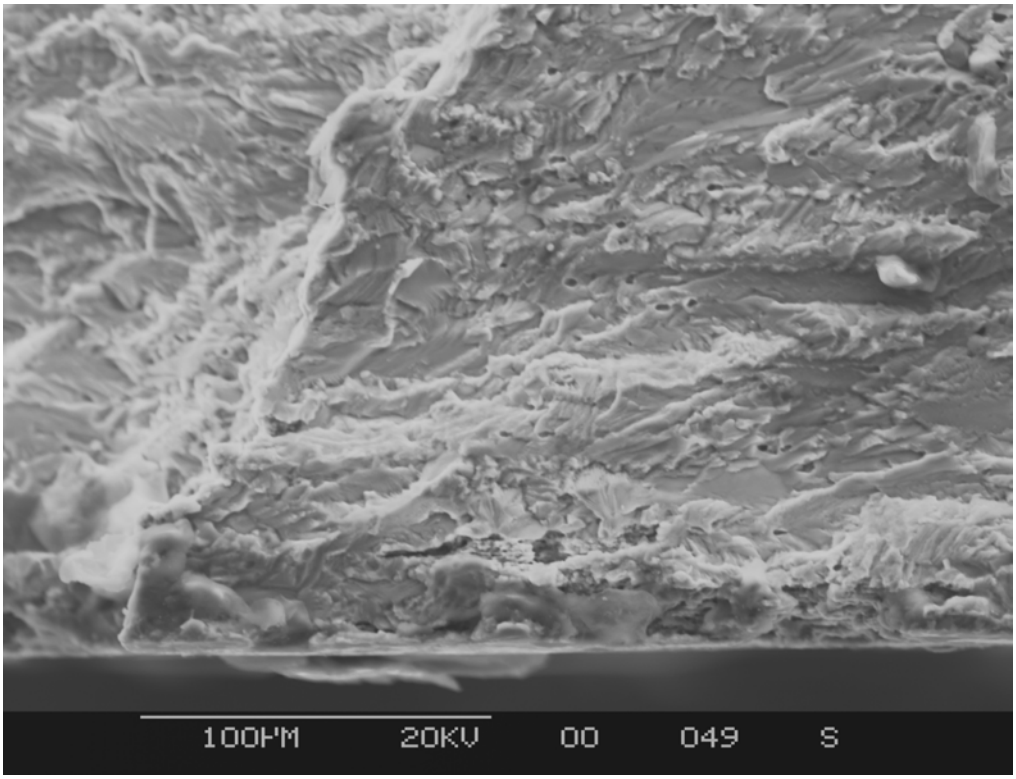

Figure B-93. Crack Origin B (Fig. B-91) on Specimen 5967.

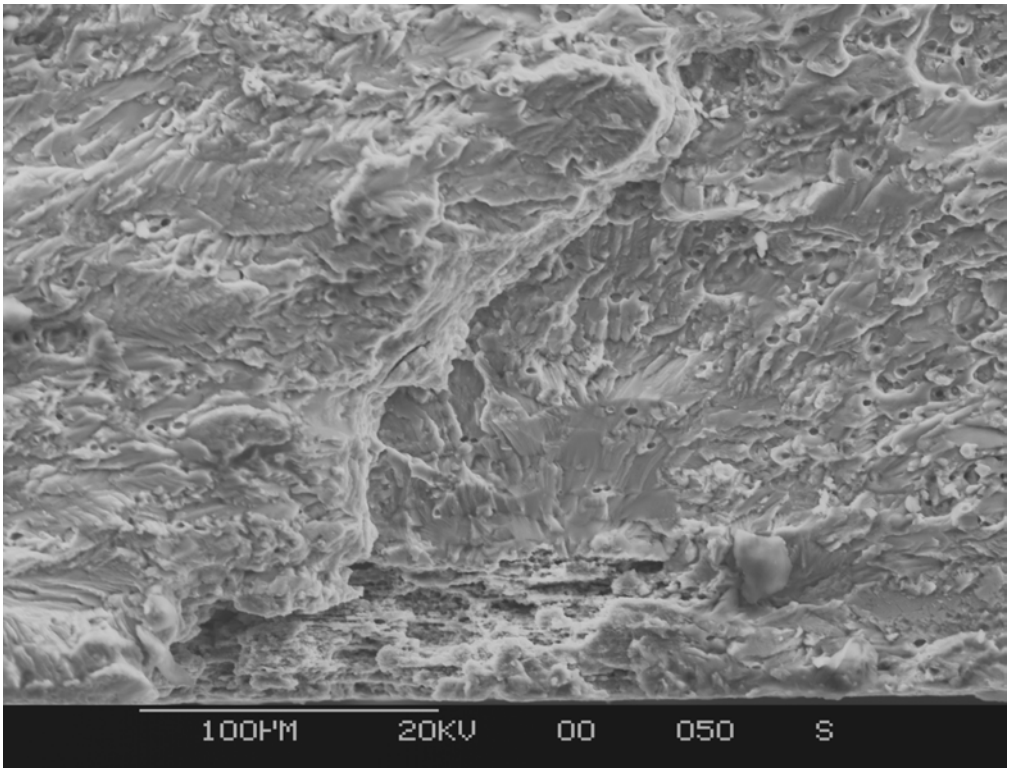

Figure B-94. Crack Origin C (Fig. B-91) on Specimen 5967.

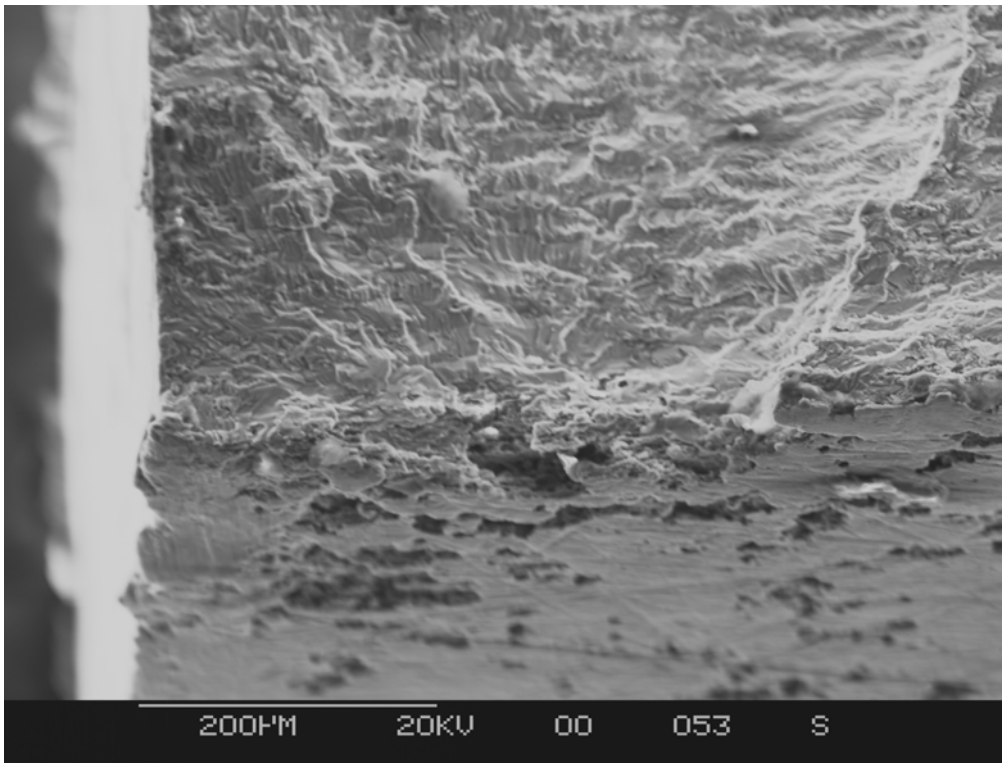

Figure B-95. Surface View of Crack Origin A on Specimen 5967.

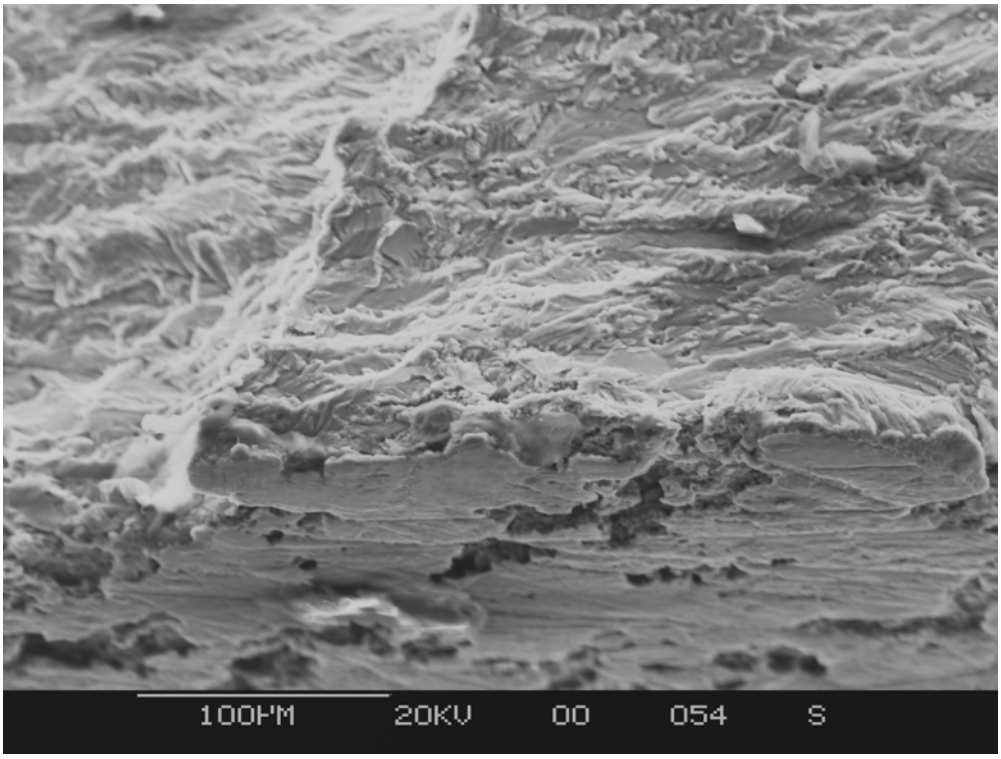

Figure B-96. Surface View of Crack Origin B on Specimen 5967.

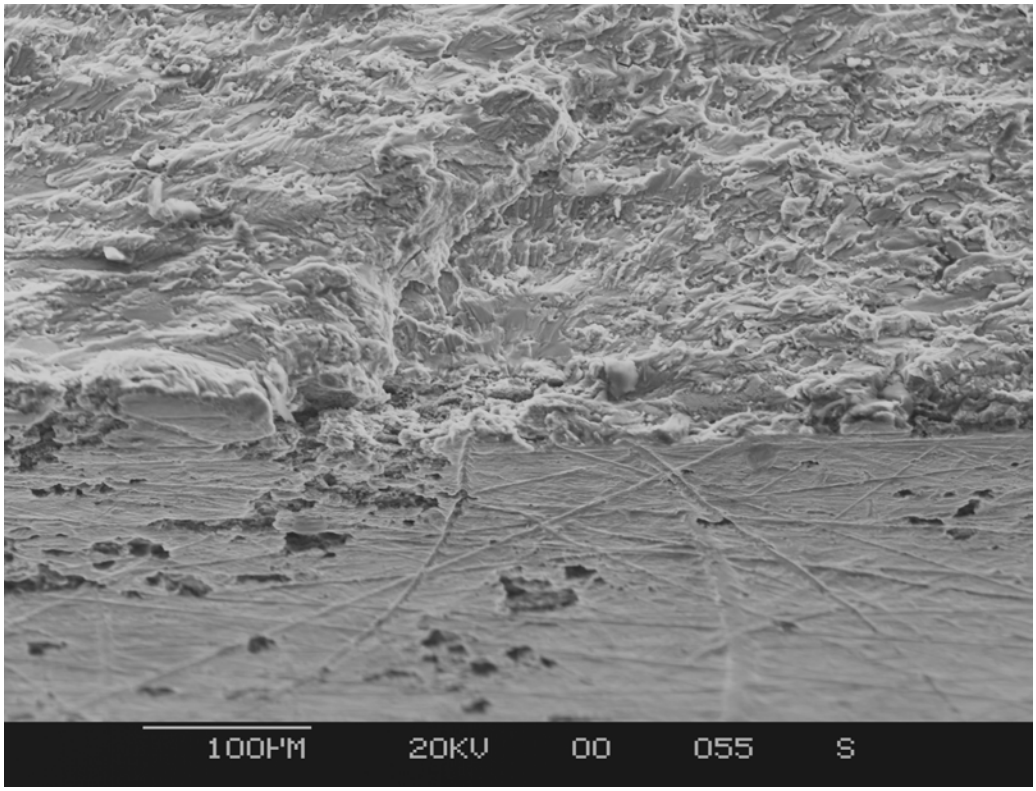

Figure B-97. Surface View of Crack Origin C on Specimen 5967.

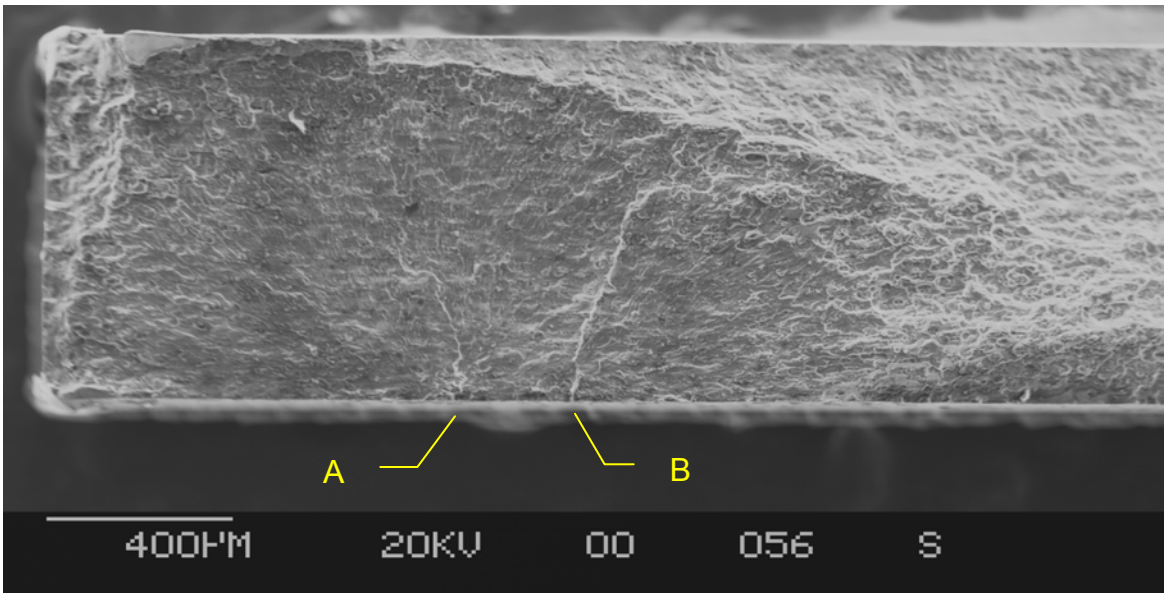

Figure B-98. Fatigue Crack on Fracture Surface of Specimen 5969.

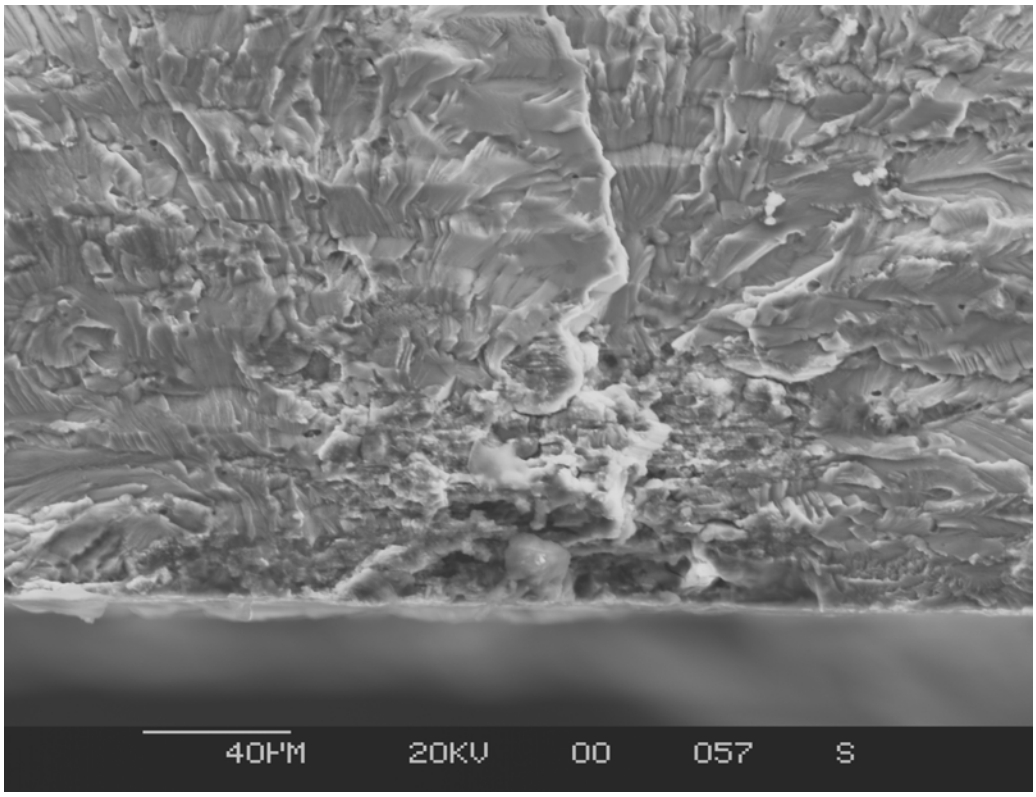

Figure B-99. Crack Origin (A in Fig. B-98) on Specimen 5969.

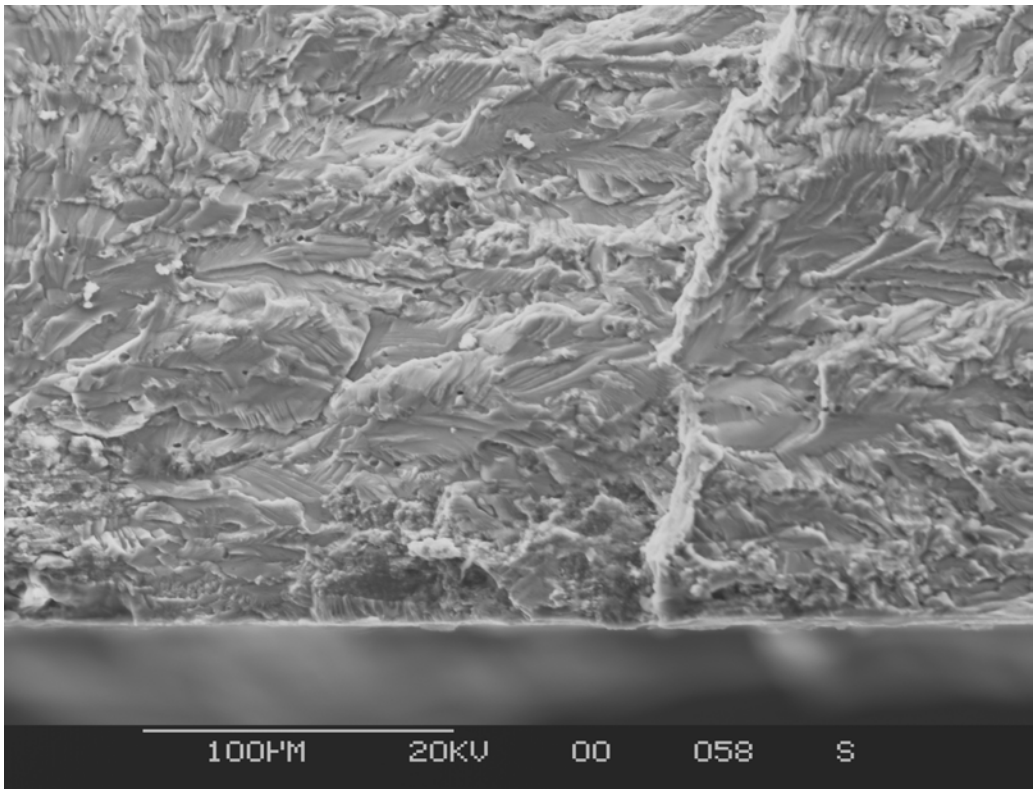

Figure B-100. Pits Adjacent to Crack Origin (B in Fig. B-98) on Specimen 5969.

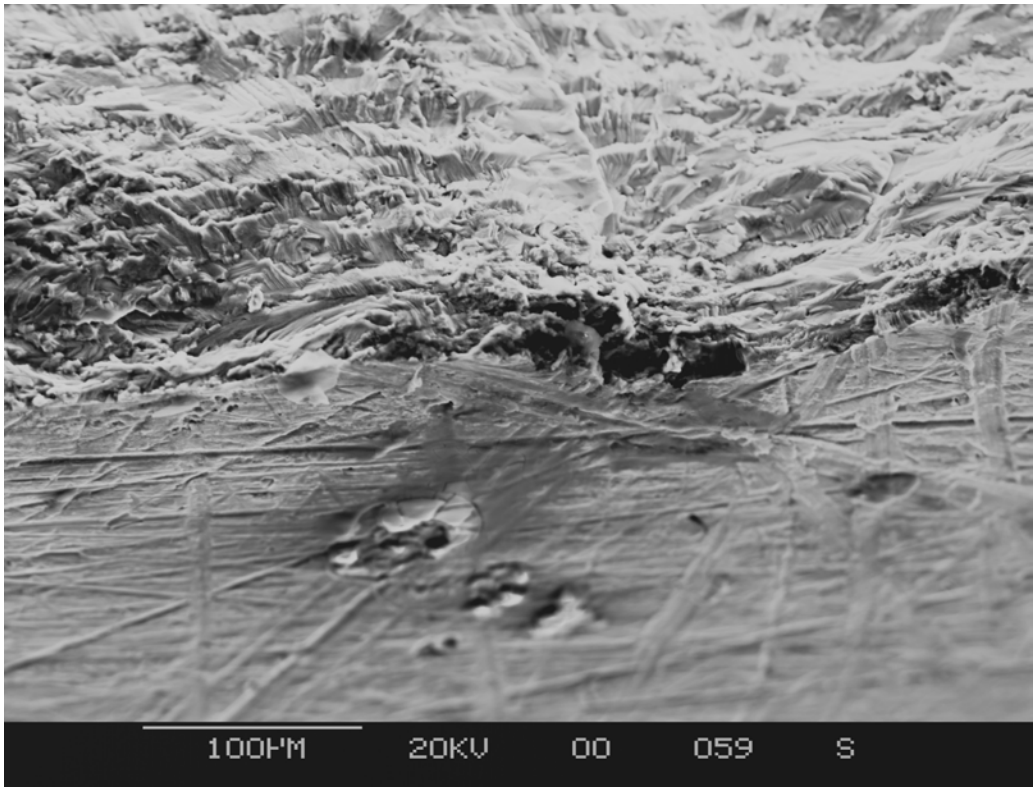

Figure B-101. Surface View of Crack Origin (A in Fig. B-98) on Specimen 5969.

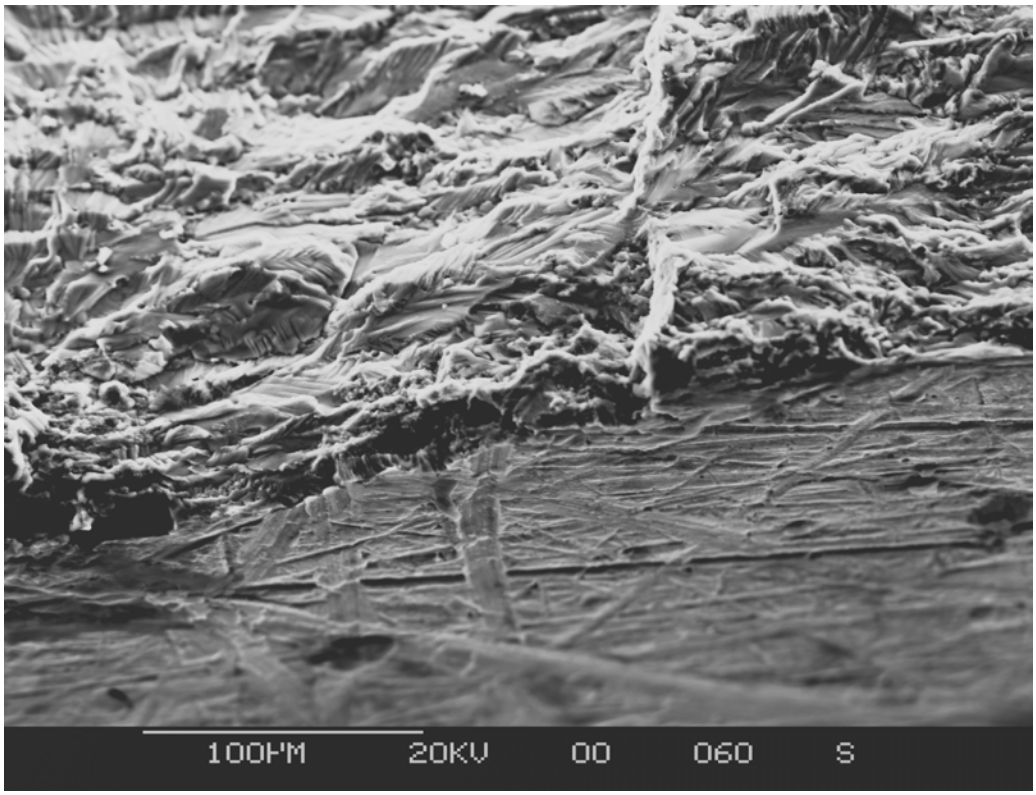

Figure B-102. Surface View of Pits Adjacent to Crack Origin (B in Fig. B-98) on Specimen 5969.

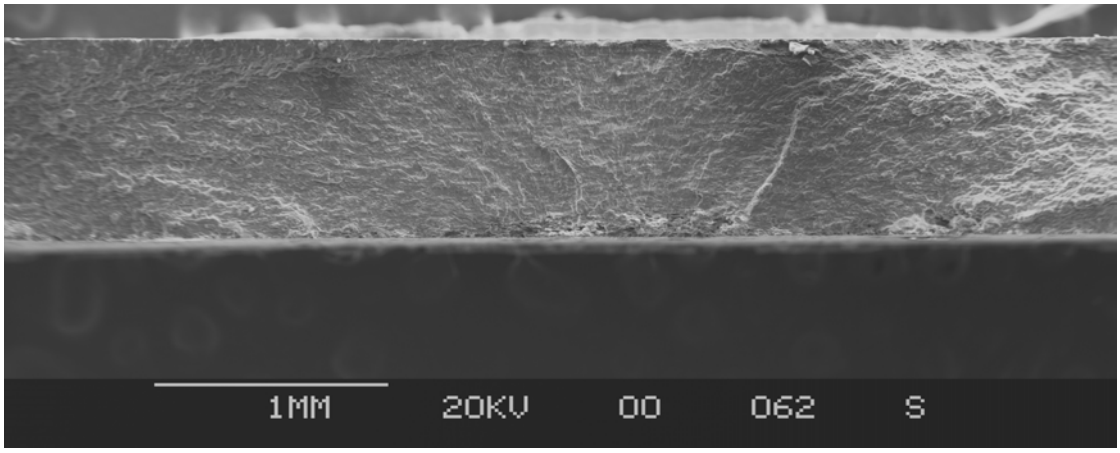

Figure B-103. Fatigue Crack on Fracture Surface of Specimen 6002 Showing Multiple Origins.

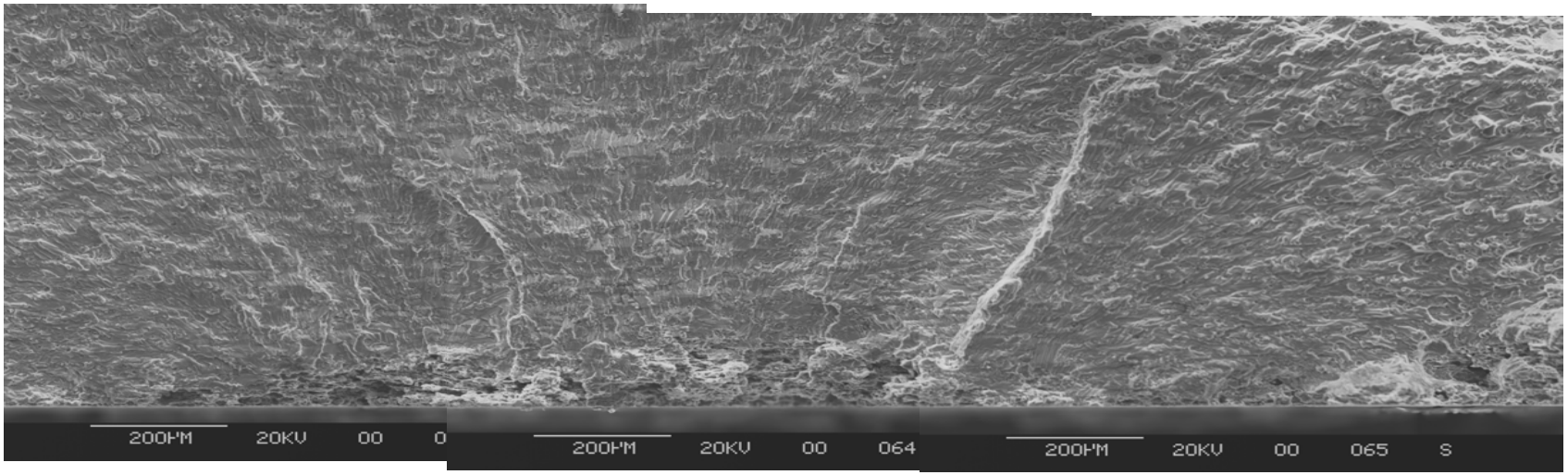

Figure B-104. Composite Photo of Crack Origins on Specimen 6002.

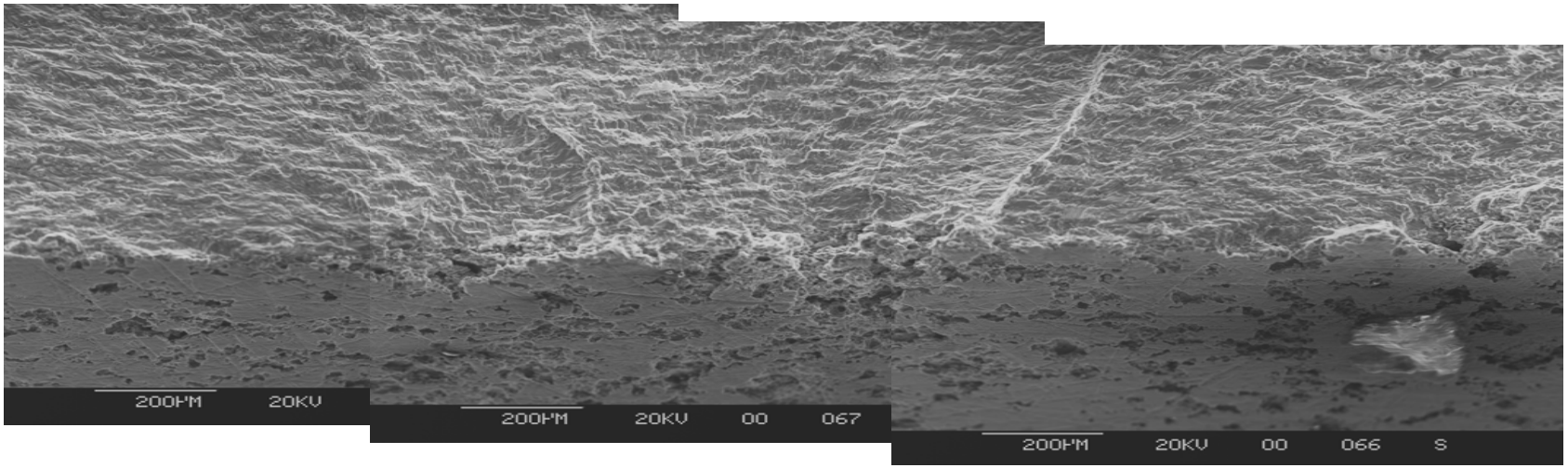

Figure B-105. Edge View of Crack Origins on Specimen 6002.

APPENDIX C: Surface Roughness Measurements for Select Specimens

Digital data was recorded at 0.025 in. (0.64 mm) intervals during a stylus travel of 0.25 in. (6.4 mm). A single trace on the front or back face was made as near as possible to the fracture surface. Software provided with the instrument converted the surface trace into a roughness profile, i.e., deviations from the mean. The roughness profiles were converted to single value representations of roughness using the following formulae.

Average roughness: $R_a = \frac{1}{N}\sum_{n=1}^{N}|r_n|$

RMS roughness: $R_q = \sqrt{\frac{1}{N}\sum_{n=1}^{N}r_n^2}$

Peak: $R_p = |\max(r_n)|$

Valley, $R_v = |\min(r_n)|$

Peak-to-Valley, $R_t = R_p + R_v$

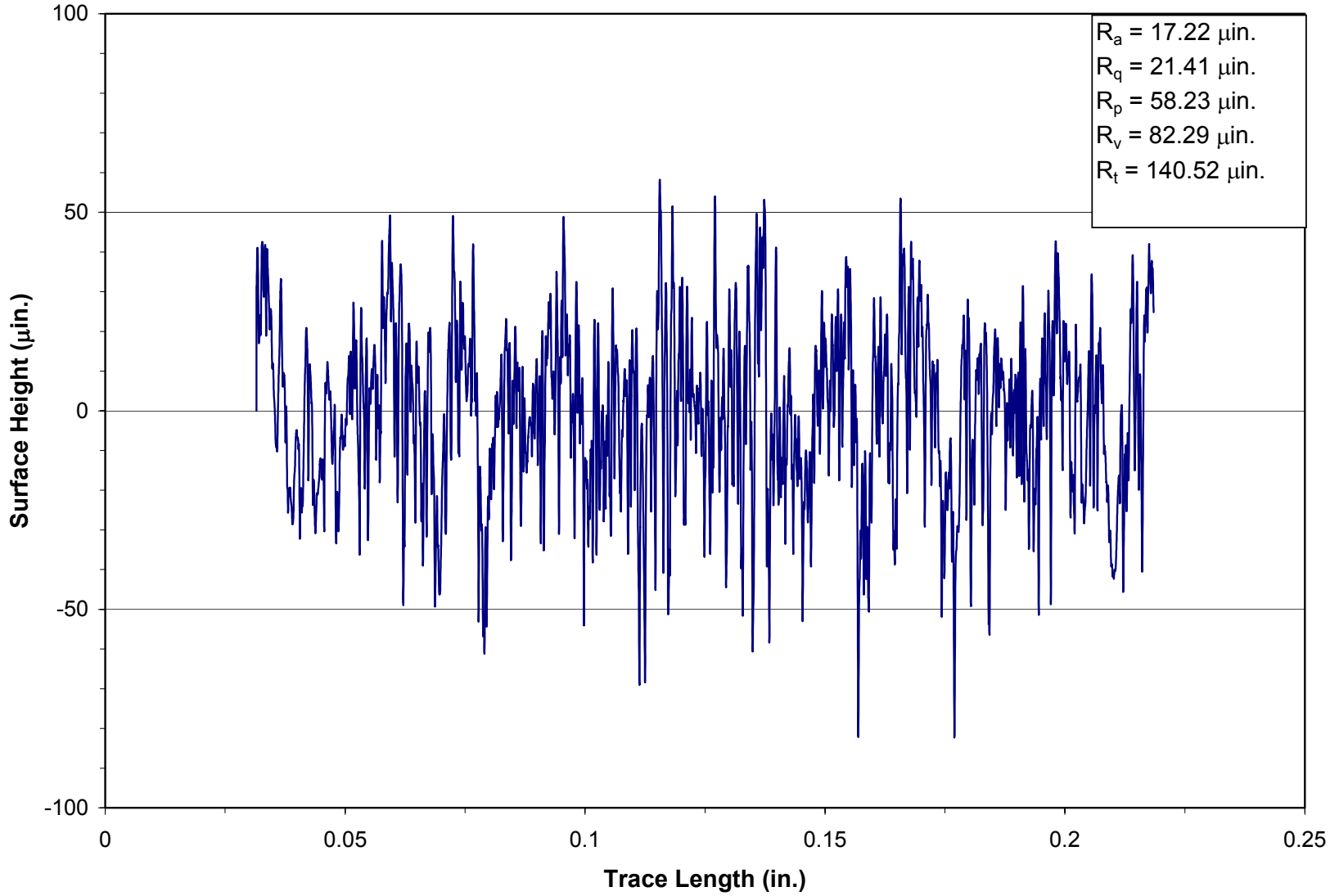

Figure C-1. Roughness Profile from Specimen N1.

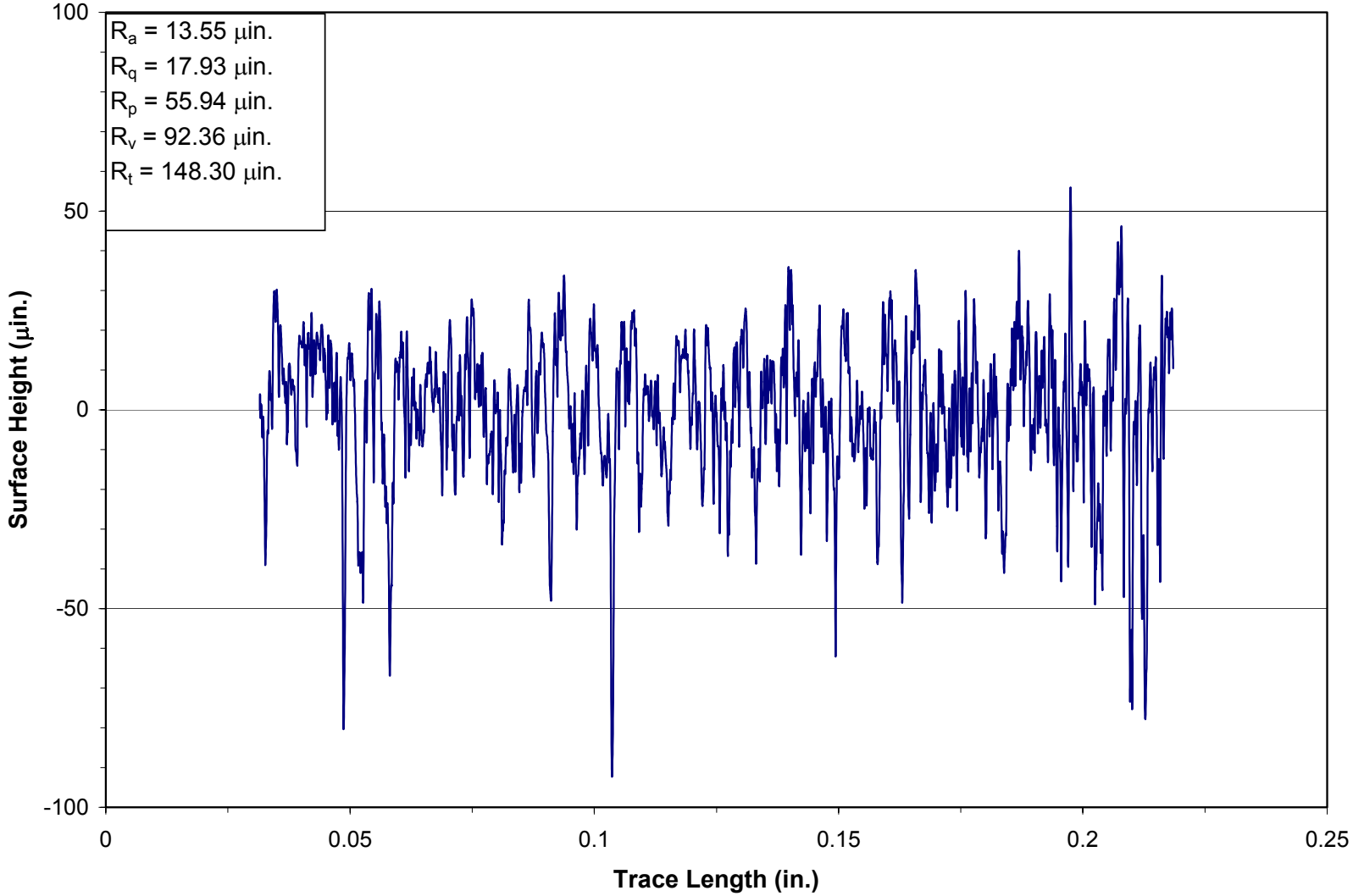

Figure C-2. Roughness Profile from Specimen N2.

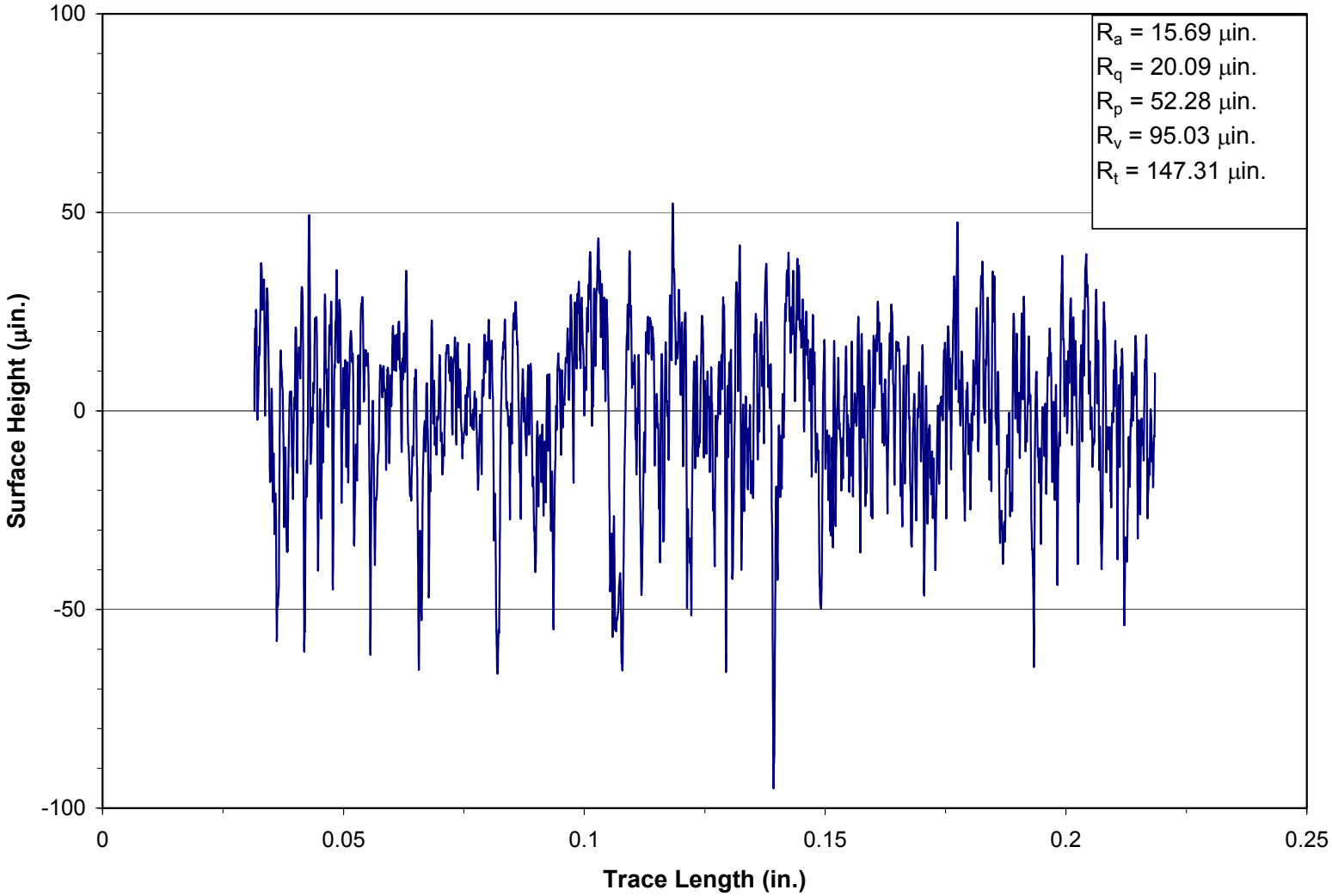

Figure C-3. Roughness Profile from Specimen N3.

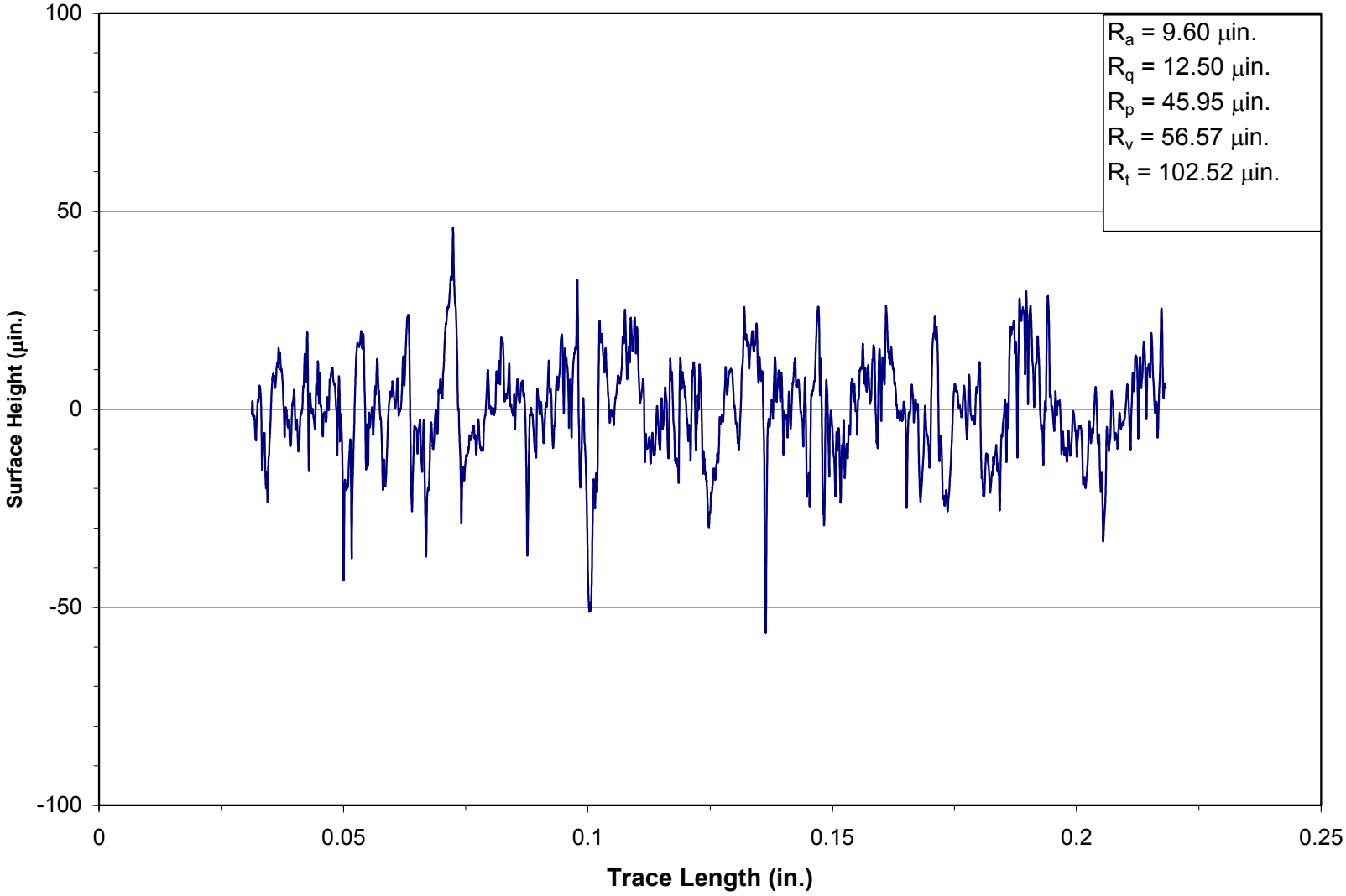

Figure C-4. Roughness Profile from Specimen 0000.

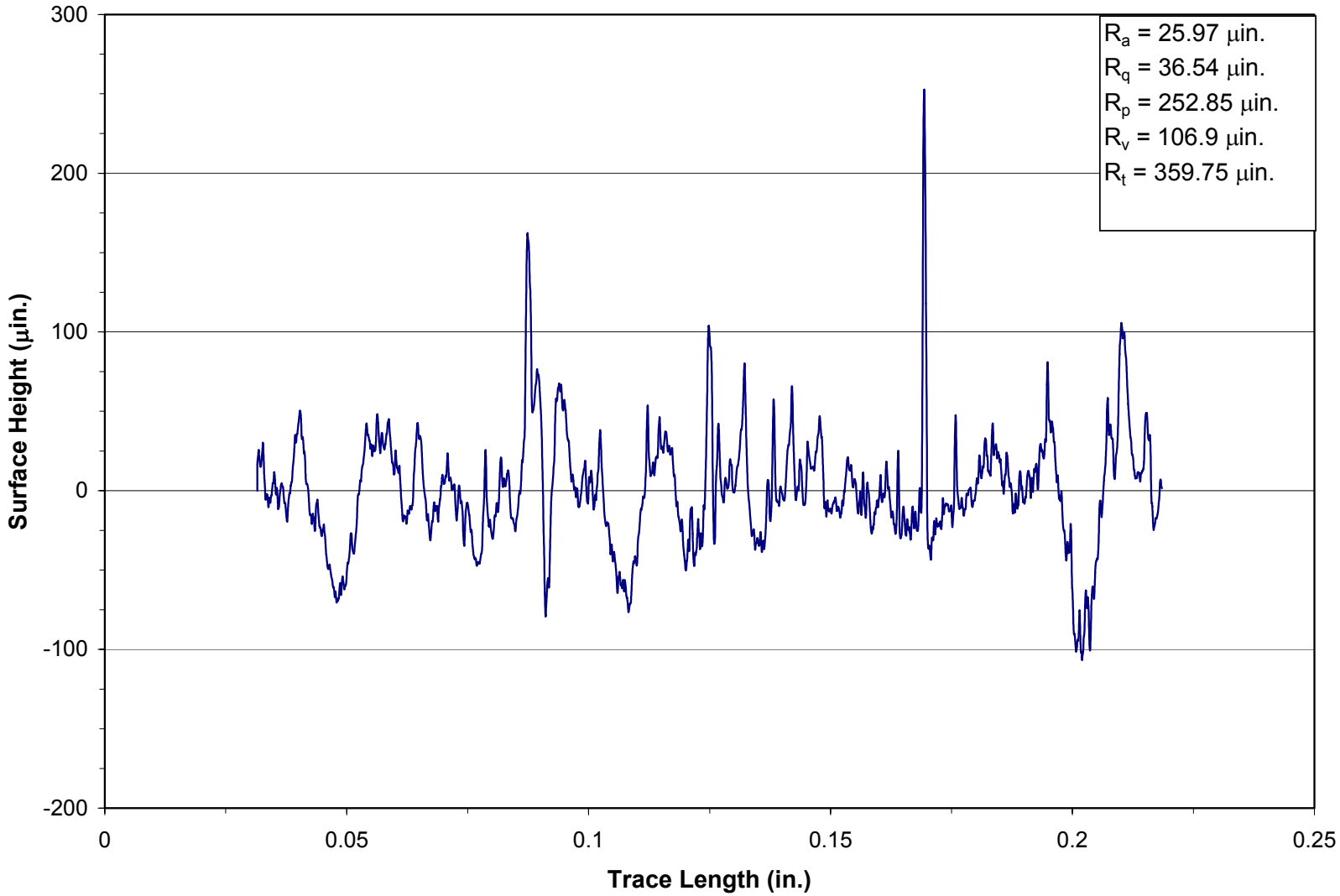

Figure C-5. Roughness Profile from Specimen 1331.

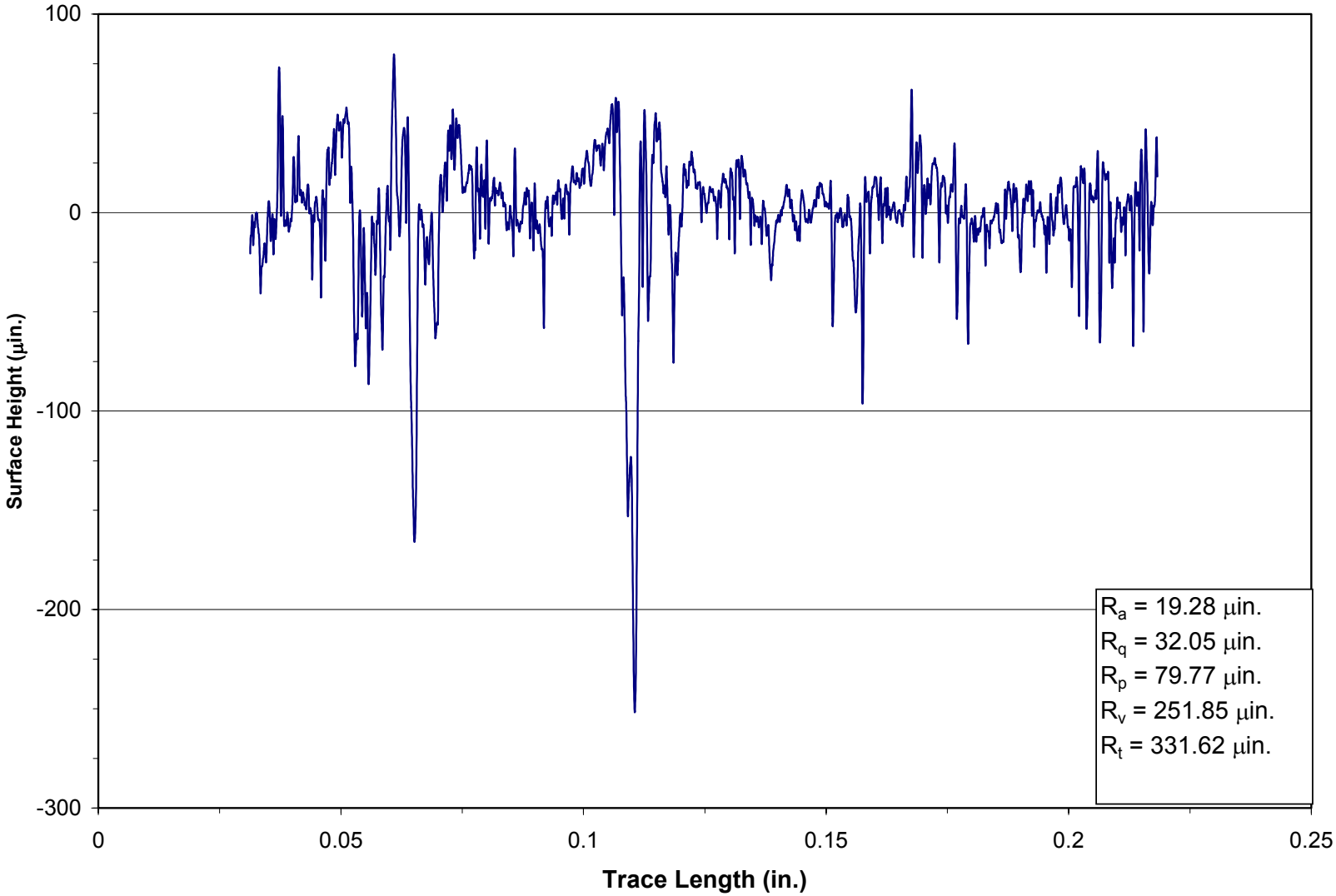

Figure C-6. Roughness Profile from Specimen 5607.

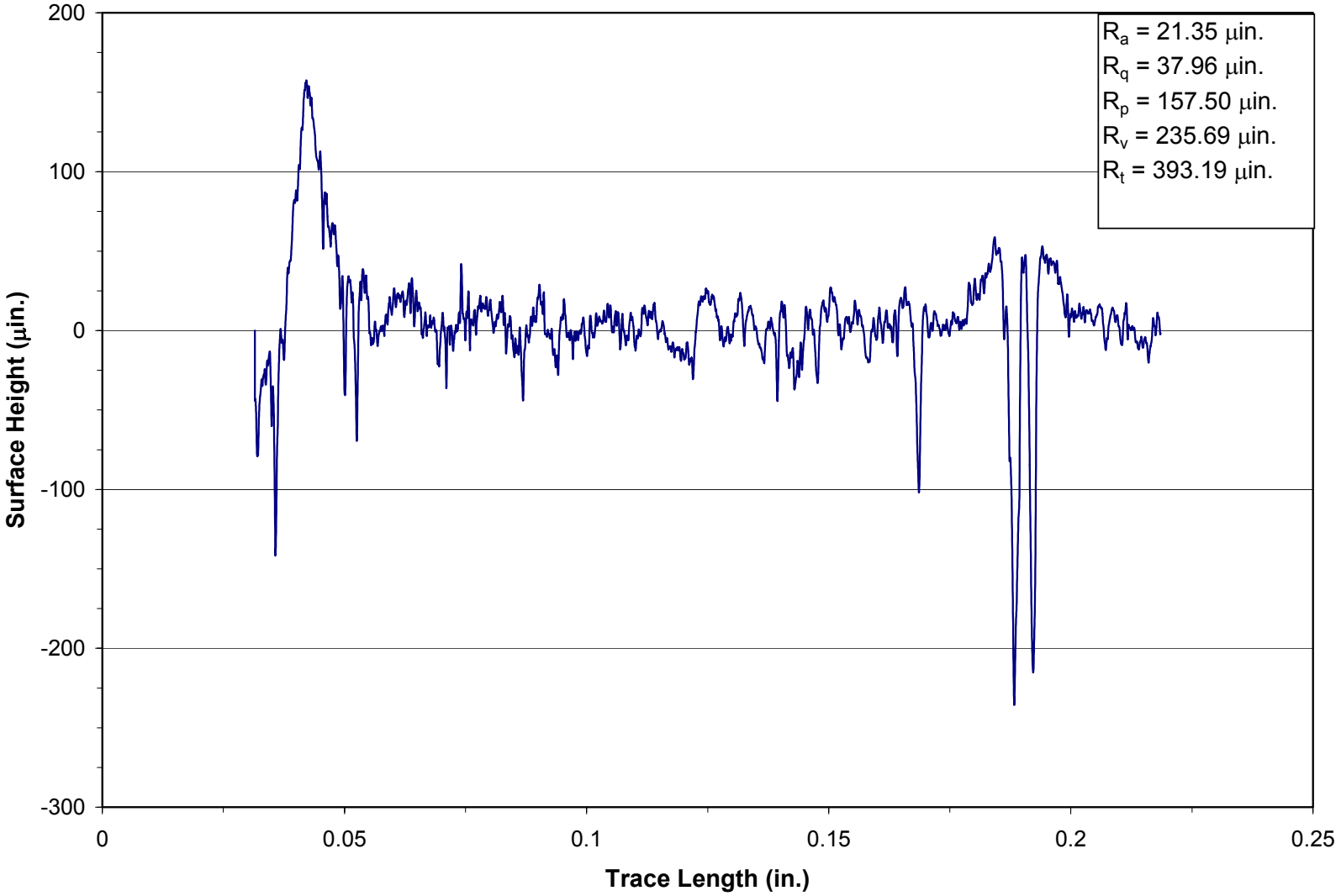

Figure C-7. Roughness Profile from Specimen 5608.

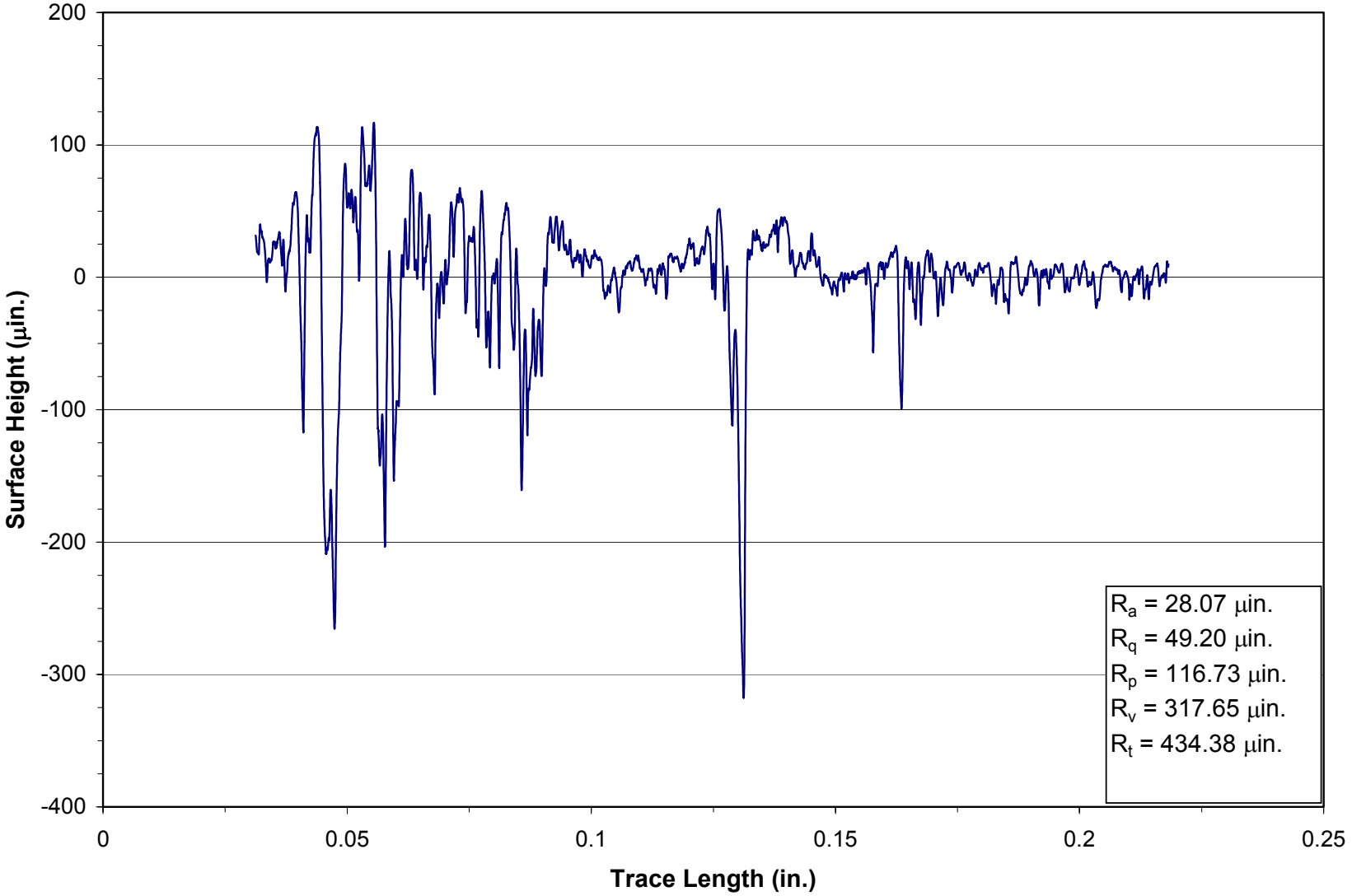

Figure C-8. Roughness Profile from Specimen 5615.

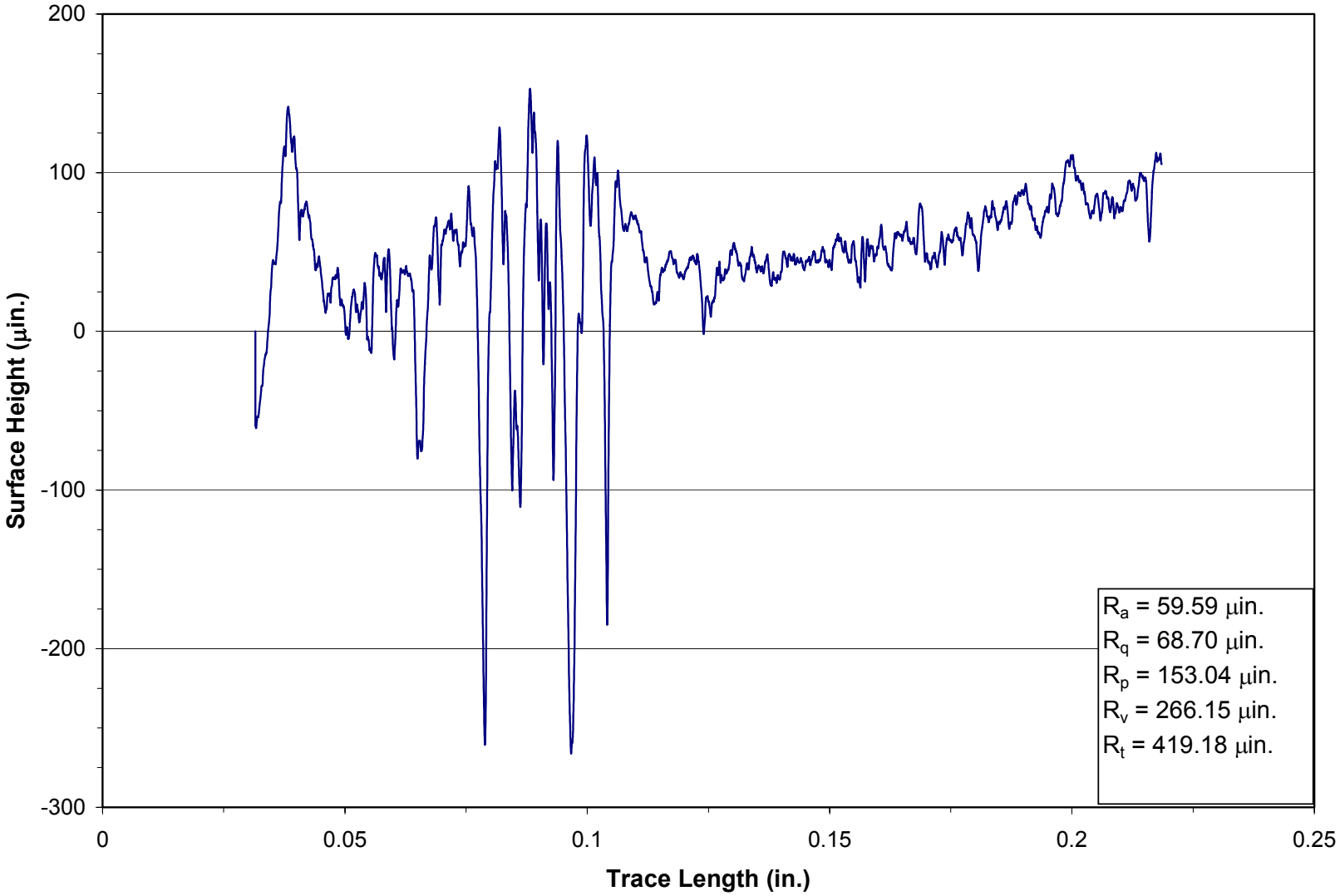

Figure C-9. Roughness Profile from Specimen 5616.

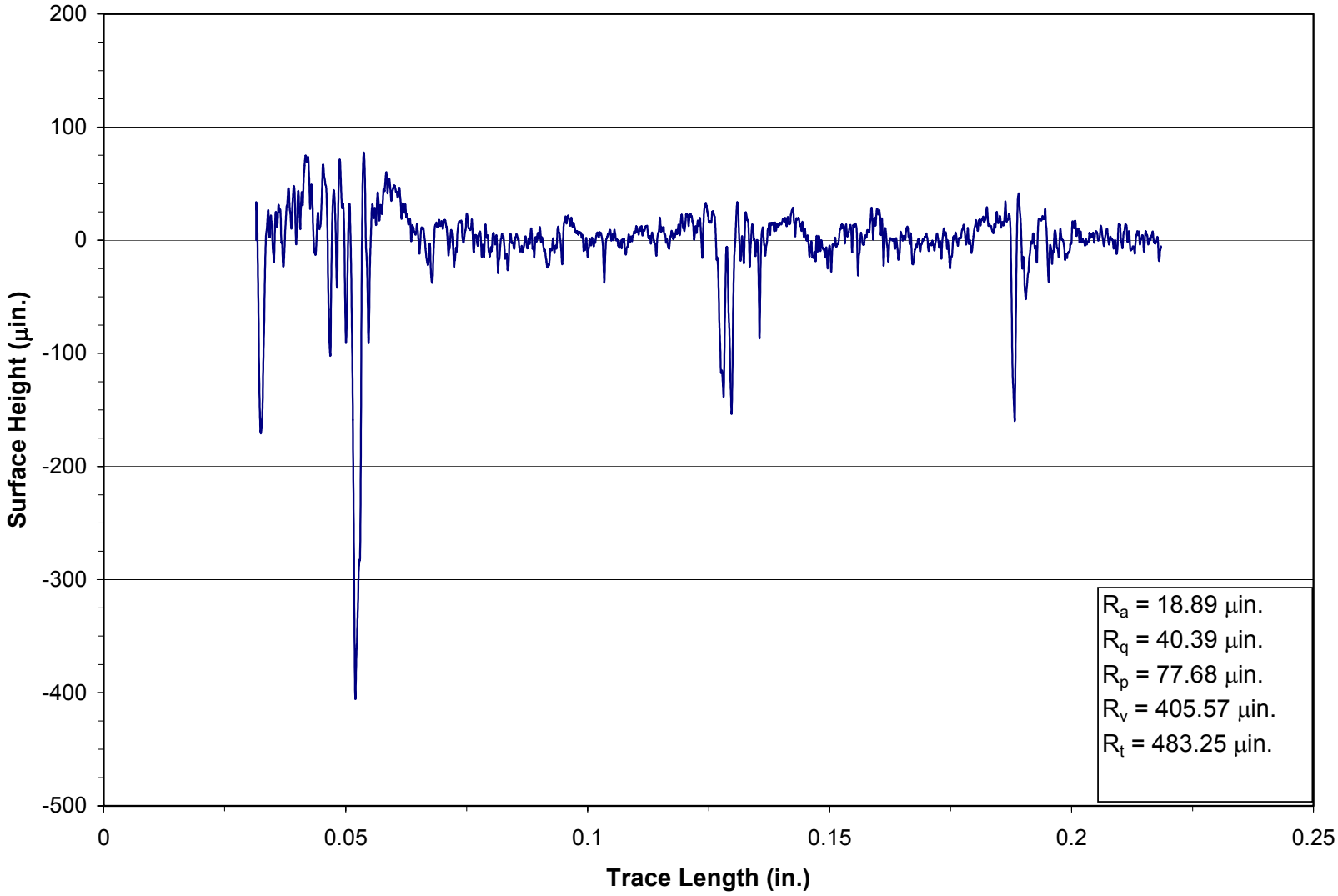

Figure C-10. Roughness Profile from Specimen 5618.

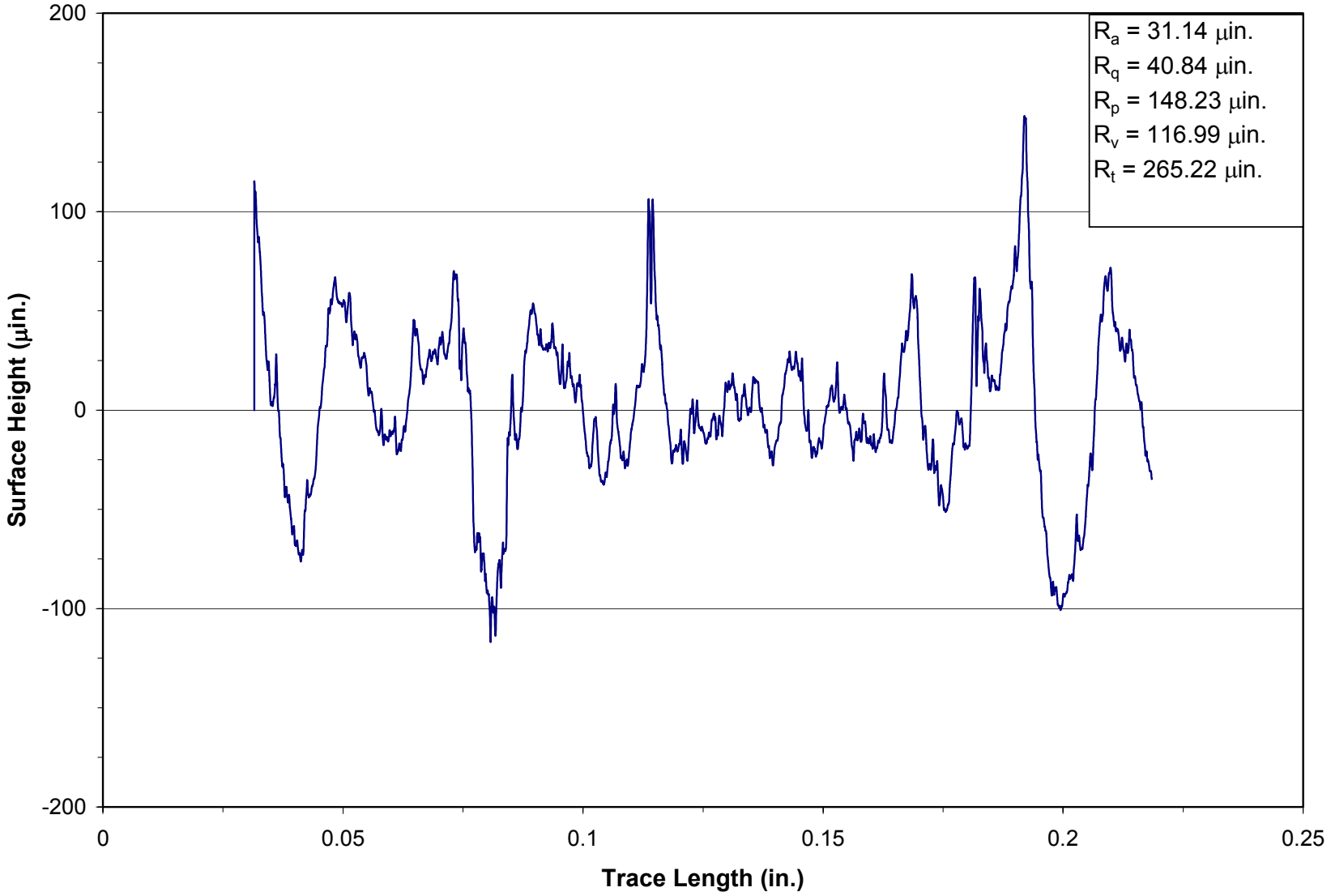

Figure C-11. Roughness Profile from Specimen 5635.

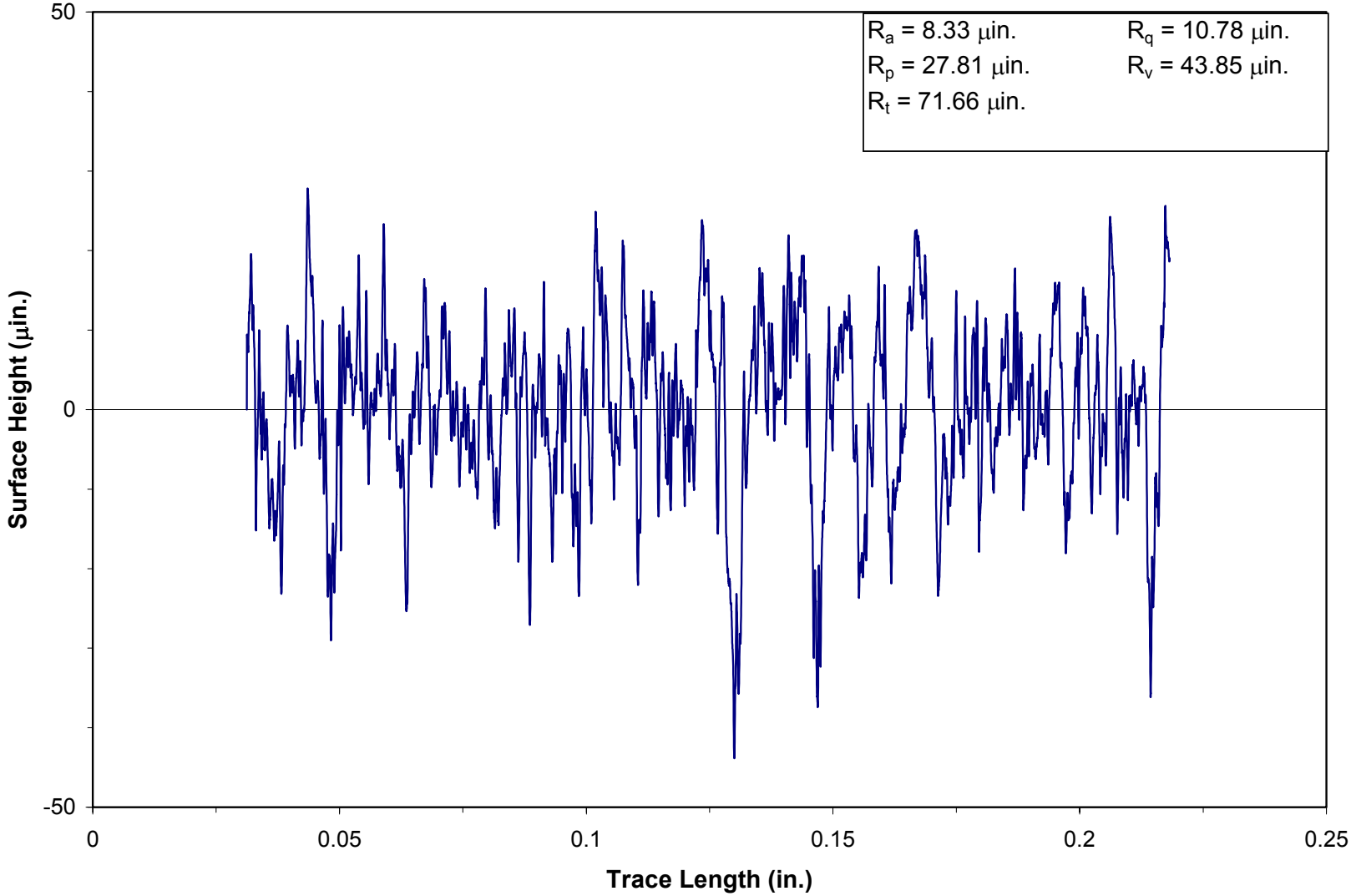

Figure C-12. Roughness Profile from Specimen 5636.

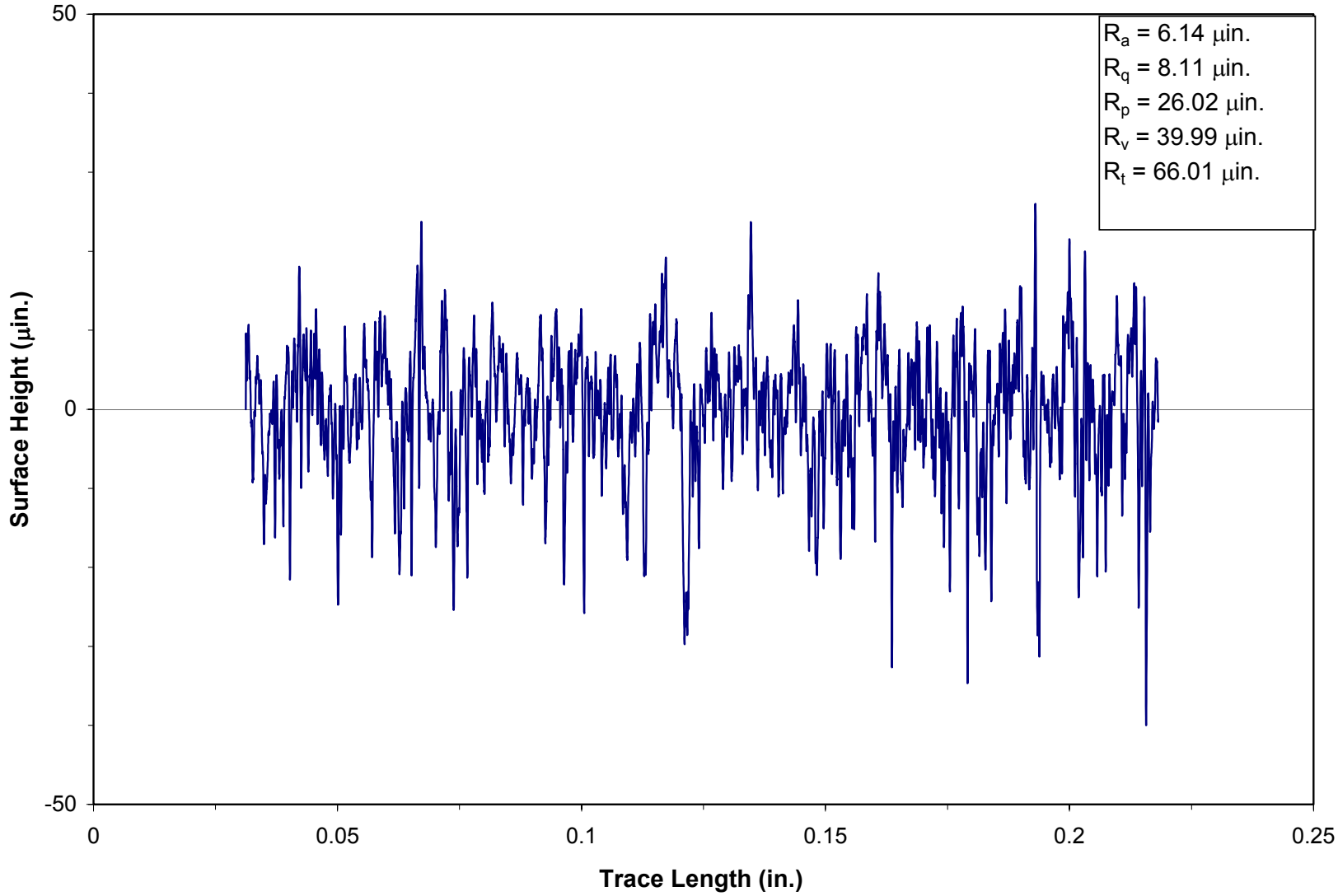

Figure C-13. Roughness Profile from Specimen 5708.

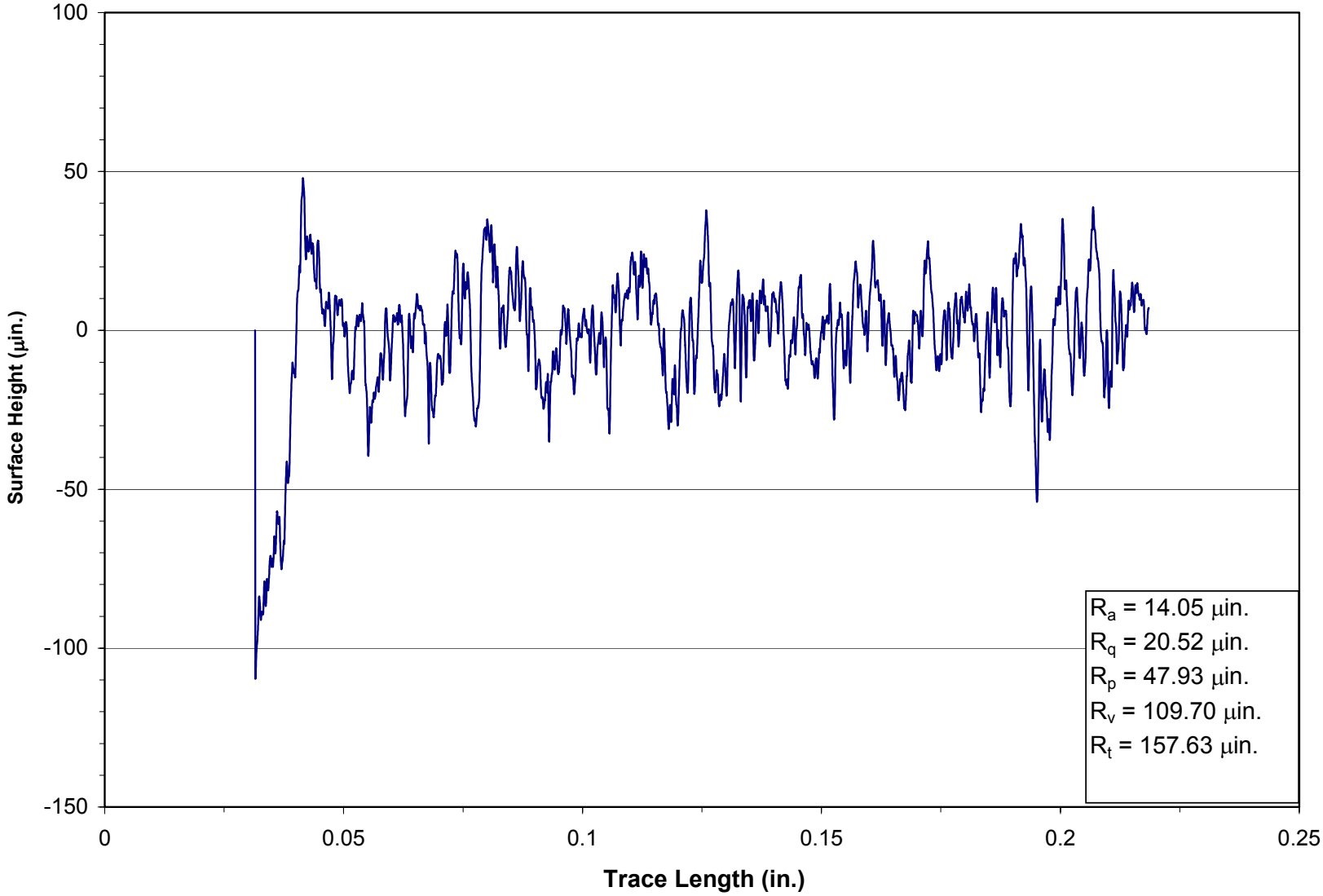

Figure C-14. Roughness Profile from Specimen 5710A.

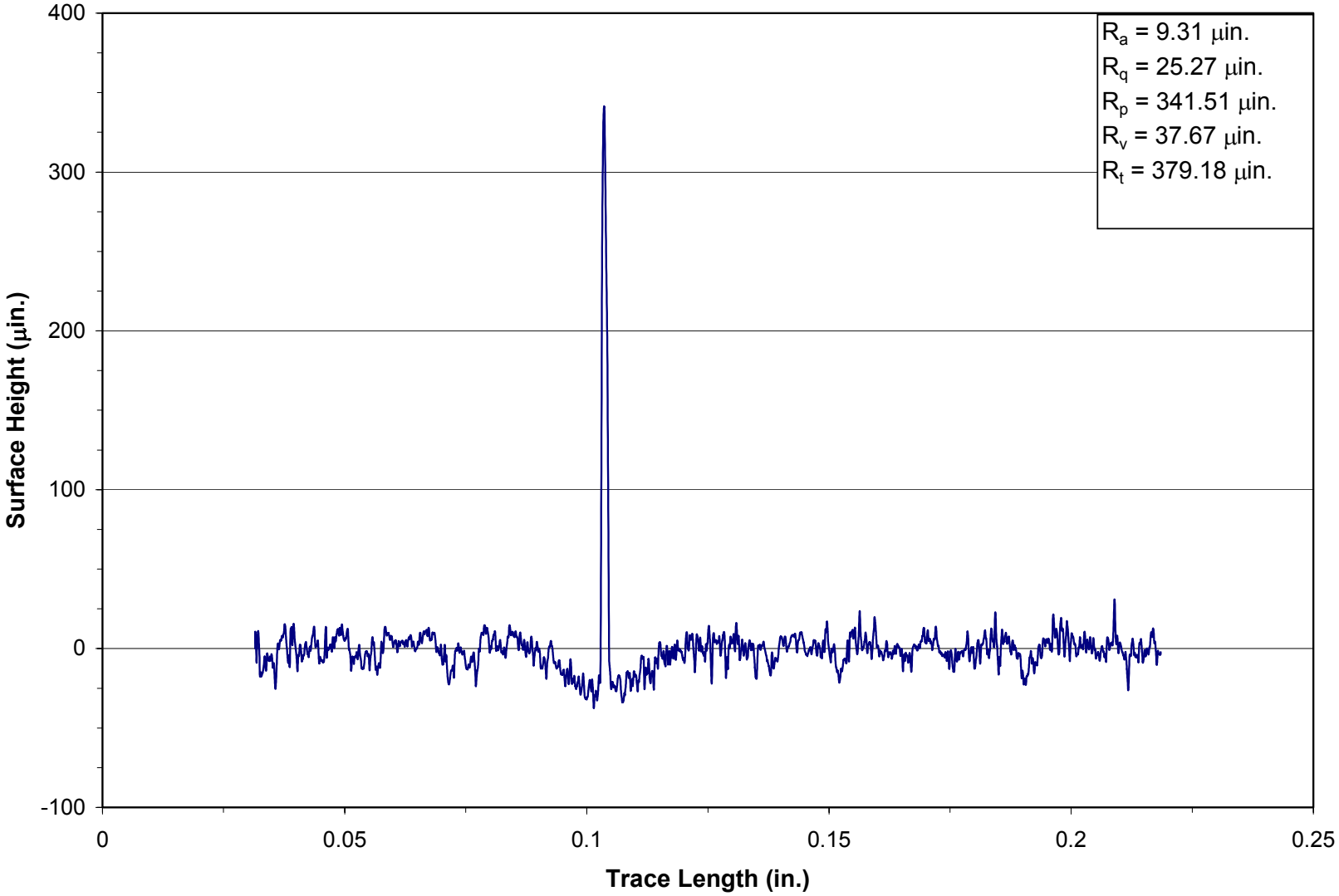

Figure C-15. Roughness Profile from Specimen 5710B.

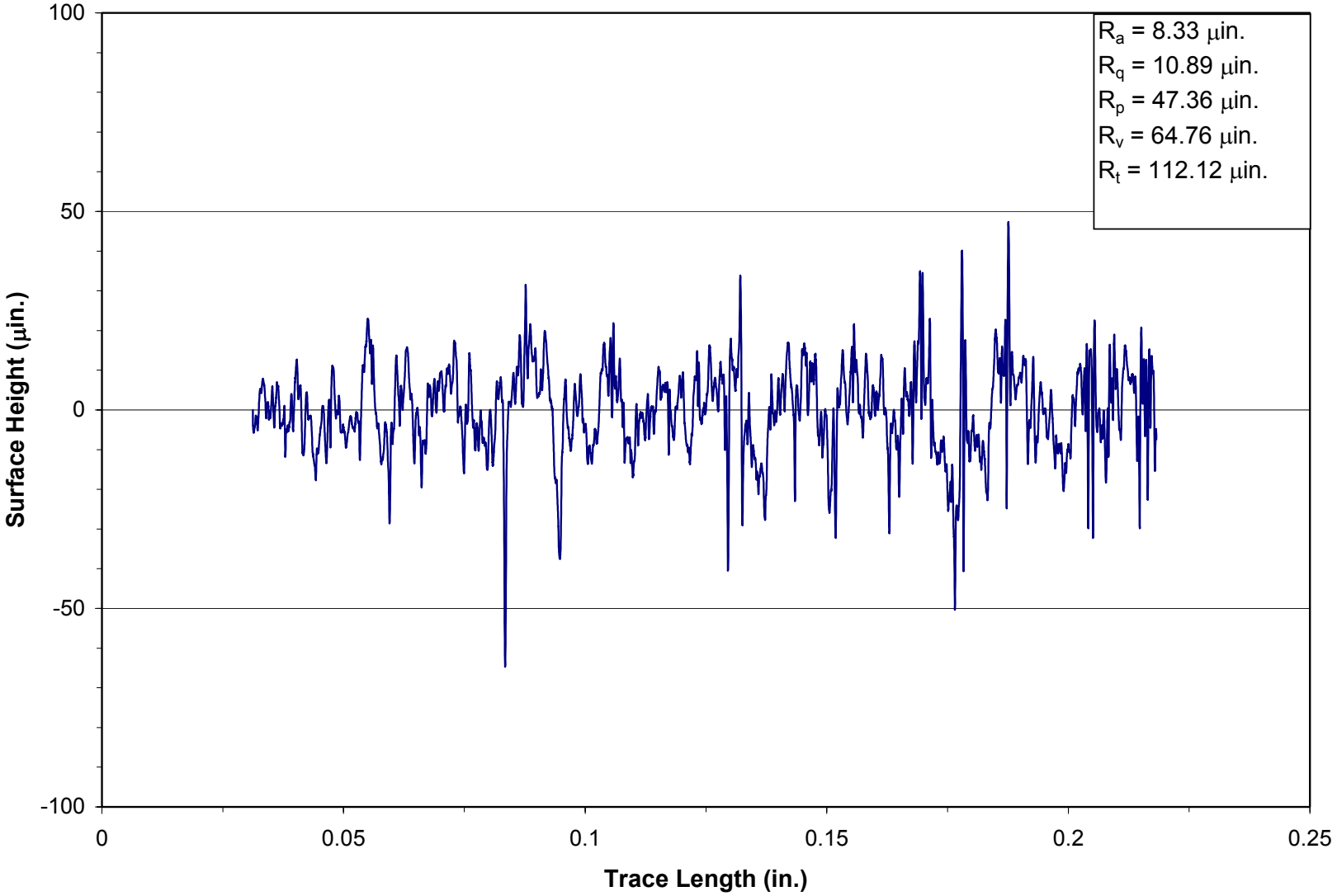

Figure C-16. Roughness Profile from Specimen 5772.

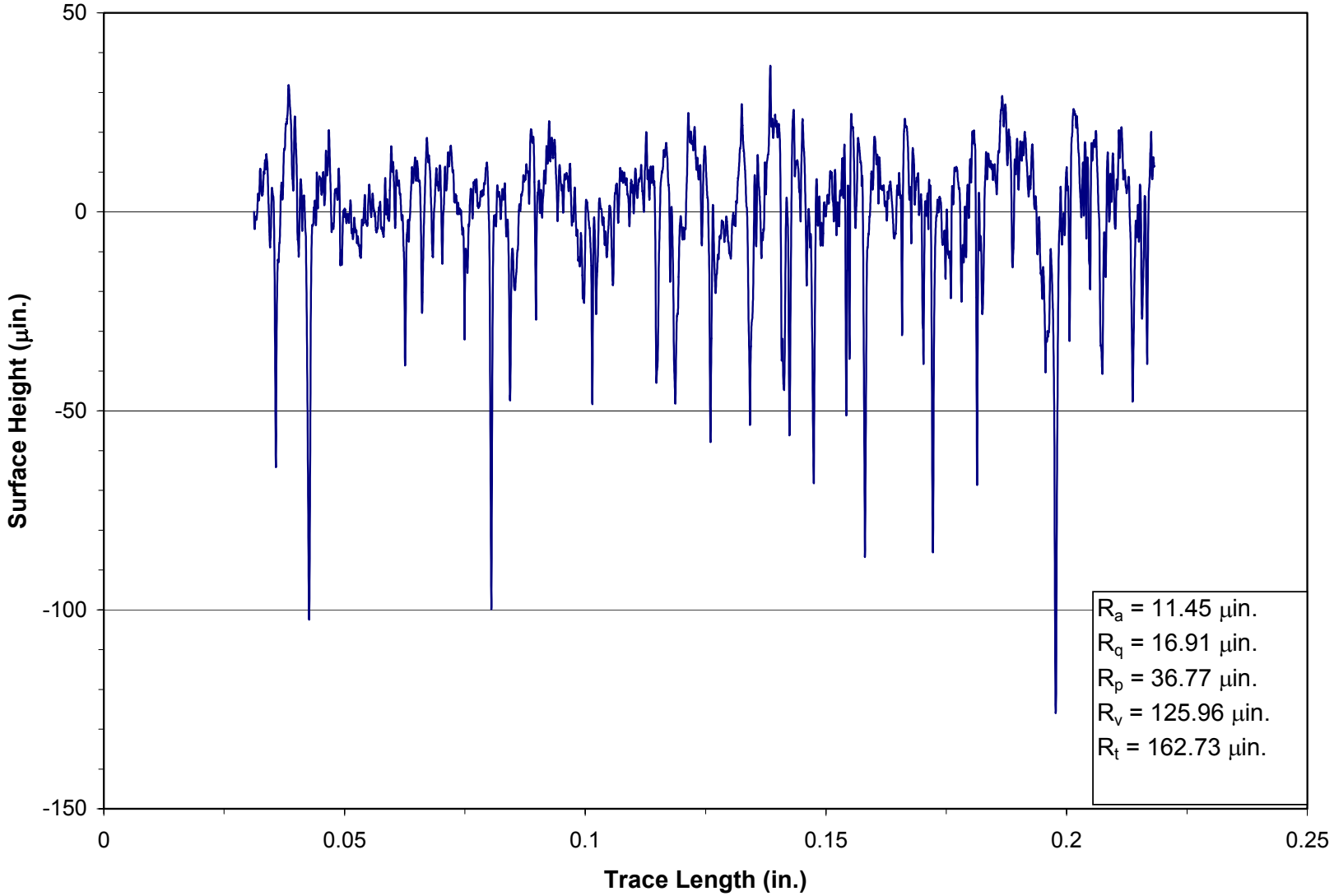

Figure C-17. Roughness Profile from Specimen 5773.

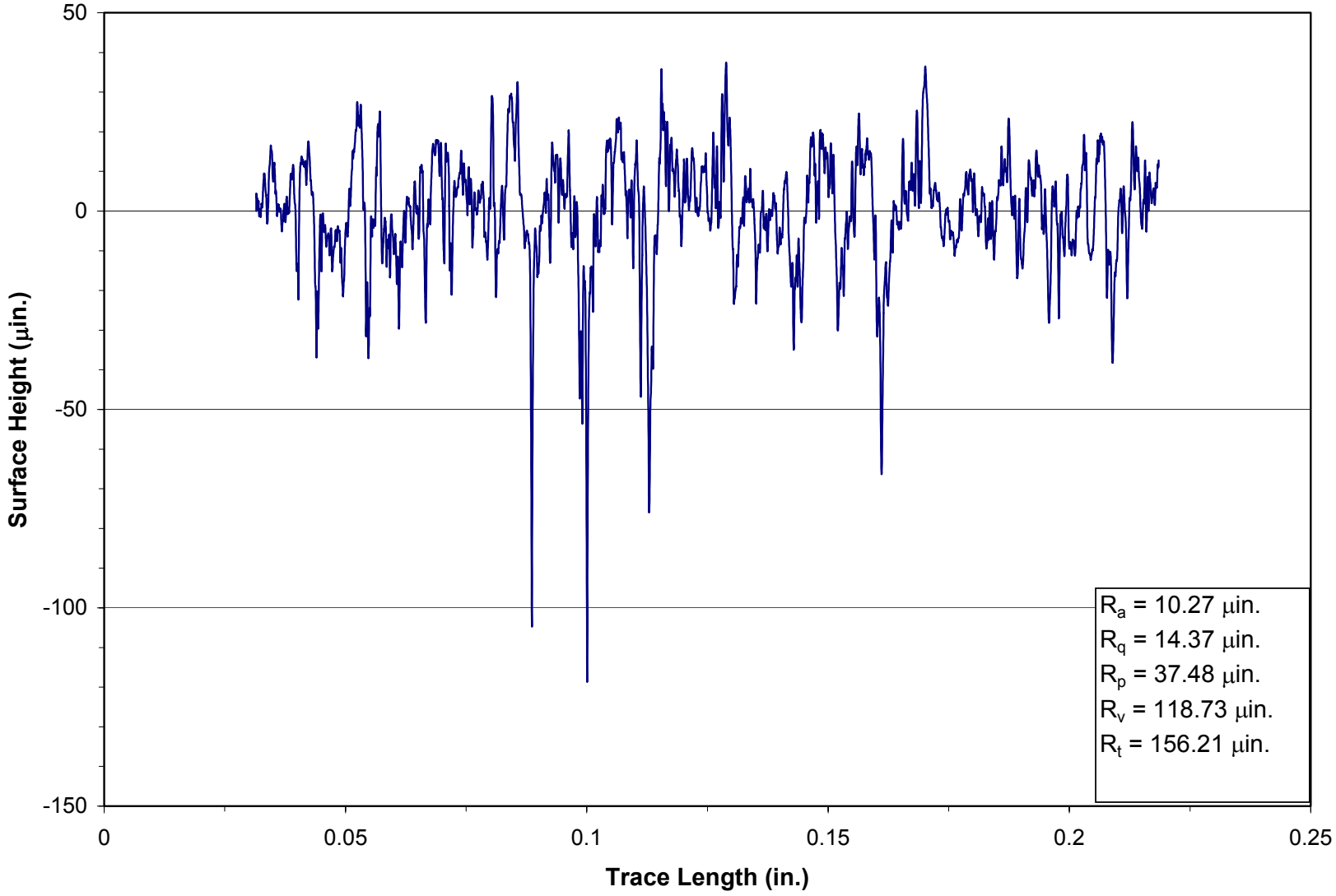

Figure C-18. Roughness Profile from Specimen 5776.

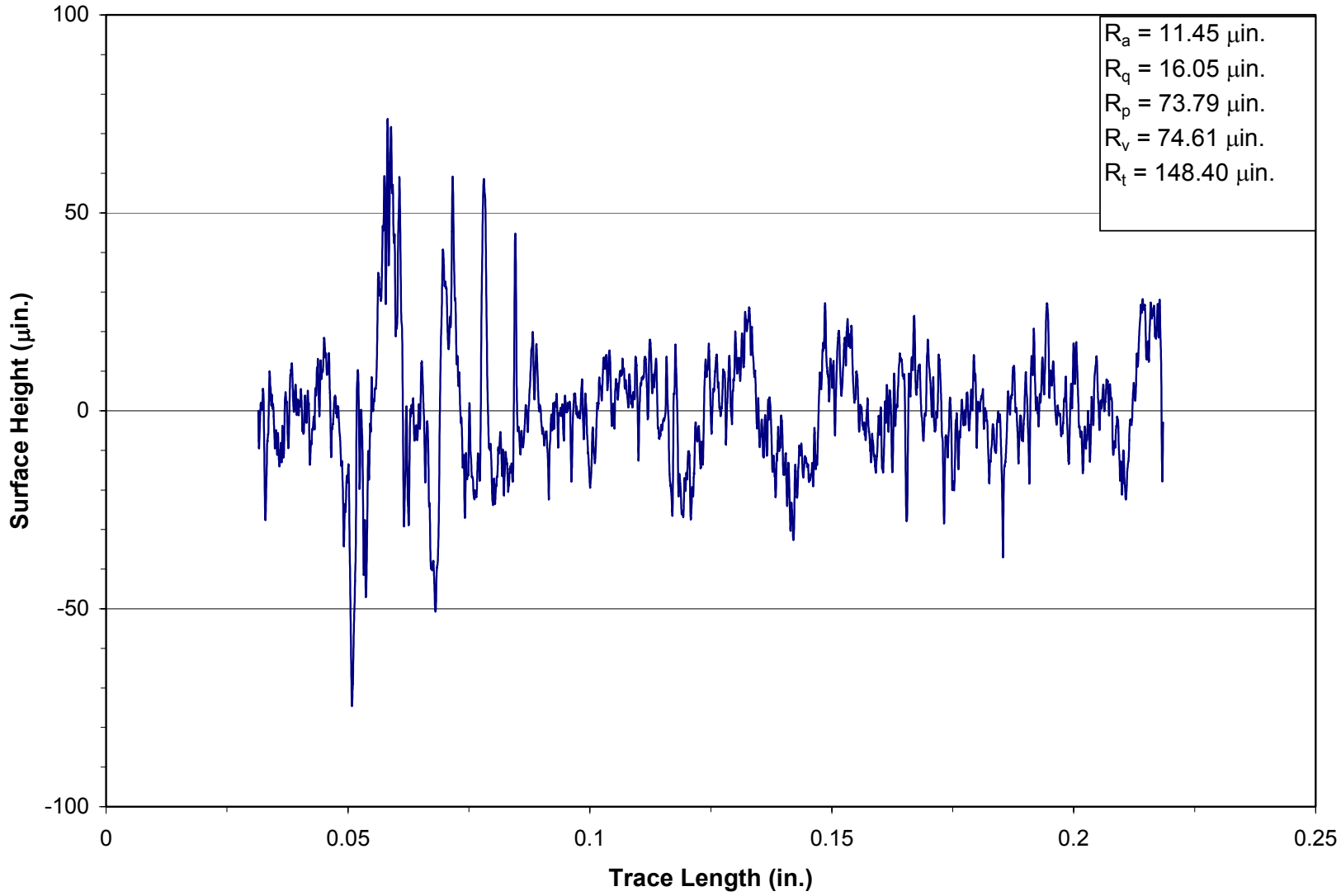

Figure C-19. Roughness Profile from Specimen 5829.

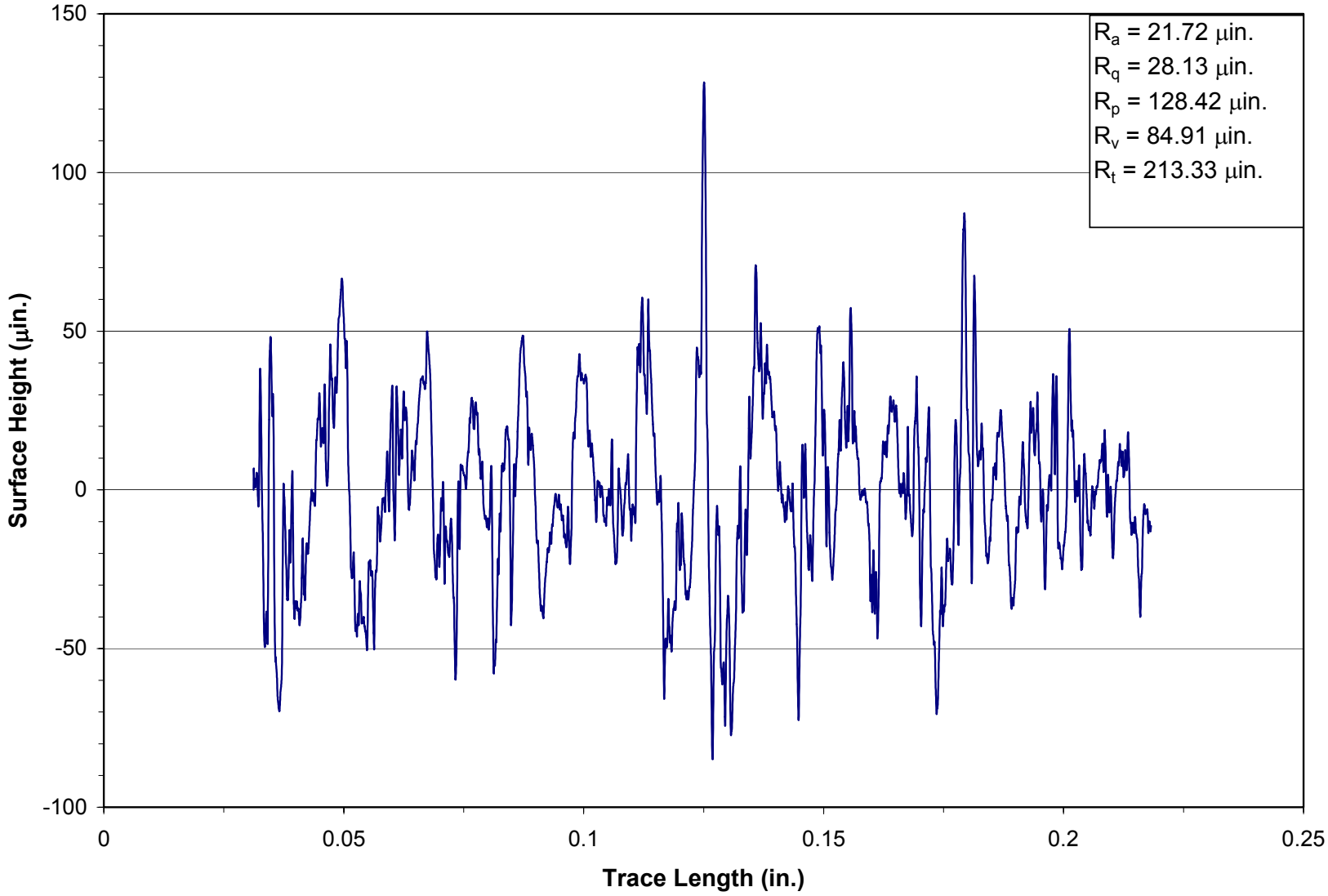

Figure C-20. Roughness Profile from Specimen 5830.

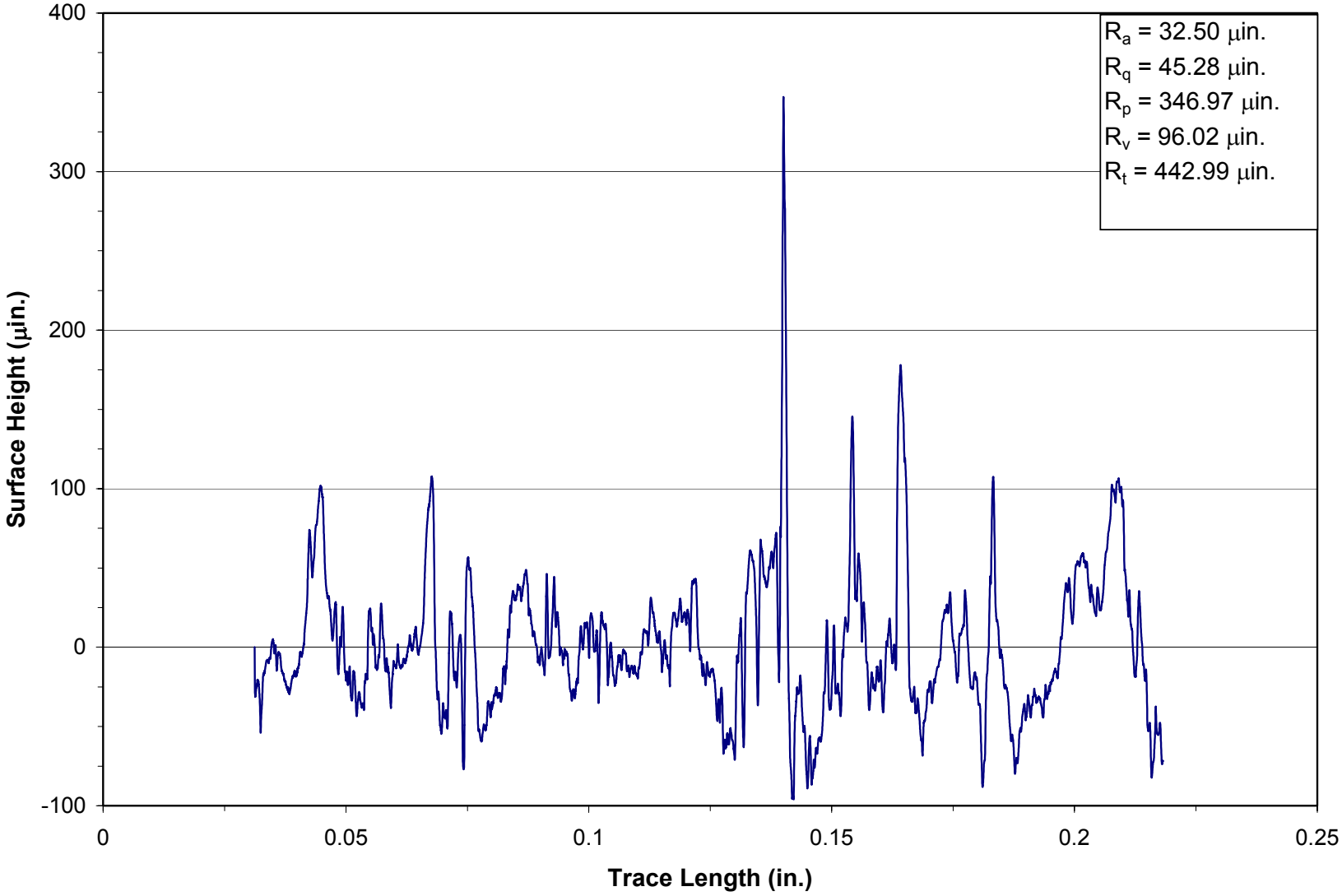

Figure C-21. Roughness Profile from Specimen 5832.

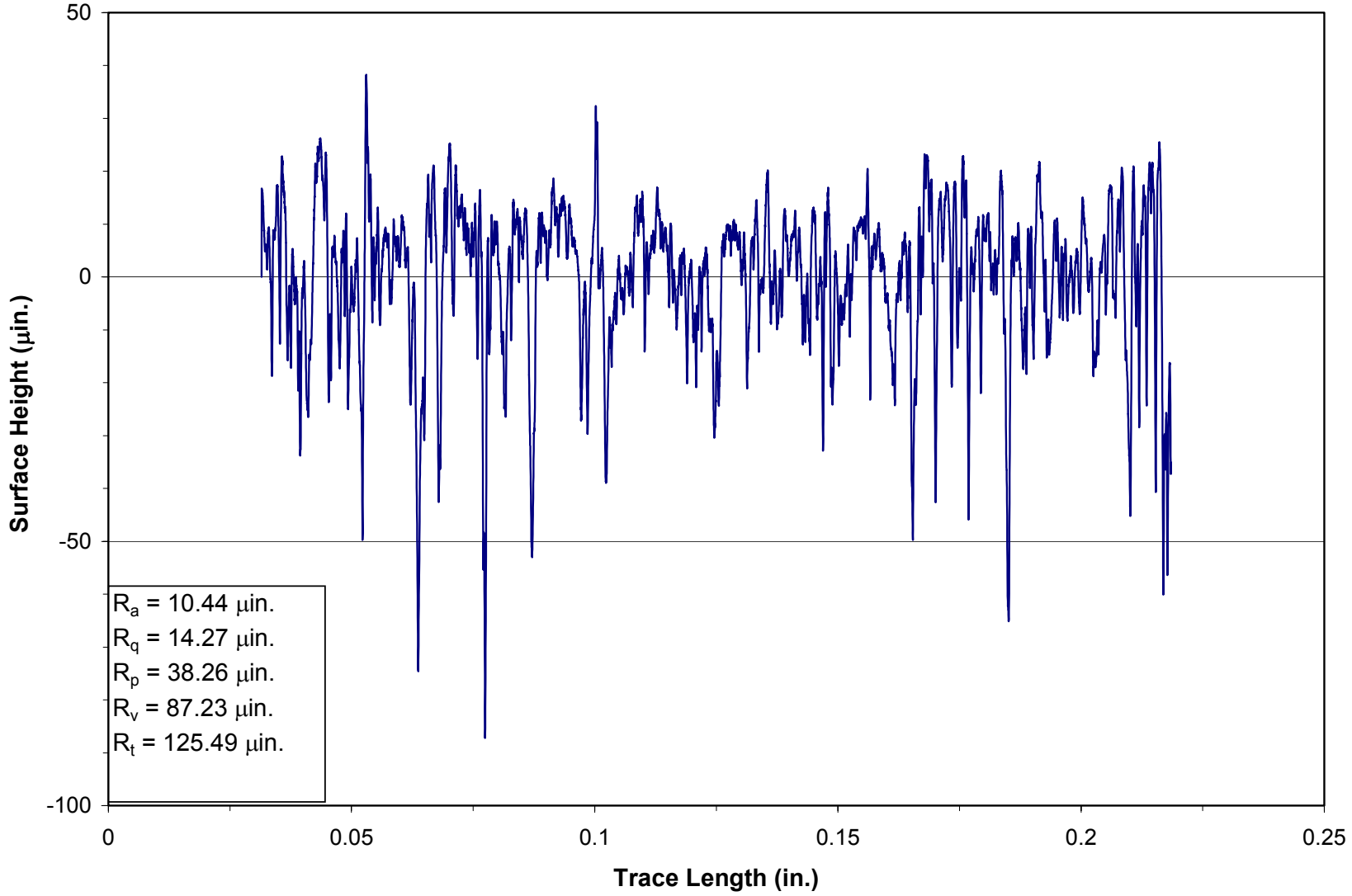

Figure C-22. Roughness Profile from Specimen 5854.

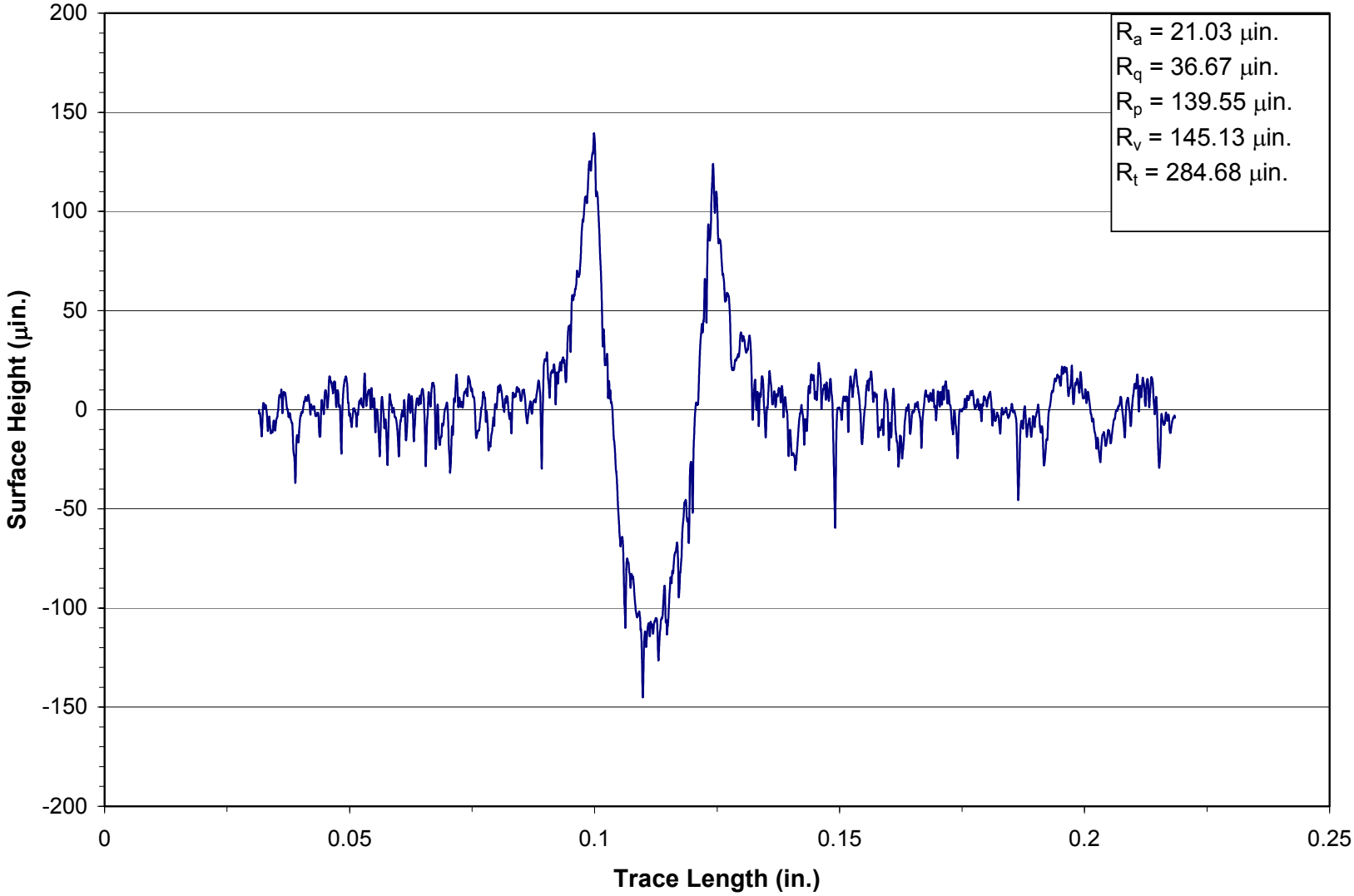

Figure C-23. Roughness Profile from Specimen 5869.

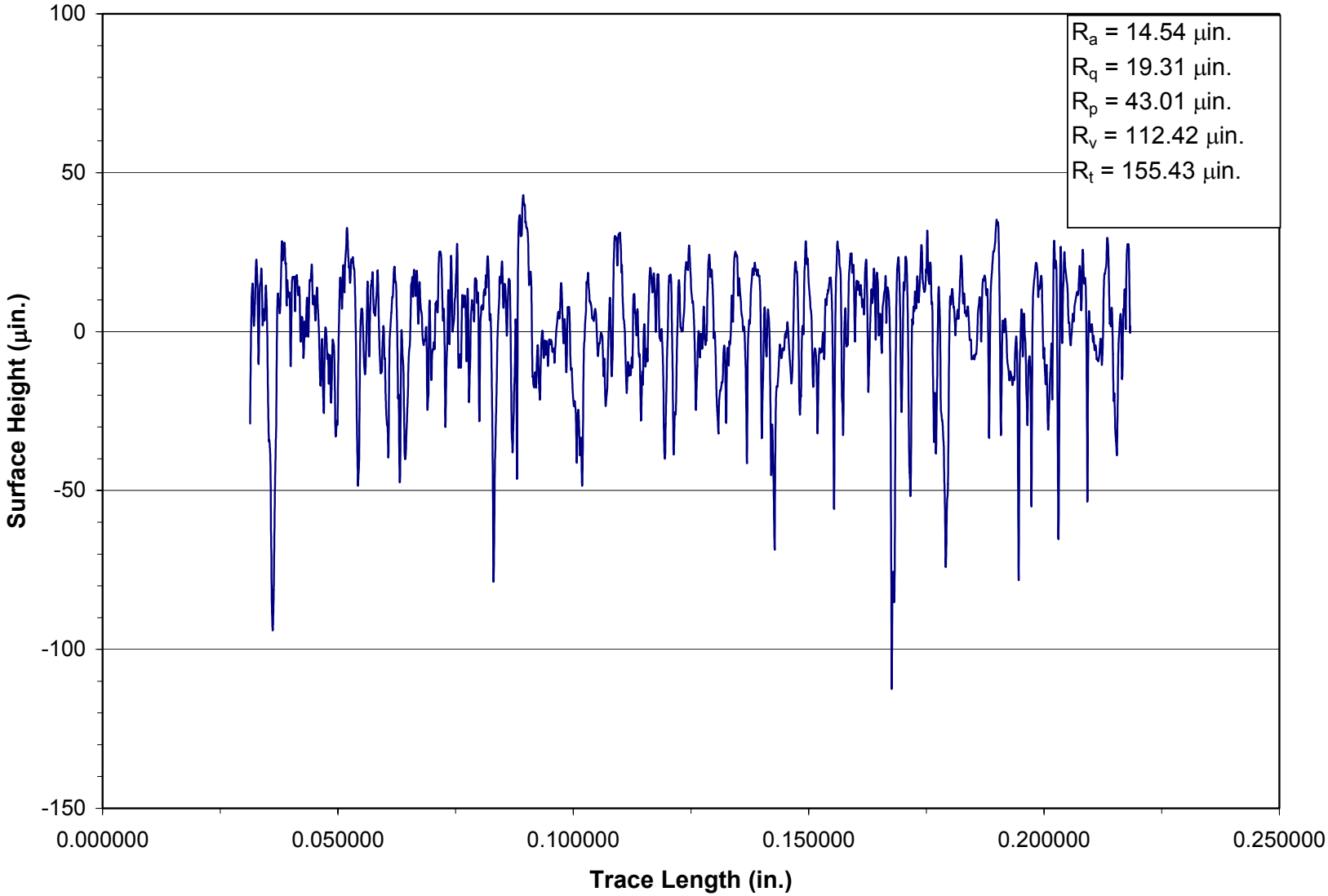

Figure C-24. Roughness Profile from Specimen 5871.

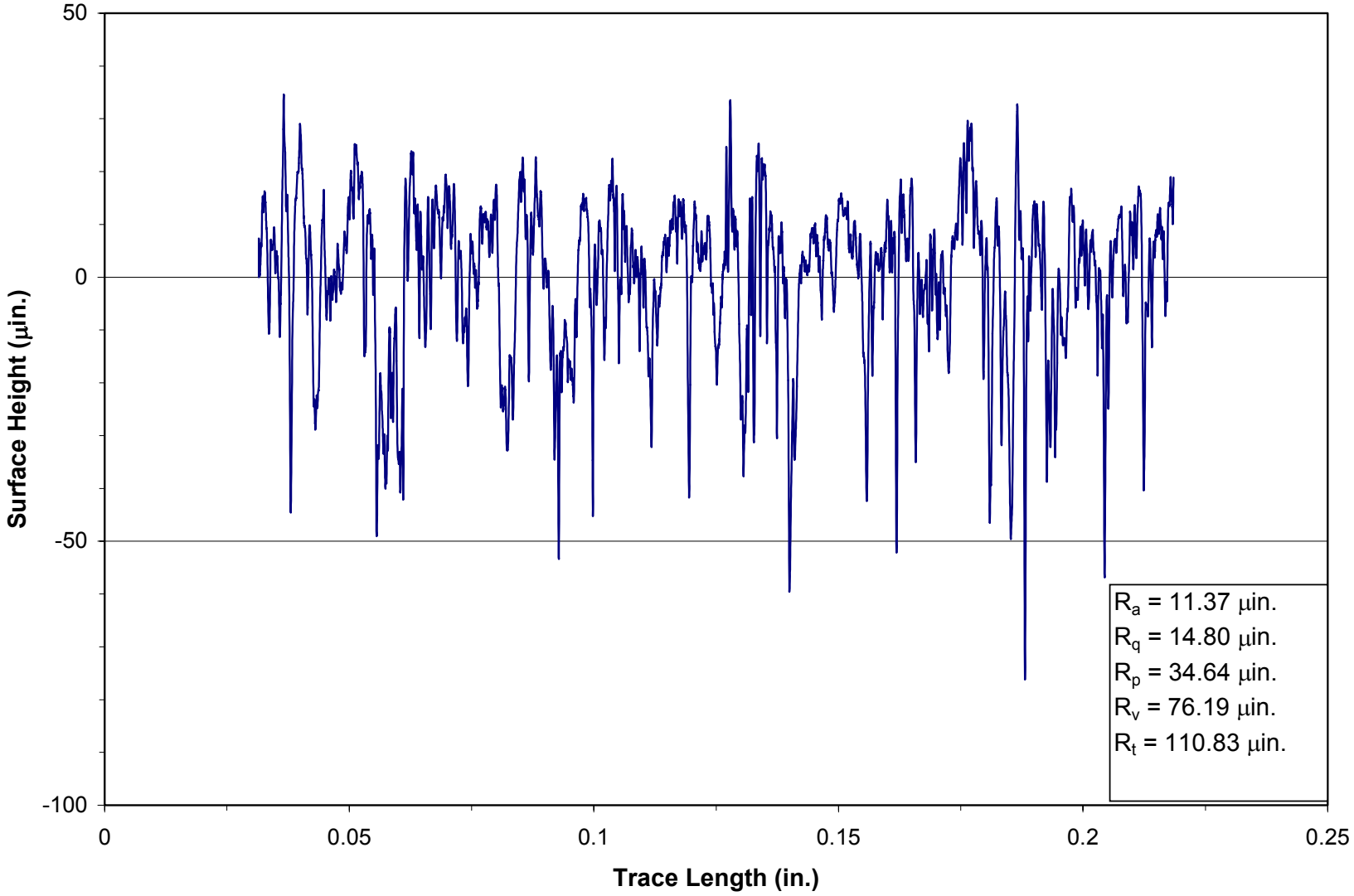

Figure C-25. Roughness Profile from Specimen 5872.

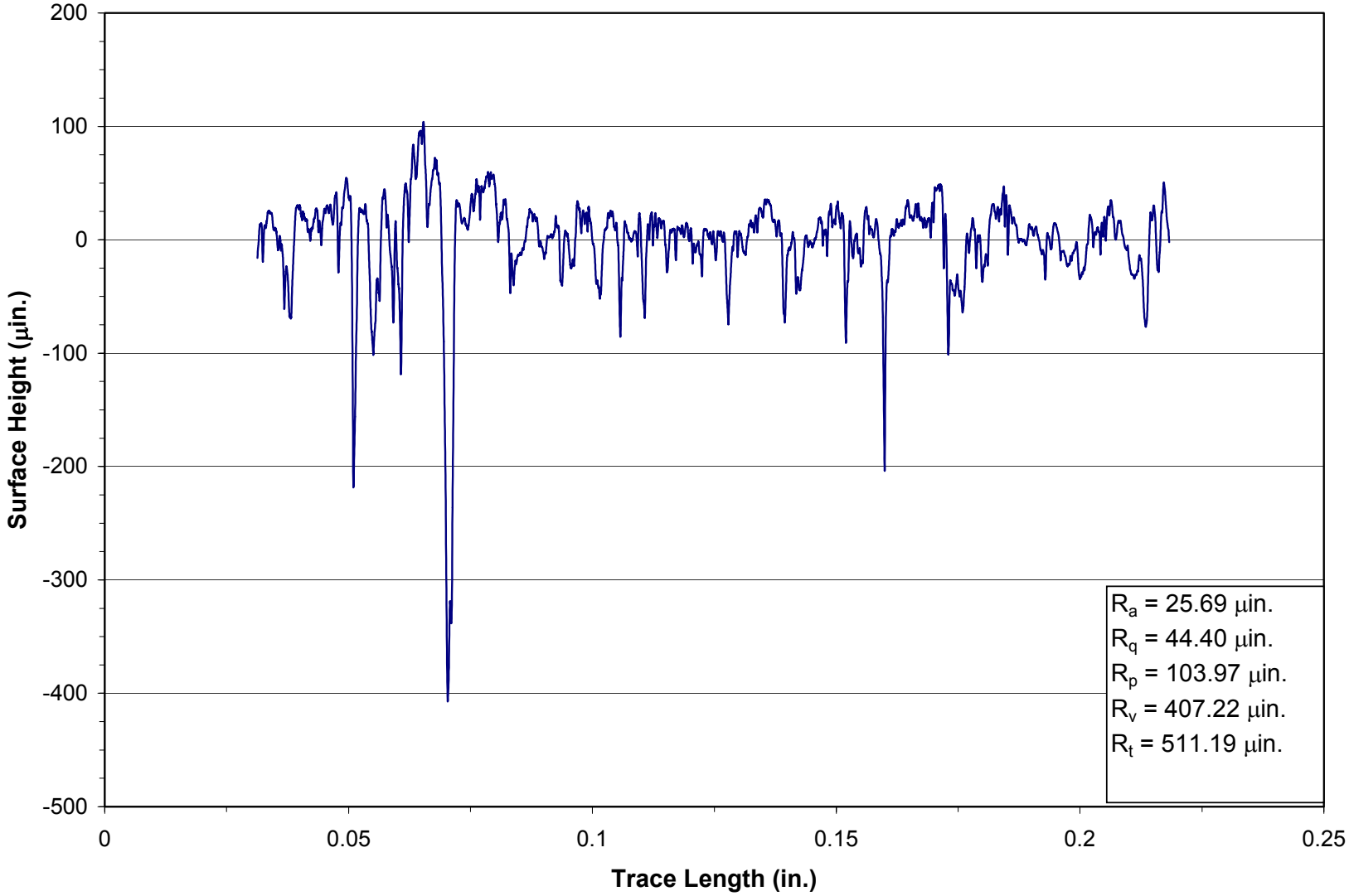

Figure C-26. Roughness Profile from Specimen 5877.

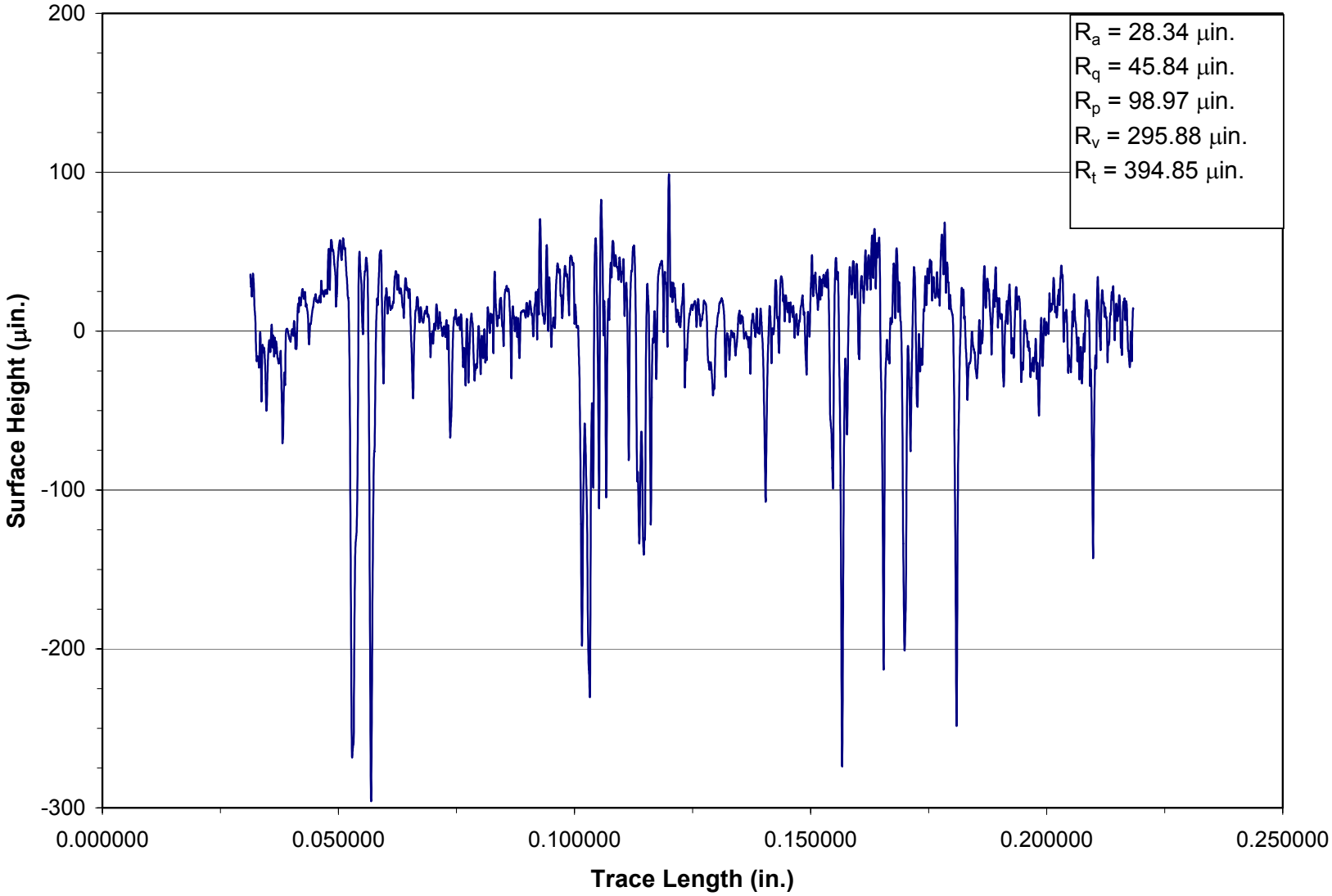

Figure C-27. Roughness Profile from Specimen 5878.

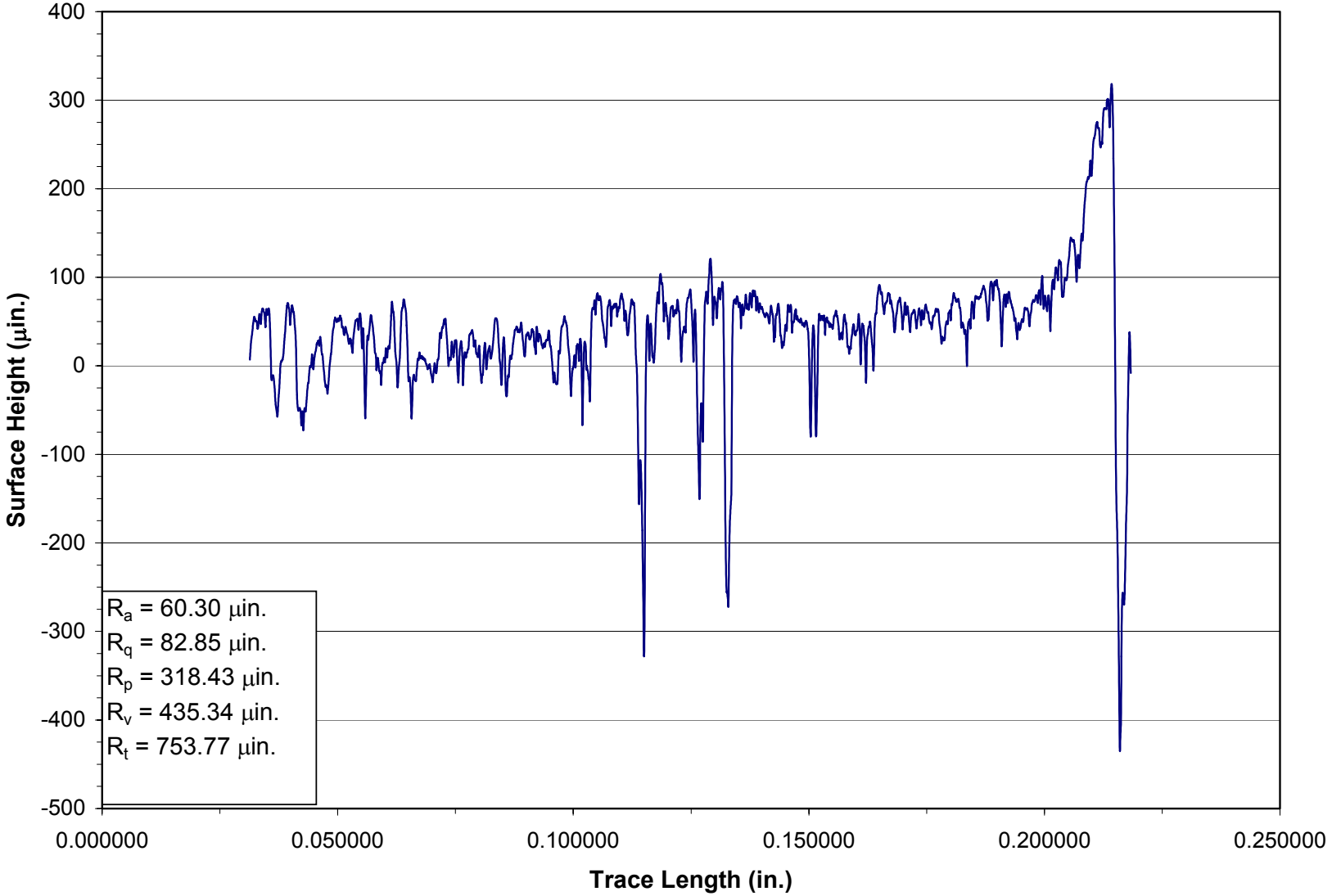

Figure C-28. Roughness Profile from Specimen 5879.

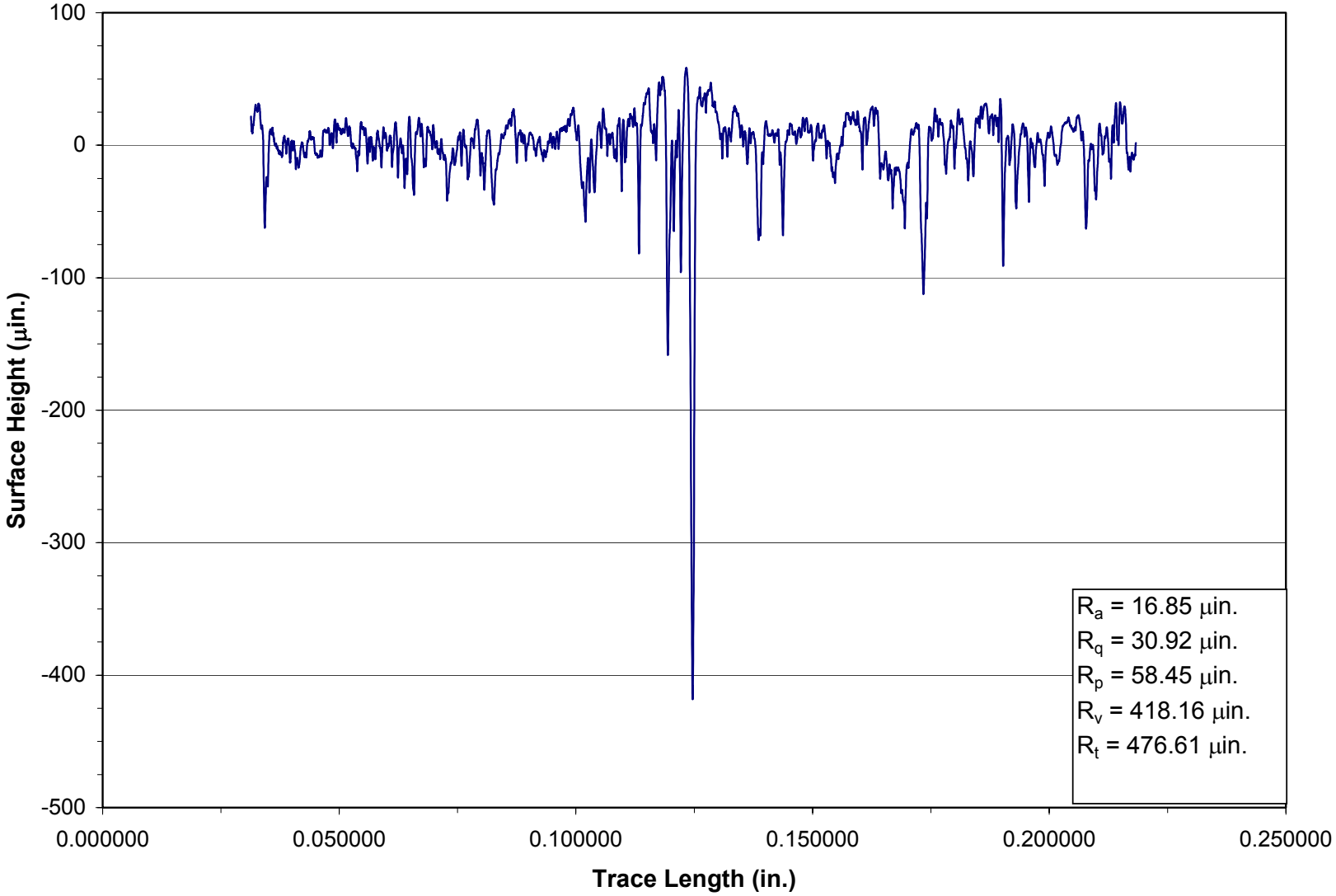

Figure C-29. Roughness Profile from Specimen 5880.

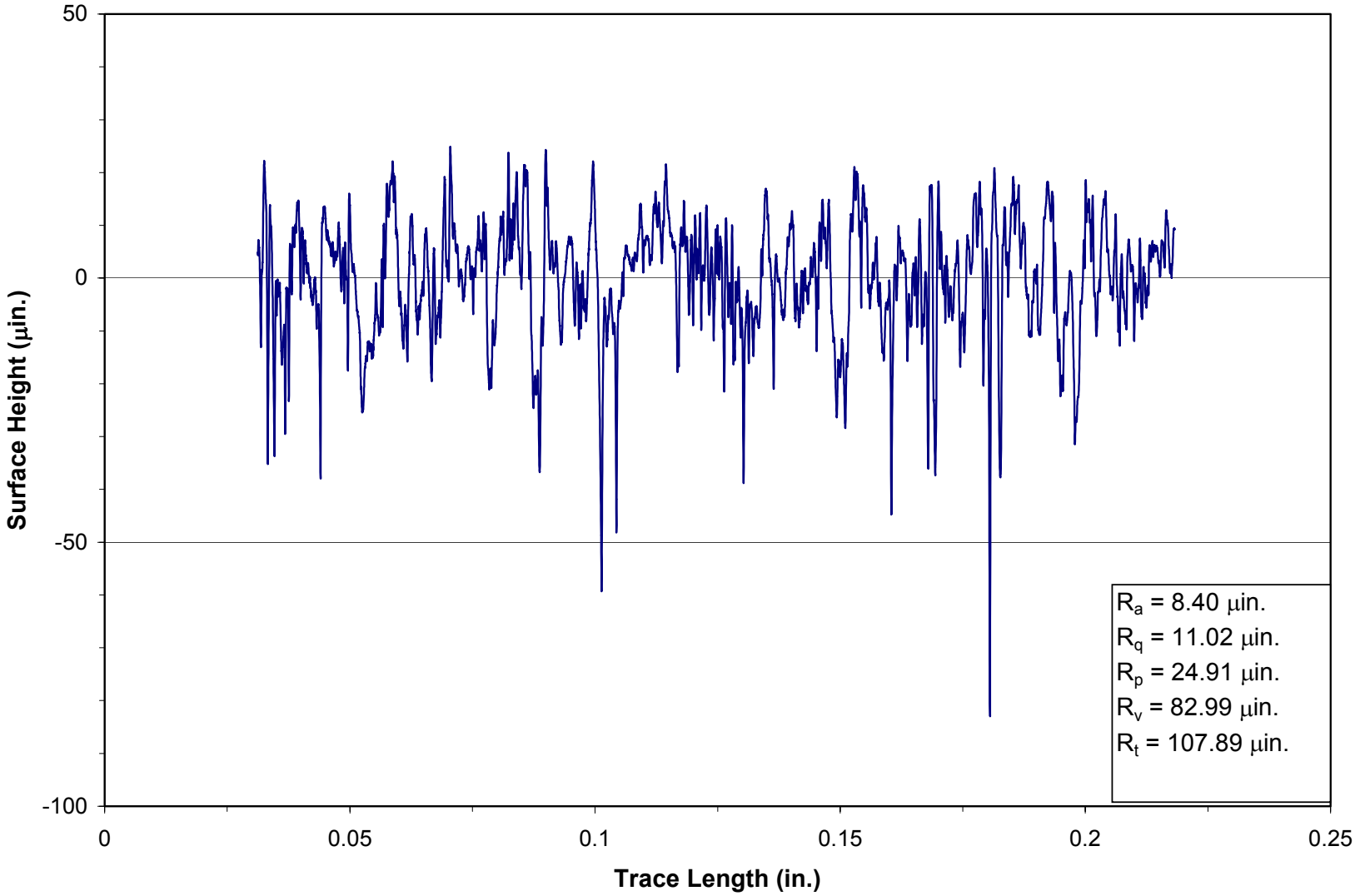

Figure C-30. Roughness Profile from Specimen 5893.

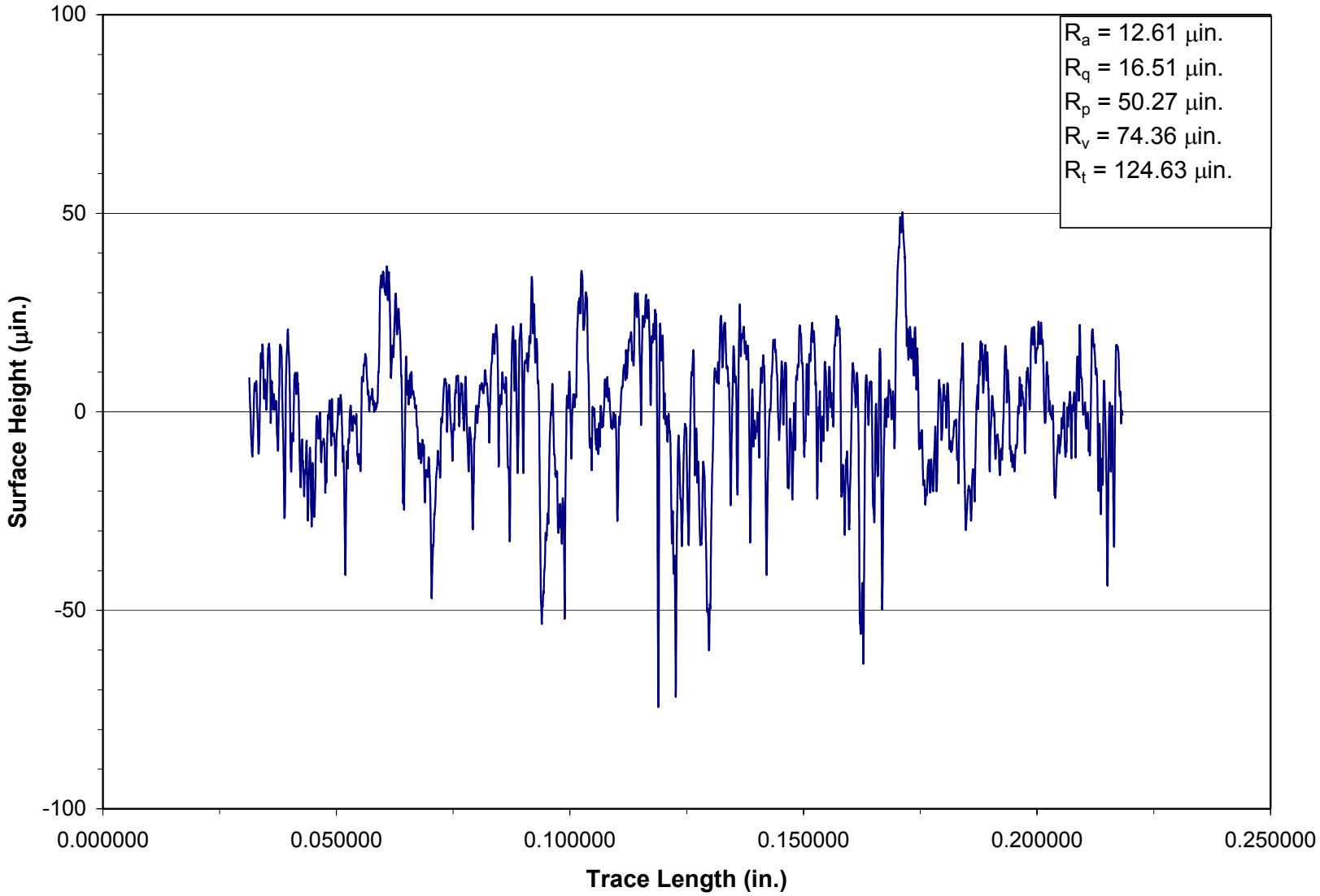

Figure C-31. Roughness Profile from Specimen 5896.

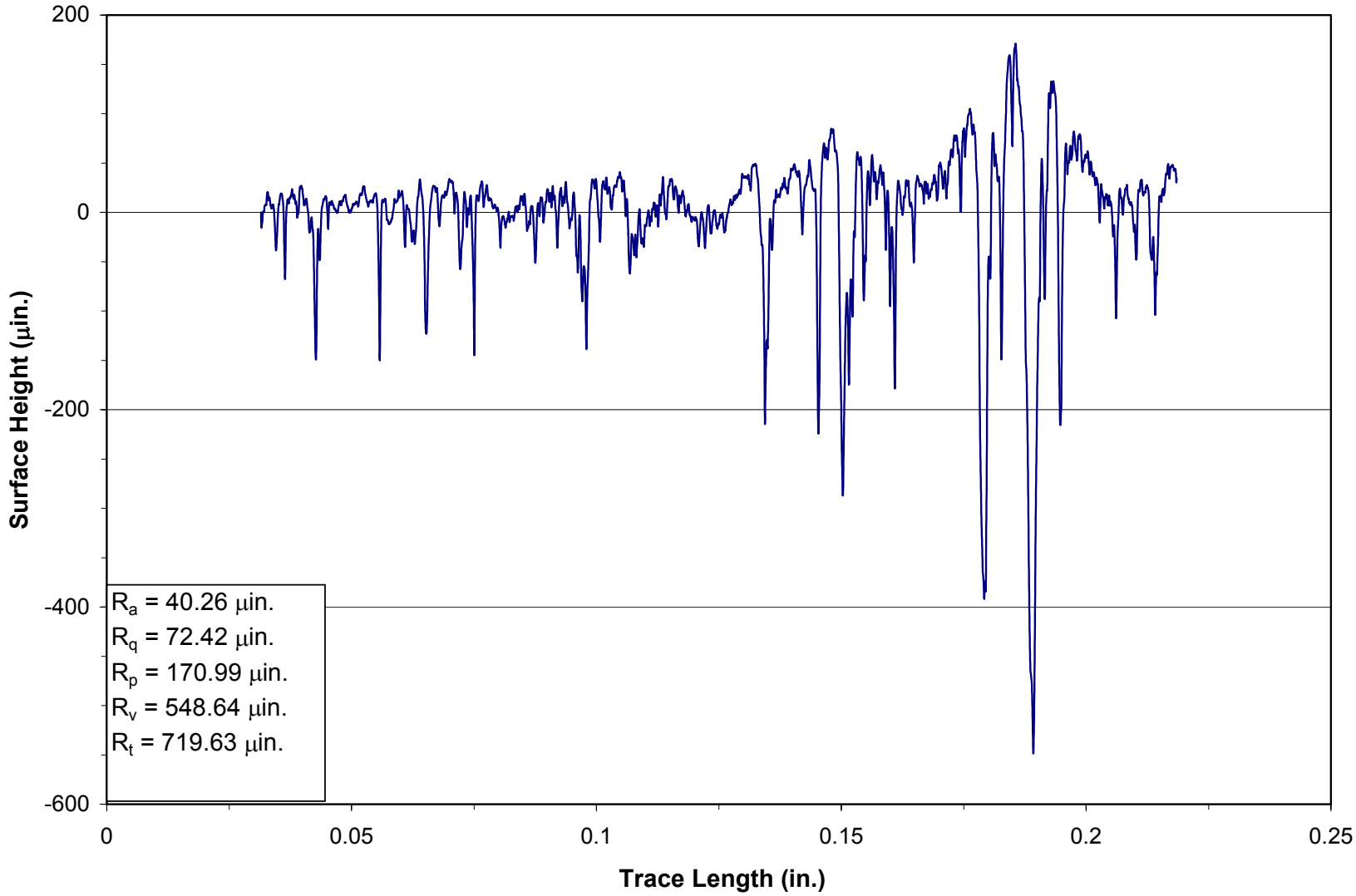

Figure C-32. Roughness Profile from Specimen 5914.

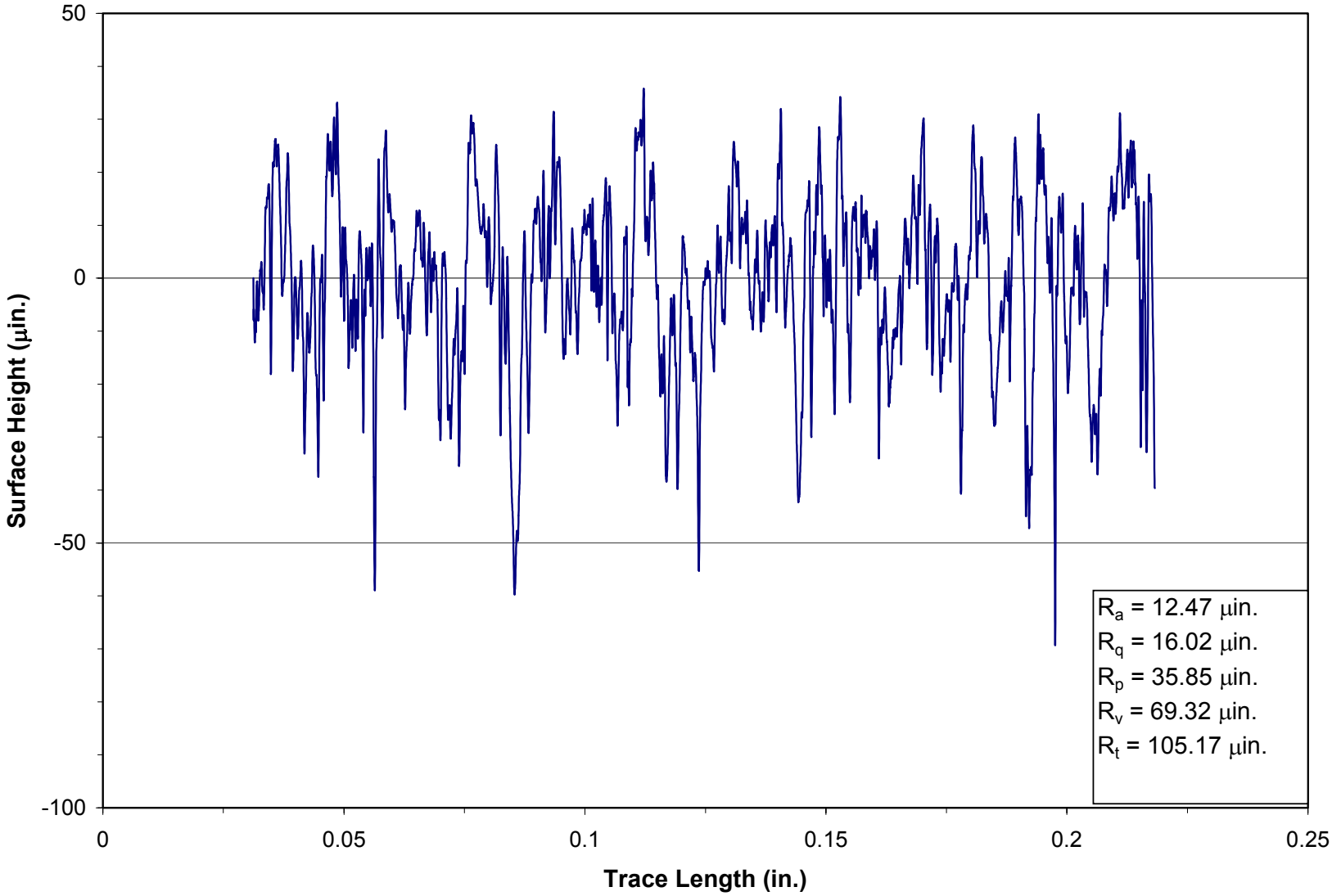

Figure C-33. Roughness Profile from Specimen 5925.

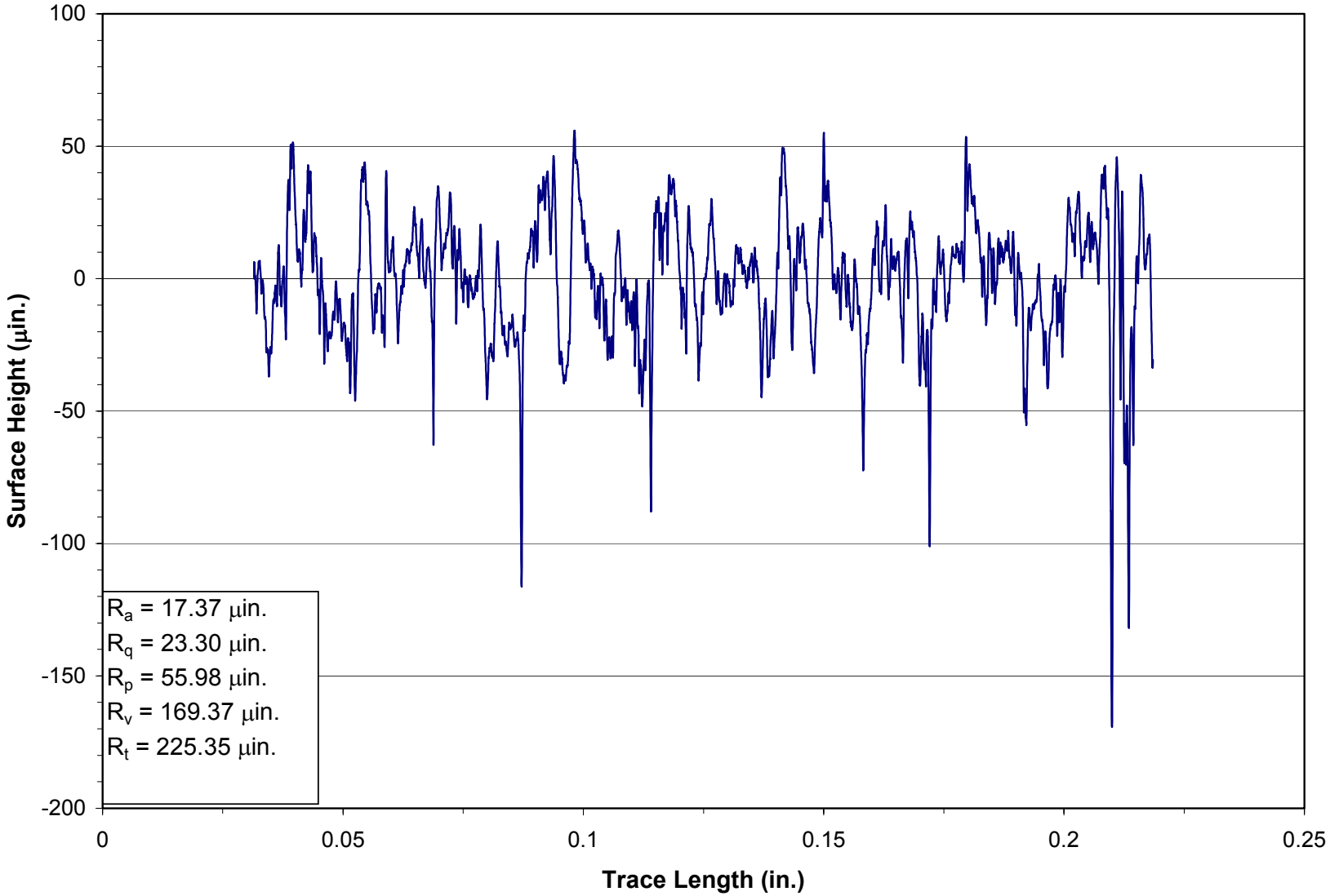

Figure C-34. Roughness Profile from Specimen 5926.

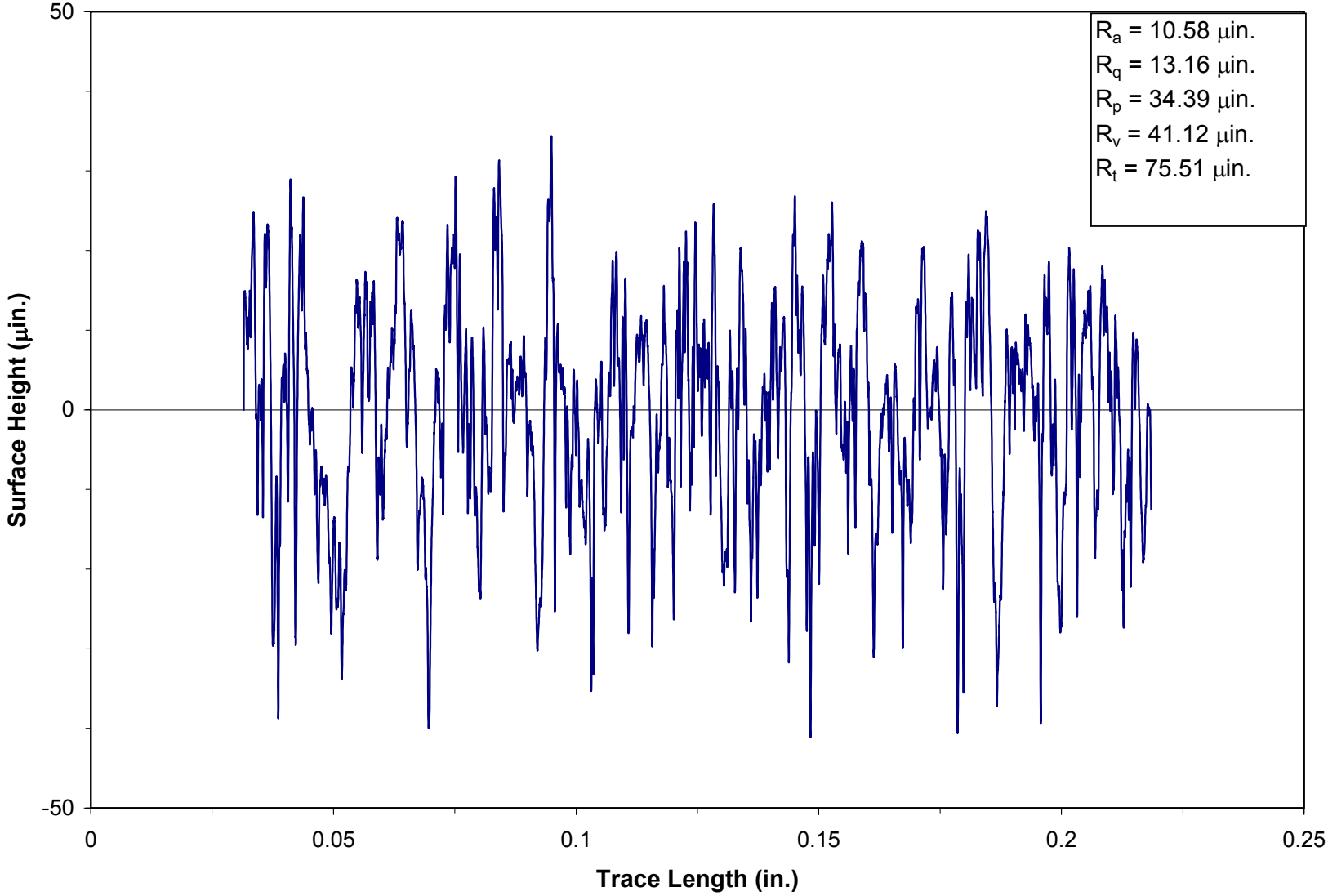

Figure C-35. Roughness Profile from Specimen 5931.

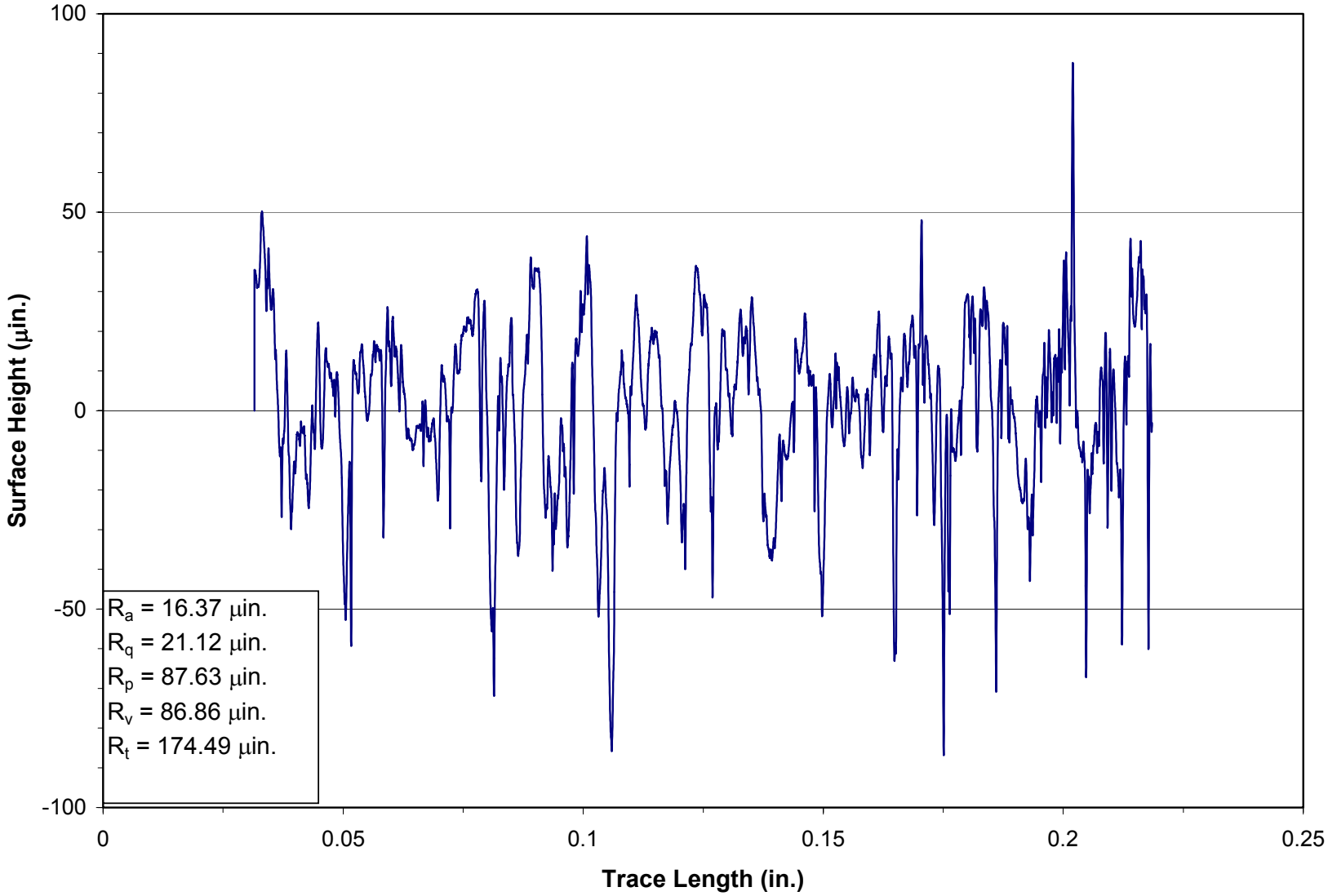

Figure C-36. Roughness Profile from Specimen 5932.

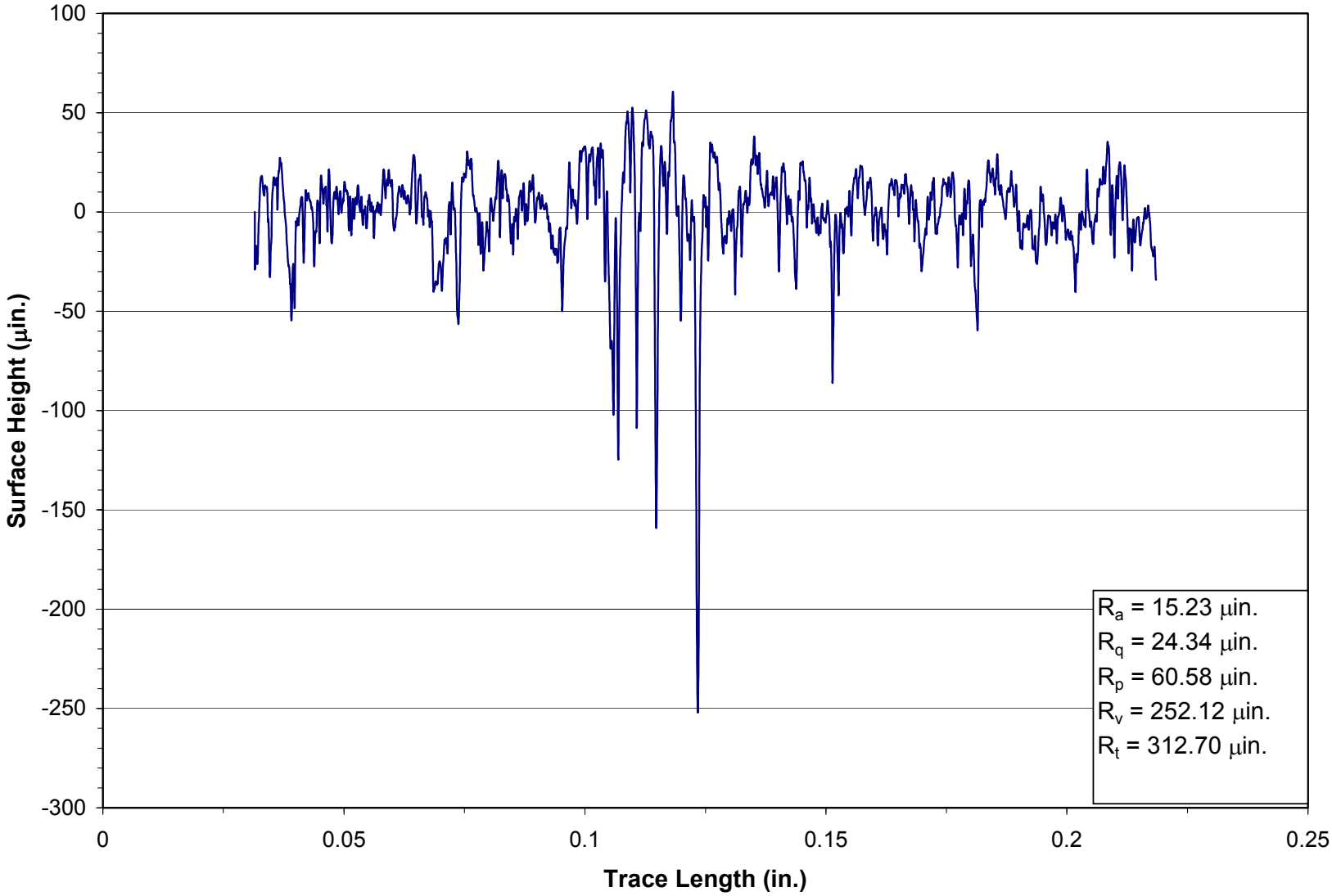

Figure C-37. Roughness Profile from Specimen 5933.

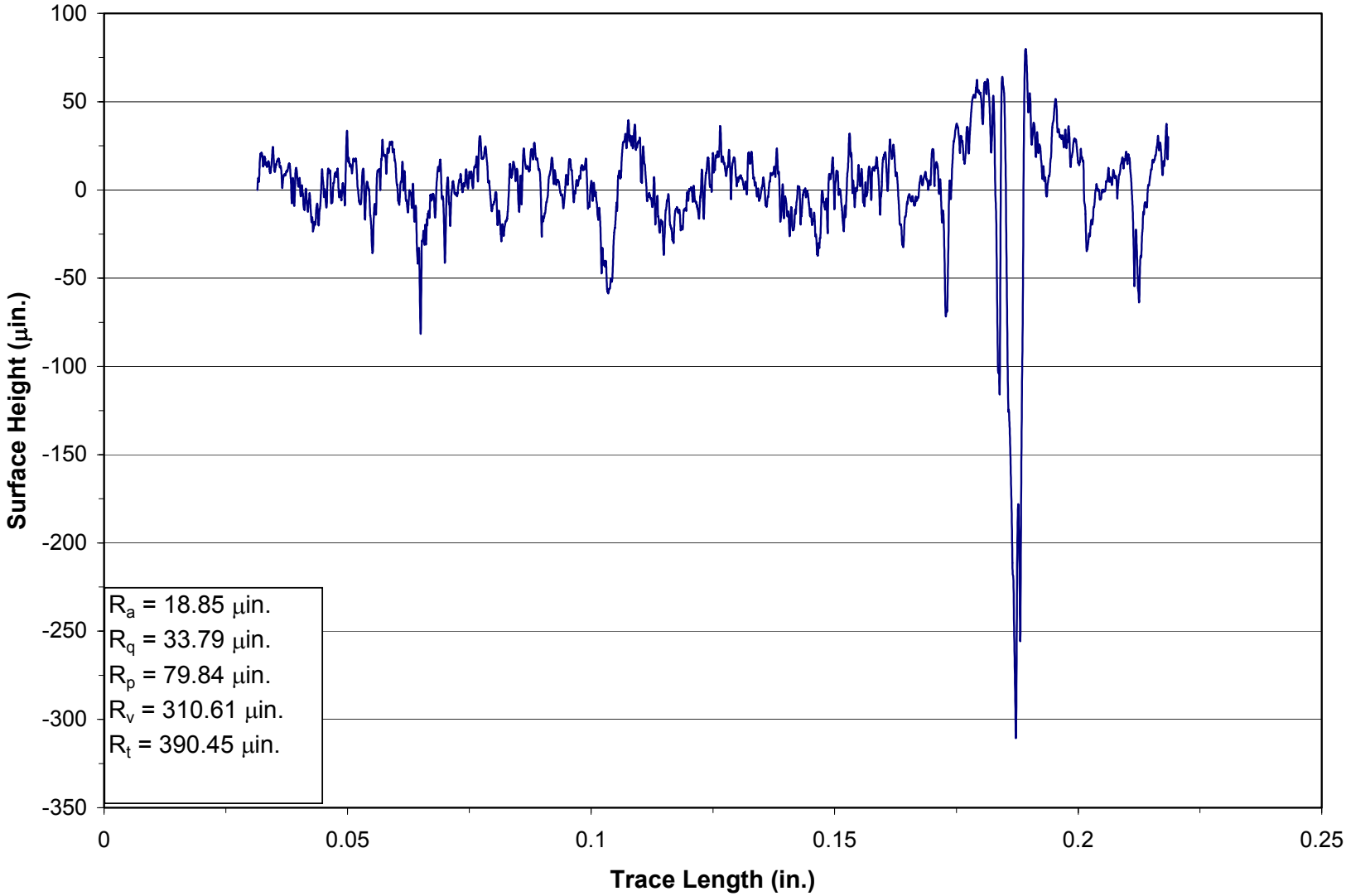

Figure C-38. Roughness Profile from Specimen 5934.

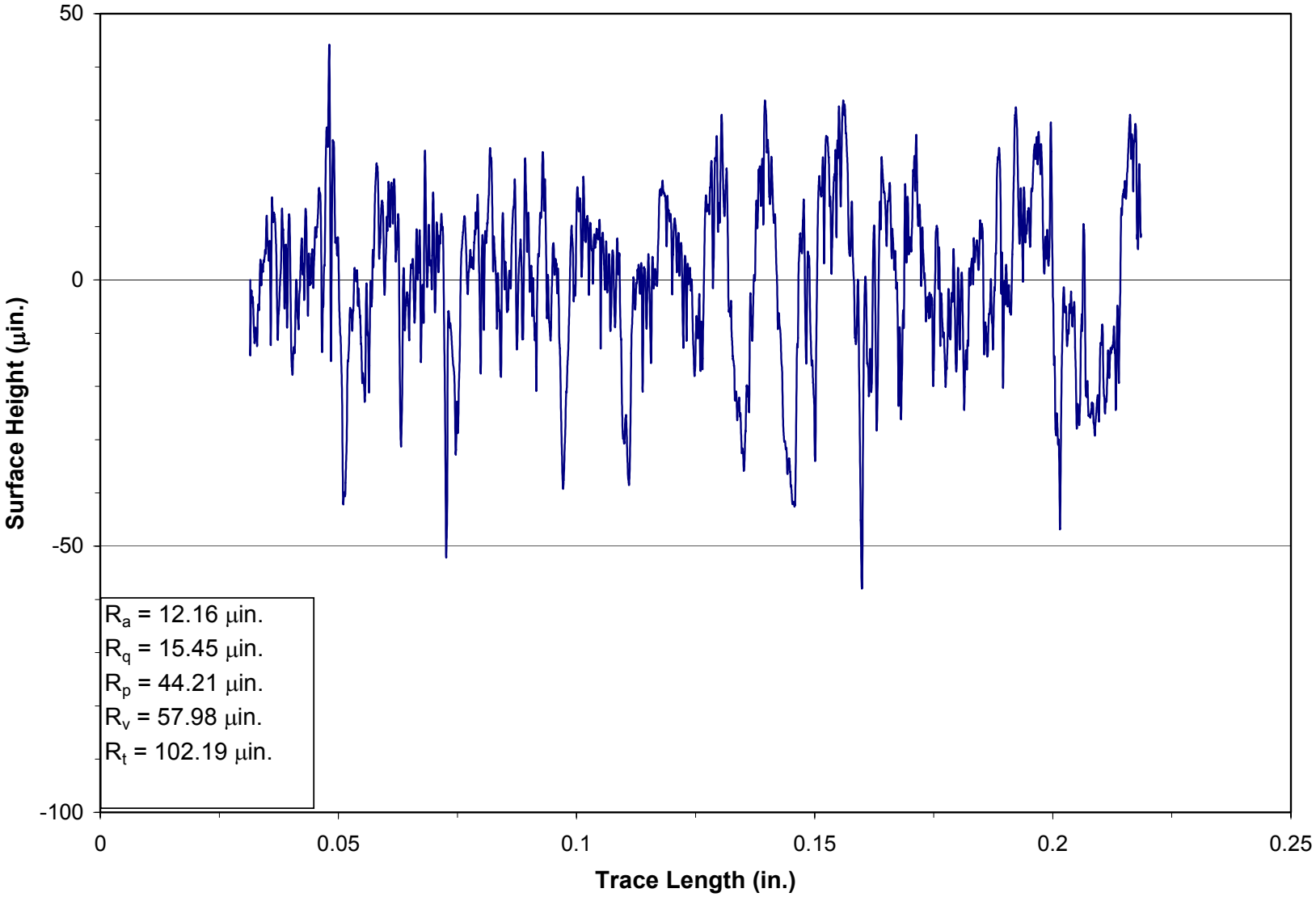

Figure C-39. Roughness Profile from Specimen 5944.

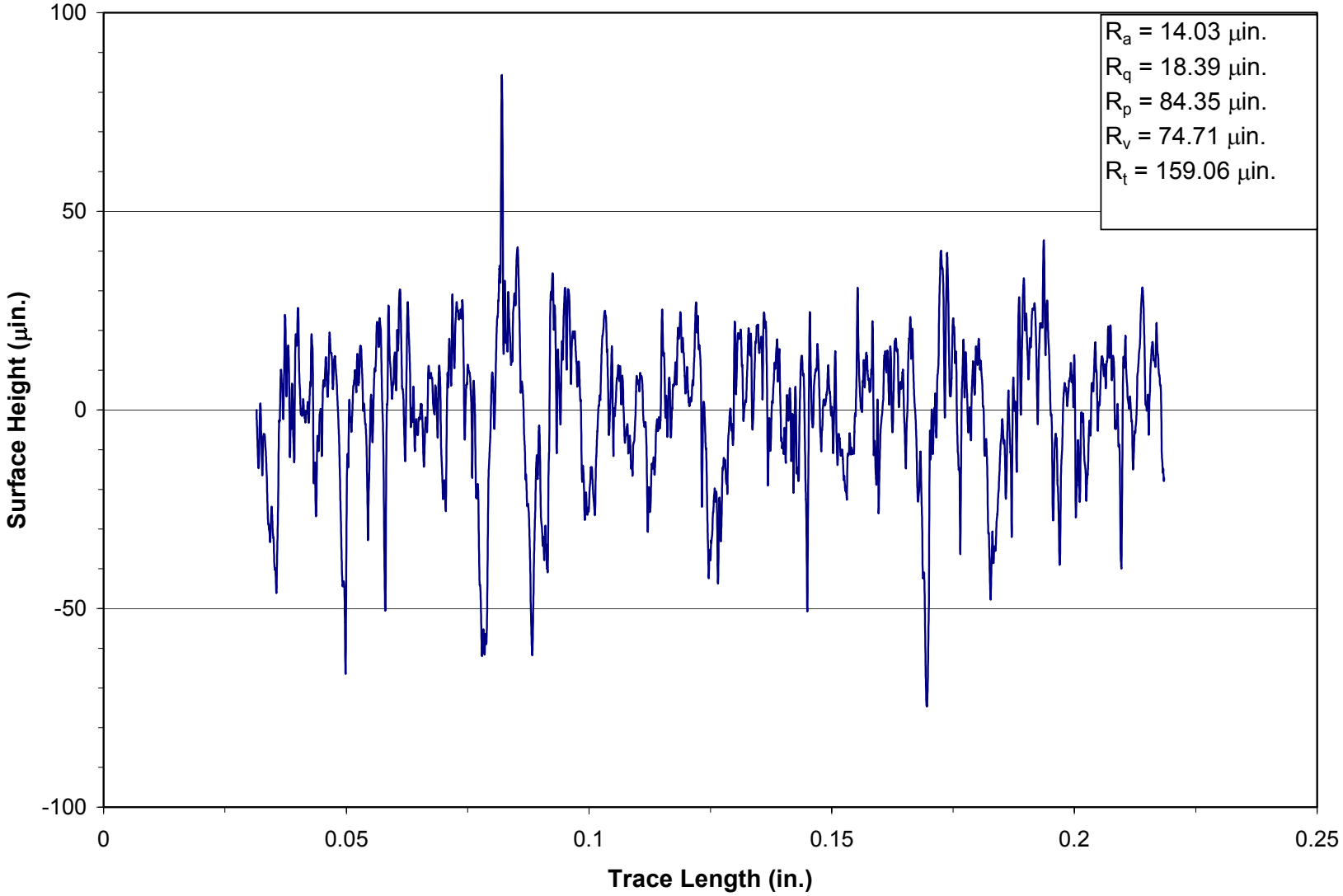

Figure C-40. Roughness Profile from Specimen 5945.

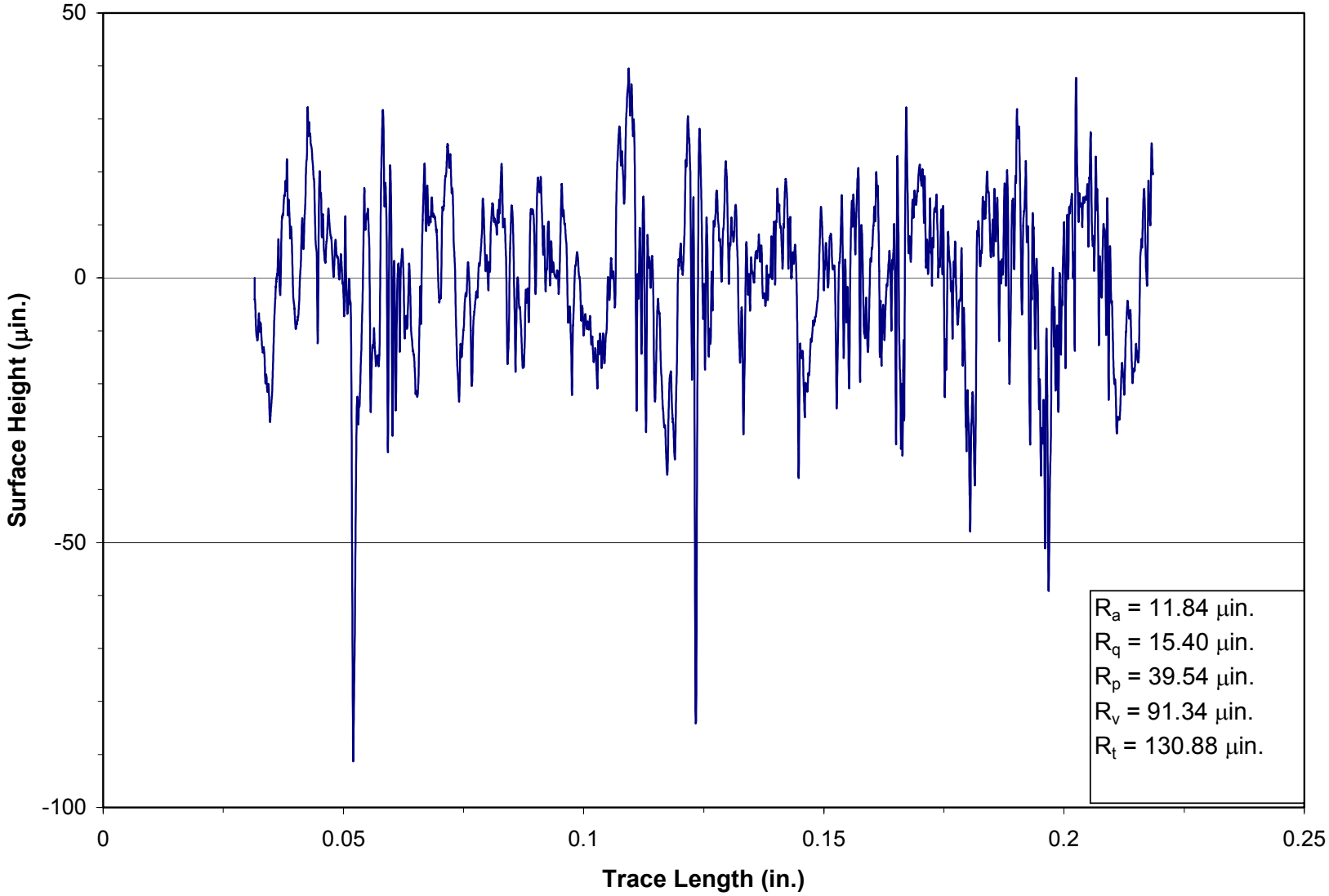

Figure C-41. Roughness Profile from Specimen 5946.

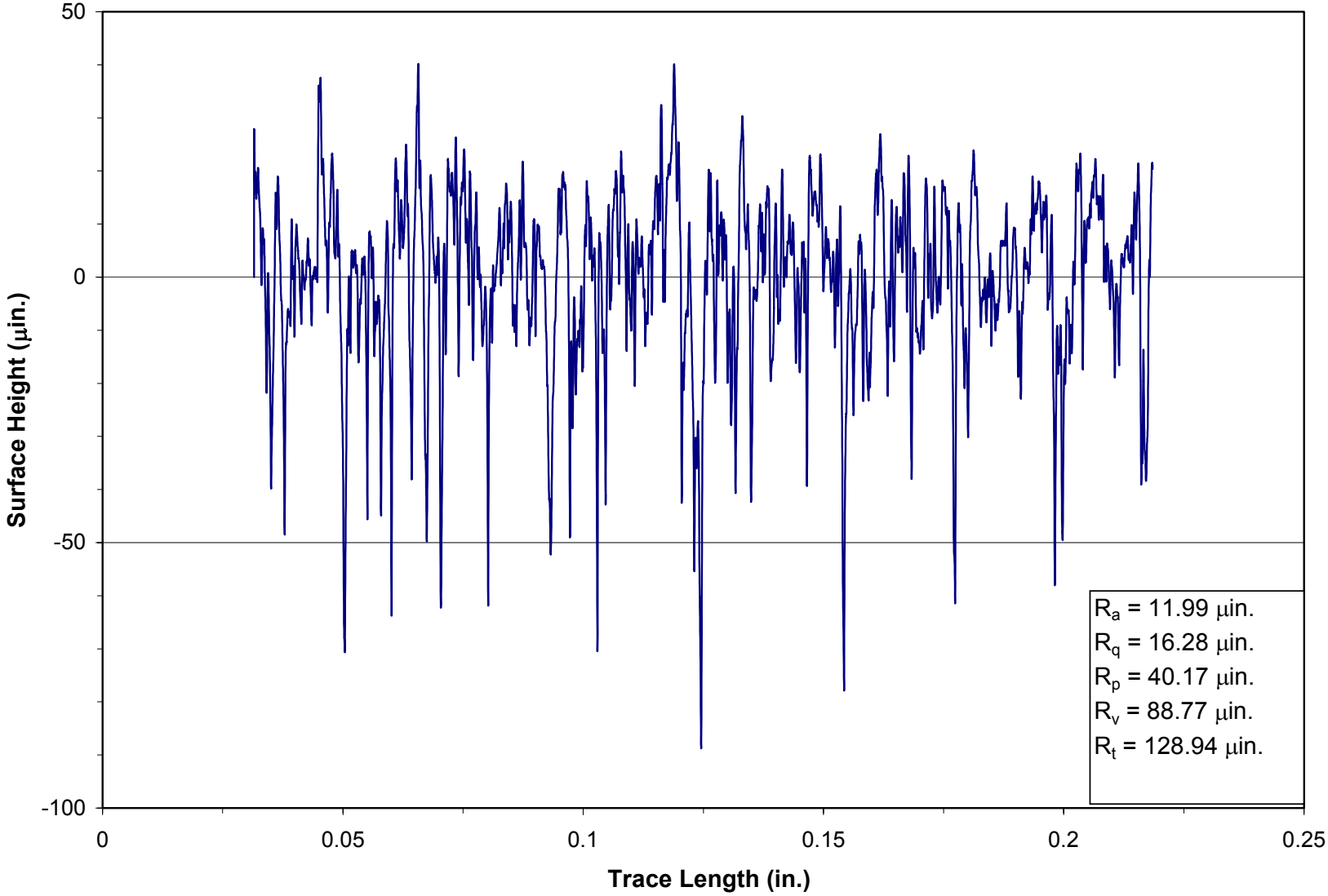

Figure C-42. Roughness Profile from Specimen 5967.

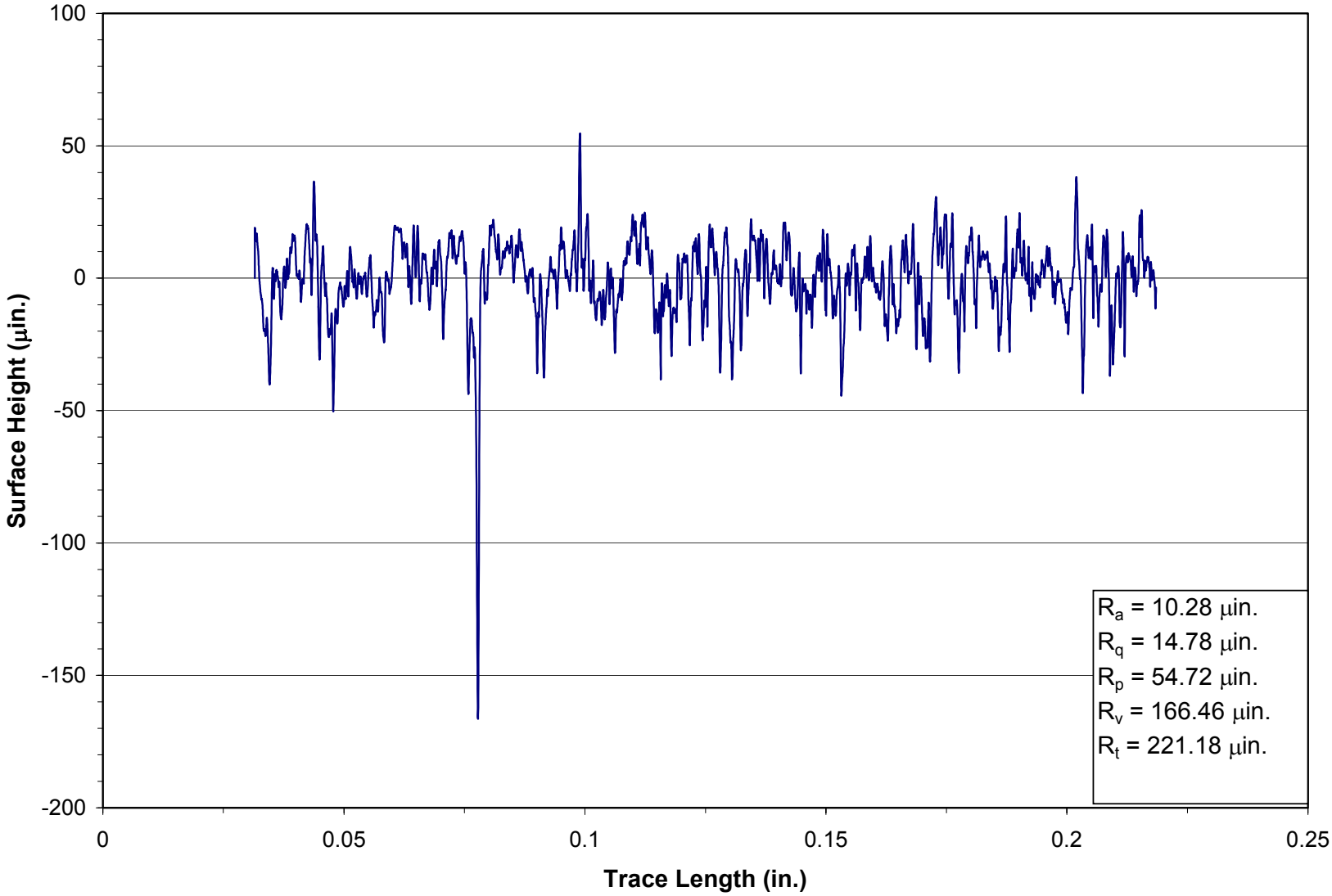

Figure C-43. Roughness Profile from Specimen 5969.

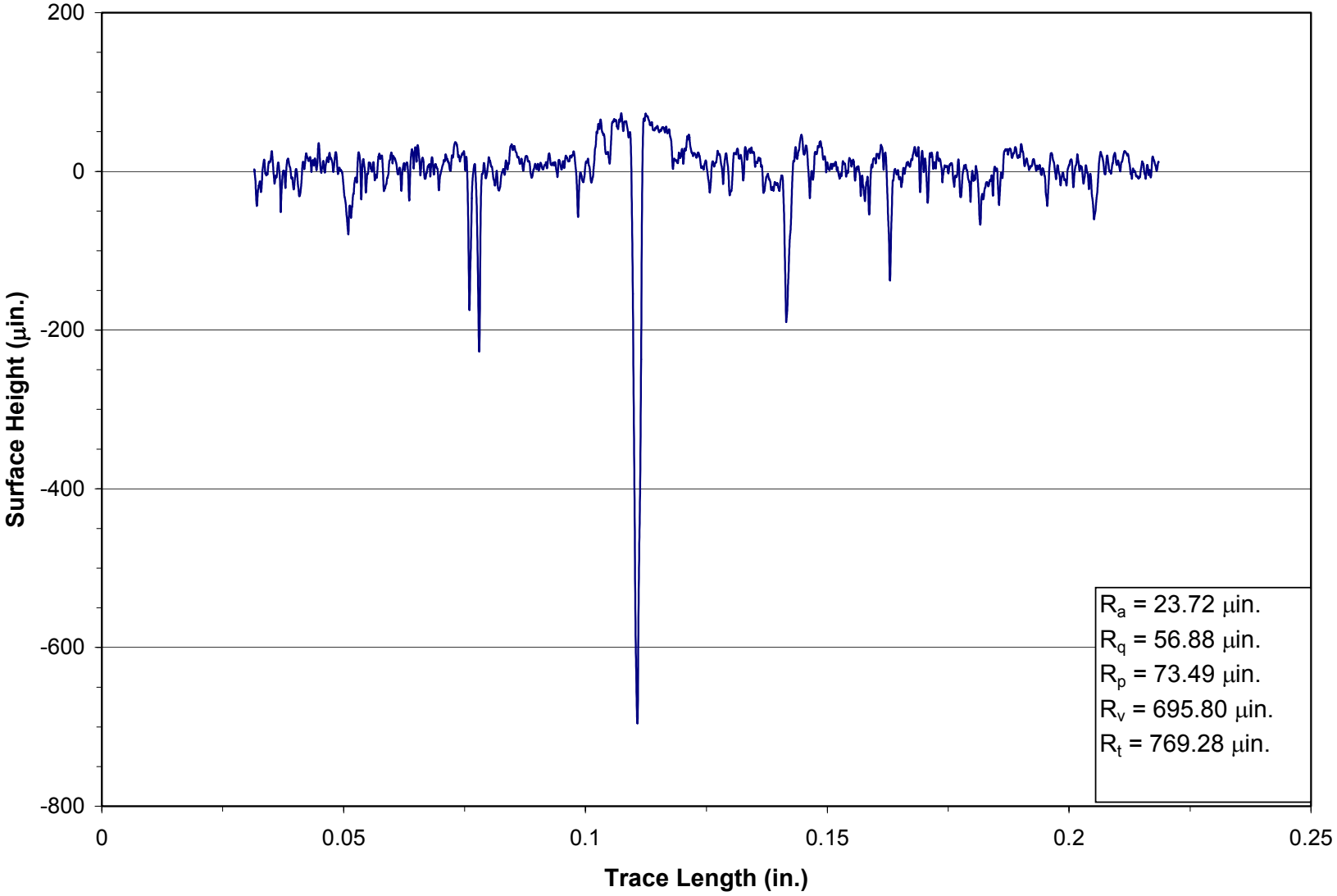

Figure C-44. Roughness Profile from Specimen 6002.

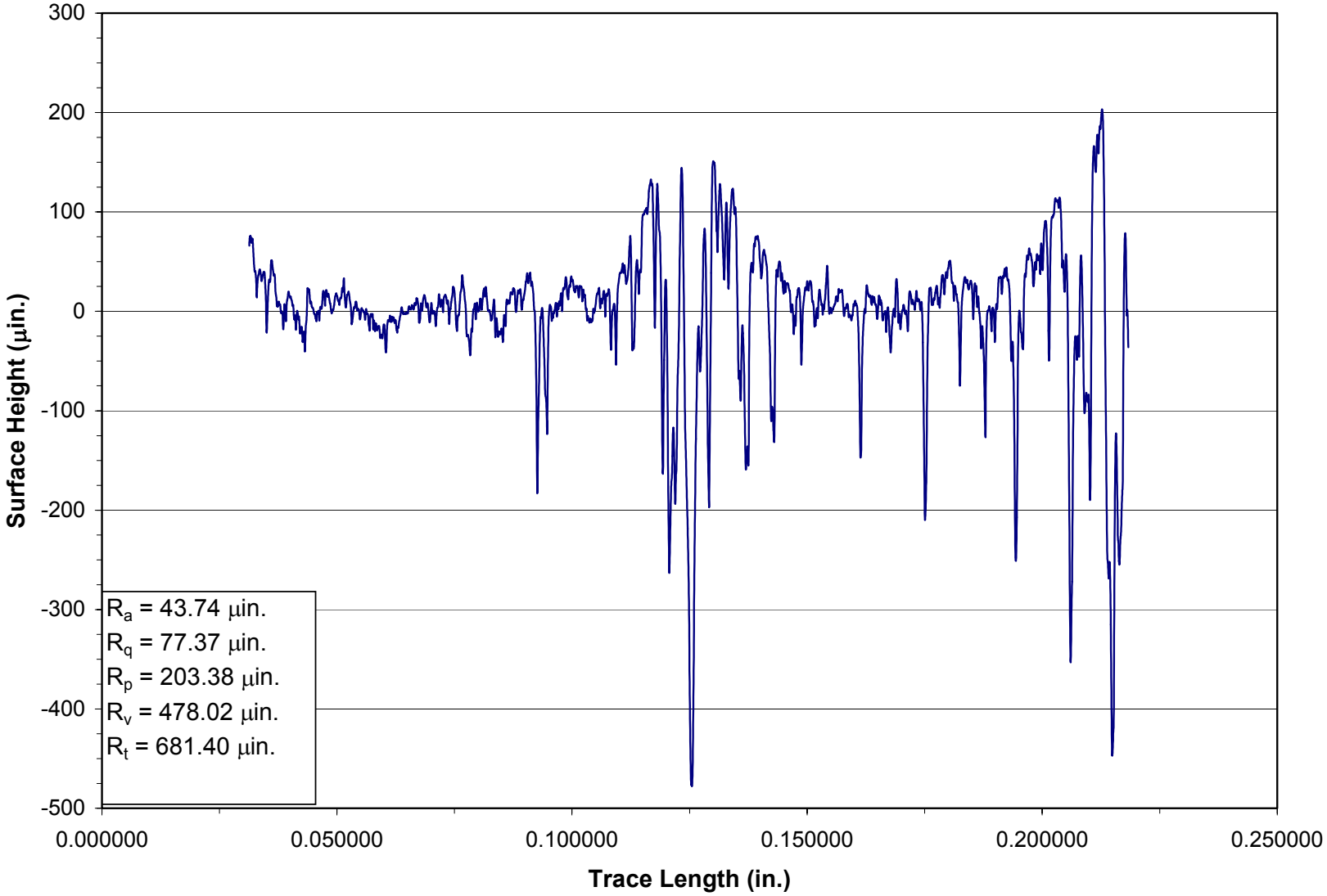

Figure C-45. Roughness Profile from Specimen 6008.